

FLOW BOILING ENHANCEMENT FOR THERMAL MANAGEMENT SYSTEMS

FINAL REPORT

January 29, 1998

Submitted to

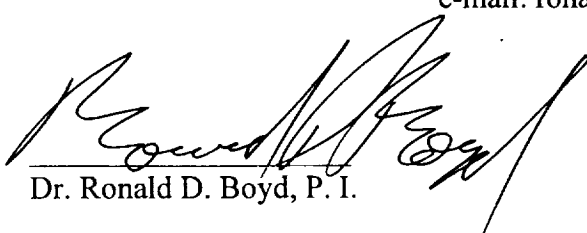
**The National Aeronautics and Space Administration (NASA)
Lyndon B. Johnson Space Center (JSC)**

From the:

THERMAL SCIENCE RESEARCH CENTER (TSRC)

by

**Dr. Ronald D. Boyd (P. I.)
Honeywell Endowed Professor of Engineering and
Director of the Thermal Science Research Center
Department of Mechanical Engineering
College of Engineering
Prairie View A&M University
P. O. Box 397
Prairie View, TX 77446-0397
(409) 857-4811, 2827, or 4023
e-mail: ronald_boyd@pvamu.edu**



Dr. Ronald D. Boyd, P. I.

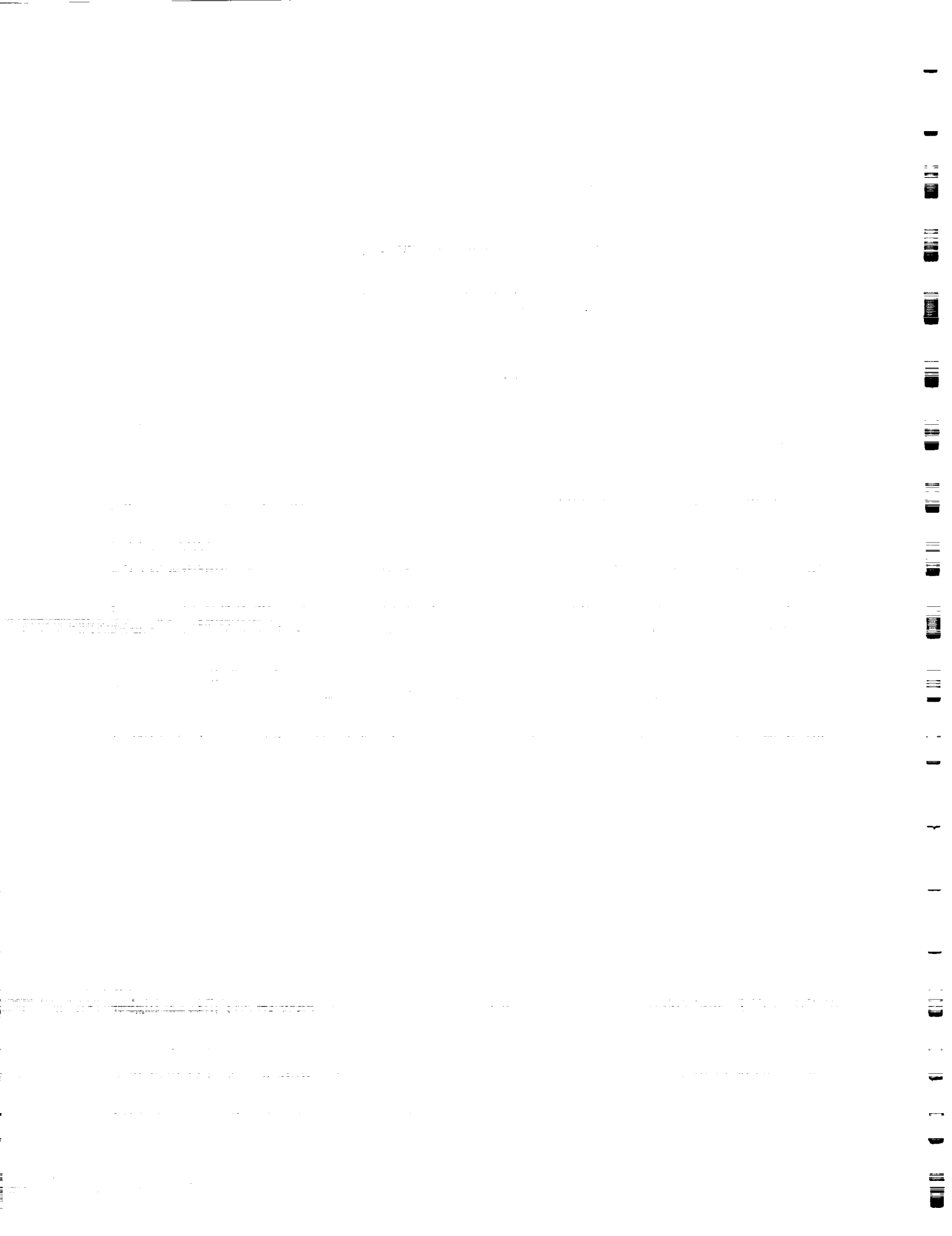
FLOW BOILING ENHANCEMENT FOR THERMAL MANAGEMENT SYSTEMS

Ronald D. Boyd (P. I.), Director of the TSRC and
Honeywell Endowed Professor of Engineering
Thermal Science Research Center (TSRC)
College of Engineering and Architecture
Prairie View A&M University
P. O. Box 397
Prairie View, TX 77446-0397
Phone: (409) 857-4811, 2827, 4023
FAX: (409) 845-9997 or 857-2325
e-mail: ronald_boyd@pvamu.edu

EXECUTIVE SUMMARY

This final report covers funded projects which include: (1) Flow Boiling Enhancement For Thermal Management Systems; and (2) a supplement to the former title, entitled Enhancement for Thermal Management Systems. As part of one of the main objectives of the proposed work, a vertical flow loop was designed and built to determine local (circumferential and axial) and mean wall temperature distributions for saturated and subcooled flow boiling in a single-side heated vertical channel with downward flow. Experimental results are given for flow with Freon-11 mass velocities of 280, 210.0, and 140.0 kg/m²s. The measurements indicate a significant circumferential variation in the temperature. The data indicate that a different mode of heat transfer is present at each circumferential location. The two-dimensional local measurements of the channel wall temperature show that corresponding local heat transfer coefficient variations will be significant.

The results for the vertical downward flow in a single-side heated channel with a Freon-11 mass velocity of 210.0 kg/m²s are summarized. The two-dimensional local (axial and circumferential) measurements of the channel outside wall temperature were obtained experimentally and the corresponding axially and circumferentially mean heat transfer coefficients **h** were calculated. This flow configuration was shown to have twenty percent higher values of **h** and forty percent higher ultimate critical heat flux than the case of a top-heated channel with horizontal flow. The data points to the existence of multiple levels of critical heat flux, which is unique to the single-side heated geometry. Finally, these averaged heat transfer



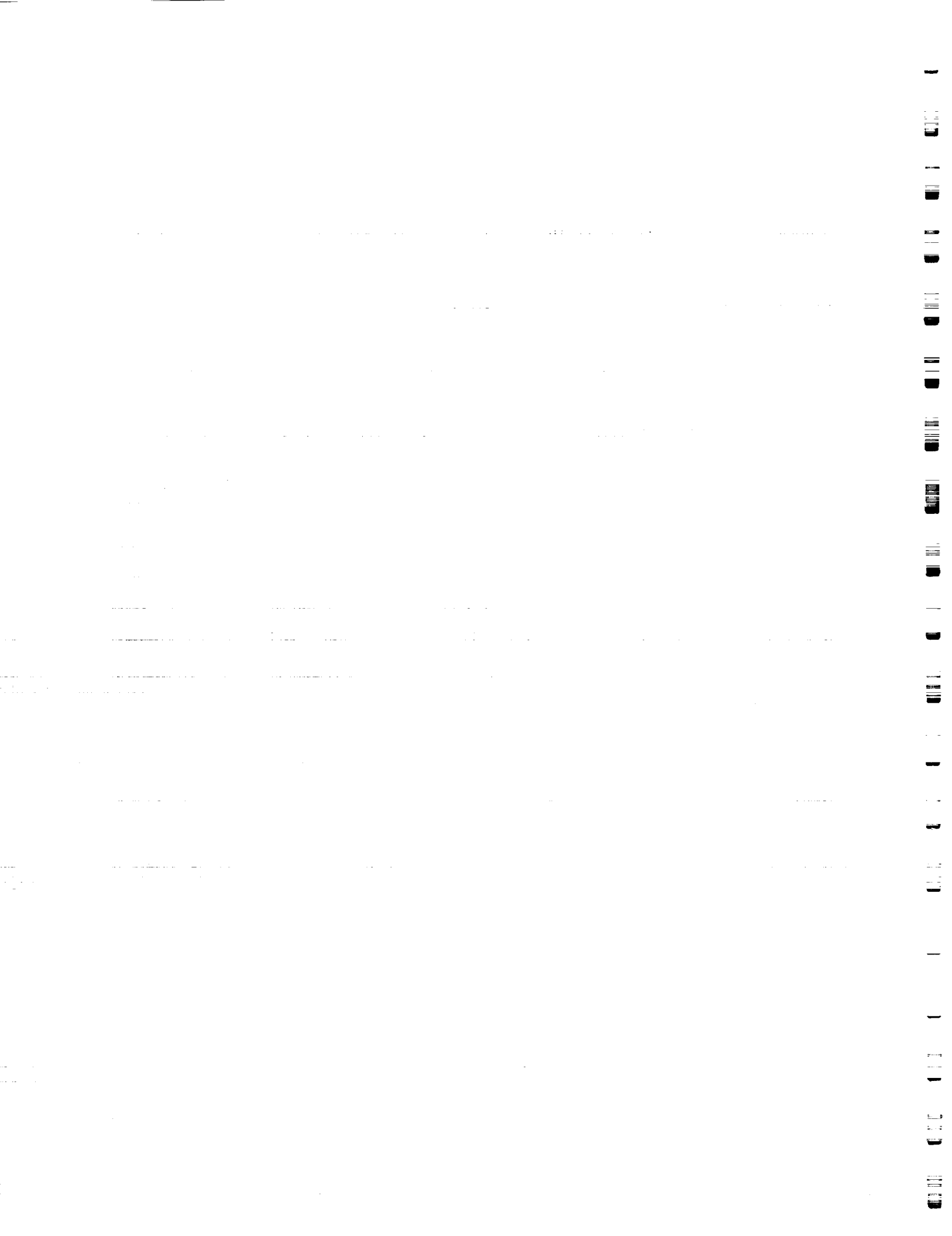
coefficients ranged from 30.0 to 230.0 W/m²K for the net heat flux range of 180.0 to 11,000.0 W/m².

The results obtained for downward flow boiling in vertical tubes were compared with identical test runs for Freon-11 flowing in horizontal channels with a top-side heating configuration. The experiments show a significant effect of flow direction on local outside wall temperatures and the averaged heat transfer coefficient.

The results of comparisons of flow boiling heat transfer in uniform and single-side heated tubes with existing single-phase and two-phase correlation are presented. Dittus-Boelter and Petukhov's single-phase correlation are used to compare experimentally obtained single-phase data; and Shah, and Liu-Winterton's two-phase correlation are used two-phase heat transfer data. The results of these comparisons show that some of our experimental data is in good agreement with the existing single-side heat transfer correlations for both uniform, and single-side heated case. Although the Liu-Winterton correlation had better agreement at low power levels and axial locations, the Shah correlation had better agreement at higher power levels and at axial locations near the center of the heated length. Both correlations overpredicted the data near the exit. Both correlations overpredicted the data near the exit. Therefore, additional correlational developmental work is needed for local (axial) heat transfer in circumferentially non-uniform heated channels.

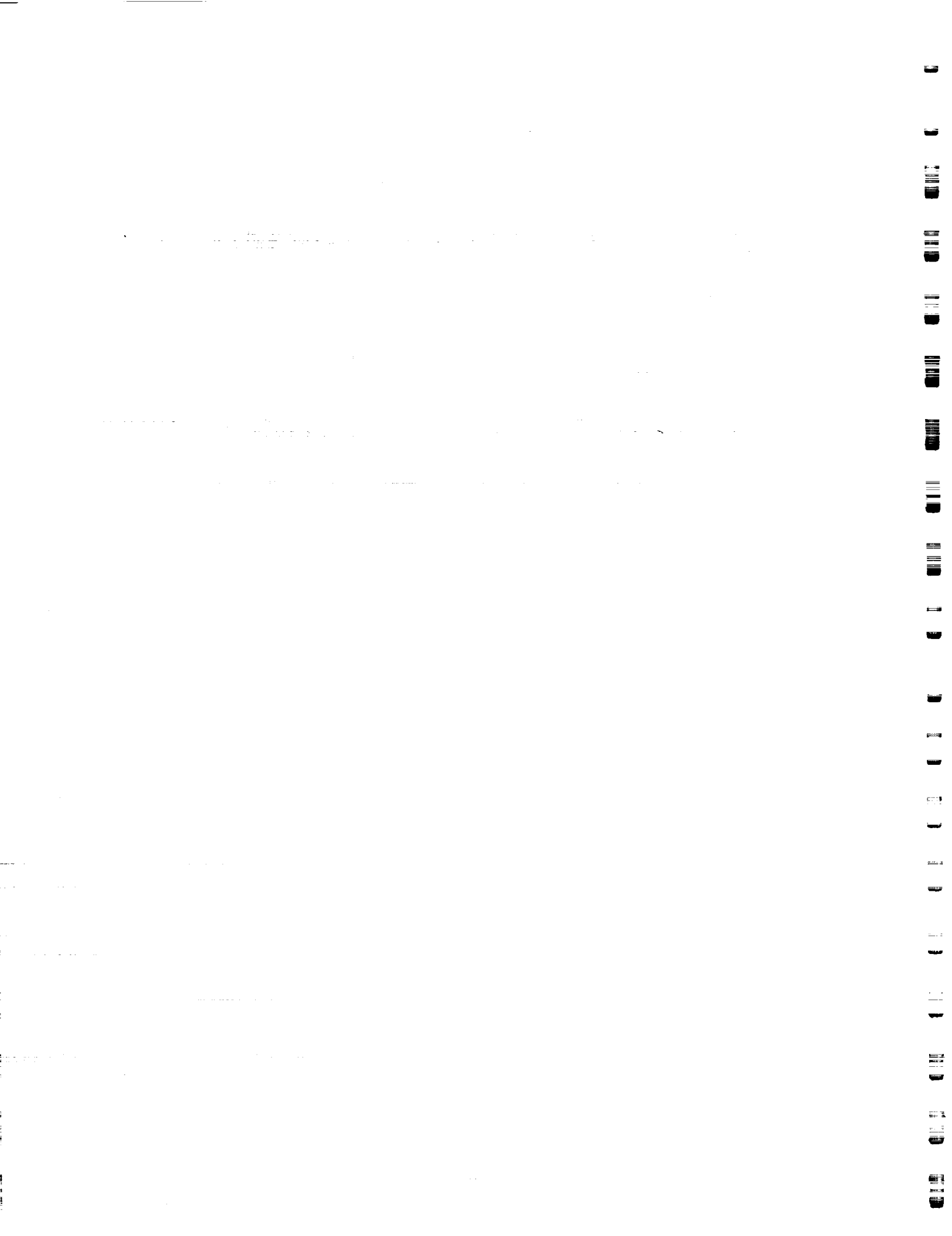
A steady state version of an inverse heat conduction (IHC) technique was used to perform two-dimensional (2-D) data reduction for selected experiments. The IHC technique is used to determine circumferential variation of heat transfer coefficient on one surface from the known values of a set of measured temperatures at specific locations and the known boundary condition on the other surface. Results on a horizontal test section top heated case show that the value of heat transfer coefficient increases from the top to a maximum value at around 45 degrees and then decreases drastically towards the unheated bottom portion.

This study has demonstrated that two-dimensional temperature variations are significant in two-phase thermal management systems which are heated from one side of the flow channels. Progress in advanced space thermal management systems requiring high heat flux removal will hinge on expanding the results of this study.



Although most of the funded NASA work at Prairie View has not resulted in technical papers in international publications, this work has resulted in the following **published technical papers** (see the Appendix for the complete reprints):

1. Boyd, R., Smith, A., and Turknett, J., 1995, "Two-Dimensional Wall Temperature Measurements and Heat Transfer Enhancement for Top-Heated Horizontal Channels with Flow Boiling," *Journal of Experimental Thermal and Fluid Science*, Vol. 11, pp. 372-386.
2. Boyd, R., Smith, A., and Turknett, J., 1994, "Measurements of Local Heat Transfer for Forced Convection and Flow Boiling in Horizontal, Uniformly Heated Smooth Tubes," *Journal of Experimental Heat Transfer*, Vol. 7, pp. 19-29.
3. Peatiwala, Q., Boyd, R., and Huque, Z., 1995 "Multi-Dimensional Wall Temperature and Boiling Curves for a Single-Side Heated Vertical Channel with Downward Flow," 1995 ASME/AIAA National Heat Transfer Conference, pp. 1-10.
4. Peatiwala, Q. and Boyd, R. D., 1995, "Forced Convection and Flow Boiling in a Single-Side Heated Vertical Smooth Channel with Downward Flow," 1995 National Heat Transfer Conference, HTD-Vol. 314, pp. 133-143.



**FLOW BOILING ENHANCEMENT FOR
THERMAL MANAGEMENT SYSTEMS**

FINAL REPORT

January 29, 1998

Submitted to

**The National Aeronautics and Space Administration (NASA)
Johnson Space Center (JSC)**

From the:

THERMAL SCIENCE RESEARCH CENTER (TSRC)

Contributors:

Ronald D. Boyd (P. I.)

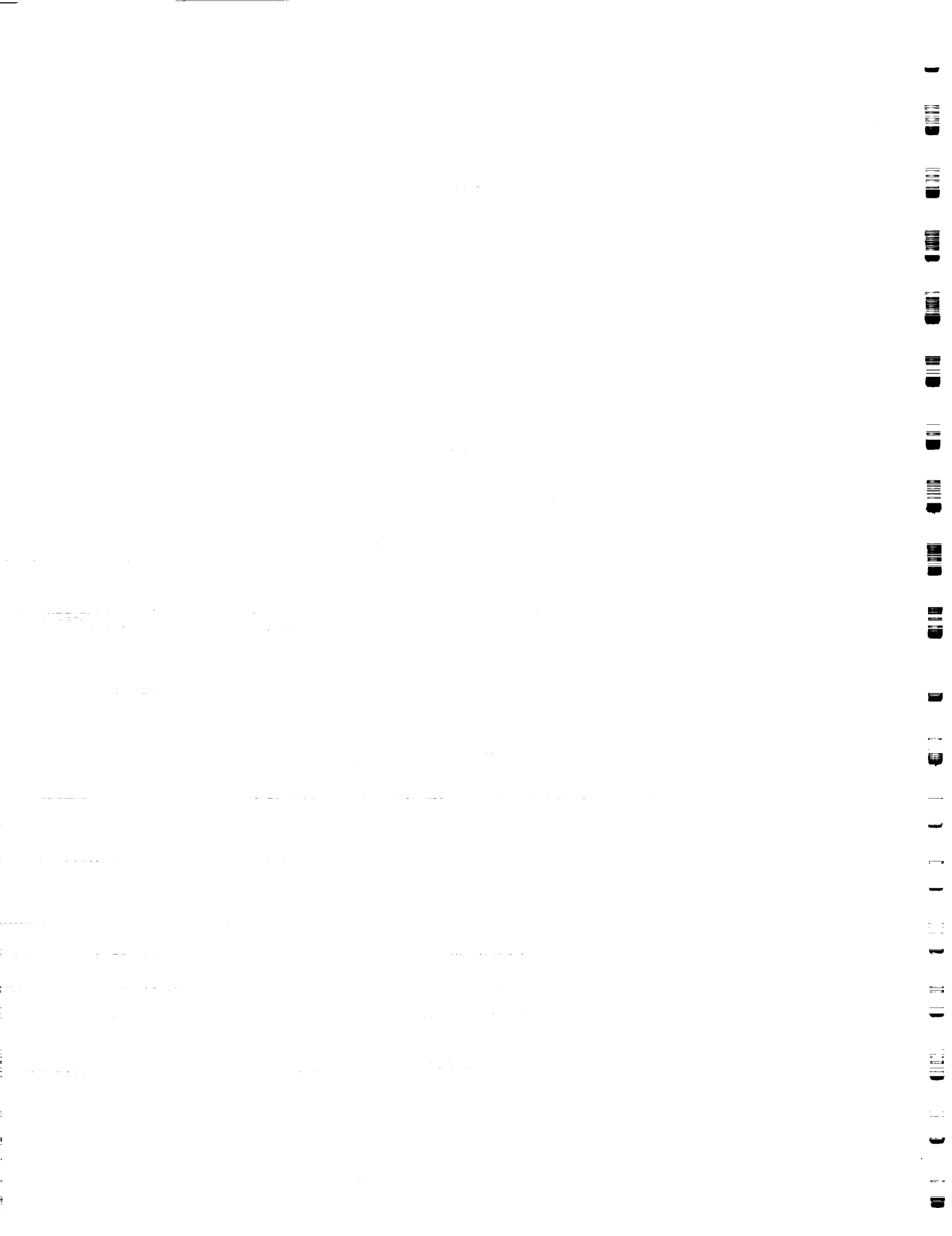
Quaid Peatiwala

Qing-Yuan Li

Ziaul Huque

Lori Davenport

Tabassum Kabir



FLOW BOILING ENHANCEMENT FOR THERMAL MANAGEMENT SYSTEMS

TABLE OF CONTENTS

EXECUTIVE SUMMARY	ii
NOMENCLATURE	vii
1.0: MULTI-DIMENSIONAL WALL TEMPERATURE AND BOILING CURVES FOR A SINGLE-SIDE HEATED VERTICAL CHANNEL WITH DOWNWARD FLOW	1
2.0: FORCED CONVECTION AND FLOW BOILING IN A SINGLE-SIDE HEATED VERTICAL SMOOTH CHANNEL WITH DOWNWARD FLOW.....	27
3.0: SUBCOOLED FLOW BOILING IN SINGLE-SIDE HEATED VERTICAL CHANNELS WITH DOWNWARD FLOW; PART I: THE EFFECT OF ORIENTATION BASED ON THE AVERAGED HEAT TRANSFER COEFFICIENT	50
4.0: SUBCOOLED FLOW BOILING IN SINGLE-SIDE HEATED VERTICAL CHANNELS WITH DOWNWARD FLOW; PART II: COMPARISONS WITH SELECTED TWO-PHASE CORRELATIONS	61
5.0: TWO-DIMENSIONAL DATA REDUCTION APPLYING INVERSE HEAT CONDUCTION (IHC) TECHNIQUE	77
6.0: CONCLUSIONS	88
ACKNOWLEDGMENTS	90
REFERENCES	91
APPENDIX (Published Technical Papers)	95
1. Journal of Experimental Thermal and Fluid Science	
2. Journal of Experimental Heat Transfer	
3. 1995 ASME/AIAA National Heat Transfer Conference	
4. 1995 National Heat Transfer Conference	
DISTRIBUTIONS	144

NOMENCLATURE

Bo	Boiling number
D	Channel inside diameter (m)
E	Sum of squared temperature error
G	Mass Velocity ($\text{kg/m}^2\text{s}$)
h	Heat transfer coefficient, ($\text{W/m}^2\text{K}$)
h_{mj}	Circumferentially-averaged but axially distributed heat transfer coefficient ($j = 1, 2, \dots, 7$)($\text{W/m}^2\text{K}$)
k	Thermal conductivity (W/m K)
L	Heated length, m
M	Total number of measuring points
M_w	Molecular Weight
N	Total number of h_i coefficients
ONB	Onset of Nucleate Boiling
Pe	Peclet number (Re Pr)
Pr	Liquid Prandtl
p_r	Reduced pressure
q	Heat flux, (W/m^2)
q_g	Heat generation rate in wall per unit area
Re	Liquid only Reynolds number
St	Stanton Number
T	Temperature (K)
T_{av}	Circumferentially averaged wall temperature (^0C)
T_c	Calculated temperature
T_m	Measured temperature
x	Quality
x^*	Equilibrium quality at the axial location where $T_w = T_{sat}$
Z	Axial coordinate or measurement location in the heated section of the test section (m)
Z_j	Axial coordinate or measurement location in the heated section of the test section (m)

Greek

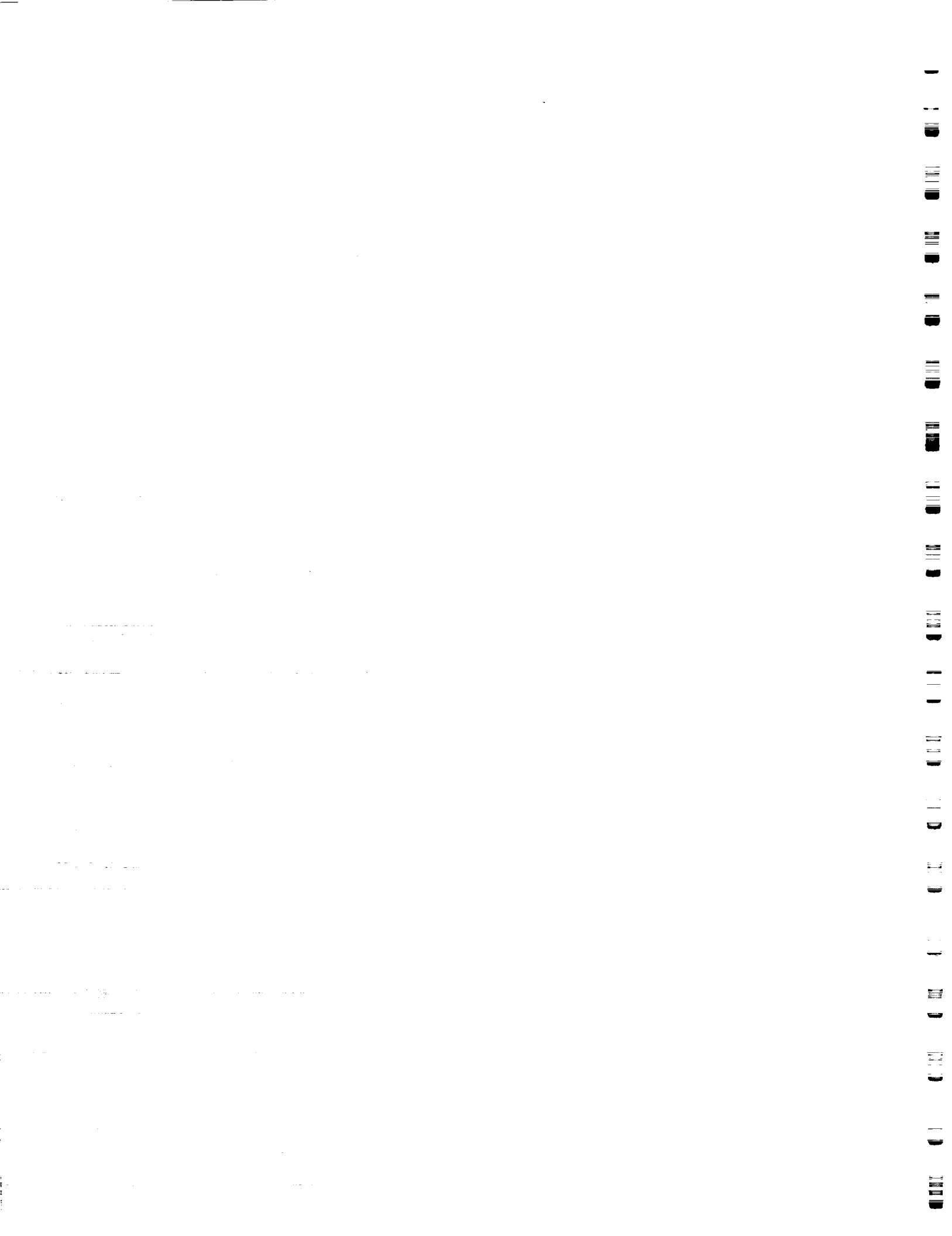
ϕ	Circumferential coordinate or measurement location (degrees)
μ	Dynamic viscosity, (N s/m^2)

SUBSCRIPTS

b	Bulk fluid
i	Circumferential location measuring points index
j	Axial location measuring points index
L	Liquid
NB	Nucleate boiling
pool	Pool boiling



s Saturation
tp Two-phase
w Wall



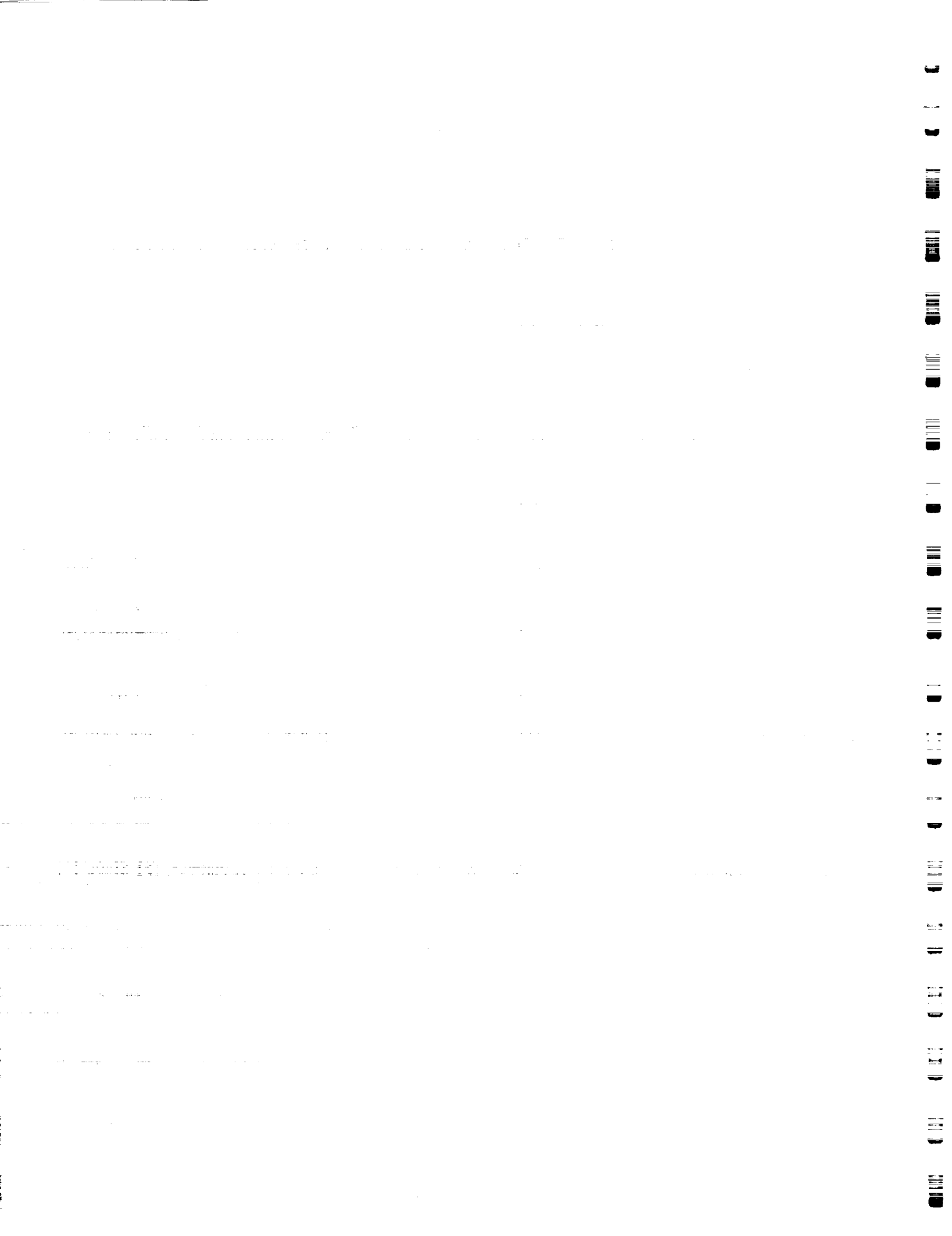
FLOW BOILING ENHANCEMENT FOR THERMAL MANAGEMENT SYSTEMS

1.0 MULTI-DIMENSIONAL WALL TEMPERATURE AND BOILING CURVES FOR A SINGLE- SIDE HEATED VERTICAL CHANNEL WITH DOWNWARD FLOW

1.1 INTRODUCTION AND OBJECTIVES

Future space programs and commercialization will require an active thermal control system (Miller et al. [1]) to provide moderate temperature heat rejection for different system modules. It is essential that the thermal rejection system selected be able to operate under a variety of complex and non-uniform heat flux distributions. Other requirements for the selected system include minimum overall system mass, and pumping power (Ungar et al. [2] and Reinarts et al. [3]). The high heat flux potential and low mass requirement of the two-phase thermal control system makes them an attractive option for advanced space applications. Although work is proceeding in studying the two-phase pressure drop [2, 3], little efforts are being devoted to studying heat transfer related topics in single-side heated systems. In particular, optimization of the heat transfer, with accompanying reduced mass and pumping power requirements, will require a knowledge of the two-dimensional wall temperature distributions in advanced and commercial space systems (Boyd et al. [4]). Implementation of two-phase thermal control system will also require additional emphasis on flow boiling phenomenon as it pertains to non-uniform heat flux distributions, resulting wall temperature distributions, heat transfer coefficients, flow channel aspect ratio, and orientation.

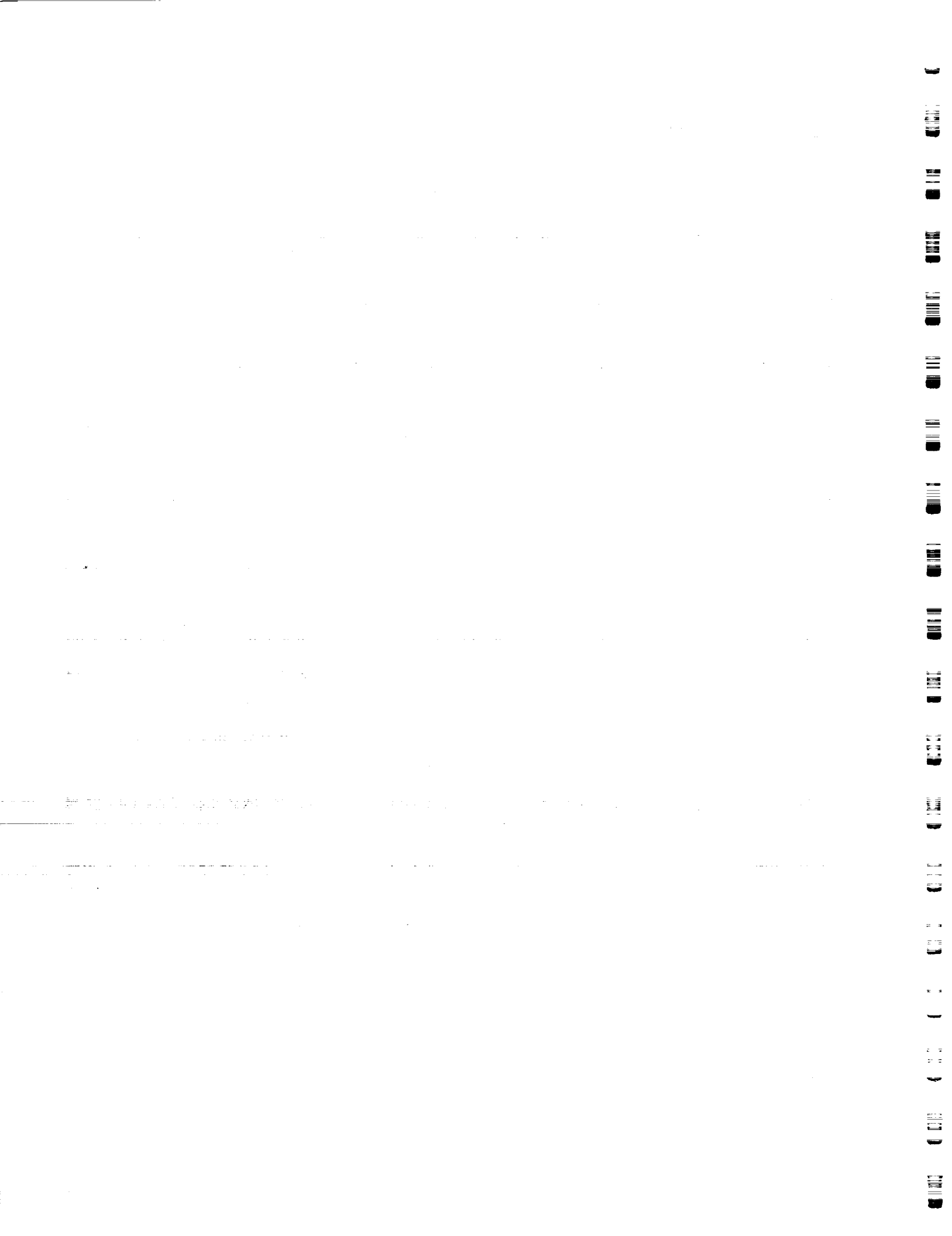
From the literature review, there has been much work completed for the two-phase heat transfer correlations for a uniform heat flux distribution. Correlations presented by Kandlikar, [5] Shah, [6] Gungor and Winterton, [7] and Boyd and Meng [8] cover different fluids, vast ranges of flow rates, the entire spectrum of quality, and low and high subcoolings. The former three correlations were only recommended for saturated flow boiling and the latter for subcooled flow boiling. These correlations are valid for only smooth tubes, and one must avoid using them when orientation is important. The former three correlations were derived from the data collected from horizontal flow boiling, where as the latter for high Froude number (> 50.0). Recently, several researchers have considered the effect of heat transfer enhancement devices (fins, and twisted tapes) and have presented correlations, but most of these



are again for horizontal flow boiling or condensation on horizontal tubes. Patankar et al., [9] Wen et al., [10] and Jaber et al., [11] have studied the effect of fins on the heat transfer coefficient for condensation. While Wen et al. [10] presented experimental data to facilitate theoretical model development of heat transfer coefficient for condensation on horizontal integral-finned tubes, Jaber et al. [11] found that the condensation heat transfer coefficient can be increased by up to 280% for copper if commercially available enhanced tubes are used in condensers over smooth copper tubes. He also looked at copper alloy tubes and found that heat transfer is enhanced by an average of over 30% with finned tubes relative to smooth tubes. Boyd et al. [4], Smith, [12] and Turknett, [13] have studied the flow boiling in horizontal channels with uniform and top-side heating with and without enhancements. They made measurements of the two-dimensional axial and circumferential wall temperature distributions, and presented results for the axial distribution of the heat transfer coefficient for four internal tube configurations.

As stated before almost all of the work done in two phase flow is for uniform heat flux and for this heat loading condition, there is no circumferential variation in wall temperature. Hence, at any power level only single mode of heat transfer is used to calculate heat transfer coefficient at a given axial location. It is understandable that by using a uniform heat flux distribution, the modeling for heat transfer coefficient is greatly simplified; but in engineering applications with non-uniform circumferential heat flux distributions, this work will show that the wall temperature variations are significant. Some applications where this may be important include thermal management for the advanced space systems, high heat flux fusion components, high heat flux electronic components, in-tube boiling systems, boilers, condensers, and heat exchangers. It should be made clear here that great care must be taken when approximating a non-uniform heat flux condition with a uniform one because by using this approximation, severe restricts or even anomalies may result. This is another reason why applications requiring single-side heating of channels with flow boiling will be better characterized by measurements of the local 2-D wall temperature and heat transfer variations.

For advanced space thermal management systems to become a reality, extensive efforts are needed to collect and correlate 2-D two-phase experimental data for heat transfer correlations for complex heat flux distributions. The long-range scope of this study includes making 2-D wall temperature measurements as a function of mass velocity, inlet subcooling, tube diameter, tube internal geometry, tube orientation, gravity level, and heating configuration. The anticipated Freon -11 mass velocity and

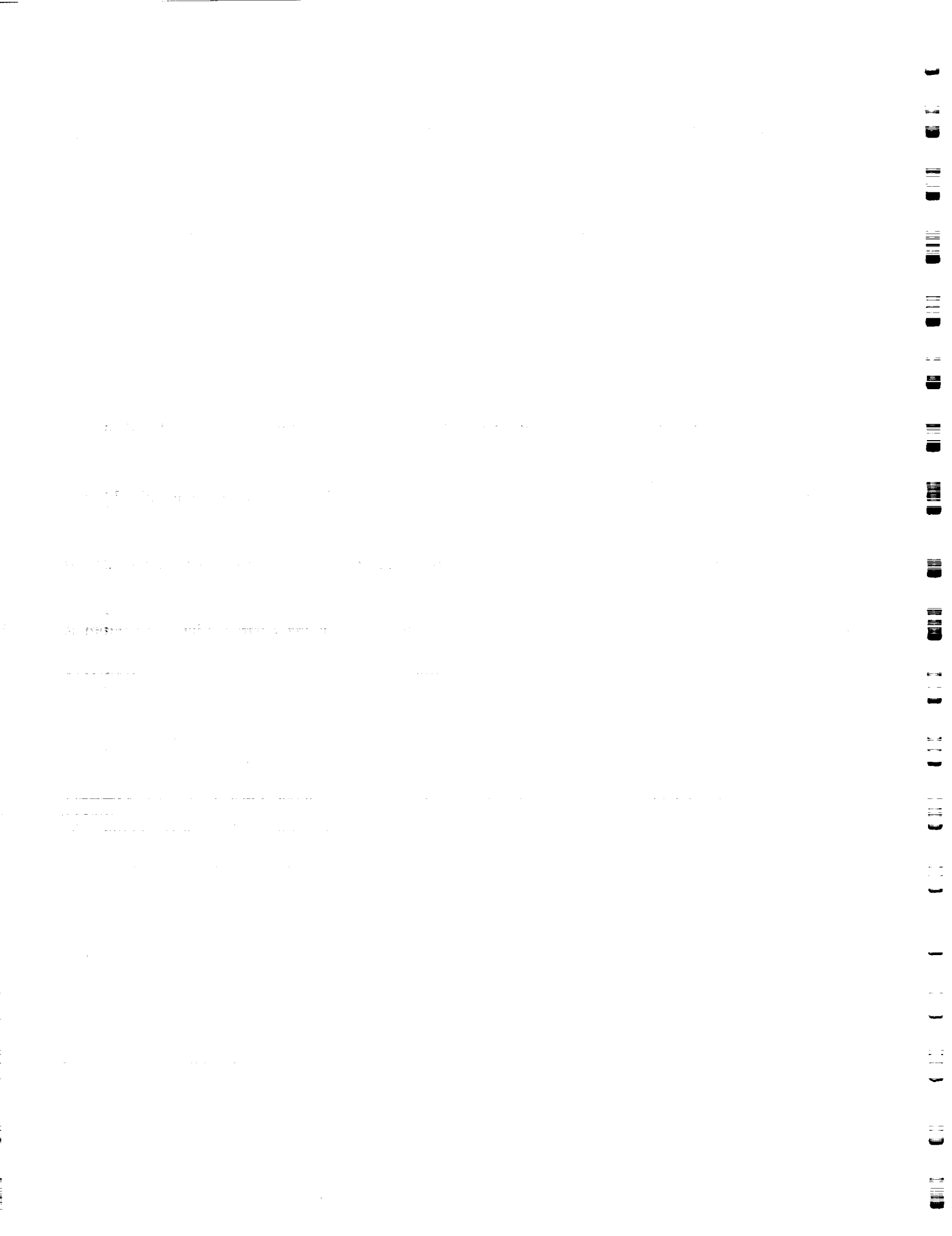


tube diameter range between 95.0 and 1,300.0 μm , and between 9.5 and 25.4 mm, respectively. The tube inside wall configuration will include smooth wall, finned wall, and combined twisted tape and finned walls. In the present paper, we present an example of 2-D outside wall temperature measurements made with subcooled Freon-11 flowing downward in a smooth vertical channel with single-sided heating and study the effects of different mass velocities on wall temperature distribution.

1.2 EXPERIMENTAL SETUP

The system used to perform forced convection boiling experiments in vertical tubes (downward flow) was based on the system initially developed by Boyd et al. [4] and later used by Smith [12], Boyd, [14] and Turknett [13]. Figure 1a shows the Freon-11 vertical flow boiling loop. This closed loop is constructed of stainless steel and copper, and operates between 3.4 kPa and 0.17 MPa. The maximum power generation capability is 2.7 kW and the maximum volume flow rate is approximately $2.97 \times 10^{-4} \text{ m}^3/\text{sec}$. The Freon-11 is stored in a reservoir which is filled using a chemical resistance centrifugal pump. After filling the reservoir, the Freon-11 is circulated through the closed loop at the desired operating pressure and flow rate. By circulating the Freon-11 before any data is recorded, any leaks in the system can be detected by using a halogen leak detector. Then the desired inlet temperature is obtained by properly adjusting the chiller/isothermal bath. The energy is transferred between the chiller and Freon-11 by way of a commonly connected heat exchanger. During testing, the outlet temperature of the chiller is adjusted to maintain a constant inlet Freon-11 temperature for a given experimental run. The working fluid for the chiller is a 60/40 ethylene glycol - distilled water mixture.

A description of the closed flow loop and the function of its components is instructive. The Freon-11 flows from the reservoir to the filter, where all the contaminants are removed before the fluid enters the positive displacement pump. The positive displacement pump requires a net positive suction of at least 0.02 MPa. This pump was selected for durability. After leaving the pump, the fluid passes through the pulsation damper. The damper reduces the pressure and flow oscillations. The pressure fluctuations are also minimized by using the pneumatically controlled metering valve. Exiting the control valve, the fluid flows to the heat exchanger, where its temperature is set at a desired value by adjusting the chiller parameters. After exiting the heat exchanger, the fluid passes through the turbine flow meter and enters the unheated "flow developing" section or upstream part of the test section which has a length greater than forty (40) times the test section diameter. The fluid then enters the heated section of the test section.



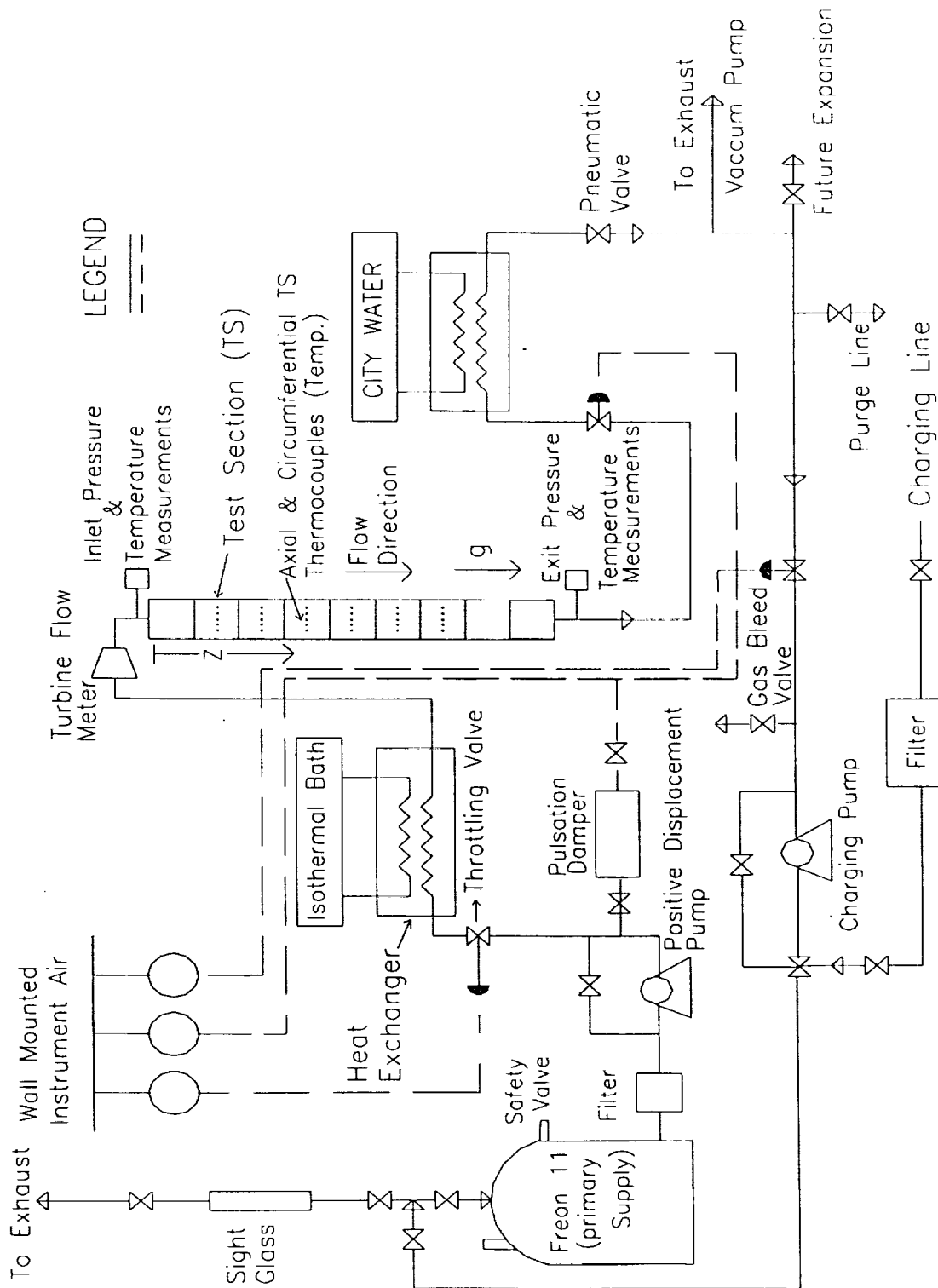


Figure 1a: Schematic of the Vertical Downward Flow Boiling Loop

A downstream pneumatically controlled valve is used to control the test section exit pressure. The heated fluid then passes through another heat exchanger where the energy generated is removed partially by using tap water. Finally, the fluid flows back to the reservoir and the flow cycle is complete.

The test sections used in this experiment are the same as used by Boyd et al. [4] The test sections are 2.235 m long copper tubes (see Figure 1b), and consists of two parts: (1) Upstream unheated section to facilitate flow development, and (2) A downstream single-side heated section. For the present case, the inside diameter (D) was 25.4 mm and the outside diameter was 28.5 mm.

The heated section has a smooth inside surface. The test section was heated with heater tapes which varied in width based on tube diameter and are 1.22 m long. Each tape has power generation capacity of 2.66 kW. The test section was designed with flexibility and ease of replacement in mind. Although, the pressure losses due to union connector at both top and bottom ends of the test section are assumed to be small, computations and additional measurements, will be performed later to estimate these losses. The entire test section was insulated to minimize the heat losses. In addition to the primary two parts of the main test section, each part had pressure-temperature measurement ports upstream and downstream of the test section.

The heated part of the test section was divided into seven .203 m axial intervals. At each of the axial locations there are seven thermocouples installed circumferentially at 0 , $\pi/4$, $3\pi/8$, $\pi/2$, $5\pi/8$, $3\pi/4$, and π degrees (see Figure 2) , with 0 being at the top heated portion of vertical symmetry plane in Figure 8. This test section thermocouple arrangement will allow better circumferential resolution of the wall temperature variation than previous test sections (Boyd, [14] Smith, [12] and Turknett, [13]) because seven circumferential locations were used rather than four.

The thermocouples were installed by using high thermal conductivity epoxy. Special care was taken when thermocouples were adhered to the tube. The thermocouple beads were placed in good contact with the tube so that as little epoxy as possible was used. Based on forty repeated measurements of the epoxy thickness between the thermocouple and the copper tube, the mean thickness was 0.194 mm, and the standard deviation was 0.007 mm.

1.3 DATA REDUCTION ANALYSIS

Forty-nine (49) local temperature measurements were made on the outside surface of the heated portion of the test section for each experiment. These outside temperatures must be related to the inside

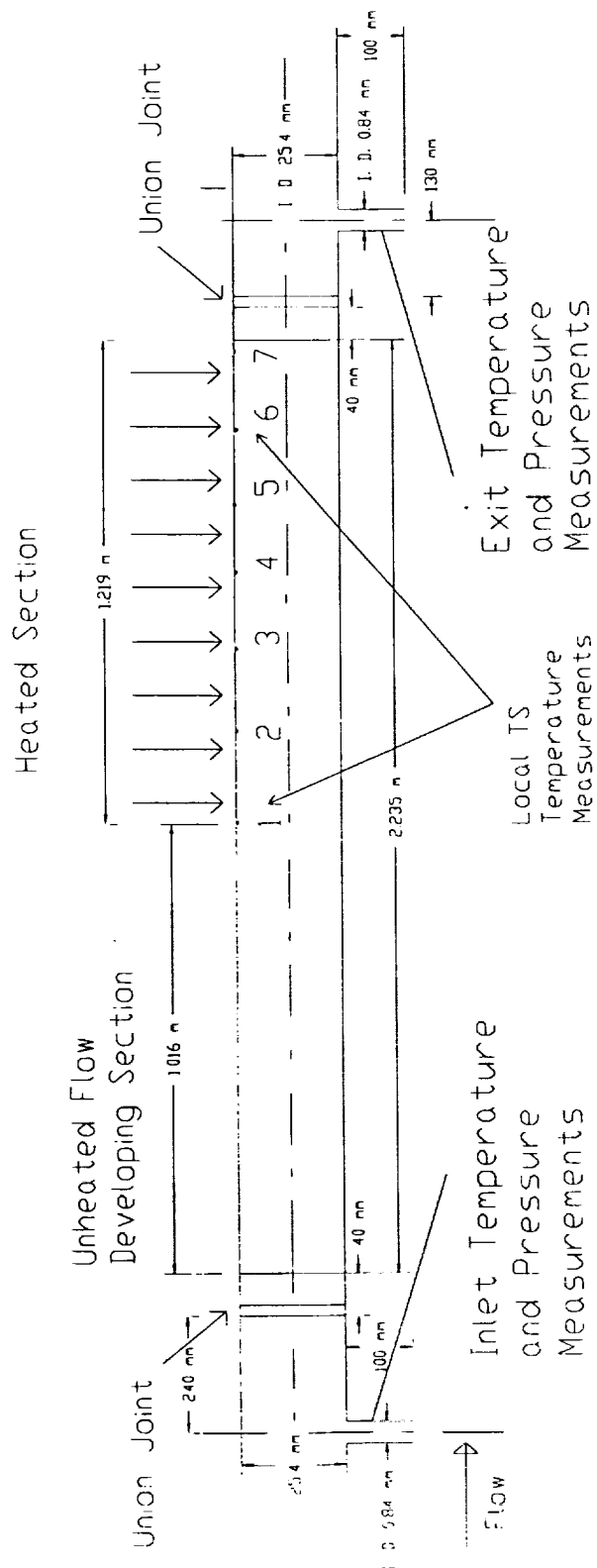


Figure 1b: Test Section Configuration for Temperature and Pressure Measurements

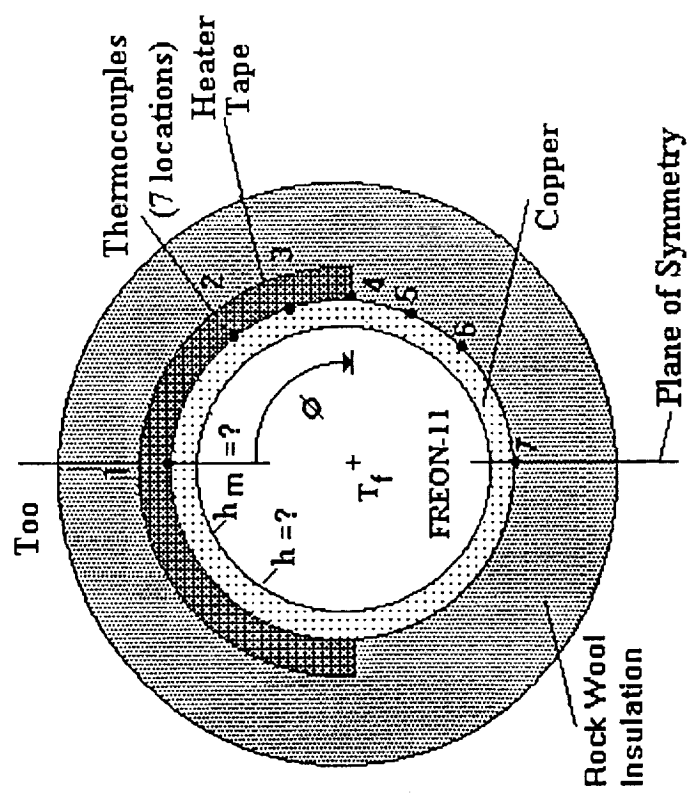
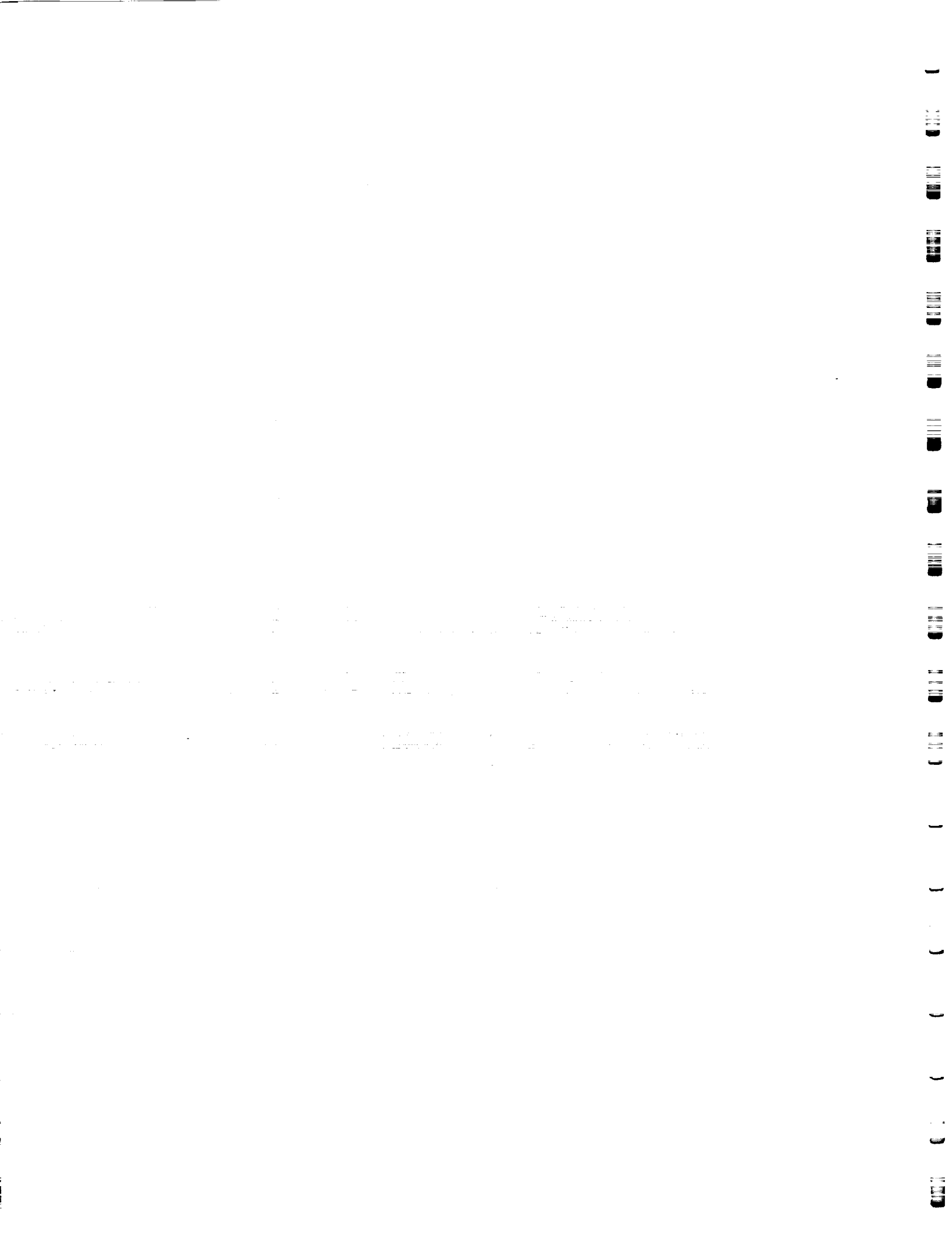


Figure 2: Cross-section of Heated Portion of the Vertical Test section



wall temperature so that the inside heat transfer coefficient can be computed. Two techniques will be used to reduce the wall temperature data: (1) the heated thermal hydraulic approach (Boyd et al. [4]), see Figure 3, and (2) a multi-dimensional inverse conduction analysis using a numerical finite element computation code called ANSYS.

The initial data reduction is based on the heated hydraulic approach used by Boyd et al. [4] In this analysis, we compute circumferentially averaged heat transfer coefficient from circumferentially averaged wall temperature. The circumferentially averaged temperature was computed from the seven wall temperature measurements made on copper tube outside surface at each axial location by using the piece-wise linear approach similar to that used by Reid et al. [15] Using their approach, the circumferentially averaged outside wall temperature can be related to the seven circumferential measured temperatures (T_{m1} at 0 degrees, T_{m2} at $\pi/4$, T_{m3} at $3\pi/8$ etc.) by the equation given below:

$$T_{av} = \frac{2T_{m1} + 3T_{m2} + 2T_{m3} + 2T_{m4} + 2T_{m5} + 3T_{m6} + 2T_{m7}}{16} \quad (1)$$

The temperature T_{av} was used with the model presented by Boyd et al. [4] to account for temperature drop across channel walls, and convective and radiative heat losses to the surroundings. Using this model, the mean heat transfer coefficient (h_{mj}) at a given axial location can be obtained. The uncertainties for each measurement in this experiment are as follows: (1) for geometric measurements, ± 0.001 mm; (2) for voltage, ± 0.05 mV; (3) for current, ± 0.005 mA; (4) for pressure, ± 0.7 Pa; (5) for flow rate, $\pm 6.3E-7$ m³/s; and the resulting uncertainty in wall temperature was estimated to be , ± 0.2 °C.

1.4 RESULTS

For a 25.4 mm inside diameter single-side heated test section, 2-D (axial and circumferential) wall temperature distribution results are presented for mass velocities (G) of 280.0, 210, and 140 kg/m²s, for an inlet temperature of 22.6 °C, and an exit pressure of 0.1843 MPa (absolute).

2-D Wall Temperature Distribution

Figures 4 through 10 show the distributions as measured outside wall temperature at different circumferential and axial locations for mass velocities of 280.0, 210, and 140 kg/m²s. The wall temperature increased as the fluid flowed from upstream to downstream (axial locations #1 to #7) in the

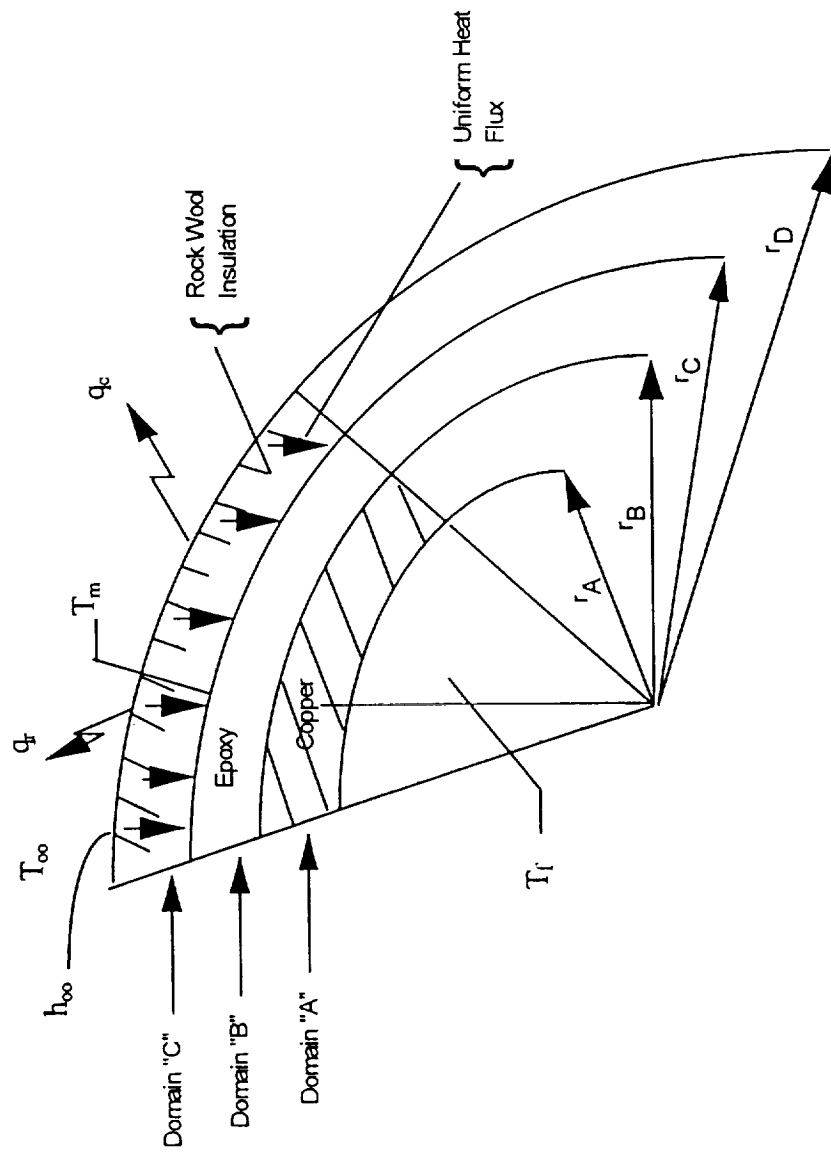


Figure 3: Thermal Hydraulic Model

Single-Side Heated Tube, $D = 25.4$ mm, Inlet Temp = 22.6°C , $\phi = 0.0$ Degrees

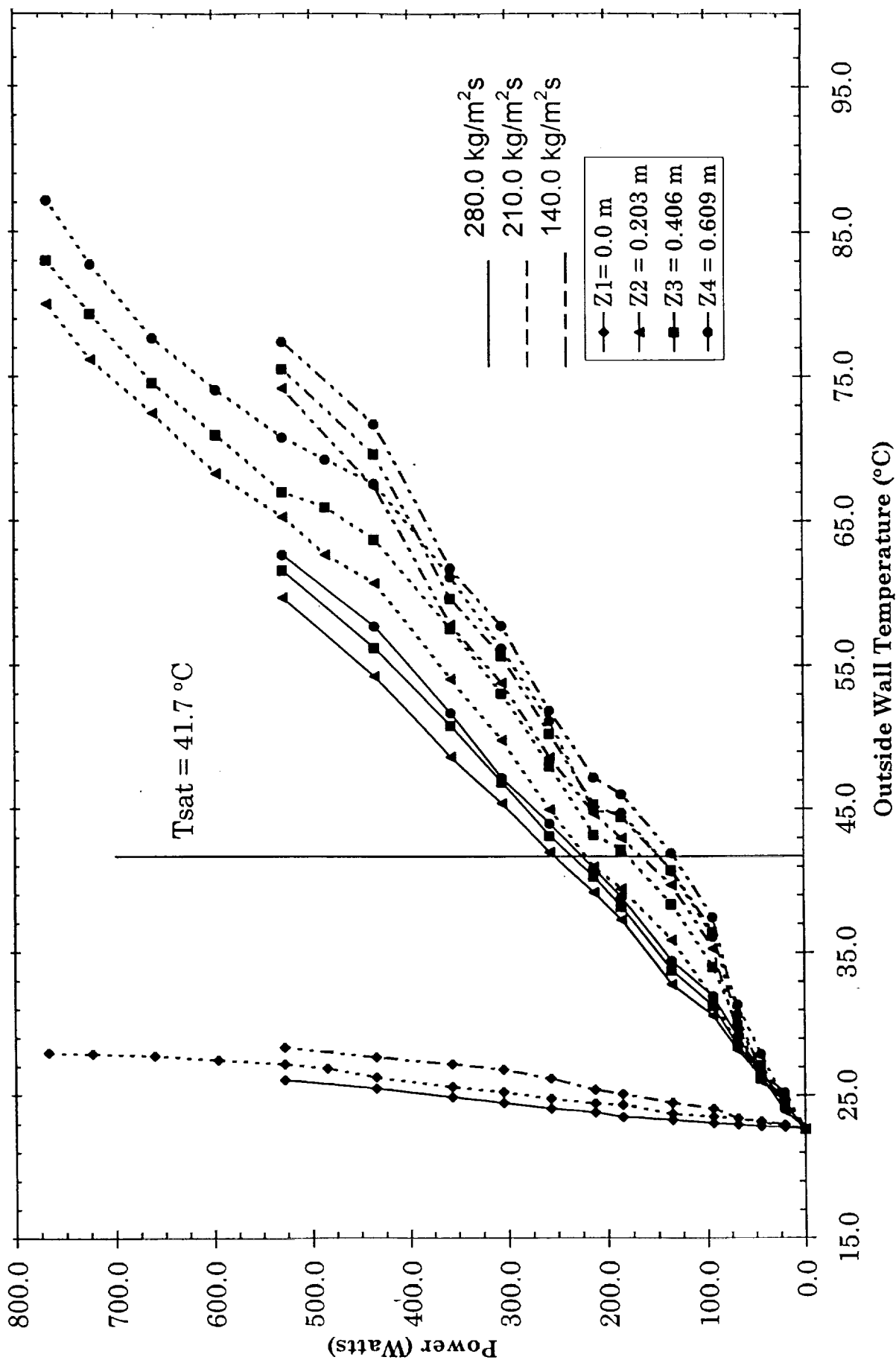
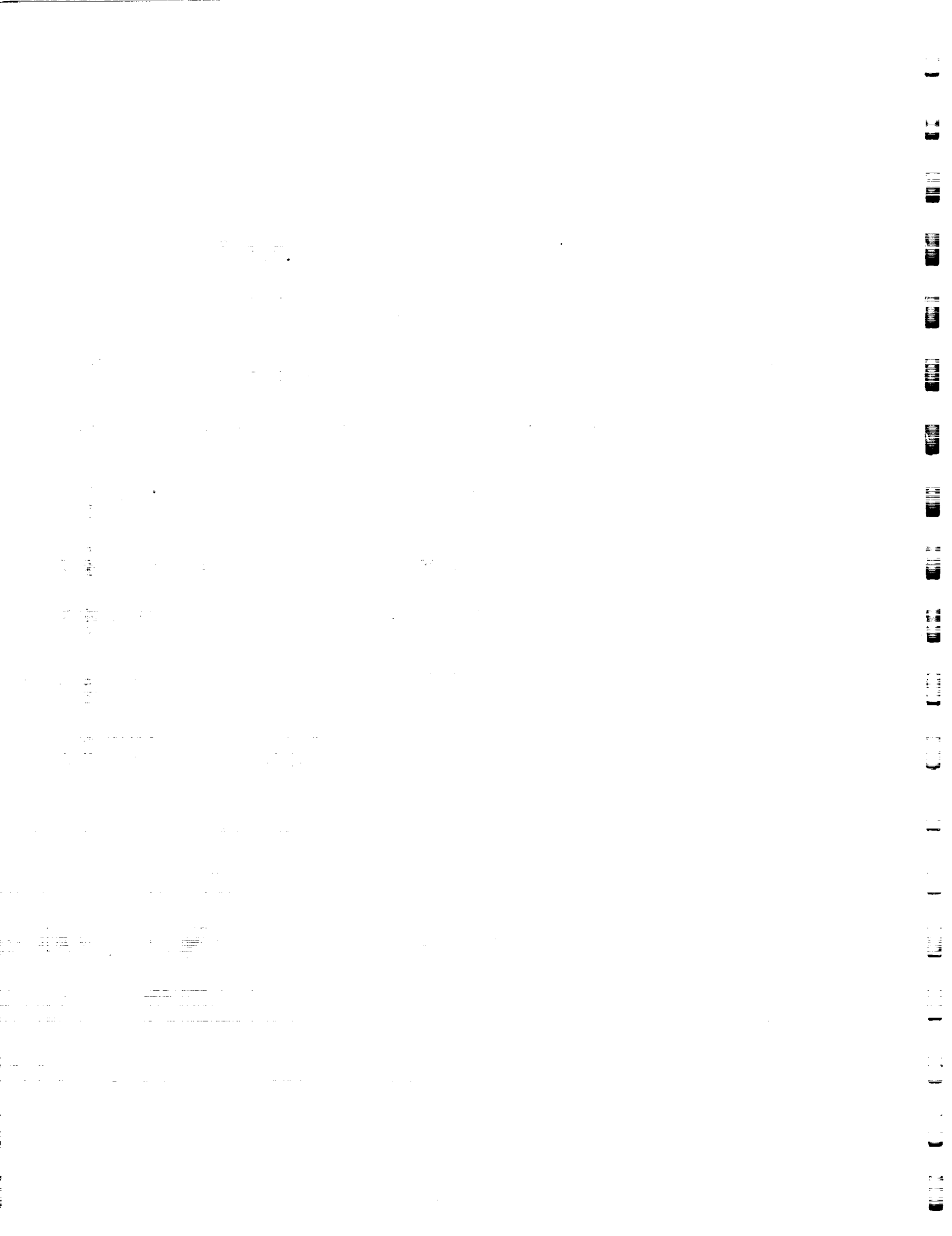


Figure 4a : Measured Outside Wall Temperature (Copper Channel) Axial Distribution as a Function of the Net Power Generation for Single-Side Heated Smooth Channel for Different Mass Velocities.



$G = 210 \text{ kg/m}^2\text{s}$, Inlet Temp = 22.6°C
 Single-Side Heated Tube, $D = 25.4 \text{ mm}$; $\phi = 45.0$ Degrees

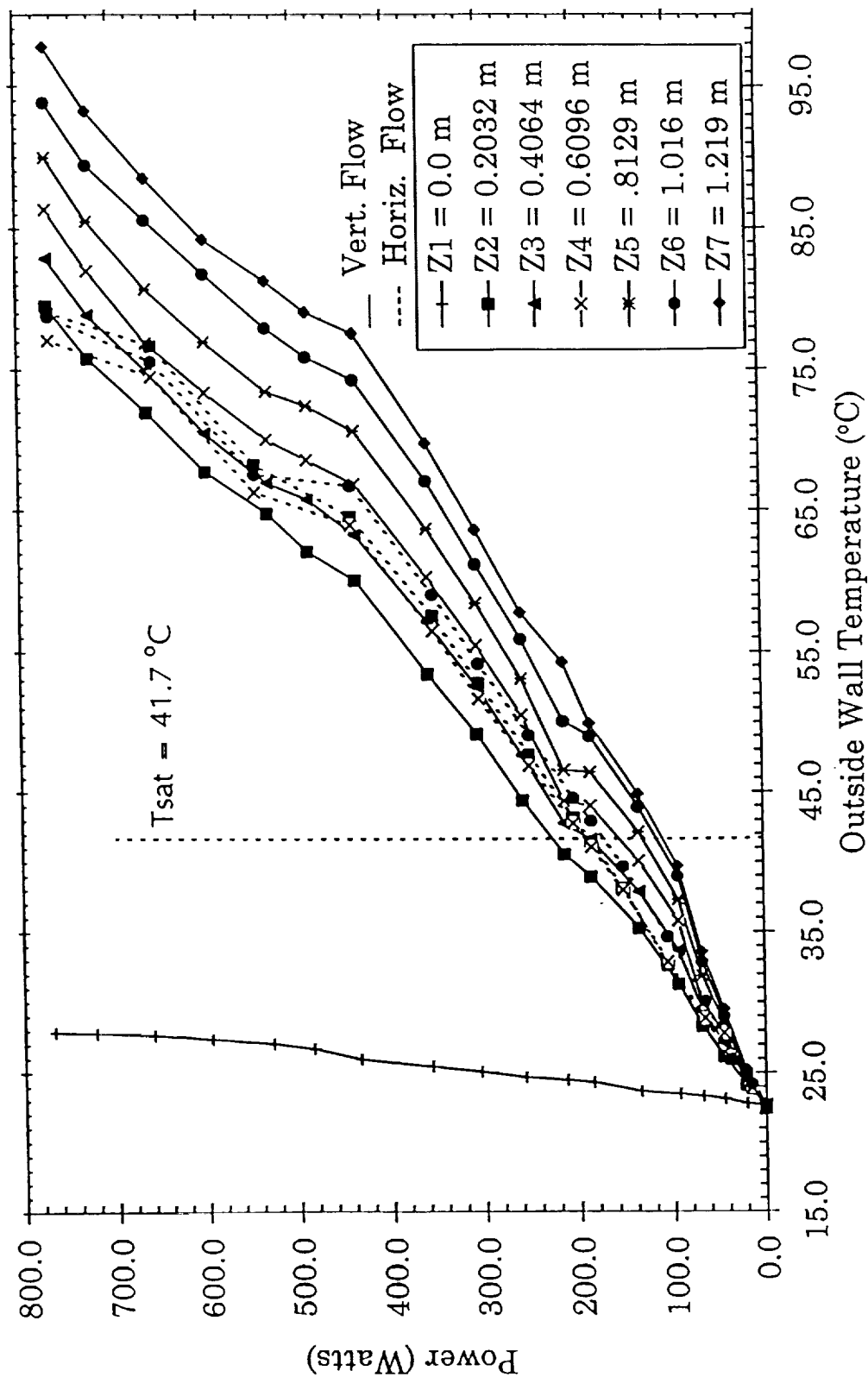


Figure 4b: Measured Outside Wall Temperature (Copper Channel) Axial Variation as a Function of the Net Power Generation for Single-Side Heated, Smooth Channel for $\phi = 45.0$ Degrees

$G = 210 \text{ kg/m}^2\text{s}$, Inlet Temp = 22.6°C
 Single-Side Heated Tube, $D = 2.54 \text{ cm}$; Power = 93.5 Watts

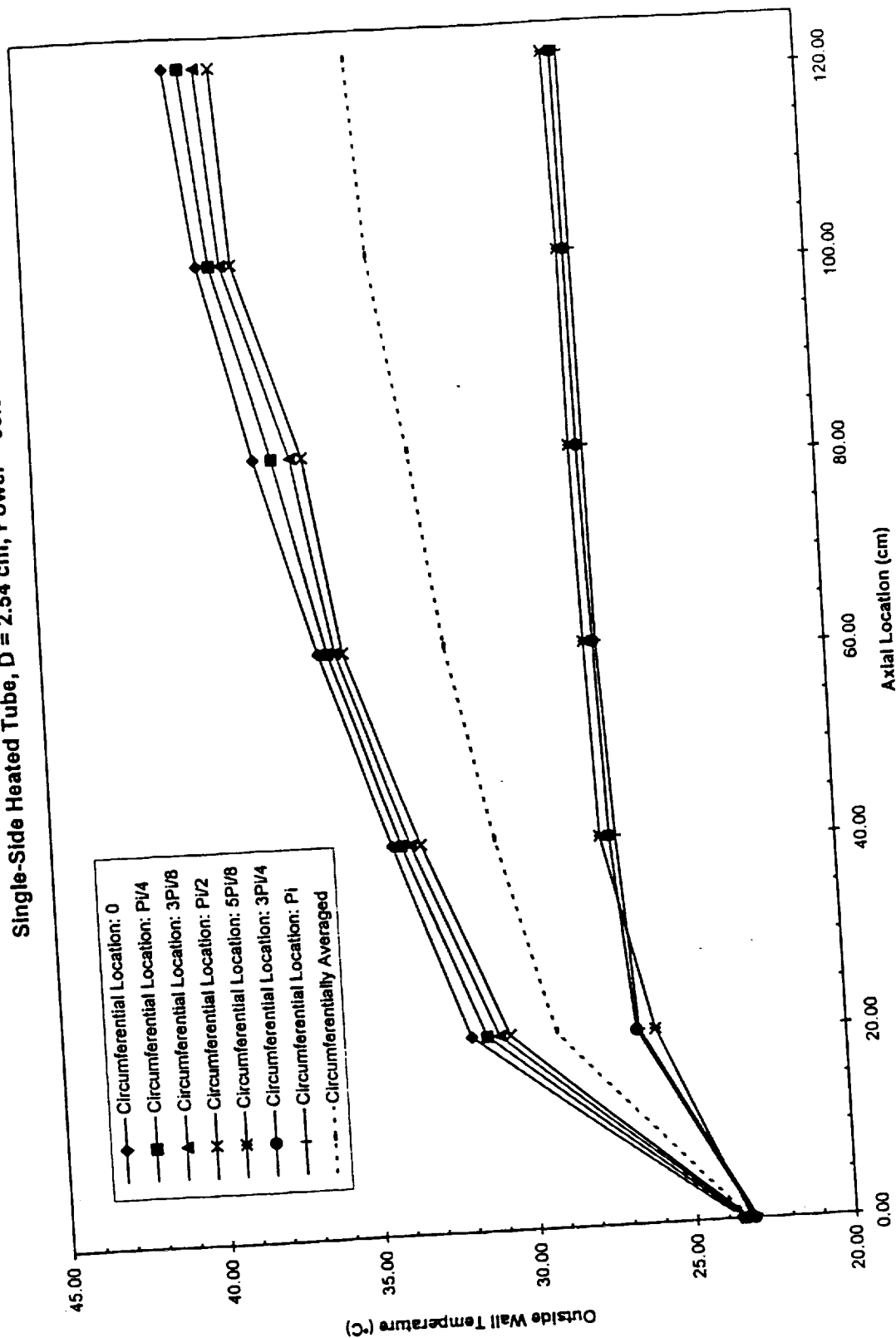


Figure 5a: Axial Distribution of the Wall Temperature for Seven Circumferential Locations for the Smooth Tube for the Net Power Generation of 93.5 Watts

$G = 210 \text{ kg/m}^2\text{s}$, Inlet Temp = 22.6°C
 Single-Side Heated Tube, $D = 2.54 \text{ cm}$; Power = 212.7 Watts

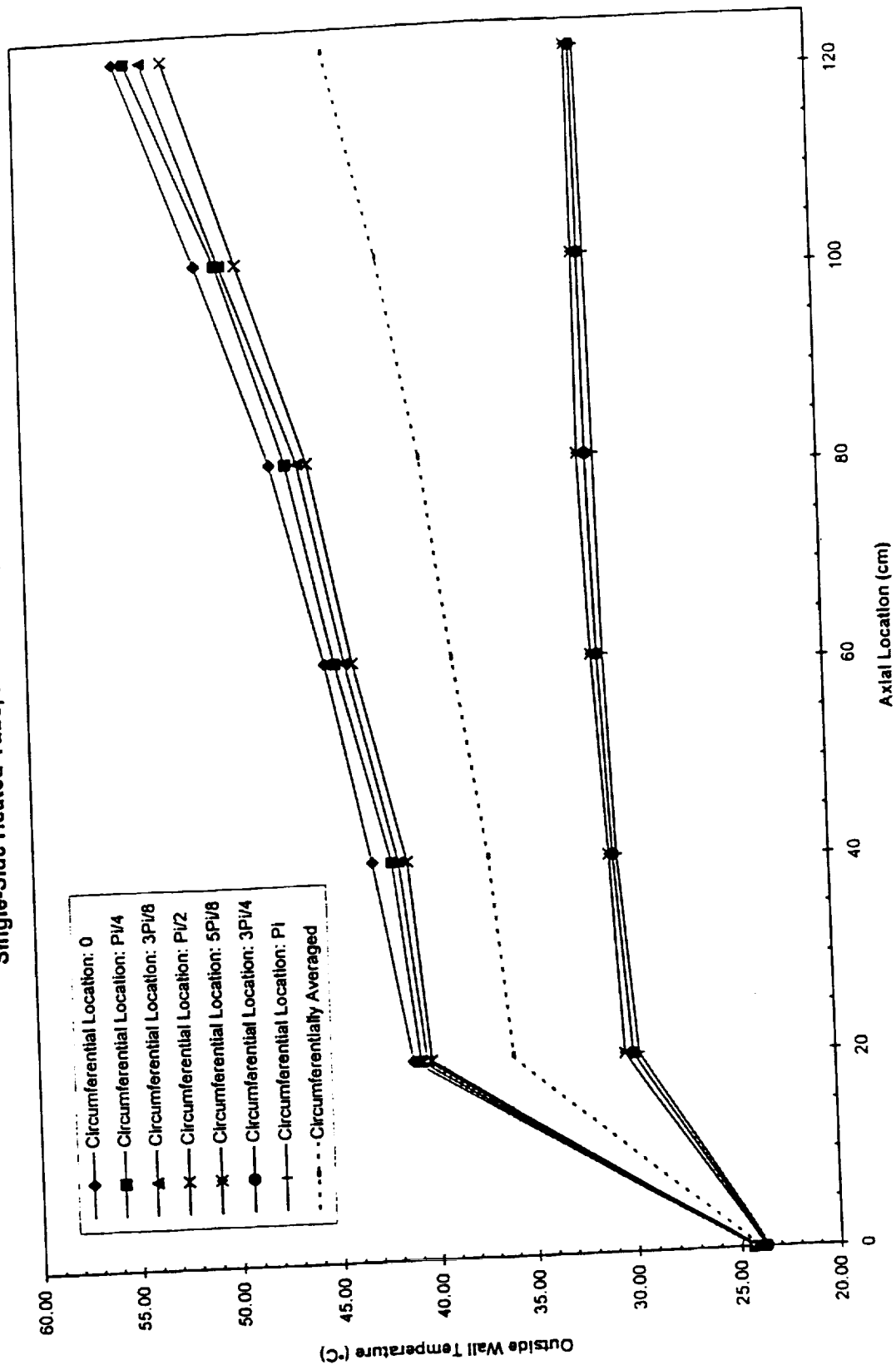
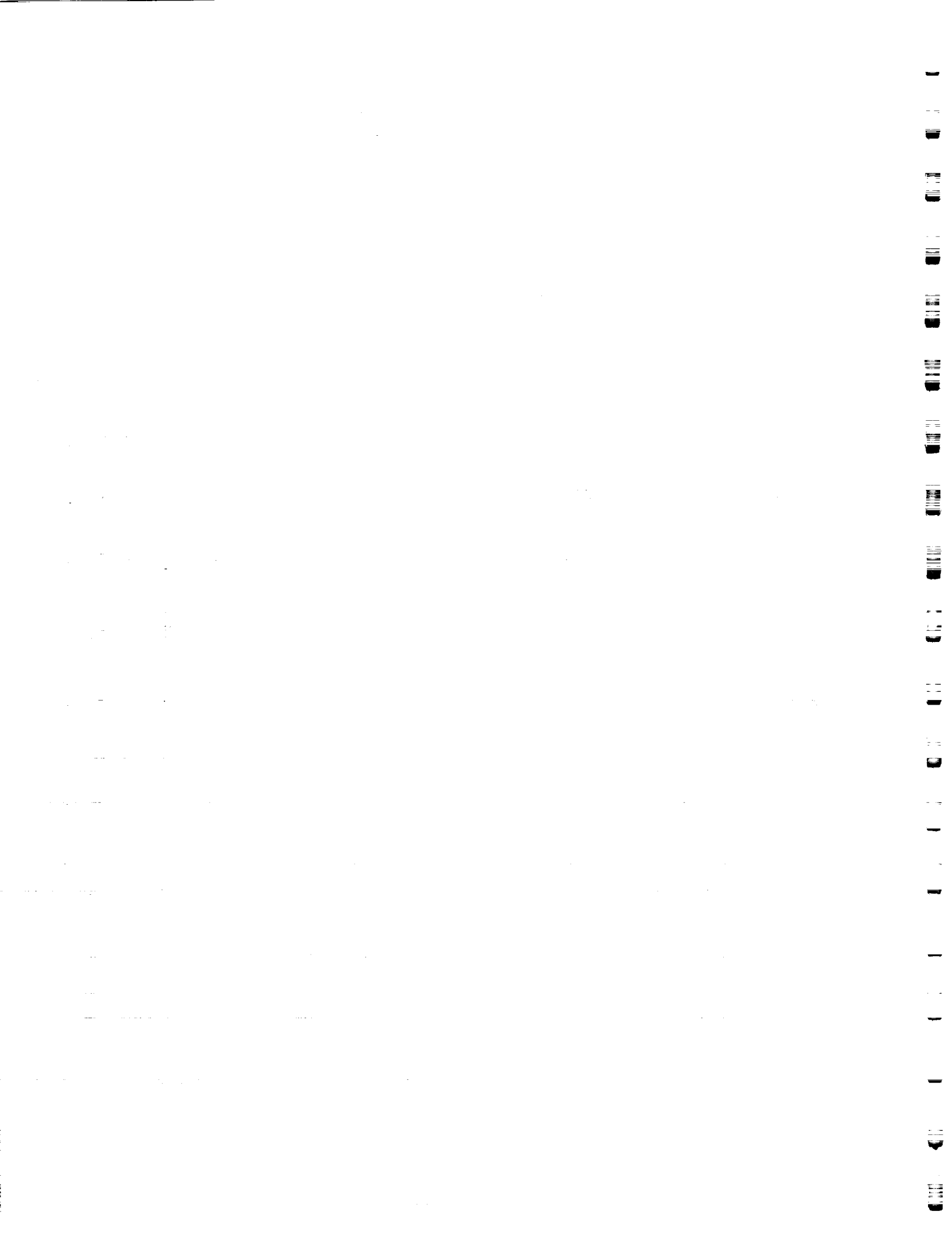


Figure 5b: Axial Distribution of the Wall Temperature for Seven Circumferential Locations for the Smooth Tube for the Net Power Generation of 212.7 Watts



Single-Side Heated Tube, $D = 25.4$ mm, Inlet Temp = 22.6°C , $\phi = 67.5$ Degrees

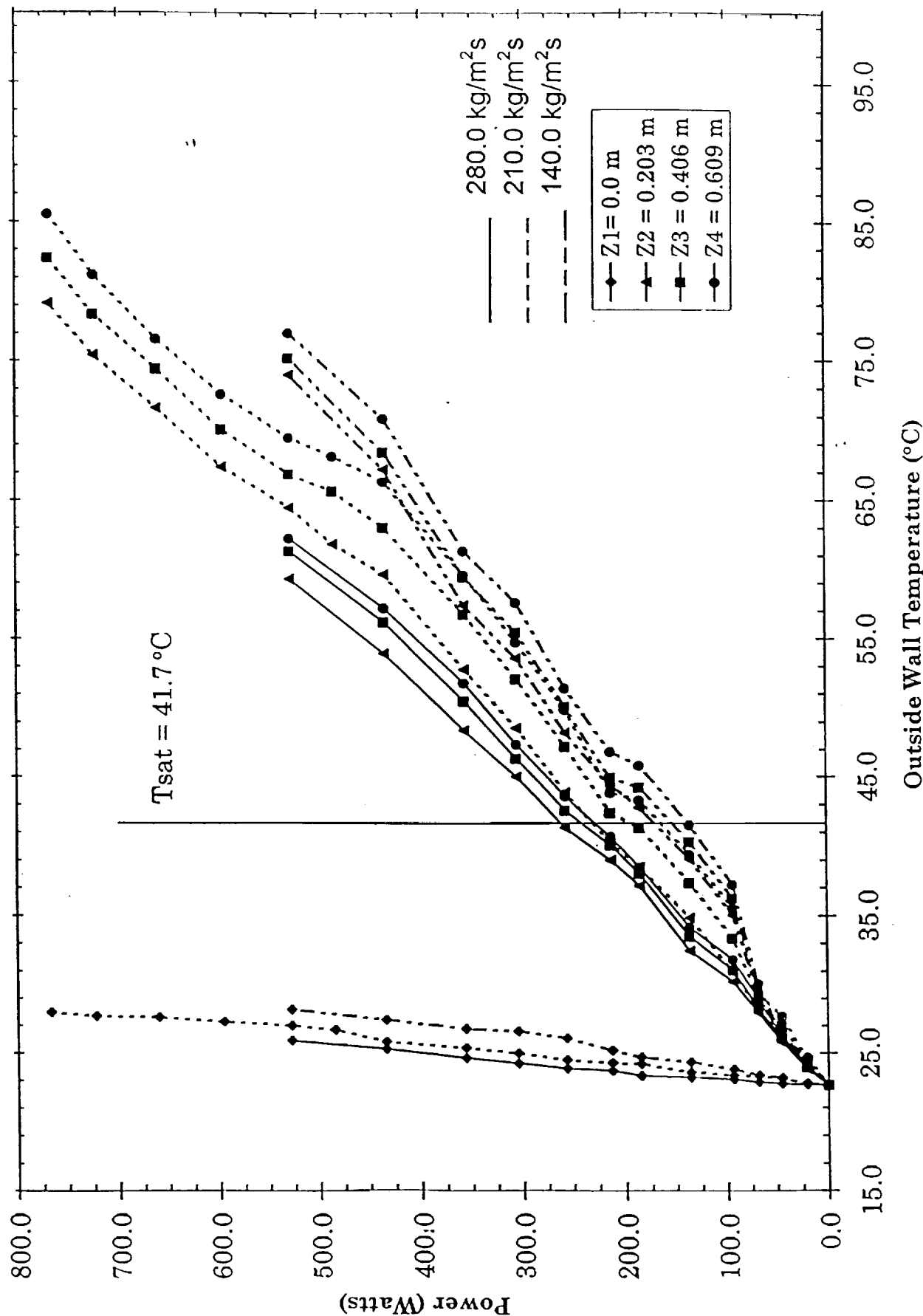


Figure 6a: Measured Outside Wall Temperature (Copper Channel) Axial Distribution as a Function of Net Power Generation for a Single-Side Heated, Smooth Channel for Different Mass Velocities.

Single-Side Heated Tube, $D = 25.4$ mm, Inlet Temp = 22.6°C , $\phi = 67.5$ Degrees

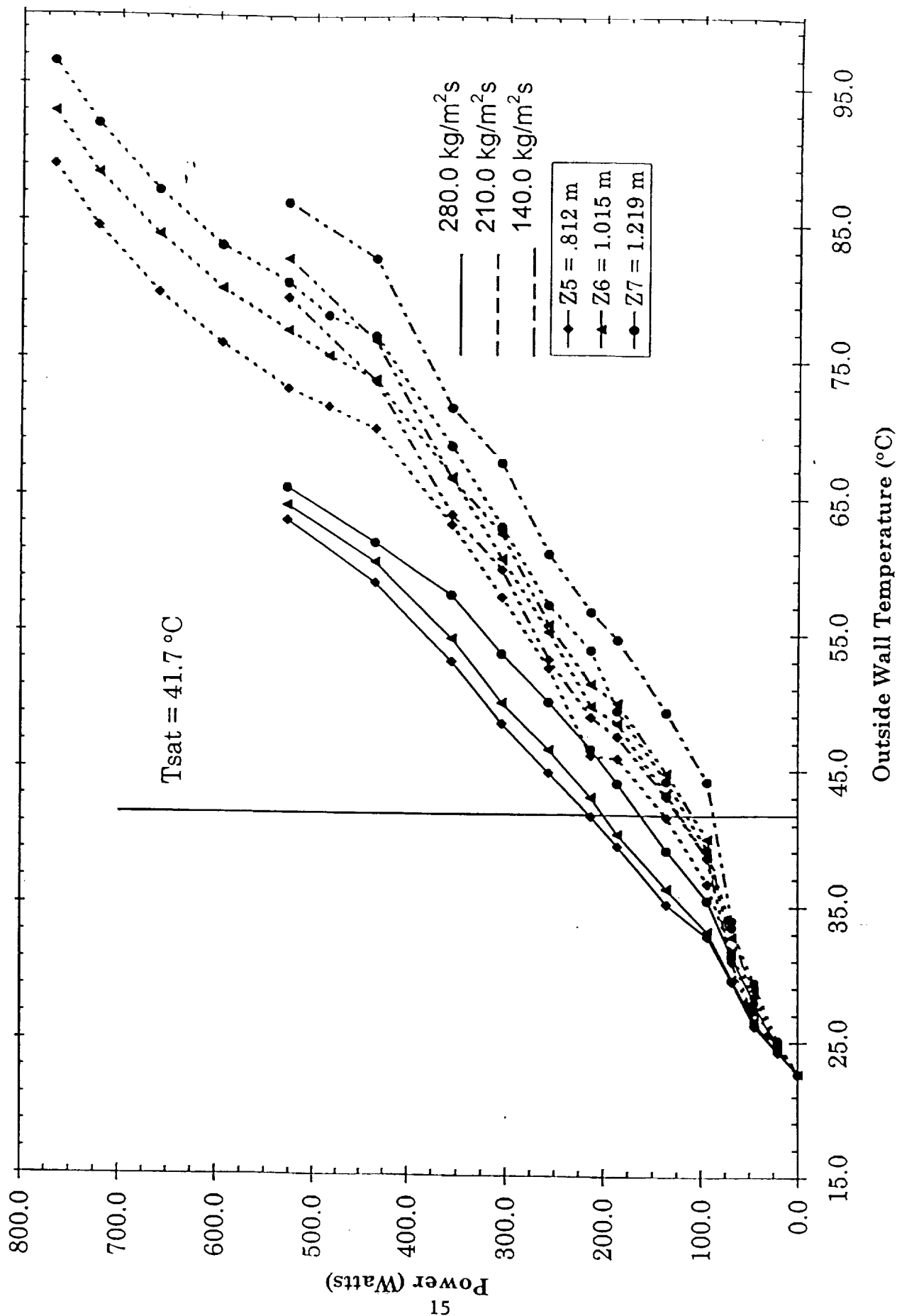
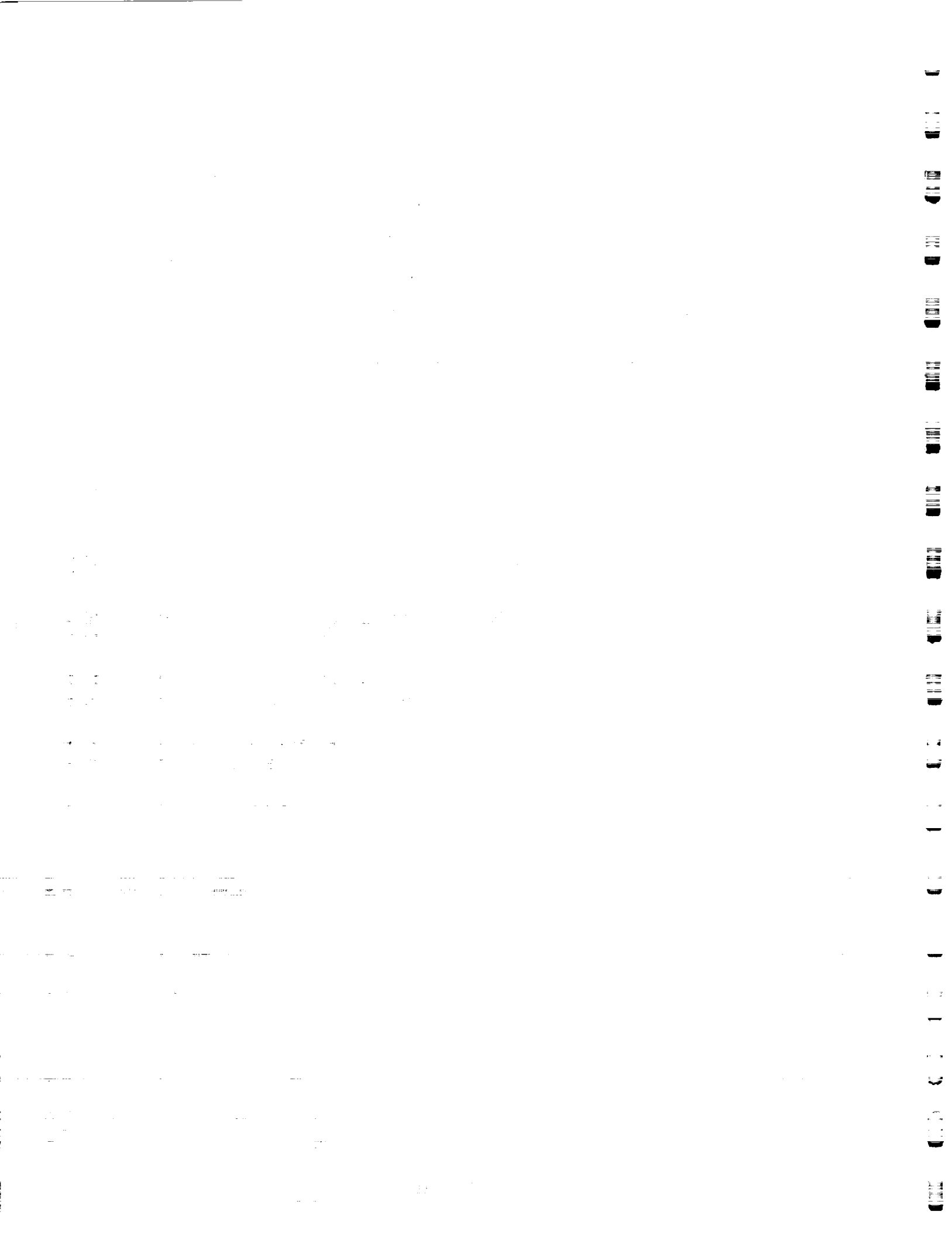


Figure 6b: Measured Outside Wall Temperature (Copper Channel) Axial Distribution as a Function of Net Power Generation for a Single-Side Heated, Smooth Channel for Different Mass Velocities.



Single-Side Heated Tube, $D = 25.4$ mm, Inlet Temp = 22.6°C , $\phi = 90.0$ Degrees

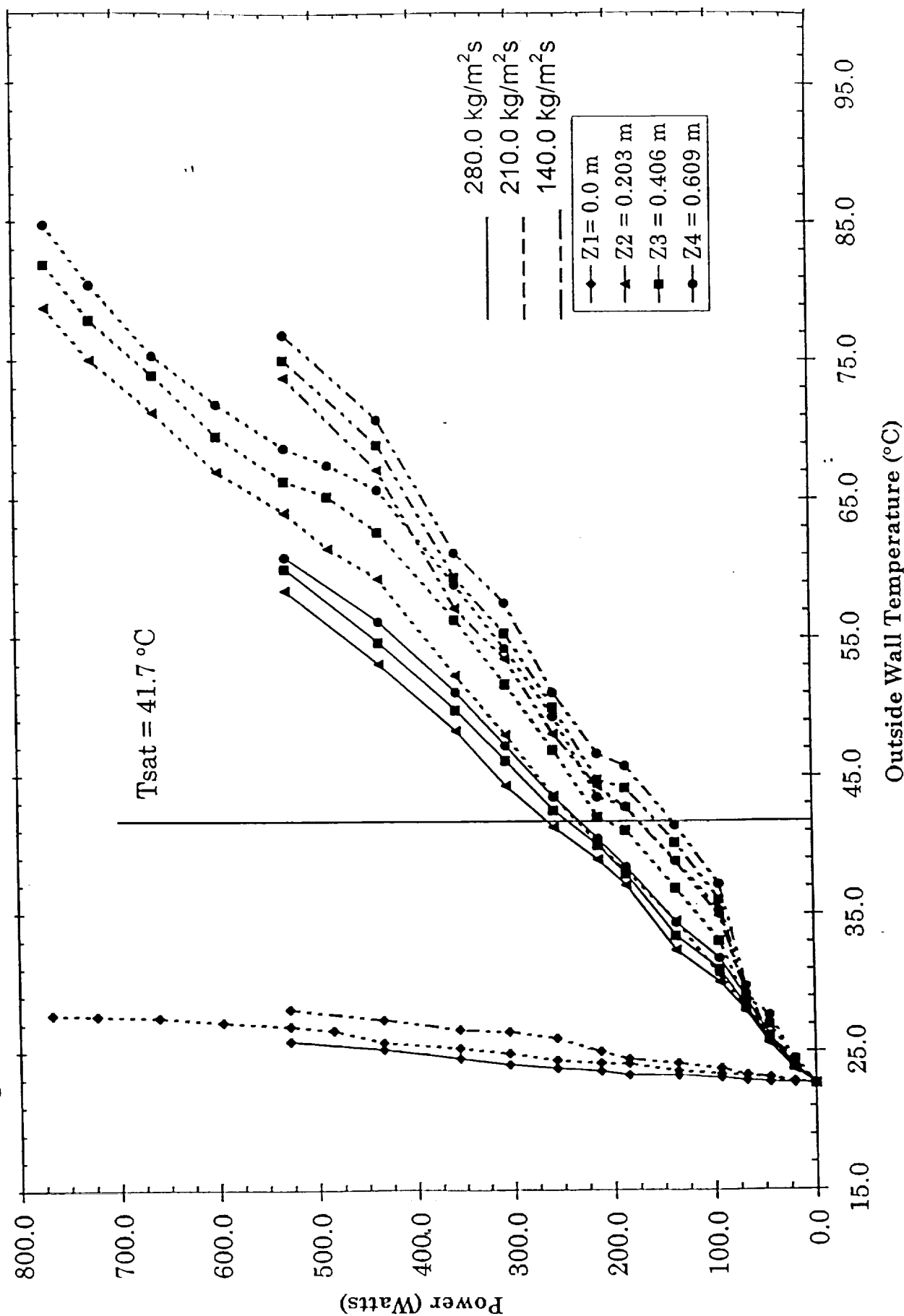


Figure 7a: Measured Outside Wall Temperature (Copper Channel) Axial Distribution as a Function of the Net Power Generation for a Single-Side Heated, Smooth Channel for Different Mass Velocities.

Single-Side Heated Tube, $D = 25.4$ mm, Inlet Temp = 22.6°C , $\phi = 90.0$ Degrees

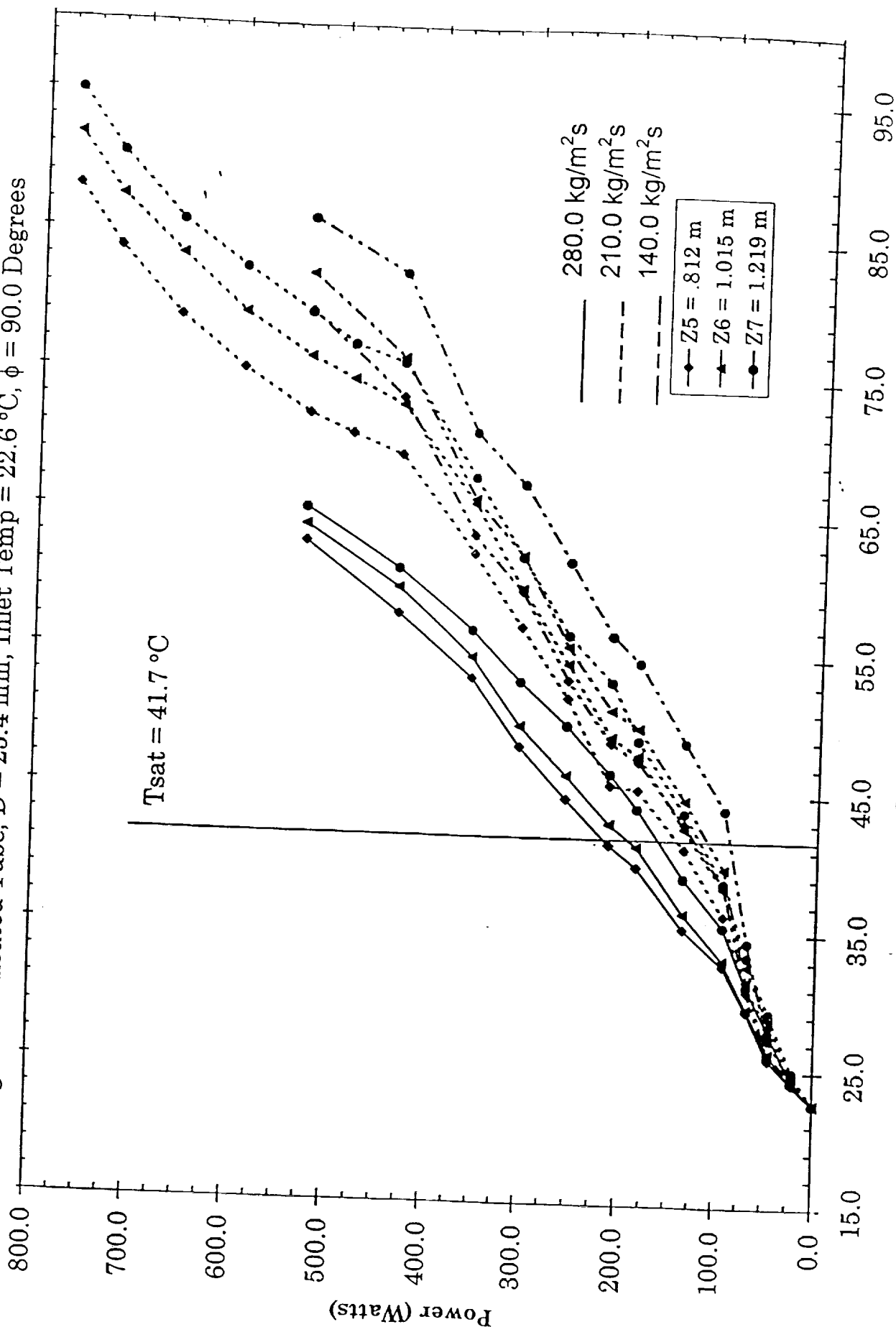
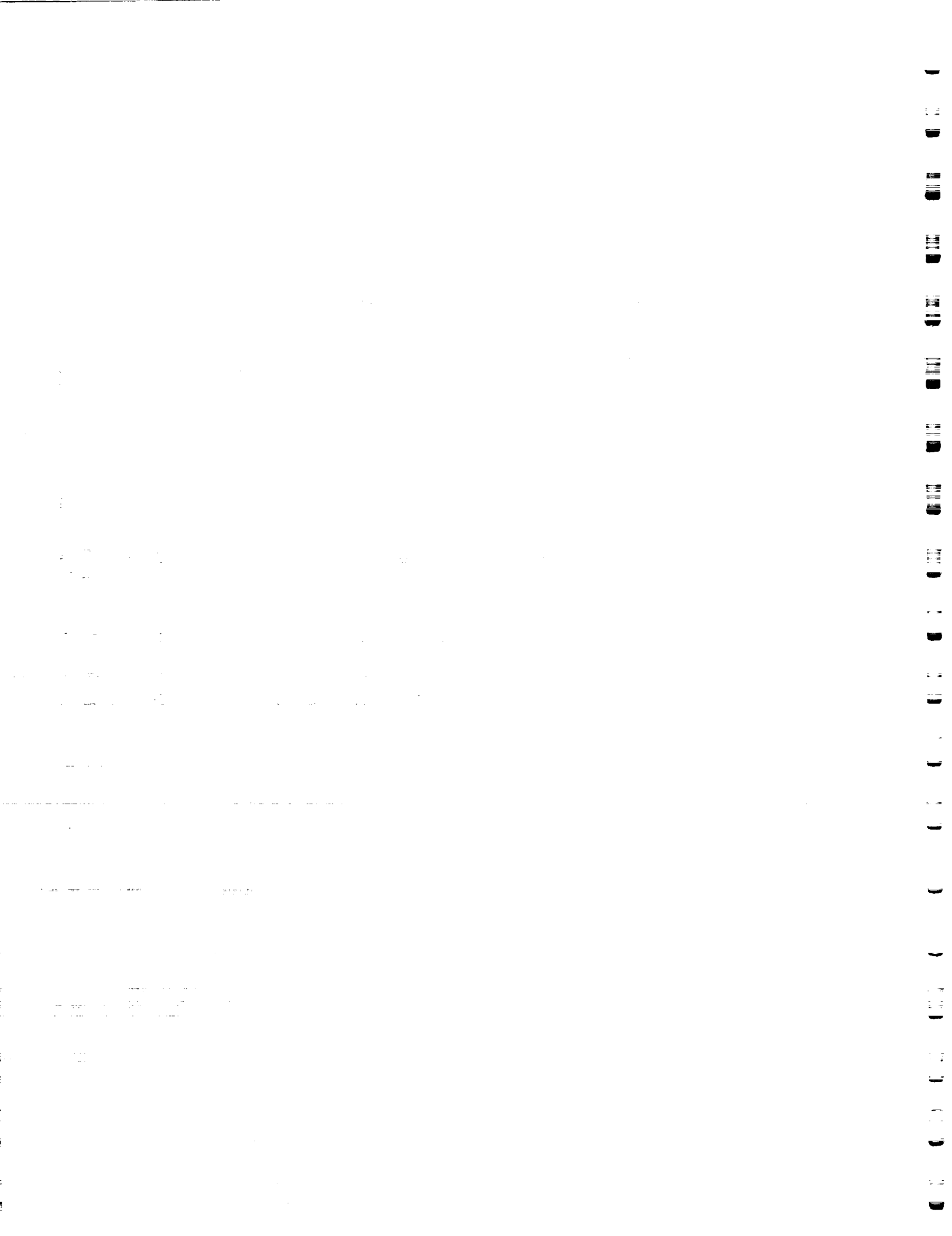
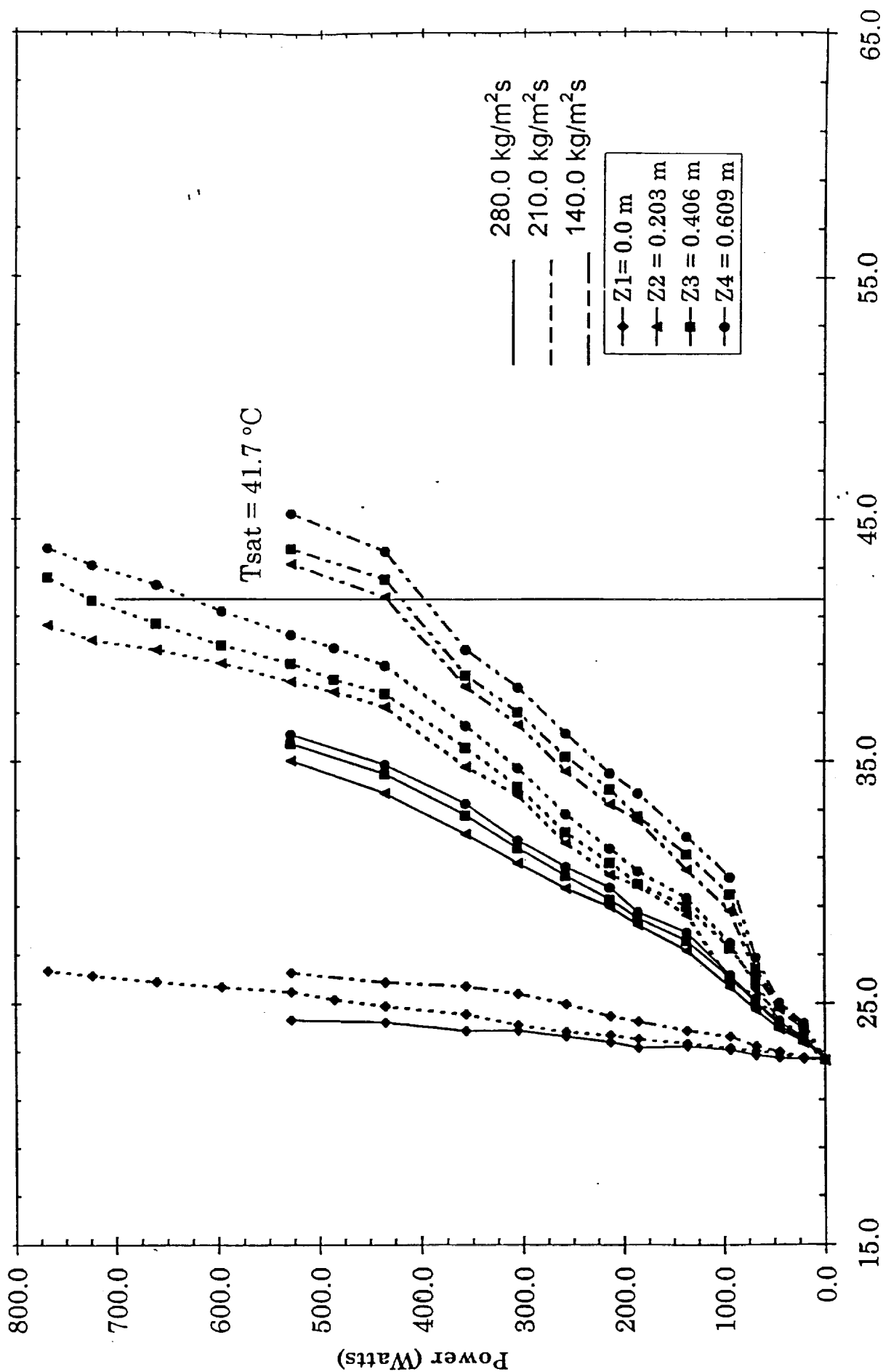


Figure 7b: Measured Outside Wall Temperature (Copper Channel) Axial Distribution as a Function of the Net Power Generation for a Single-Side Heated.

Smooth Channel for Different Mass Velocities.

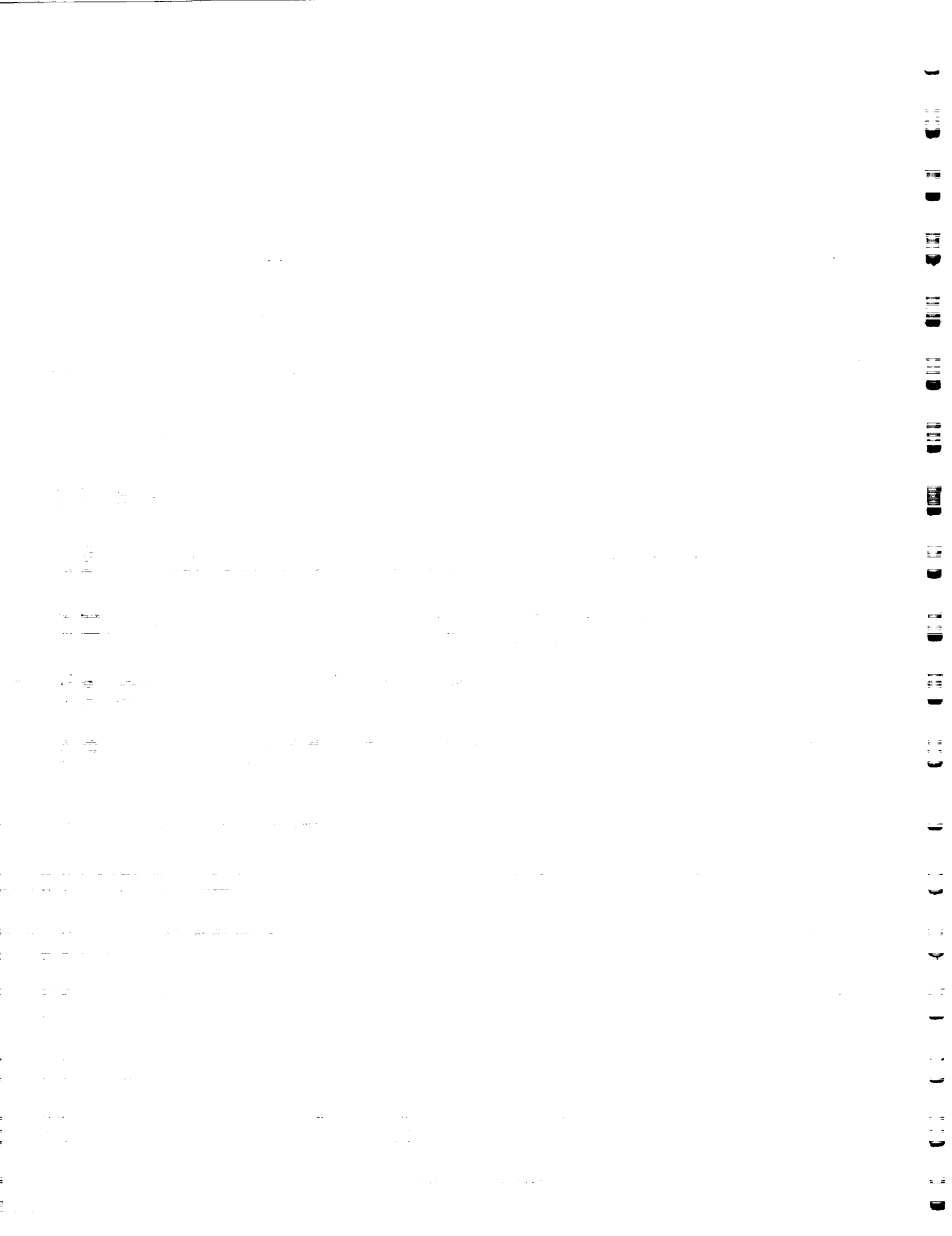


Single-Side Heated Tube, $D = 25.4$ mm, Inlet Temp = 22.6°C , $\phi = 112.5$ Degrees



Outside Wall Temperature ($^\circ\text{C}$)

Figure 8a: Measured Outside Wall Temperature (Copper Channel) Axial Variation as a Function of the Net Power Generation for a Single-Side Heated Smooth Channel for Different Mass Velocities.



Single-Side Heated Tube, $D = 25.4$ mm, Inlet Temp = 22.6°C , $\phi = 112.5$ Degrees

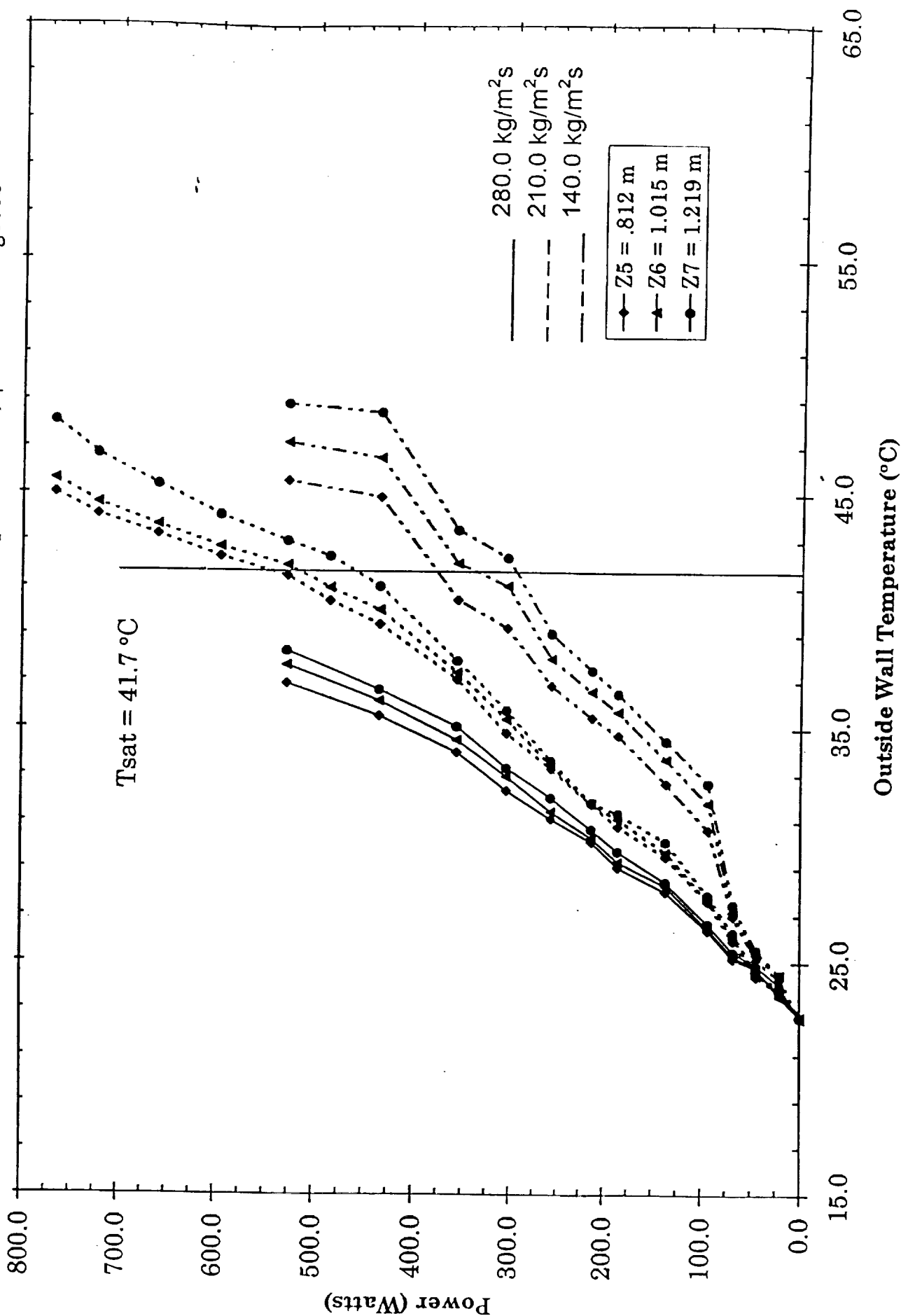
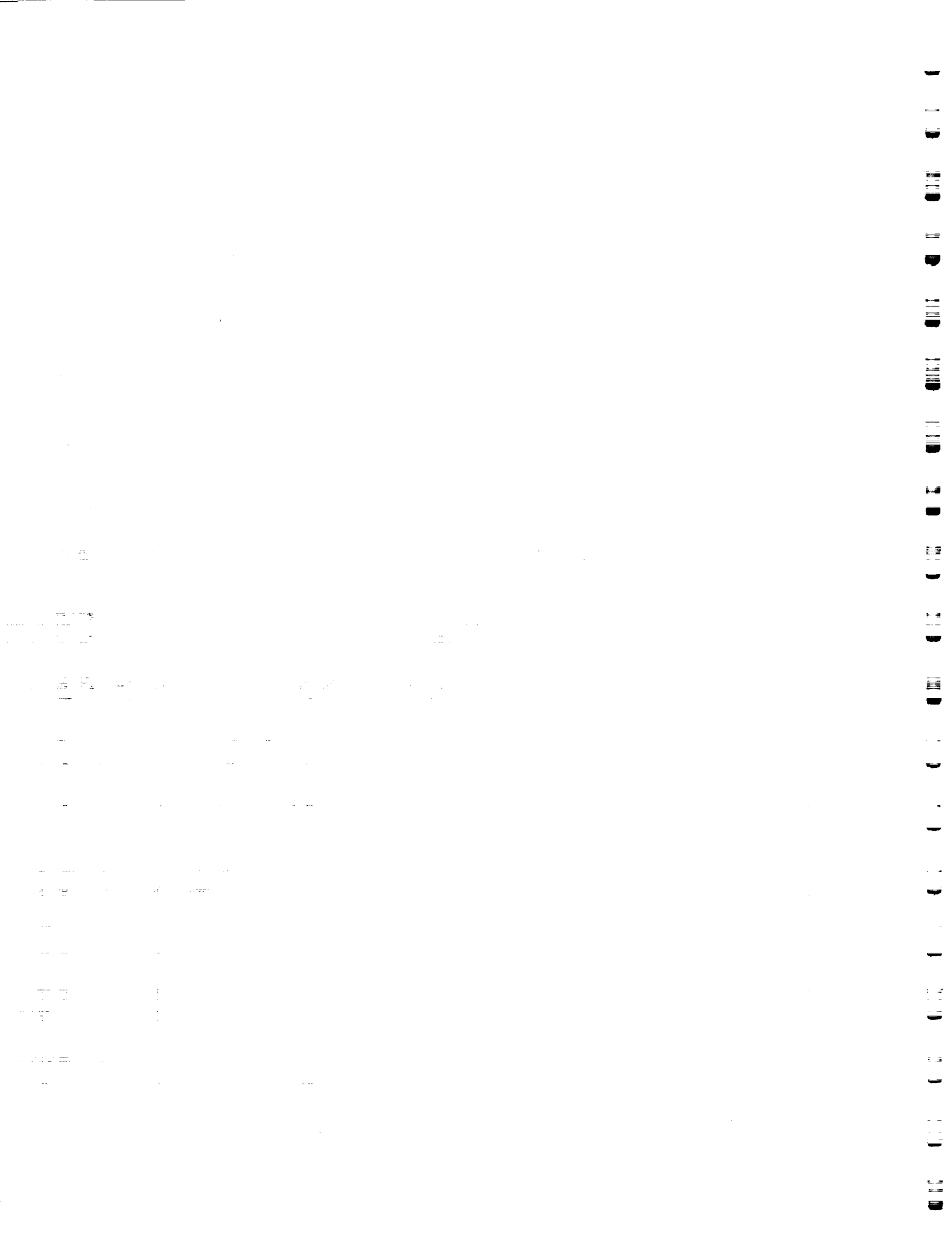


Figure 8b: Measured Outside Wall Temperature (Copper Channel) Axial Variation as a Function of the Net Power Generation for a Single-Side Heated Smooth Channel for Different Mass Velocities.



Single-Side Heated Tube, $D = 25.4$ mm, Inlet Temp = 22.6°C , $\phi = 135.0$ Degrees

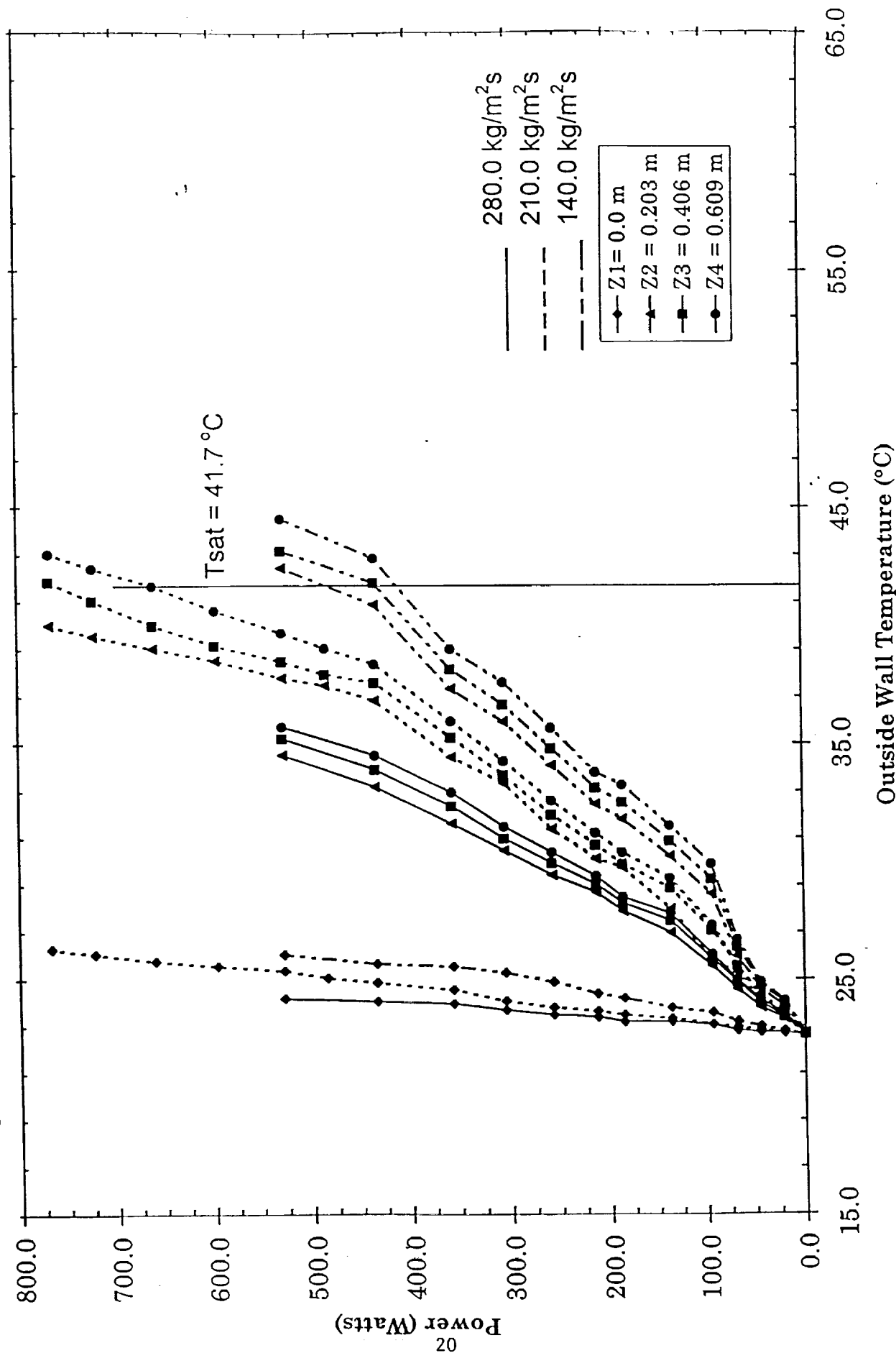
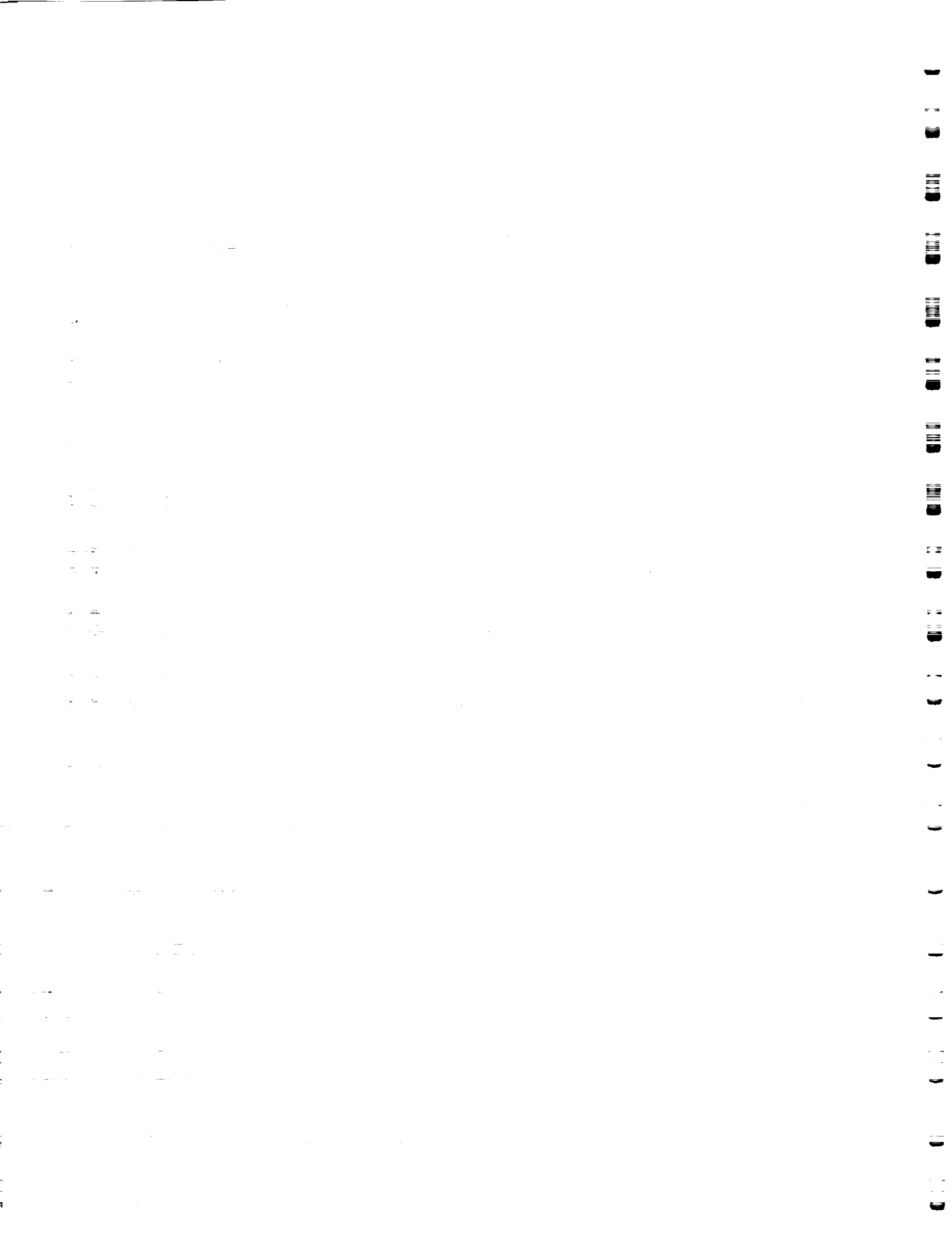


Figure 9a: Measured Outside Wall Temperature (Copper Channel) Axial Variation as a Function of the Net Power Generation for a Single-Side Heated Smooth Channel for Different Mass Velocities.



Single-Side Heated Tube, $D = 25.4$ mm, Inlet Temp = 22.6°C , $\phi = 135.0$ Degrees

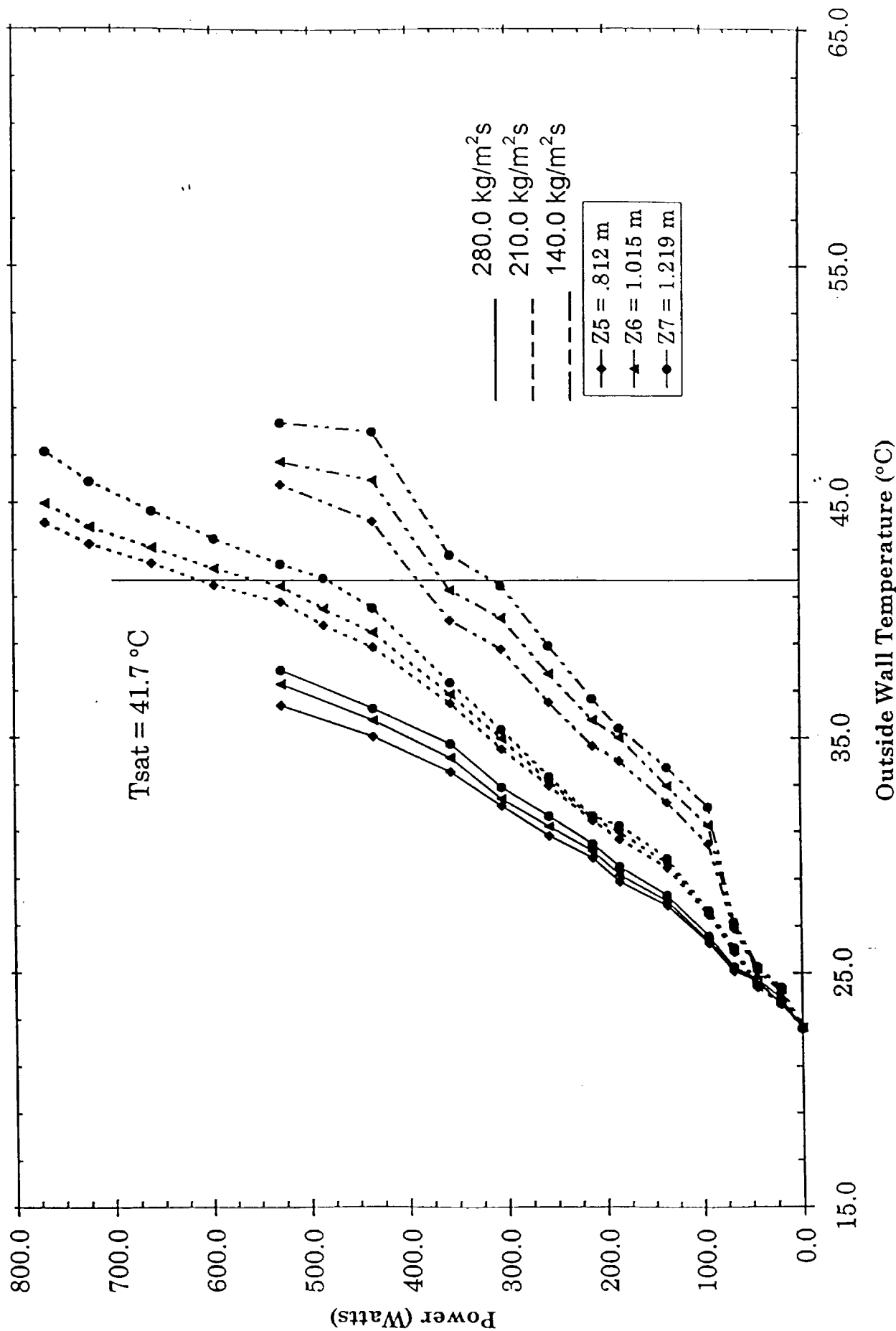


Figure 9b: Measured Outside Wall Temperature (Copper Channel) Axial Variation as a Function of the Net Power Generation for a Single-Side Heated Smooth Channel for Different Mass Velocities.

Single-Side Heated Tube, $D = 25.4$ mm, Inlet Temp = 22.6°C , $\phi = 180.0$ Degrees

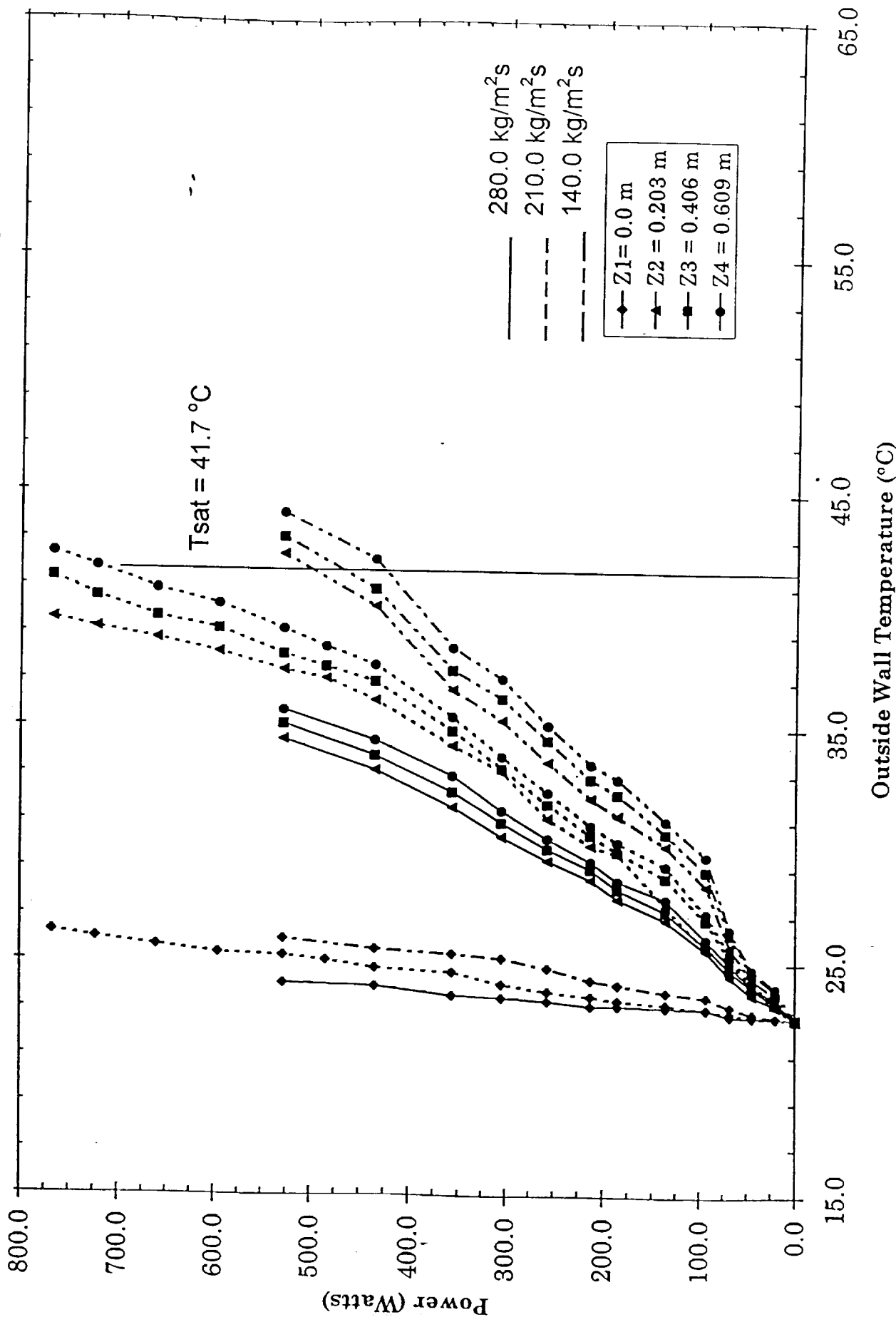


Figure 10a: Measured Outside Wall Temperature (Copper Channel) Axial Variation as a Function of the Net Power Generation for a Single-Side Heated Smooth Channel for Different Mass Velocities.

1. The first part of the document is a list of the names of the persons who have been appointed to the various positions of the Board of Directors of the Corporation.

2. The second part of the document is a list of the names of the persons who have been appointed to the various positions of the Board of Directors of the Corporation.

3. The third part of the document is a list of the names of the persons who have been appointed to the various positions of the Board of Directors of the Corporation.

4. The fourth part of the document is a list of the names of the persons who have been appointed to the various positions of the Board of Directors of the Corporation.

5. The fifth part of the document is a list of the names of the persons who have been appointed to the various positions of the Board of Directors of the Corporation.

6. The sixth part of the document is a list of the names of the persons who have been appointed to the various positions of the Board of Directors of the Corporation.

7. The seventh part of the document is a list of the names of the persons who have been appointed to the various positions of the Board of Directors of the Corporation.

8. The eighth part of the document is a list of the names of the persons who have been appointed to the various positions of the Board of Directors of the Corporation.

9. The ninth part of the document is a list of the names of the persons who have been appointed to the various positions of the Board of Directors of the Corporation.

10. The tenth part of the document is a list of the names of the persons who have been appointed to the various positions of the Board of Directors of the Corporation.

11. The eleventh part of the document is a list of the names of the persons who have been appointed to the various positions of the Board of Directors of the Corporation.

12. The twelfth part of the document is a list of the names of the persons who have been appointed to the various positions of the Board of Directors of the Corporation.

13. The thirteenth part of the document is a list of the names of the persons who have been appointed to the various positions of the Board of Directors of the Corporation.

14.

15.

Single-Side Heated Tube, $D = 25.4$ mm, Inlet Temp = 22.6°C , $\phi = 180.0$ Degrees

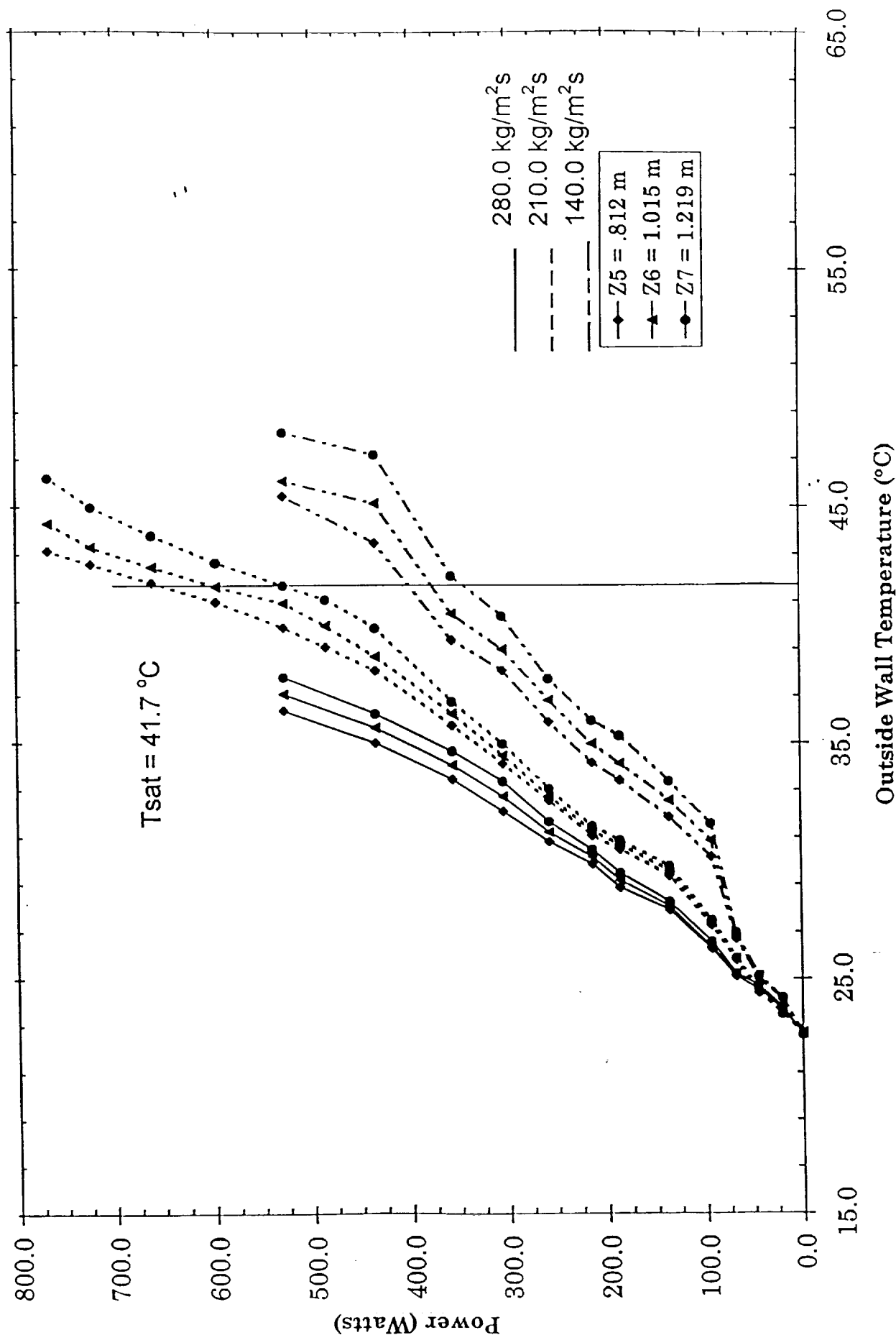


Figure 10b: Measured Outside Wall Temperature (Copper Channel) Axial Variation as a Function of the Net Power Generation for a Single-Side Heated Smooth Channel for Different Mass Velocities.

test section. Furthermore as ϕ varied from 0 to π , the temperature decreased circumferentially because of a change from a circumferentially heated region ($\phi = 0$ to $\pi/2$) to a non-heated one ($\phi = 5\pi/8$ to π) for all the flow rates. This change in temperature can be observed clearly in Figures 10 through 16.

It is desired to present the local 2-D wall temperature profile with respect to the net power generation for all forty-nine axial and circumferential locations for three different levels of mass velocity. In order to facilitate this, Figures 4 through 10 contain the profiles for $\phi = 0$ to 180.0 degrees, where Figures a and b (e.g., 4a and 4b) in this figure series contain profiles for different axial locations. Figures 4a, 5a, 6a, etc. each contain profiles for axial location Z_1 , Z_2 , Z_3 , and Z_4 . Finally, Figures 4b, 5b, 6b, etc. each contain profiles for axial locations Z_5 , Z_6 , and Z_7 .

From these figures, it can be seen that the wall temperature distributions are closely spaced for $\phi = 0$ to $\pi/2$ and $\phi = 5\pi/8$ to π . This is to be expected because of single-side heating. From the plots, one can also observe that the wall temperature at $\phi = 0$ remains above the saturation temperature ($T_{sat} = 41.65^\circ\text{C}$) and the wall temperatures at $\phi = 5\pi/8$, $3\pi/4$, and π were consistently below T_{sat} for all the mass velocities except at the highest power levels.

Although the data analysis is continuing, preliminary computations using the Davis-Anderson correlation (Davis and Anderson, [16]) indicate that the onset to nucleate boiling occurs at a wall temperature of 45.7°C , 44.1°C , and 42.45°C for mass velocities of 280, 210, and $140 \text{ kg/m}^2\text{s}$, respectively. For the computations, all Freon-11 properties were evaluated at the saturation temperature using Perry's handbook [17]. Using these computations as a basis and the basic characteristics of the boiling curve, both axial and circumferential influences on the quasi-boiling curve are displayed in Figure 4 through 10. Figure 4 ($\phi = 0.0$ degrees) through Figure 7 ($\phi = 90.0$ degrees) show that the onset of nucleate boiling (ONB) at $G = 210.0 \text{ kg/m}^2\text{s}$ does occur slightly above 41.7°C simultaneously over the heated section. For the conditions shown, this occurred at a power below 181.2 W simultaneously at all axial locations between locations #2 and #6. For $G = 280.0 \text{ kg/m}^2\text{s}$, ONB in a similar fashion occurred below 312.0 W. The onset to fully developed boiling (OFDB) for $G = 210.0 \text{ kg/m}^2\text{s}$ occurred simultaneously at all these locations at a power level of 181.2 W. Although further data reduction is needed to determine actual inside wall temperatures, it is clear from the figures that the boiling curve will shift to the right with higher values of Z . The data also show a slight increase in $[T_w]_{out}$ (outside wall temperature) in the circumferential direction from $\phi = 90.0$ degrees to 0.0 degrees. These data provide a quantitative record which shows the regions or patches where various simultaneous boiling phenomena



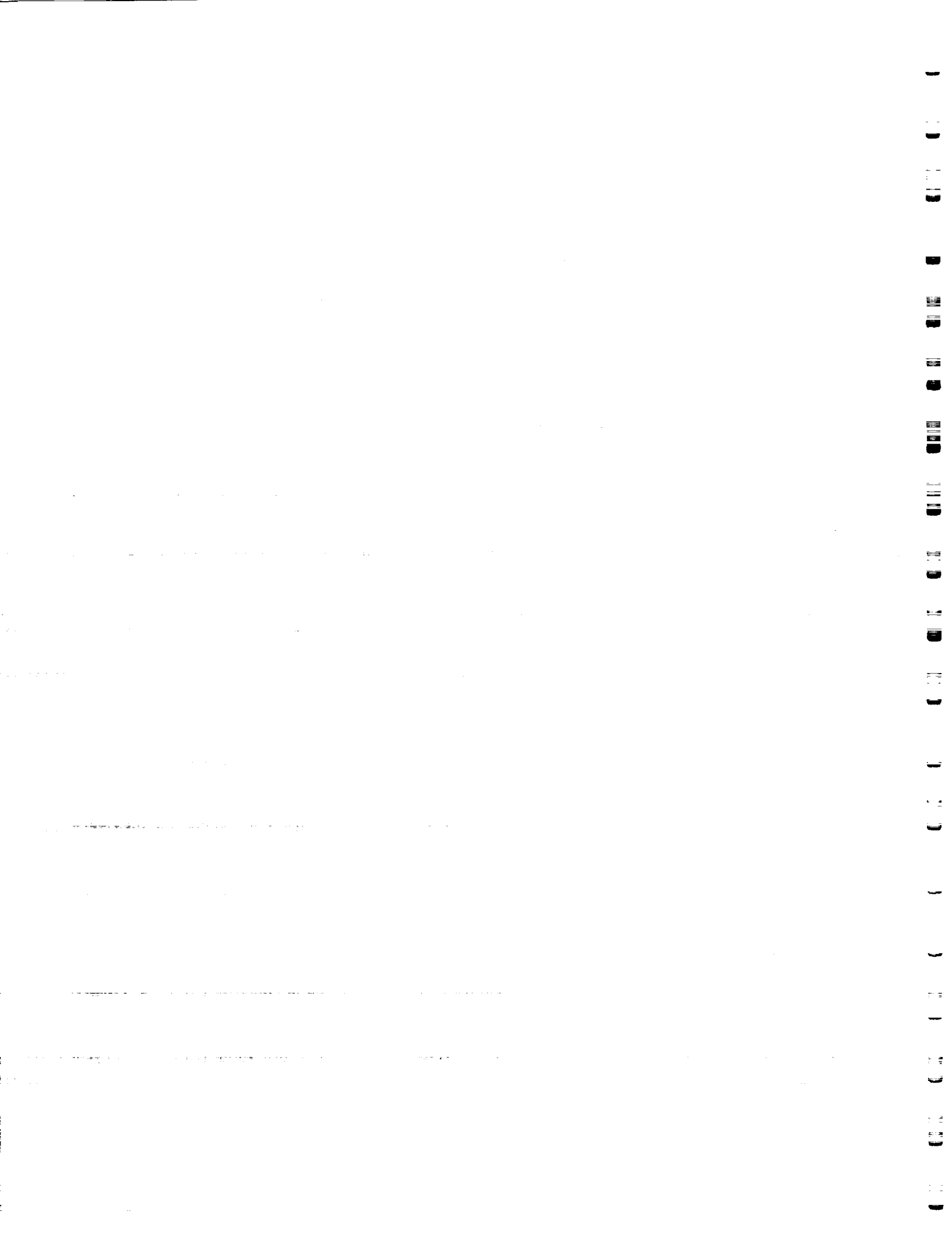
occurred. Even though the test section was made of highly conducting copper, the measured outside wall temperatures cannot be used directly to correlate ONB or CHF. However, these measurements are closely linked to the local variations of the inside wall temperature and hence are related to the local two-dimensional boiling heat transfer at the inside wall.

From the above discussion of wall temperature distributions, some additional characteristics of the curves become apparent. The critical heat flux occurred between $\phi = 0.0$ and 90.0 degrees at power levels above 212.7 W for 210.0 , and near 212.7 W for 140.0 kg/m²s. The data for 280.0 kg/m²s must be extended so that similar observations can be made.

Effect of Mass Velocity Variations

In this work, we have presented the complete wall temperature profile for three different mass velocities namely, 280.0 , 210.0 and 140.0 kg/m²s for the same tube of inside diameter of 24.5 mm. Figures 4 through 10 show the complete profile of the wall temperature for all the three mass velocities. From these plots, it is clear that there is significant effect of mass velocity on the wall temperature for this single-side heating configuration. From Figures 4 through 10, the effect of mass velocity at lower power levels on wall temperature and mode of heat transfer are not significant. However for higher power levels, increases in the mass velocity shift the quasi-boiling curve to the left with a corresponding increase in slope in both the heated and unheated regions.

Figures 4 through 10 show also a clear change in the shape of the boiling curve with respect to both mass velocity and circumferential orientation. For ϕ less than or equal to 90.0 degrees, increasing the mass velocity by identical increments from 140.0 kg/m²s to 210.0 kg/m²s and from 210.0 kg/m²s to 280.0 kg/m²s results in greater heat transfer enhancement for the latter range. Further, these figures show that for moderate power levels the flow structure results in the boiling curves for the former range almost overlaying one another. However, the boiling curves for latter or higher mass velocity range are completely separated one from another. At the higher mass velocities and for $\phi < 90.0$ degrees, the slope of the boiling curves increases and later decreases as ϕ increases. This emphasizes the three dimensional nature of the flow, and in particular the circumferential dependence due to single-side heating. Finally, the circumferential propagation of the boiling front can be seen by comparing Figures 4 through 7 with Figures 8 through 10 for $G = 140.0$ kg/m²s. At lower values of ϕ , ONB occurs below 181.0 W; however for larger ϕ , ONB occurs near 420.0 W. So as ϕ increases from 90.0 degrees, the stratified nature of the

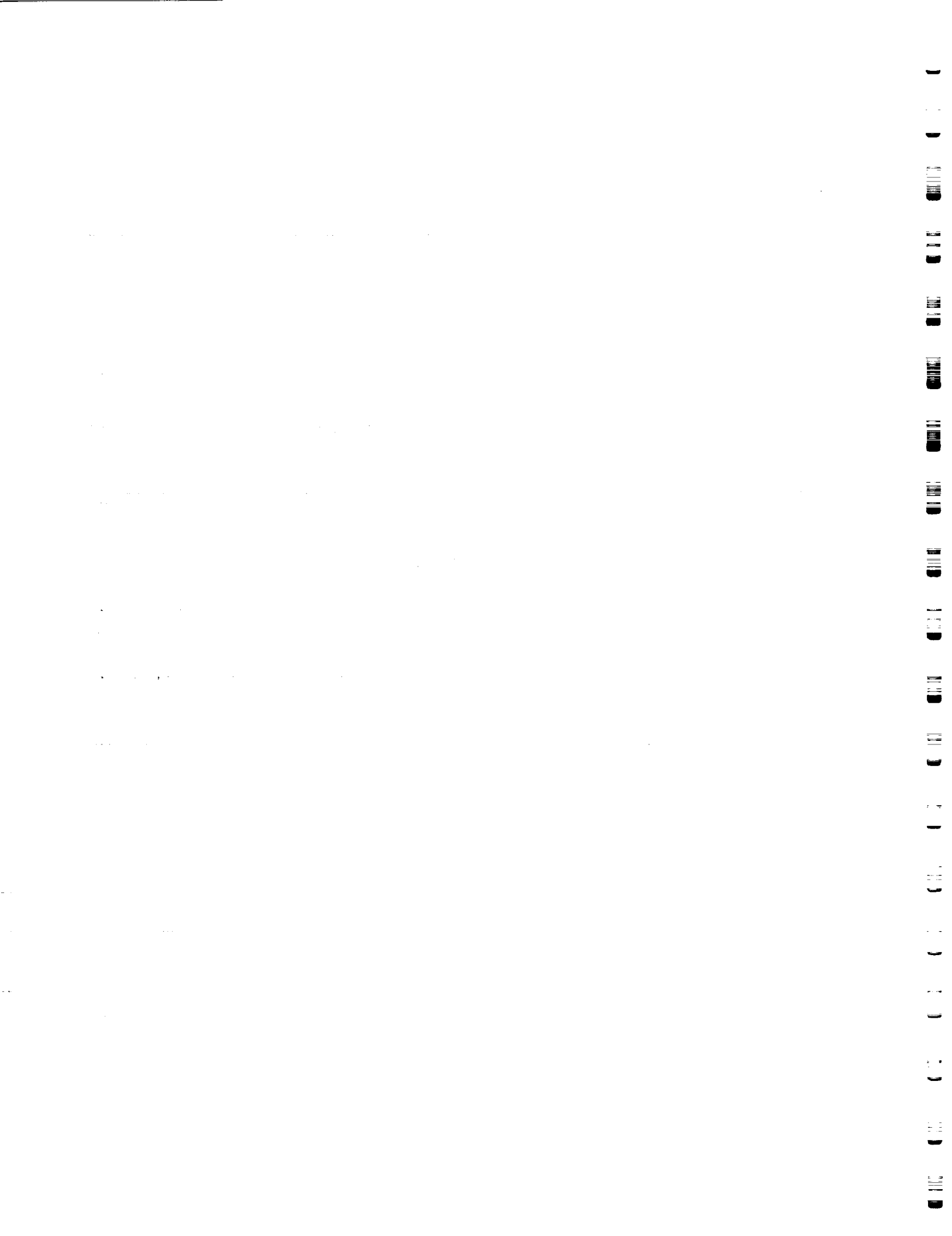


flow is obvious at all axial locations and all mass velocities for this downward vertical flow in a single-side heated channel.

In section 4, the axial distribution of the circumferentially averaged heat transfer coefficient using the thermal hydraulic approach (Boyd et al. [4]) for different diameters and different mass flow rates. Further work is needed to obtain the local (axial and circumferential) heat transfer coefficient using a non-linear inverse conduction approach (Huque and Boyd [18]).

1.5 SUMMARY

Two-dimensional wall temperature measurements were presented for the forced convection boiling of Freon-11 in a single-side heated vertical channel with downward flow for a mass flow rate of 280.0, 210.0, and 140.0 kg/m²s. Experimental data was obtained for circumferential and axial wall temperature distributions. The measurements show that the boiling curve changes significantly at higher mass velocities and with respect to both circumferential and axial coordinates. Due to circumferential transport, the slope of the boiling curve changes in a non-monotonic fashion as ϕ increases.



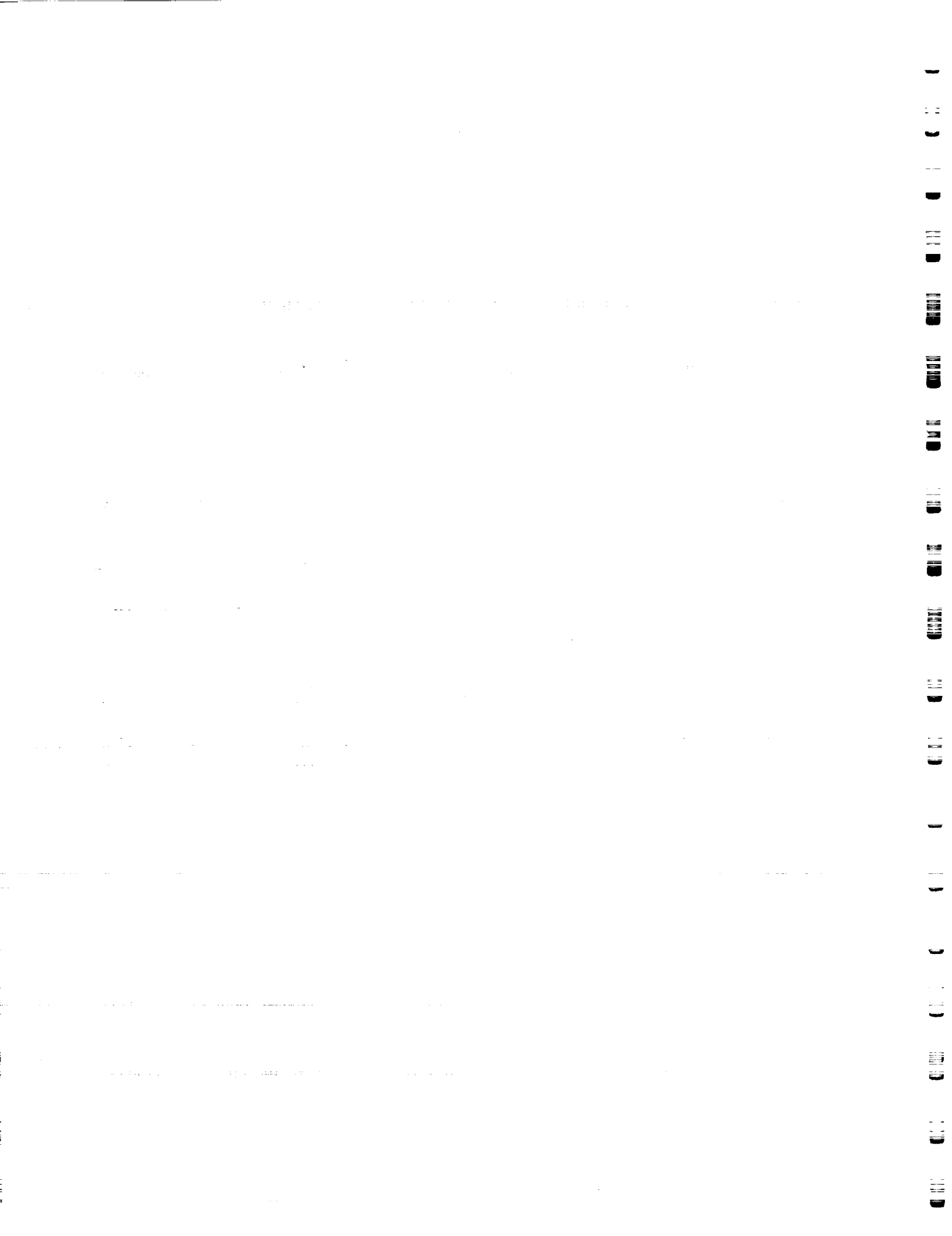
2.0 FORCED CONVECTION AND FLOW BOILING IN A SINGLE-SIDE HEATED VERTICAL SMOOTH CHANNEL WITH DOWNWARD FLOW

2.1 INTRODUCTION AND OBJECTIVES

Near and long term missions of the National Aeronautics and Space Administration (NASA), including Space Station Freedom and contemplated missions to the Moon and to Mars, will require the use of advanced thermal control concepts to efficiently transport large amount waste heat over long distances (Miller et al., [1]). These missions will require an active thermal control system to provide moderate temperature heat rejection for different system modules. It is essential that the thermal rejection system selected be able to operate under a variety of complex and non-uniform heat flux distributions. Other requirements for the selected system include minimum overall system mass, and pumping power (Ungar et al., [2]). The high heat flux potential and low mass requirement of the two-phase thermal control system makes them an attractive option for advanced space applications.

Before a two-phase thermal control system can be implemented in the space project, there are several phenomena that must be clearly understood. Among the many important aspects of two-phase thermal control and transfer systems meeting further study are the two-phase pressure drops and the two-dimensional (2-D) heat transfer coefficient distributions in smooth and enhanced tubes for various gravity levels including normal earth gravity, zero gravity, lunar gravity, and Martian gravity (Reinarts et al. [3], and Ungar et al., [2]). For the case of normal earth gravity, this study investigates 2-D wall temperature variations, and mean heat transfer coefficient variations as a function of applied power. Other gravity conditions will be considered in future studies.

Recently, increased emphasis has been placed on understanding the pressure drop in two-phase flows in earth, low gravity lunar, and Martian environments. Ungar et al. [2] and Reinarts et al. [3] studied the pressure drop and flow profiles for lunar-g and Martian-g two-phase flow. They have developed an extensive data base for these two reduced gravities and have recommended correlation's for two-phase pressure drop under these conditions. Miller et al. [1] reviewed many two-phase frictional pressure drop prediction methods for smooth tubes under normal and microgravity conditions. For qualities greater than 0.05, they recommended



Troniewski and Ulbrich's correlation. However for qualities less than 0.50, the Lockhart-Martinelli/Chisholm correlation was recommended.

Another important aspect of two-phase thermal control system is the development and understanding of fundamental characteristics of flow boiling heat transfer at different gravity levels. In particular, optimization of the heat transfer, with accompanying reduced mass and pumping power requirements, will require a knowledge of the two-dimensional heat transfer coefficient distributions in advanced and commercial space systems (Boyd et al., [4]). Implementation of two-phase thermal control system will also require additional emphasis on flow boiling phenomenon as it pertains to non-uniform heat flux distribution, resulting heat transfer coefficients, flow channel aspect ratio, and orientation.

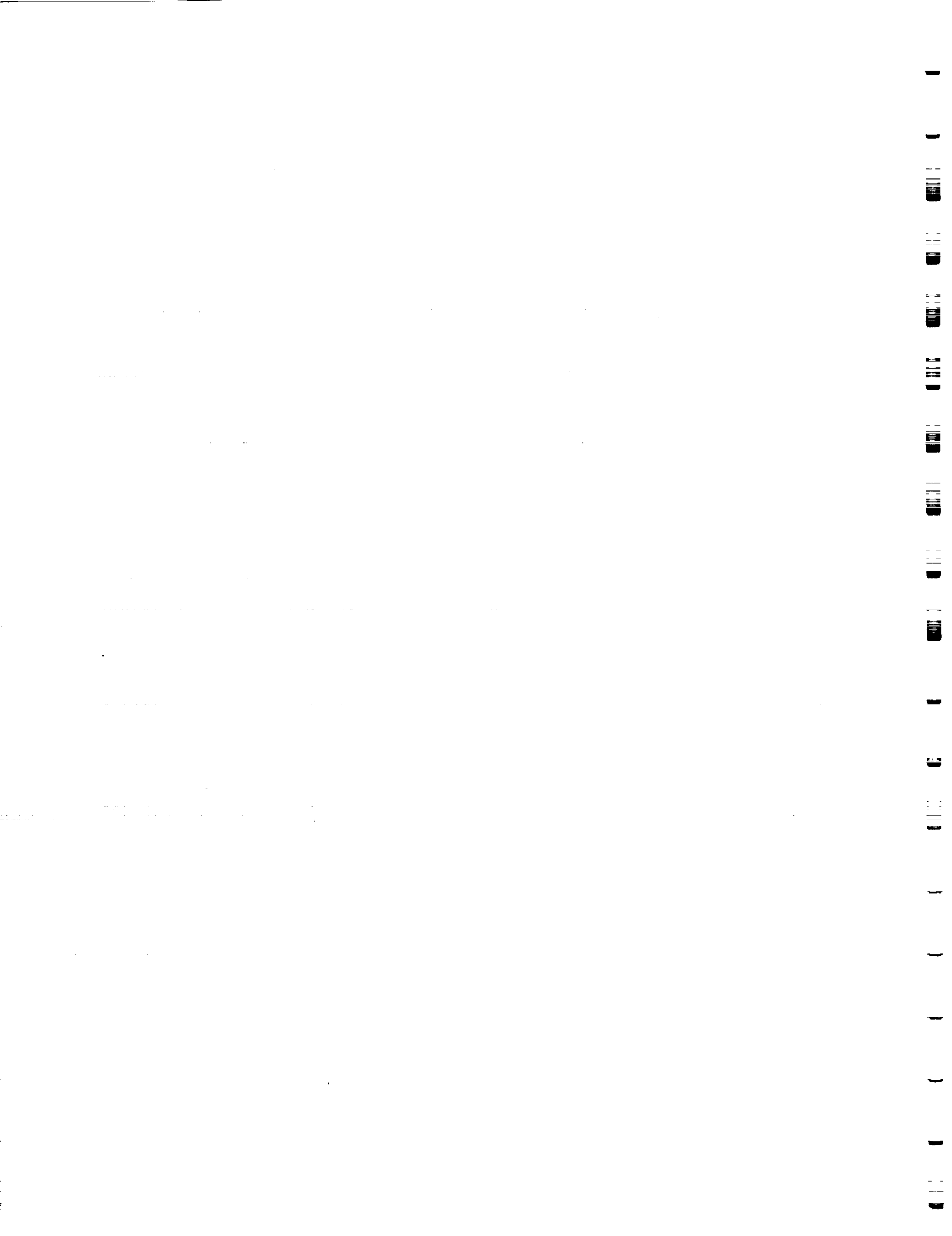
From the literature review, it is clear that progress is being made on the prediction of pressure drop for two-phase thermal control systems for various gravity levels and flow conditions. However, the same cannot be said for the local heat transfer coefficients for two-phase flow boiling. There has been much work completed for the two-phase heat transfer correlations for a uniform heat flux distribution. Correlations presented by Kandlikar [5], Shah [6], Gungor and Winterton [7], and Boyd and Meng [8] cover different fluids, vast ranges of flow rates, the entire spectrum of quality, and low and high subcooling. The former three correlations were only recommended for saturated flow boiling and the latter for subcooled flow boiling. These correlations are valid for only smooth tubes, and one must avoid using them when orientation is important. The former three correlations were derived from the data collected from horizontal flow boiling, whereas the latter for high Froude number (> 50.0). Recently, several researchers have considered the effect of heat transfer enhancement devices (fins, and twisted tapes) and have presented correlations, but most of these are again for horizontal flow boiling or condensation on horizontal tubes. Patankar et al. [9], Wen et al. [10], and Jaber et al. [11], have studied the effect of fins on the heat transfer coefficient for condensation. While Wen et al. [10] presented experimental data to facilitate theoretical model development of heat transfer coefficient for condensation on horizontal integral-finned tubes, Jaber et al. [11] found that the condensation heat transfer coefficient can be increased by up to 280% for copper if commercially available enhanced tubes are used in condensers over smooth copper tubes. He also looked at copper alloy tubes and found that heat transfer is enhanced by an average of over 30% with

finned tubes relative to smooth tubes. Boyd et al. [4], Smith [12], and Turknett [13] have studied the flow boiling in horizontal channels with uniform and top-side heating with and without enhancements. They made measurements of the two-dimensional axial and circumferential wall temperature distributions, and presented results for the axial distribution of the heat transfer coefficient for four internal tube configurations.

The literature search suggests that: (1) there is a lack of local experimental data and local heat transfer correlations for an external single-side heat flux distribution, and (2) very few studies have been completed on investigating the flow aspect ratio, and orientation effects for uniform and non-uniform heat flux distributions.

In addition to the advanced space system, single-side heat flux boundary conditions appears in many other applications. Such advanced applications include high heat fusion components, high heat flux electronic components, in-tube boiling systems, boilers, condensers, and heat exchangers. Therefore, advanced applications requiring flow boiling will necessitate better characterizations of the local 2-D heat transfer variations for single-side heated conditions.

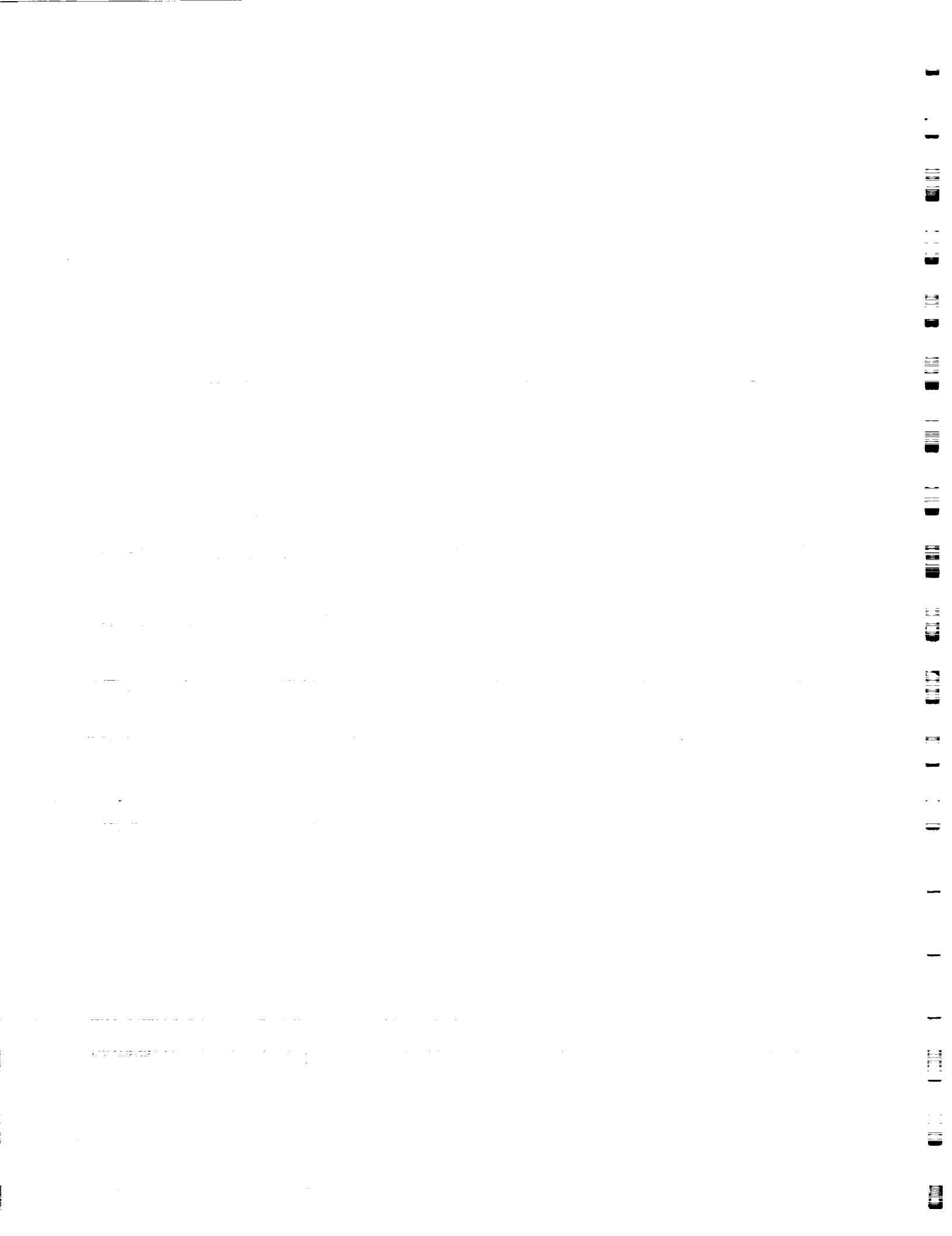
For optimized 2-D two-phase thermal management systems to become a reality, extensive efforts are needed to collect and correlate experimental data for heat transfer correlations for complex heat flux distributions. This is the **long-term objective** of future funded work which is directly related to the present study. The long-range scope of this study includes making 2-D wall temperature measurements as function of mass velocity, inlet subcooling, tube diameter, tube internal geometry, tube orientation, gravity level, and heating configuration. The anticipated Freon-11 mass velocity and tube diameter range between 95.0 and 1,300.0 kg/m²s, and between 9.5 and 25.4 mm, respectively. The tube inside wall configuration will include smooth wall, finned wall, and combined twisted tape and finned walls. In the present work, we present an example of 2-D outside wall temperature measurements made with subcooled Freon-11 flowing downward in a smooth vertical channel with single-sided heating. These wall temperature data were then used to obtain circumferentially and axially averaged heat transfer coefficients. Finally, comparisons were made with a similar flow in a horizontal channel (Boyd et al., [4]).



2.2 EXPERIMENTAL SETUP

The system used to perform forced convection boiling experiments in vertical tubes (downward flow), was based on the system initially developed by Boyd et al. [4] and later used by Smith [12], Boyd [14], and Turknett [13]. Figure 11a shows the Freon-11 (R-11) vertical flow boiling loop. This closed loop is constructed of stainless steel and copper, and operates between 3.4 kPa and $.17 \text{ MPa}$. The maximum power generation capability is 2.7 kW and the maximum volume flow rate is approximately $2.97E-4 \text{ m}^3/\text{sec}$. The Freon-11 is stored in a reservoir which is filled using a chemical resistance centrifugal pump. After filling the reservoir, the *R-11* is circulated through the closed loop at the desired operating pressure and flow rate. By circulating the *R-11* before any data is recorded, any leaks in the system can be detected by using a halogen leak detector. Then the desired inlet temperature is obtained by properly adjusting the chiller/isothermal bath. The energy is transferred between the chiller and *R-11* by way of a commonly connected heat exchanger. During testing, the outlet temperature of the chiller is adjusted to maintain a constant inlet *R-11* temperature for a given experimental run. The working fluid for the chiller is a *60/40 ethylene glycol-distilled water* mixture.

A description of the closed flow loop and the function of its components is instructive. The *R-11* flow from the reservoir the filter, where all the contaminants are removed before the fluid enters the positive displacement pump. The positive displacement pump requires a net positive suction of at least 0.02 MPa . This pump was selected for durability. After leaving the pump, the fluid passes through the pulsation damper. The damper reduces the pressure and flow oscillations. The pressure fluctuations are also minimized by using the pneumatically controlled metering valve. Exiting the control valve, the fluid flows to the heat exchanger, where its temperature is set at a desired value by adjusting the chiller parameters. After exiting the heat exchanger, the fluid passes through the turbine flow meter and enters the unheated "flow developing" section or upstream part of the test section which has a length greater than forth (40) times the test section diameter. The fluid then enters the heated section of the test section. A downstream pneumatically controlled valve is used to control the test section exit pressure. The heated fluid then passes through another heat exchanger where the energy generated is removed partially by using tap water. Finally, the fluid flows back to the reservoir and the flow cycle is complete.



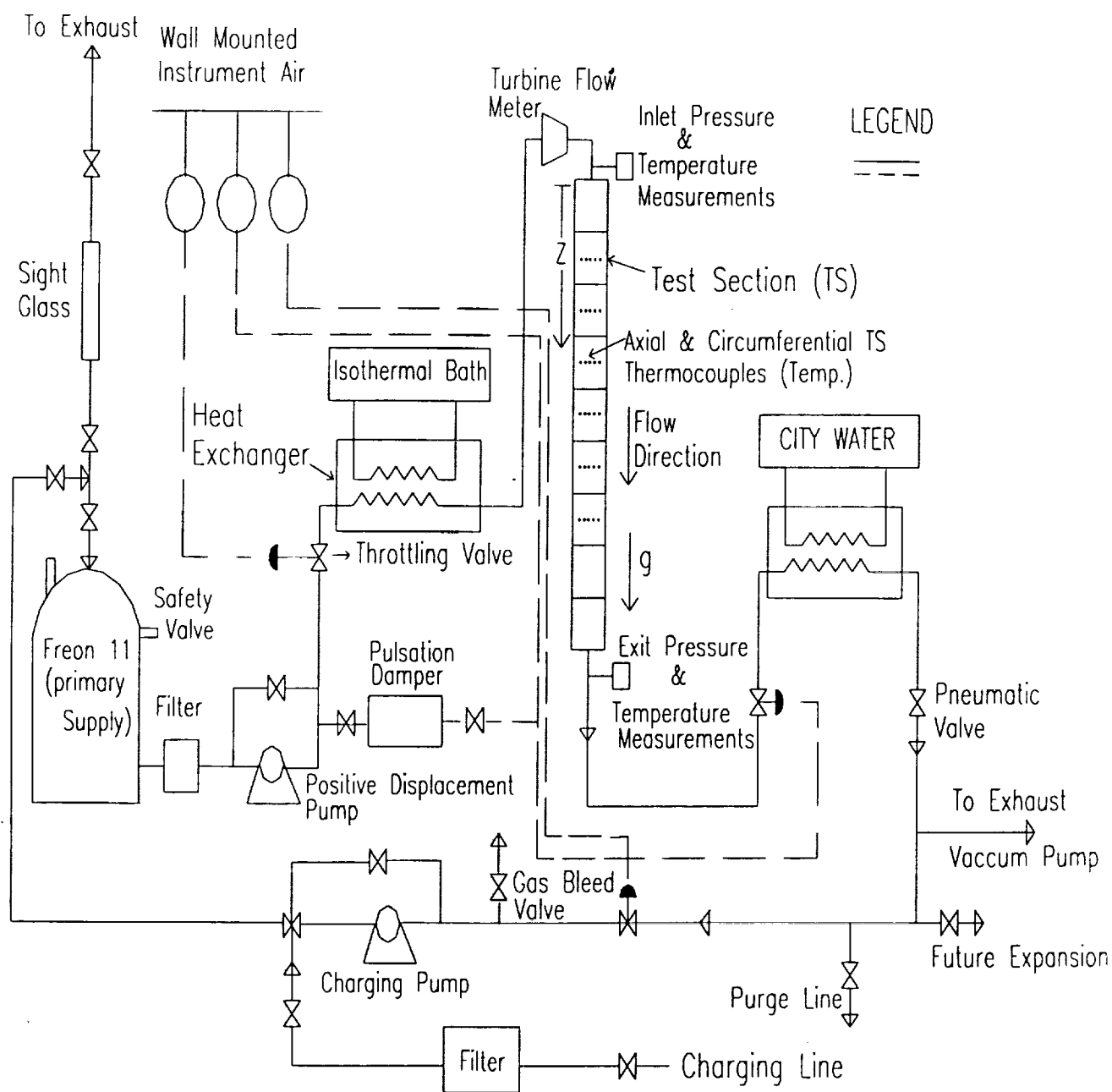
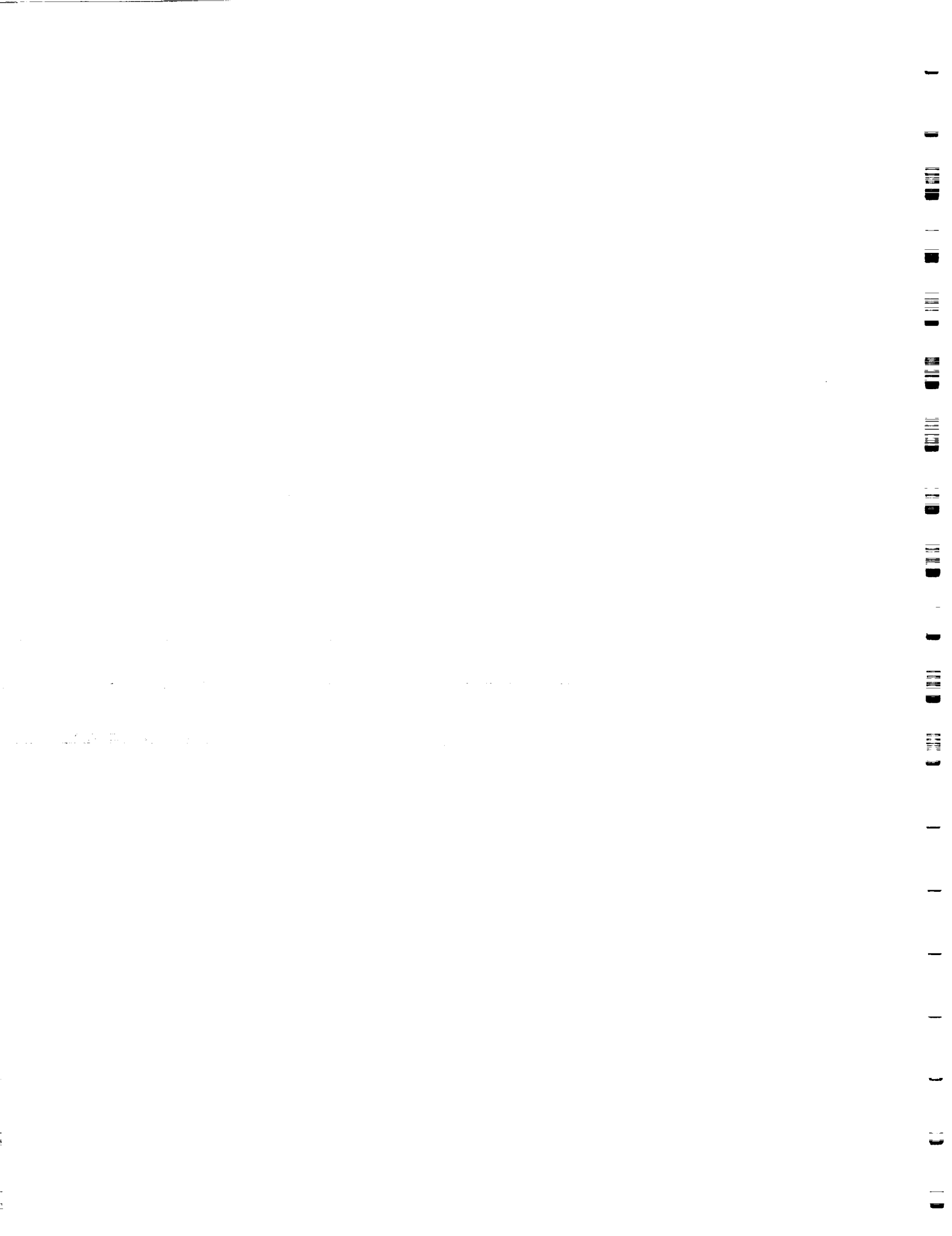


Figure 11a Schematic of the Vertical Downward Flow Boiling Loop



2.3 TEST SECTION DESCRIPTION

The test sections used in this experiment are the same as used by Boyd et al. [4]. The test sections are 2.235 m long copper tubes (see Figure 11b), and consists of two parts: (1) Upstream unheated section to facilitate flow development, and (2) A downstream single-side heated section. For the present case, the inside diameter (D) was 25.4 mm and the outside diameter was 28.5 mm.

The heated section has a smooth inside surface. The test section is heated with heater tapes which vary in width based on tube diameter and are 1.22 m long. Each tape has power generation capacity of 2.66 kW. The test section was designed with flexibility and ease of replacement in mind. Although, the pressure losses due to union connector at both top and bottom ends of the test section are assumed to be small, computations and additional measurements, will be performed later to estimate these losses. The entire test section was insulated to minimize the heat losses. In addition to the primary two parts of the main test section, each part had pressure-temperature measurement ports upstream and downstream of the test section.

The heated part of the test section was divided into seven .203 m axial intervals. At each of the axial locations there are seven thermocouples installed circumferentially at 0 , $\pi/4$, $3\pi/8$, $\pi/2$, $5\pi/8$, $3\pi/4$, and π , and degrees (see Figure 12), with 0 being at the top heated portion of vertical symmetry plane in Figure 12. This test section thermocouple arrangement will allow better circumferential resolution of the wall temperature variation than previous test sections (Boyd, [14], Smith, [12], and Turknett, [13]) because seven circumferential locations are used rather than four.

The thermocouples were installed by using high thermal conductivity epoxy. Special care was taken when thermocouples were adhered to the tube. The thermocouples beads were placed in good contract with the tube so that as little epoxy as possible was used. Based on repeated measurements (forty) of the epoxy thickness between the thermocouple and the copper tube, the mean thickness was 0.194 mm, and the standard deviation was 0.007 mm.



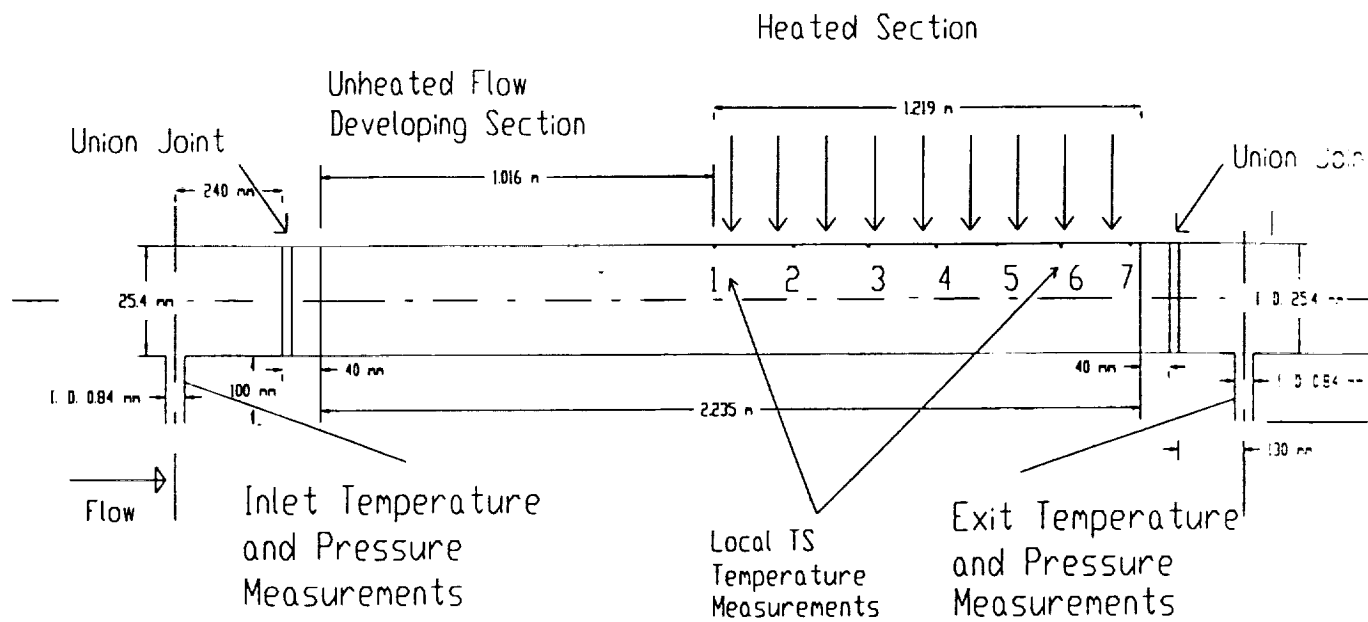


Figure 11b: Test Section (TS) Configuration for Temperature and Pressure Measurements



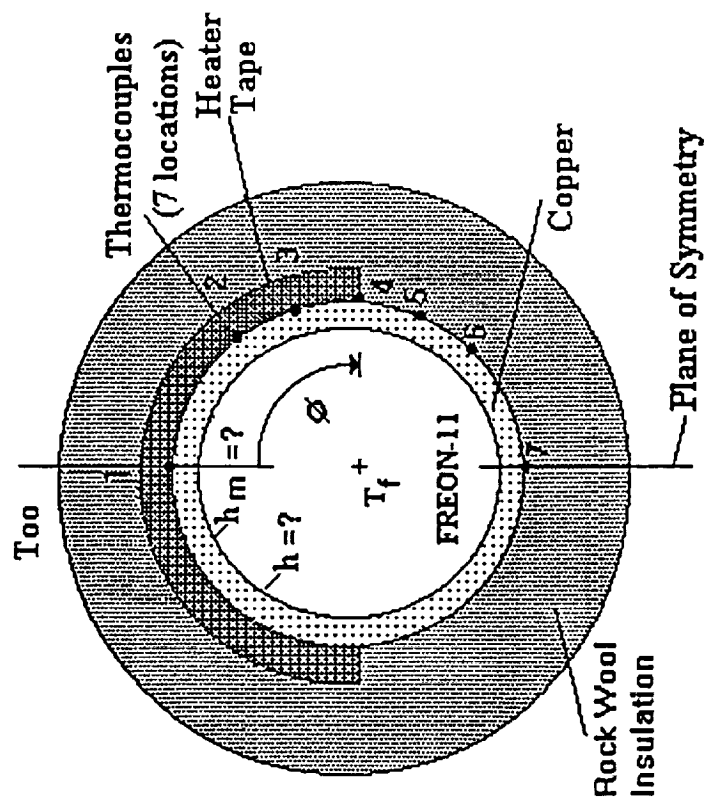


Figure 12: Cross-section of Heated Portion of the Vertical Test section

2.4 DATA REDUCTION ANALYSIS

Forty-nine (49) local temperature measurements were made on the outside surface of the heated portion of the test section for each experiment. These outside temperatures must be related to the inside wall temperature in order for us to calculate the inside heat transfer coefficient. Two techniques will be used to reduce the wall temperature data: (1) the heated thermal hydraulic approach (Boyd et al., [4]; see Figure 13), and (2) a multi-dimensional inverse conduction analysis using numerical finite element computation code called ANSYS.

The initial data reduction is based on the heated hydraulic approach used by Boyd et al. [14]. In this analysis, we compute circumferentially averaged heat transfer coefficient from circumferentially averaged wall temperature. The circumferentially averaged temperature is computed from the seven wall temperature measurements made on copper tube outside surface at each axial location by using the piece-wise linear approach used by Reid et al. [15]. Using their approach, the circumferentially averaged outside wall temperature can be related to the seven circumferential measured temperatures (T_{m1} at 0 degrees, T_{m2} at $\pi/4$, T_{m3} at $3\pi/8$ etc.) by equation (1) given above. The temperature T_{av} was used with the model presented by Boyd et al. [4] to account for temperature drop across channel walls, and convective and radiative heat losses to the surroundings. Using this model, the mean heat transfer coefficient (h_{mj}) at a given axial location was obtained.

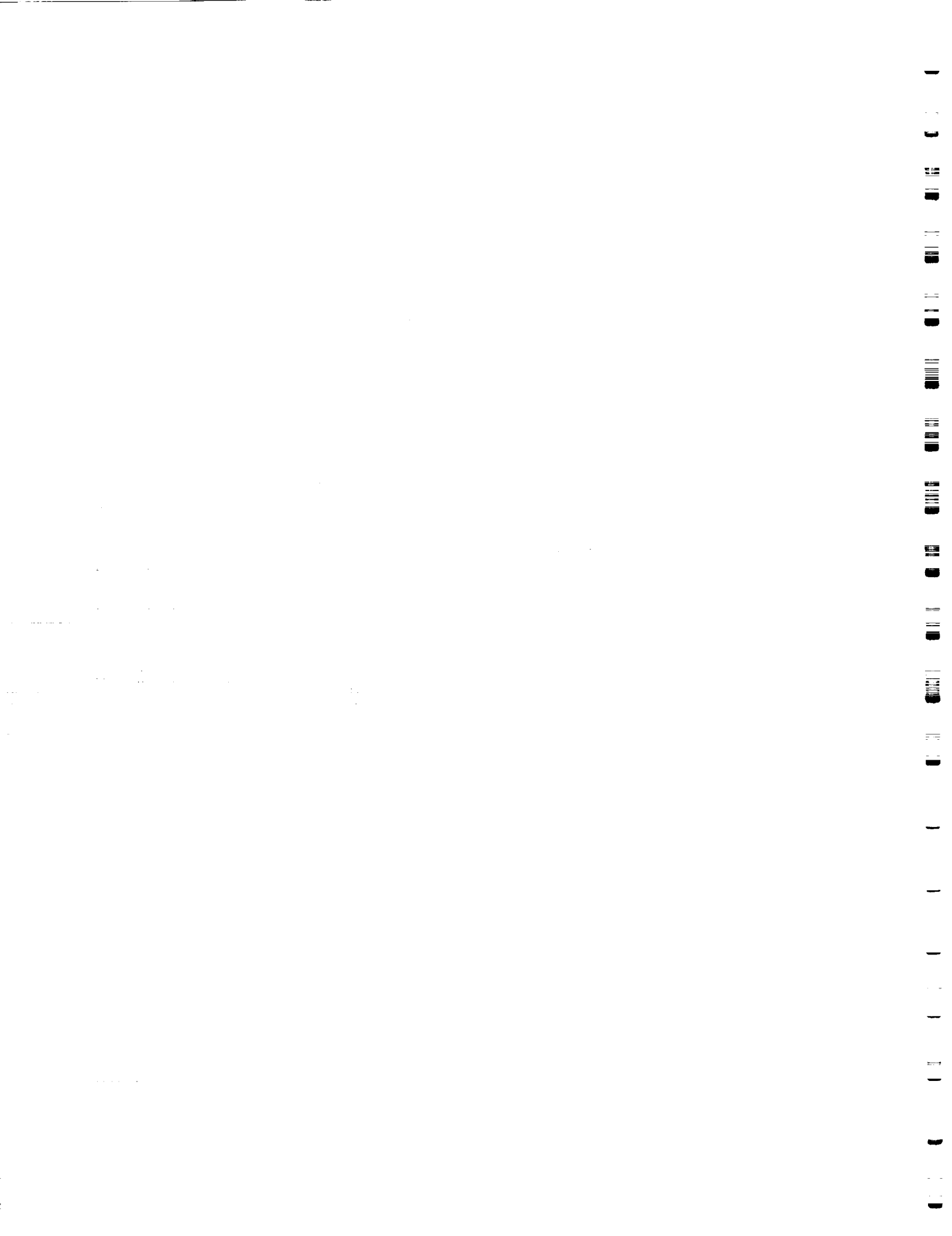
The uncertainties for each measurement in this experiment are as follows: (1) for geometric measurements, ± 0.001 mm; (2) for voltage, ± 0.05 mV; (3) for current, ± 0.005 mA; (4) for pressure, ± 0.7 Pa; (5) for flow rate, $\pm 6.3E-7$ m³/s; (6) for temperature, ± 0.17 °C. The resulting uncertainty in heat transfer coefficient was estimated by Boyd et al. [4], and Huque et al. [16] to be less than 10 percent.

2.5 RESULTS

For a 25.4 mm inside diameter single-side heated test section, results are presented for a mass velocity (G) of 210.0 kg/m²s, an inlet temperature of 22.6 °C, and an exit pressure of 0.1843 MPa (absolute). The results include: (1) 2-D (axial and circumferential) wall temperature



Figure 13: Thermal Hydraulic Model



distributions; (2) Axial distributions of mean wall temperature (circumferentially averaged); and (3) Axially and circumferentially averaged mean heat transfer coefficient distributions.

2-D Wall Temperature Distribution

Figures 14a-14g, and Figure 15, show the distributions as measured outside wall temperature at different circumferential and axial locations. The wall temperature increased as the fluid flowed from upstream to downstream (axial locations #1 to #7) in the test section. Furthermore as ϕ varied from 0 to π , the temperature decreased circumferentially because of a change from a circumferentially heated region ($\phi = 0$ to $\pi/2$) to a non-heated one ($\phi = 5\pi/8$ to π).

This change in temperature can be observed clearly in Figure 15. This figure shows the axial distributions for the wall temperature for seven circumferential locations, as well as the circumferentially averaged wall temperature (dotted line). From these figures, it can be seen that the wall temperature distributions are closely spaced for $\phi = 0$ to $\pi/2$ and $\phi = 5\pi/8$ to π . This is to be expected because of single-side heating. From the plots, one can also observe that the wall temperature at $\phi = 0$ remains above the saturation temperature ($T_{sat} = 41.65^\circ\text{C}$) and the wall temperature at $\phi = 5\pi/8$, $3\pi/4$, and π were consistently below T_{sat} .

Although the data analysis is continuing, preliminary computations using the Davis-Anderson correlation (Davis and Anderson, [17]) indicate that the onset to nucleate boiling occurs at a wall temperature of 44.1°C . For the computations, all Freon-11 properties were evaluated at the saturation temperature using Perry's handbook [18]. Using this computation as a basis and the basic characteristics of the boiling curve, both axial and orientation influences on the quasi-boiling curve are displayed in Figure 14a through 14g. Figure 14a ($\phi = 0.0$ degrees) through Figure 14d ($\phi = 90.0$ degrees) show that the onset of nucleate boiling (ONB) does occur slightly above 41.7°C simultaneously over the heated section from $\phi = 0.0$ to 90.0 degrees. For the conditions shown, this occurred at a power below 181.2 W simultaneously at all axial locations between locations #2 and #6 but at different outside wall temperatures. Similarly, the onset to fully developed boiling (OFDB) occurred simultaneously at all these locations at a power level of 181.2 W. Although further data reduction is needed to determine actual inside wall temperatures, it is clear from the figures that the boiling curve will shift to the right with higher values of Z . The data also show a slight increase in $[T_w]_{out}$ (outside wall temperature) in

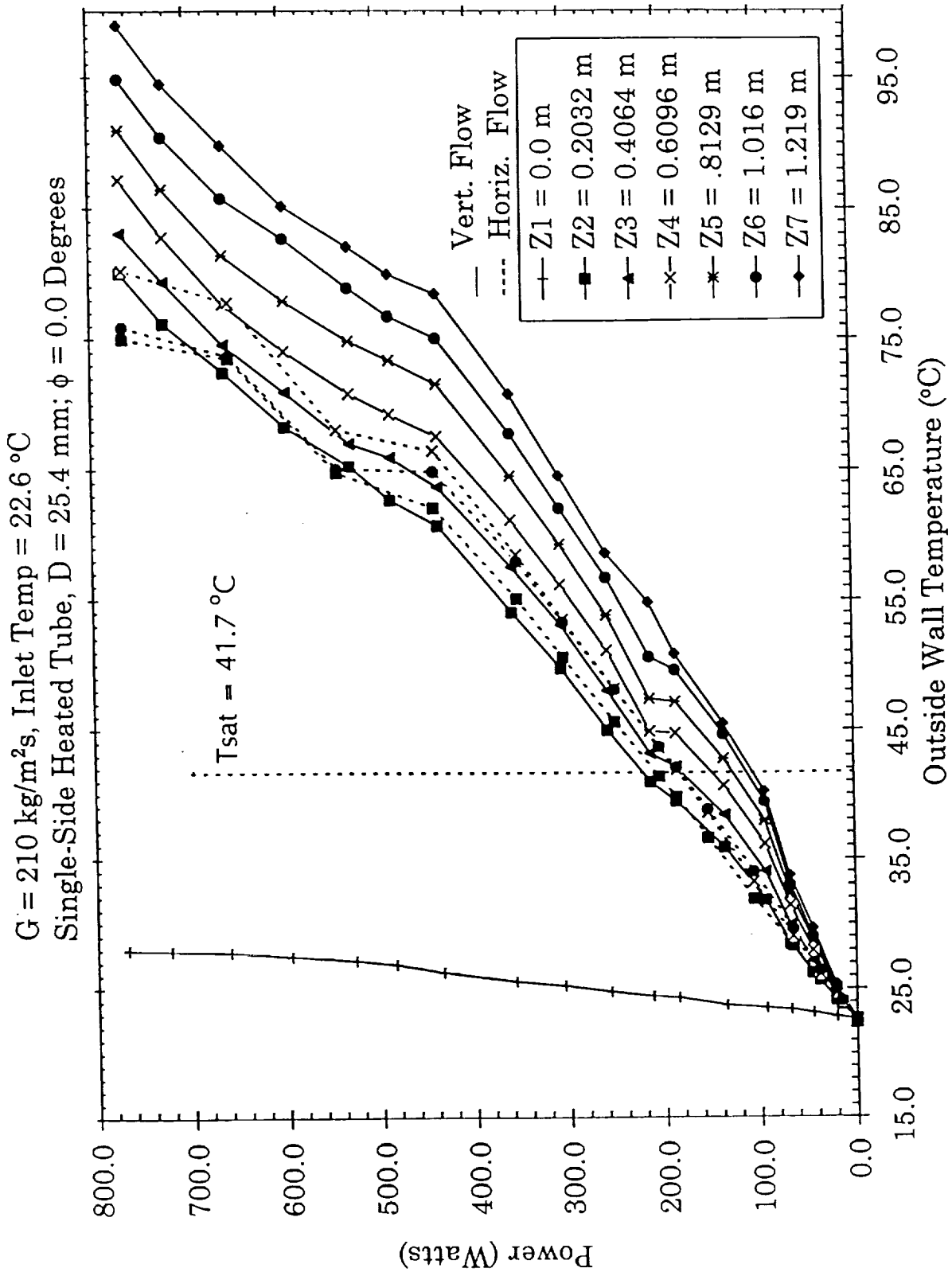


Figure 14a: Measured Outside Wall Temperature (Copper Channel) Axial Variation as a Function of the Net Power Generation for a Single-Side Heated, Smooth Channel for $\phi = 0.0$ Degrees

$G = 210 \text{ kg/m}^2\text{s}$, Inlet Temp = 22.6°C
 Single-Side Heated Tube, $D = 25.4 \text{ mm}$; $\phi = 45.0^\circ\text{Degrees}$

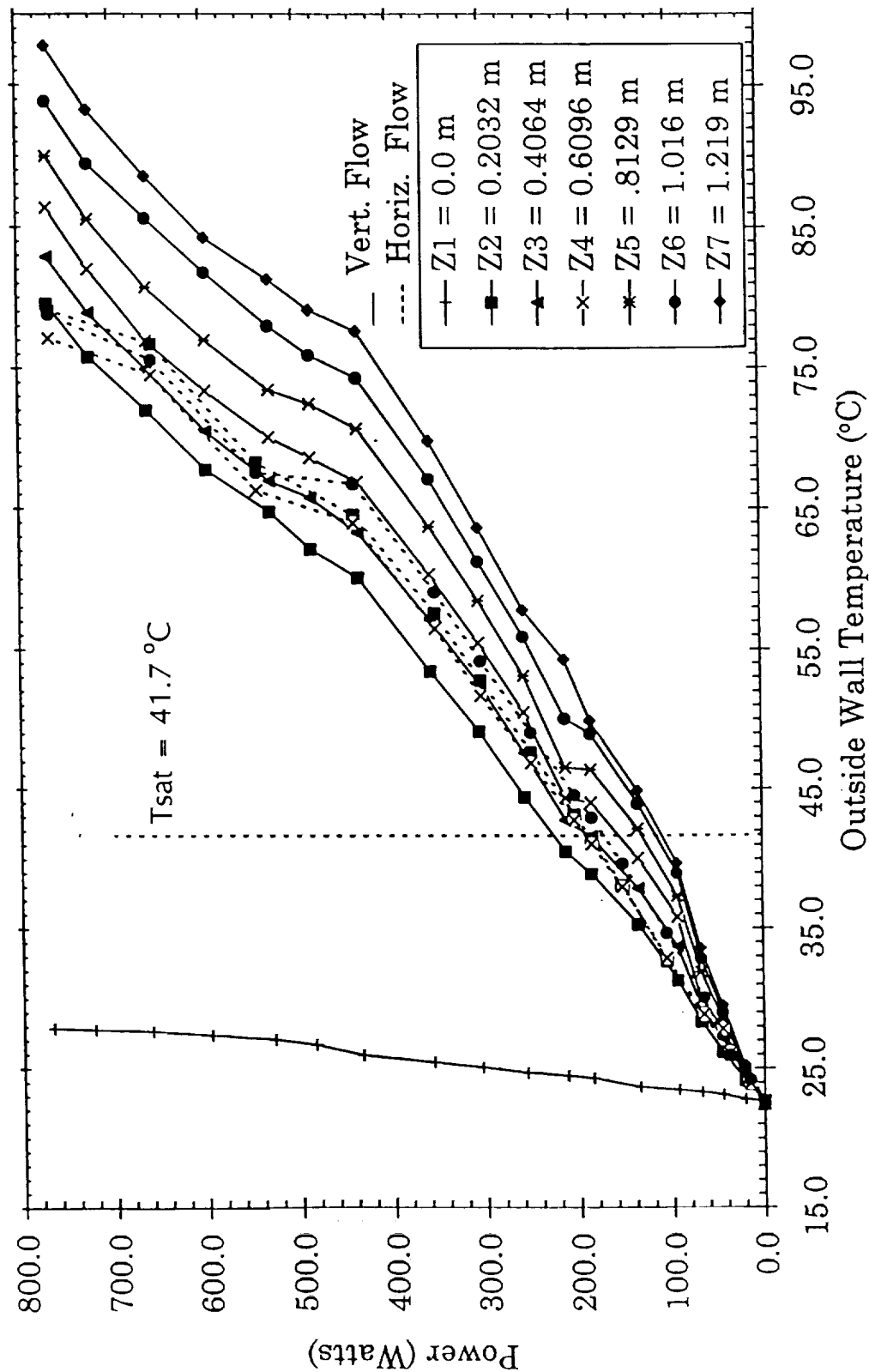
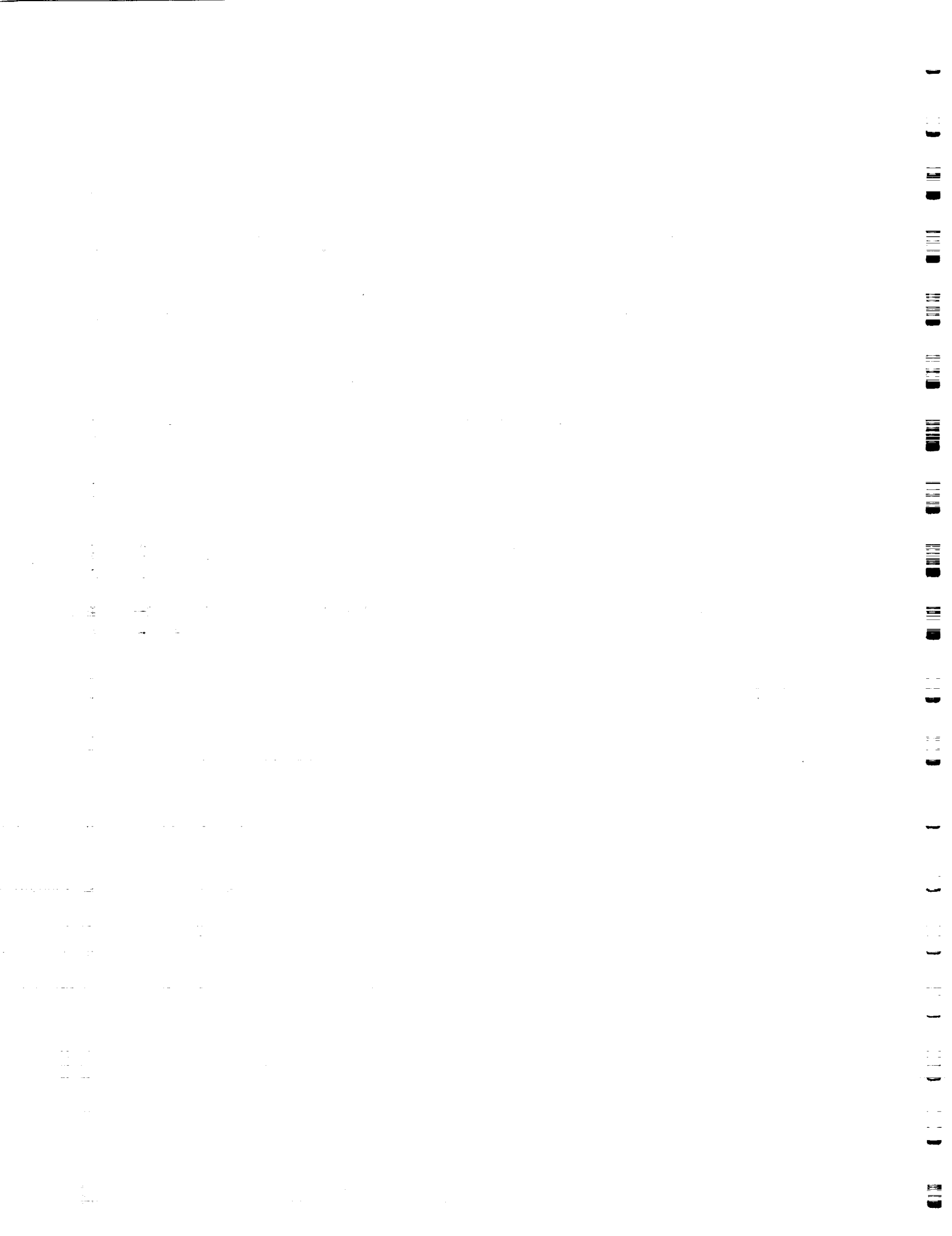


Figure 14b; Measured Outside Wall Temperature (Copper Channel) Axial Variation as a Function of the Net Power Generation for Single-Side Heated, Smooth Channel for $\phi = 45.0^\circ\text{Degrees}$



$G = 210 \text{ kg/m}^2\text{s}$, Inlet Temp = 22.6°C
 Single-Side Heated Tube, $D = 25.4 \text{ mm}$; $\phi = 67.5$ Degrees

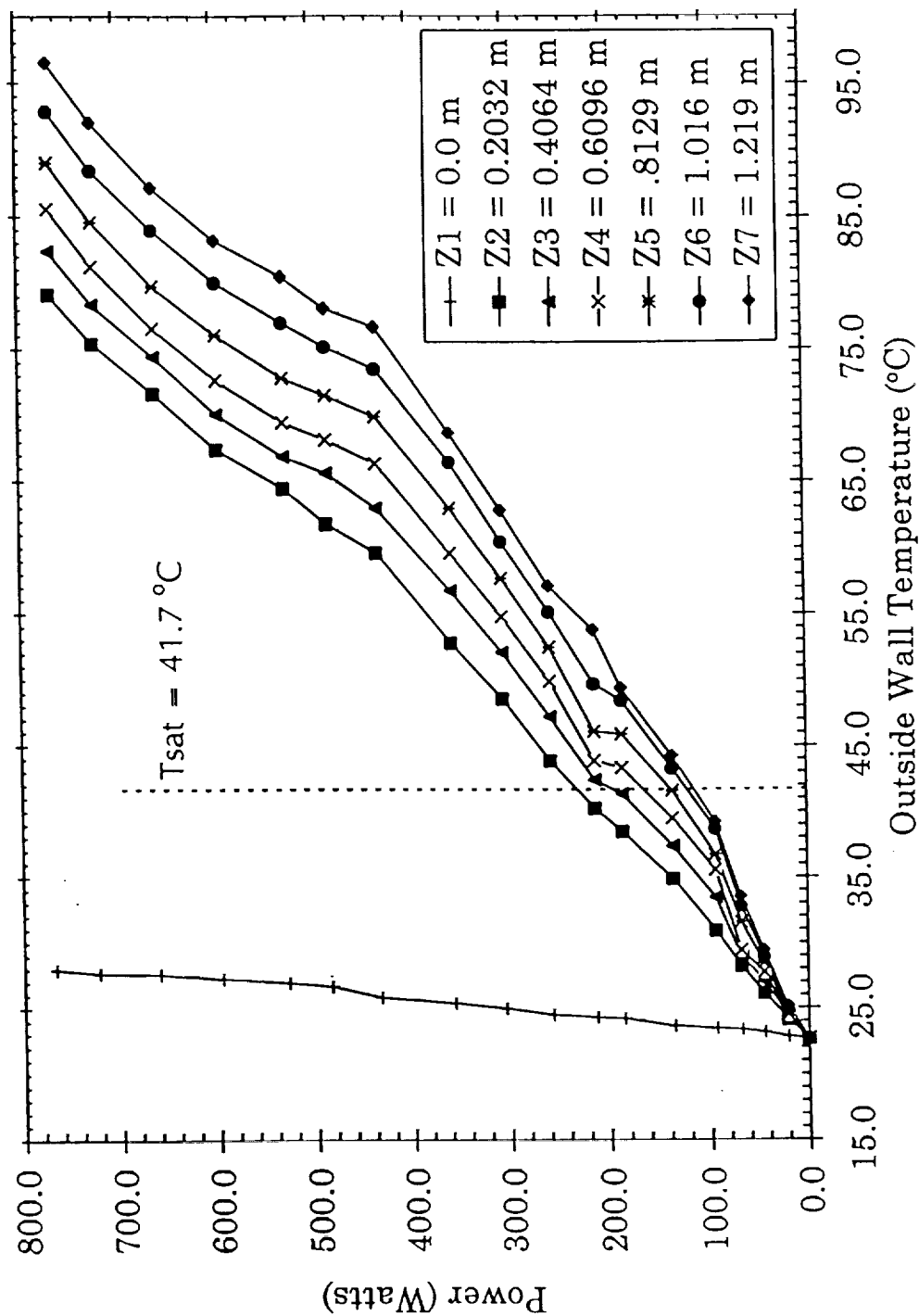
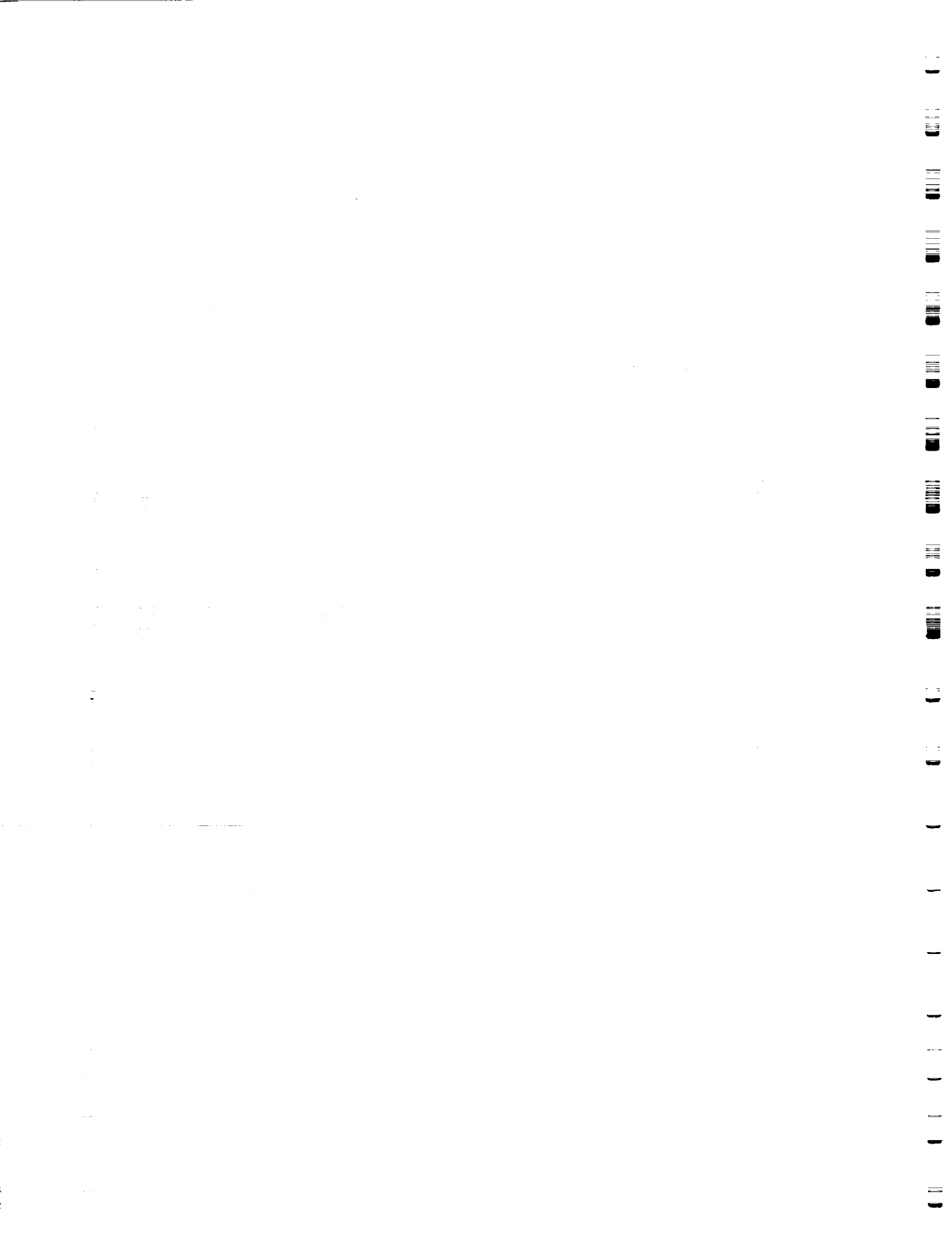


Figure 14c: Measured Outside Wall Temperature (Copper Channel) Axial Variation as a Function of Net Power Generation for a Single-Side Heated, Smooth Channel for $\phi = 67.5$ Degrees



$G = 210 \text{ kg/m}^2\text{s}$, Inlet Temp = 22.6°C
 Single-Side Heated Tube, $D = 25.4 \text{ mm}$; $\phi = 90.0$ Degrees

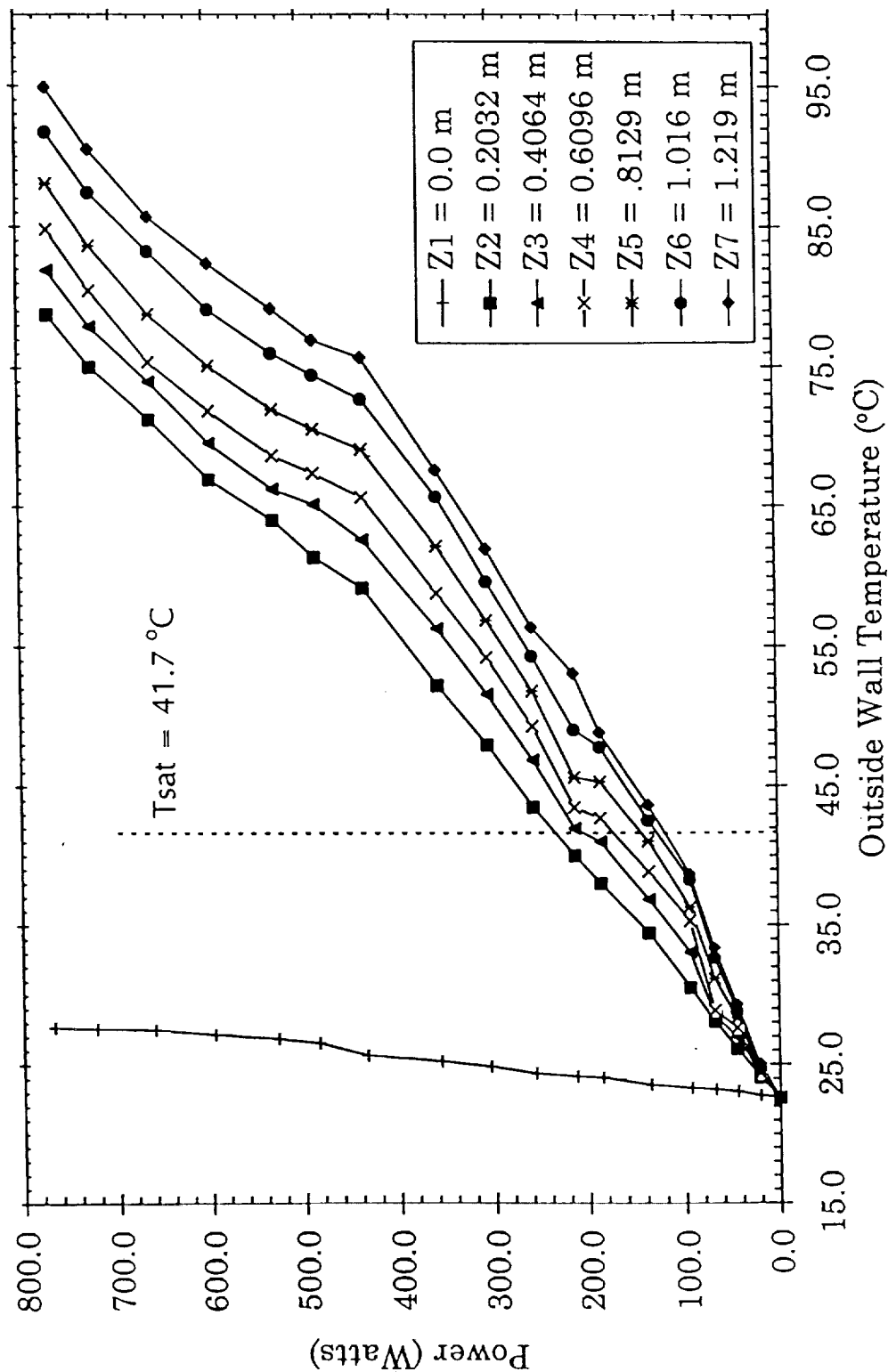
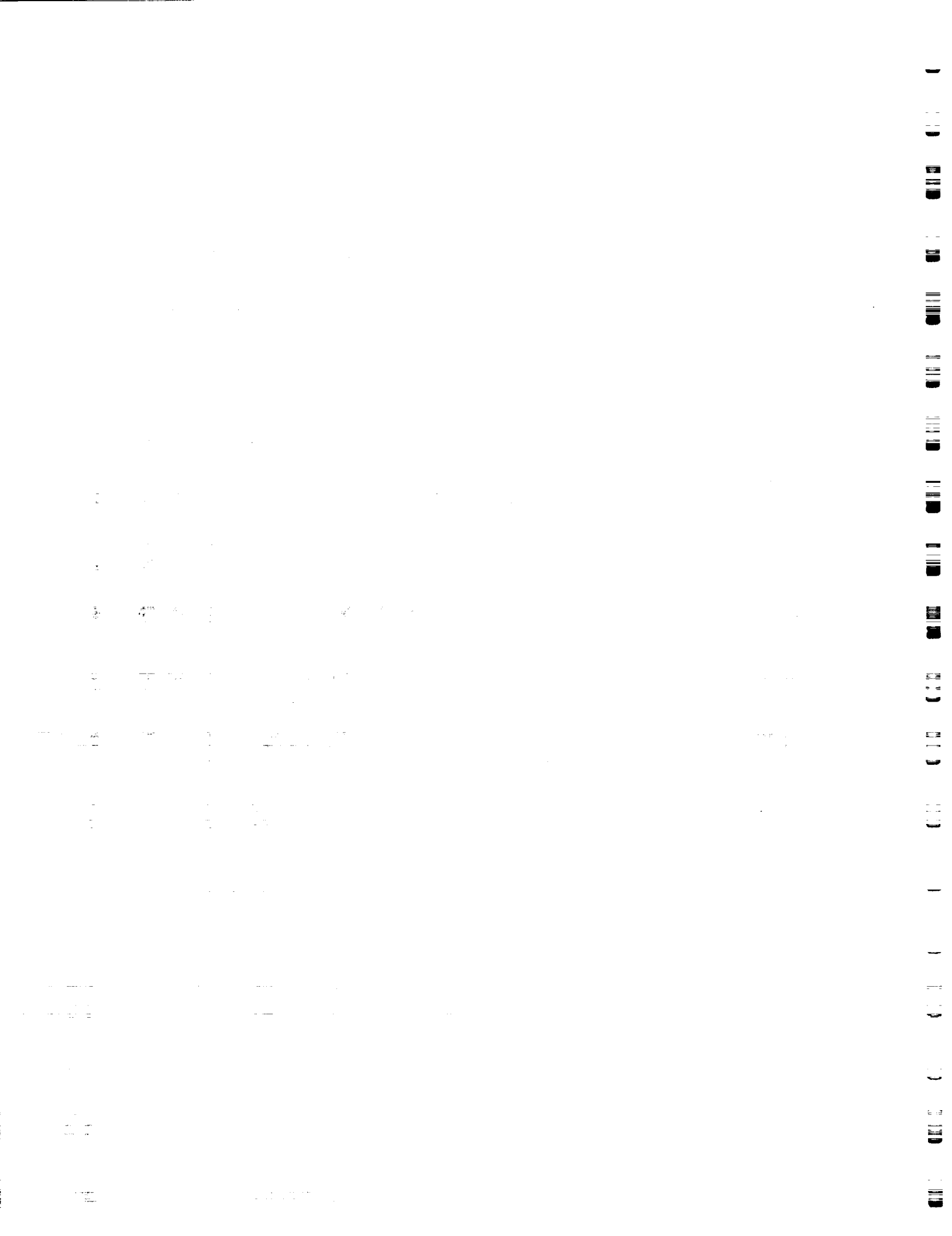


Figure 14d : Measured Outside Wall Temperature (Copper Channel) Axial Variation as a Function of the Net Power Generation for Single-Side Heated, Smooth Channel for $\phi = 90.0$ Degrees



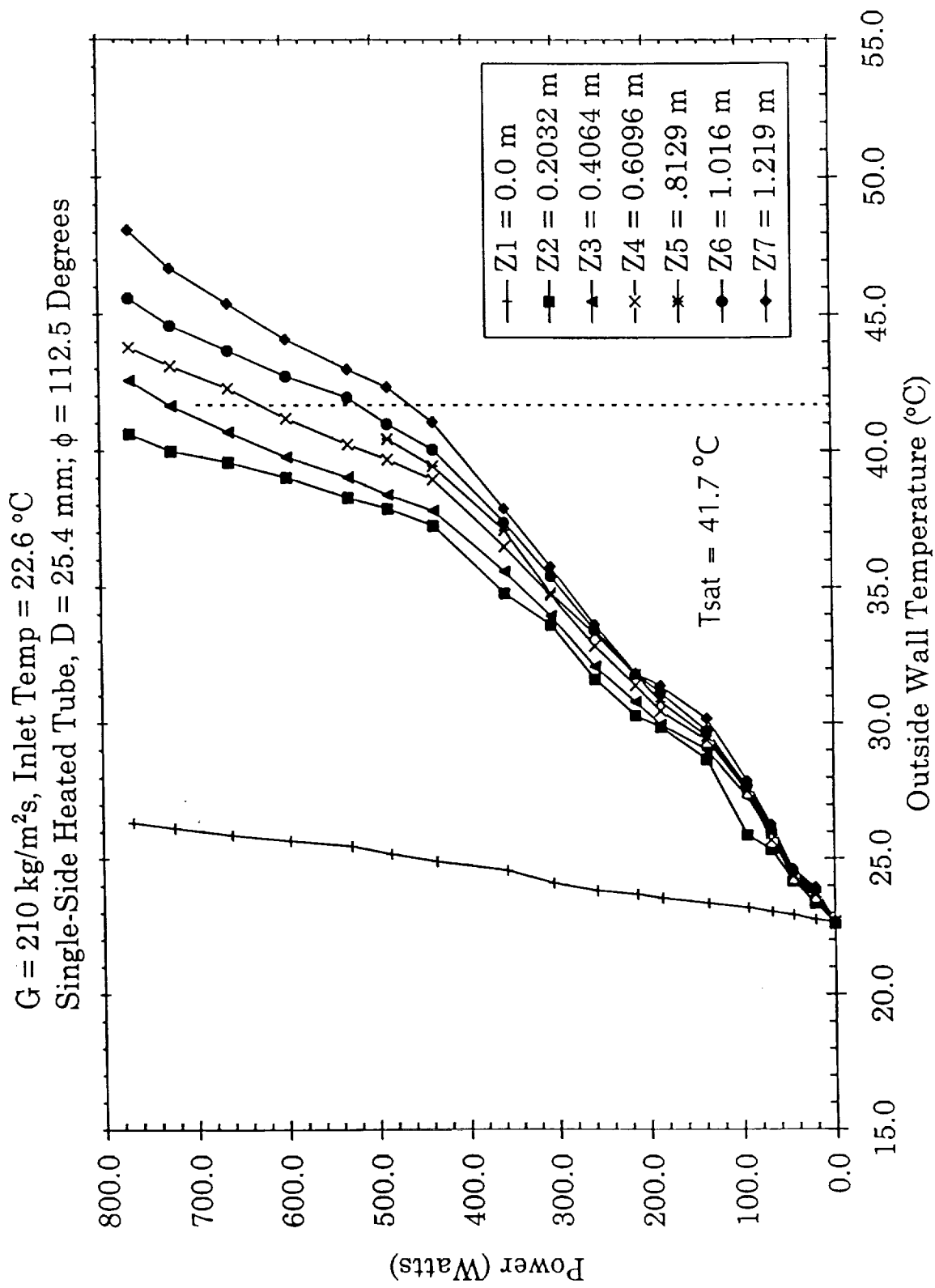


Figure 14e: Measured Outside Wall Temperature (Copper Channel) Axial Variation as a Function of the Net Power Generation for a Single-Side Heated, Smooth Channel for $\phi = 112.5^\circ$ Degrees

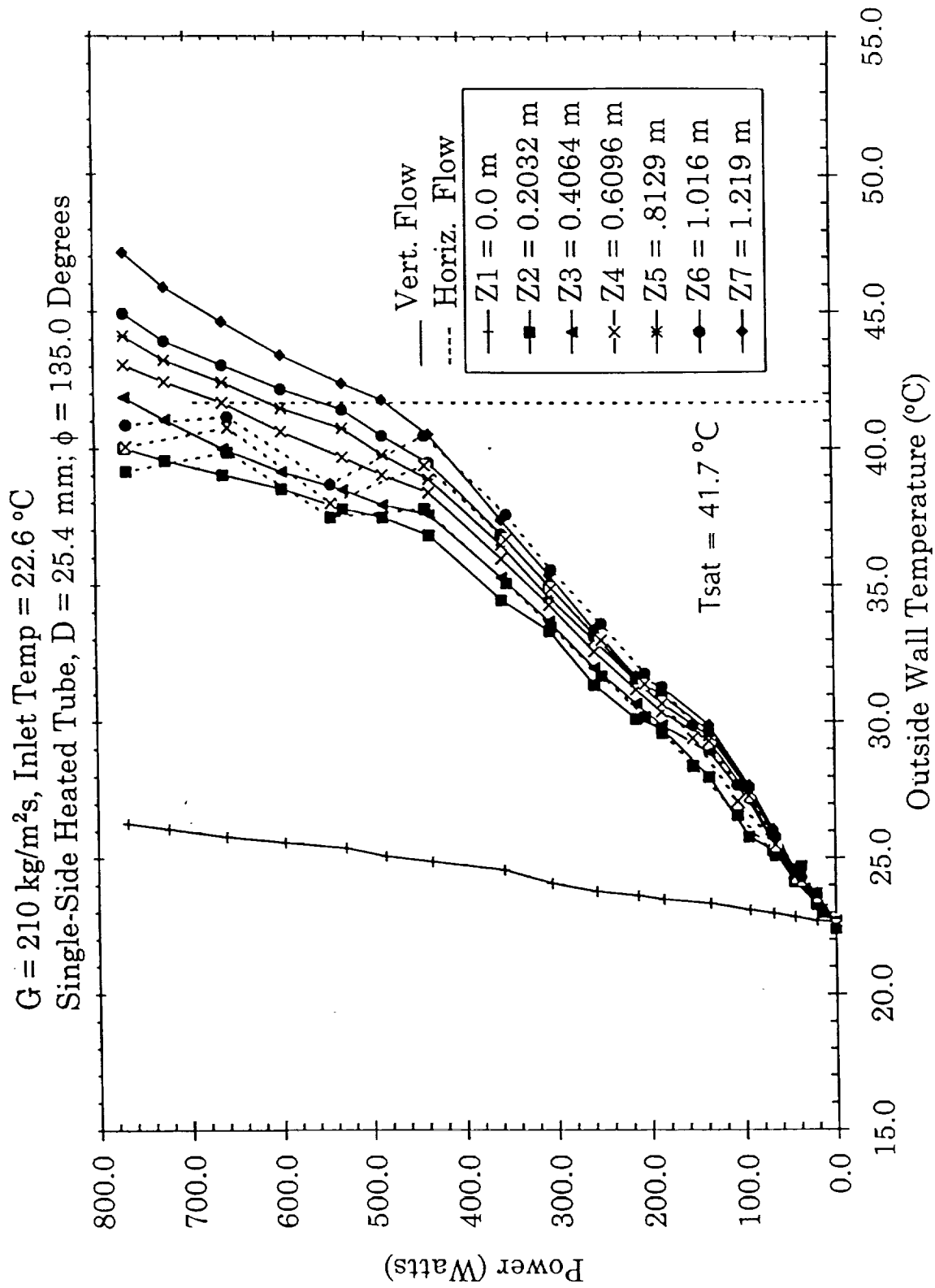


Figure 14f: Measured Outside Wall Temperature (Copper Channel) Axial Variation as a Function of the Net Power Generation for a Single-Side Heated, Smooth Channel for $\phi = 135.0^\circ$ Degrees

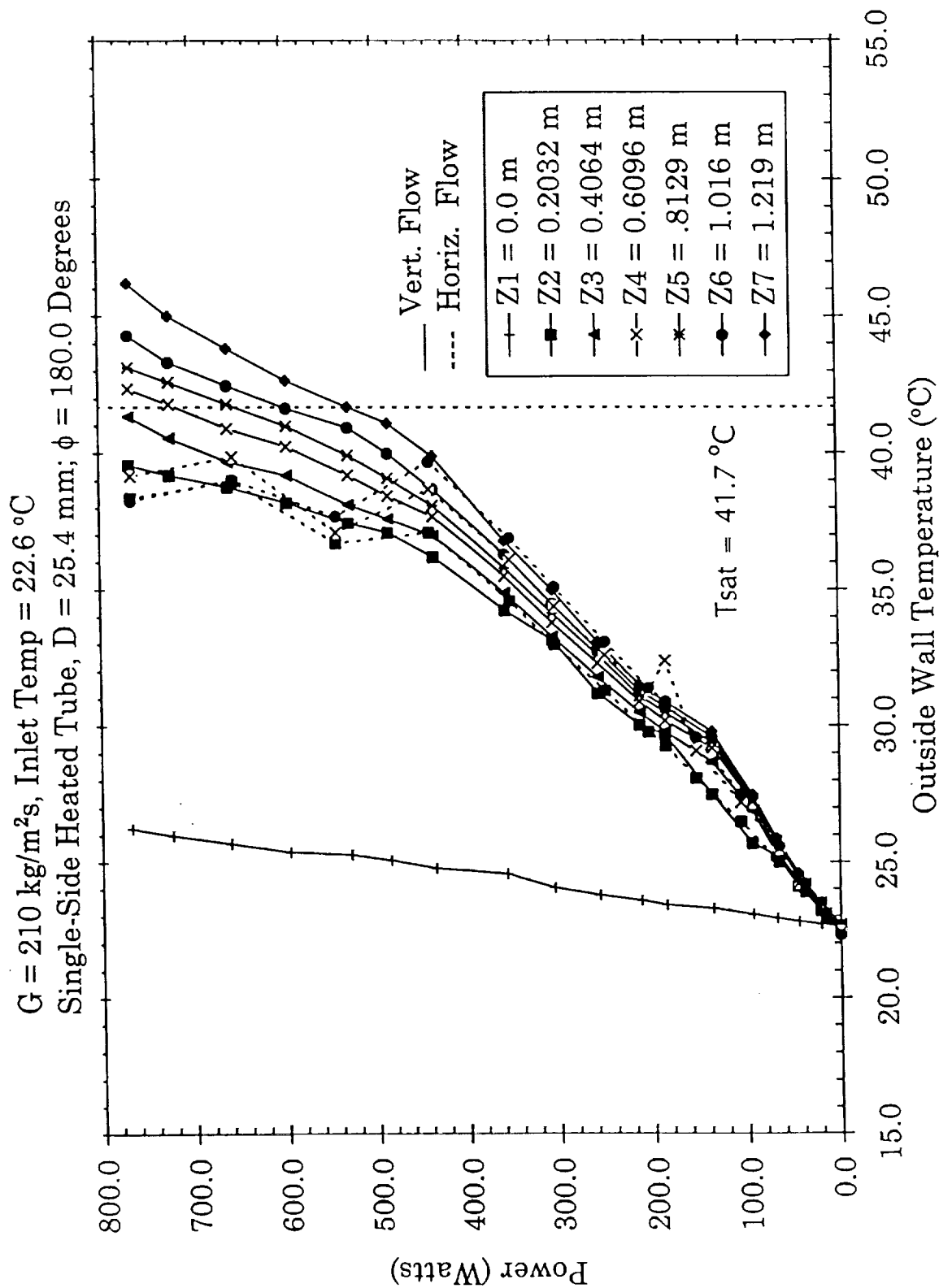


Figure 14g: Measured Outside Wall Temperature (Copper Channel) Axial Variation as a Function of Net Power Generation for a Single-Side Heated, Smooth Channel for $\phi = 180.0^\circ$ Degrees

**$G = 210 \text{ kg/m}^2\text{s}$, Inlet Temp = 22.6°C
Single-Side Heated Tube, $D = 25.4 \text{ mm}$; Power = 528.1 Watts**

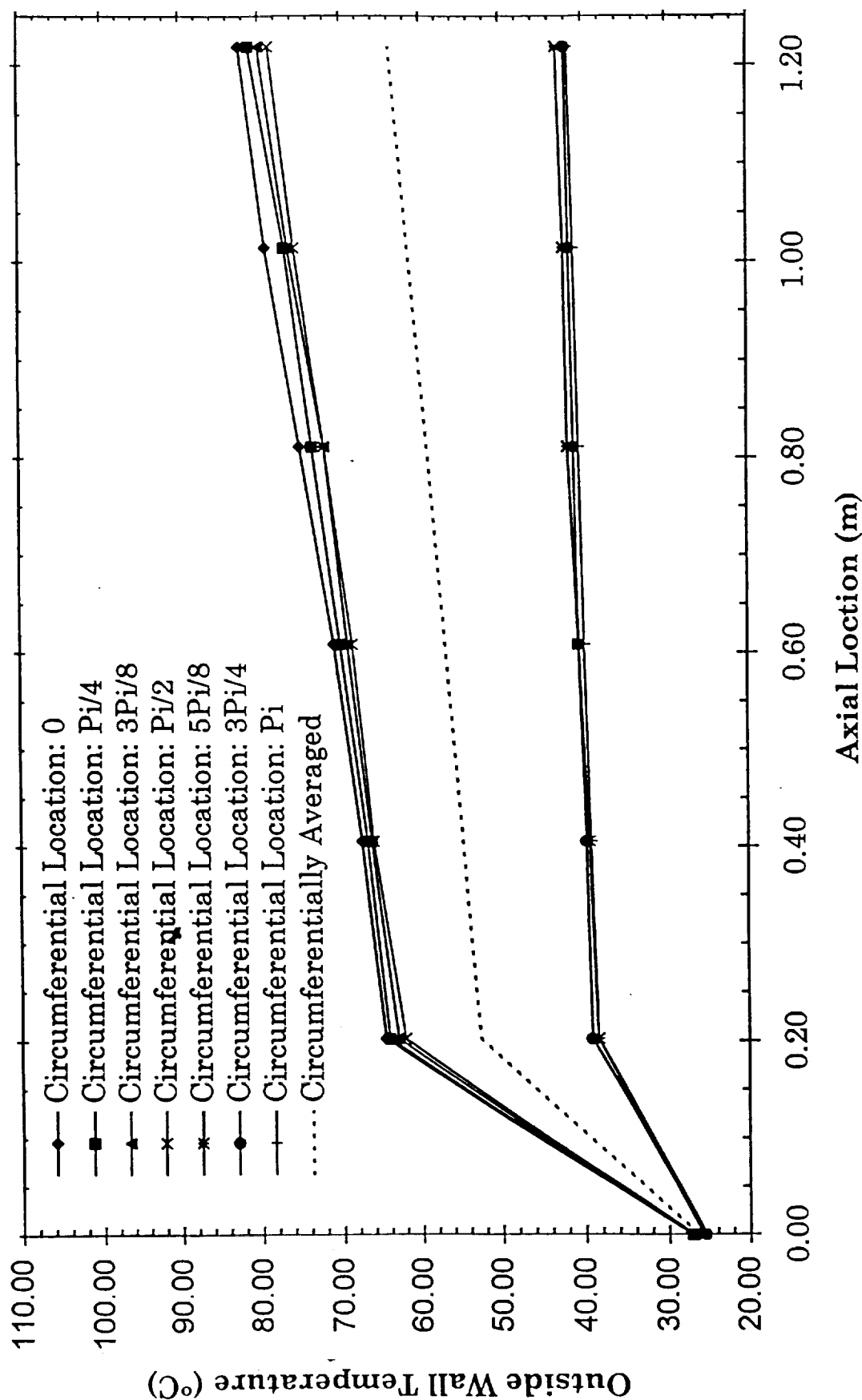


Figure 15: Axial Distribution of the Wall Temperature for Seven Circumferential Locations for the Smooth Tube for the Net Power Generation of 528.1 Watts

the circumferential direction from $\phi = 90.0$ degrees to 0.0 degrees. These data provide a quantitative record which shows the regions or patches where various simultaneous boiling phenomena occurred. Even though the test section was made of highly conducting copper, the measured outside wall temperatures cannot be used directly to correlate ONB or CHF. However, these measurements are closely linked to the local variations of the inside wall temperature and hence are related to the local two-dimensional boiling heat transfer at the inside wall.

Heat Transfer Coefficient

Once the local wall temperature distribution was obtained, the mean (circumferentially averaged) wall temperature was computed and this temperature was used in the heated thermal hydraulic approach (Boyd et al., [14]) to obtain the circumferentially averaged heat transfer coefficient for each axial location and for different power levels. Then, this circumferentially averaged heat transfer coefficient (h_{mj}) was used to obtain overall (circumferentially and axially mean) heat transfer coefficient using the equation (2), which is based on a linear piece-wise approximation between each axial location. The 1st and the 7th axial locations are not included due to end losses. Hence, the axially and circumferentially mean heat transfer coefficient was defined as

$$h = \frac{h_{m2} + 2h_{m3} + 2h_{m4} + 2h_{m5} + h_{m6}}{8.0} \quad (2)$$

The mean heat transfer coefficient distribution for the mass flow rate of $210.0 \text{ kg/m}^2\text{s}$ is given on Figure 116. From the above discussion of wall temperature distribution, the OFDB occurred at power level of 181.2 W , and the critical heat flux occurred between $\phi = 0.0$ and 90.0 degrees at a power level of 212.7 W . This can be confirmed again from the mean h distribution given in Figure 16. It is clear from Figure 16 that, at the OFDB, there is an increase in the mean h which occurs at a power of 181.2 W . This agrees with the above noted predictions using the Davis-Anderson correlation.

Since the flow channel is heated from one side, the CHF occurred locally in a small circumferential angular interval $\Delta\phi$ directly below the heater and extending from $\phi = 0$ to $\phi = \Delta\phi$. As the power level is increased, $\Delta\phi$ increases and the ONB occurs is denoted by ϕ_{ONB} , then the:

Heat Transfer Coefficient Comparison for Horizontal (Top Heated) And Downward Vertical Flow (Single-Side heated).

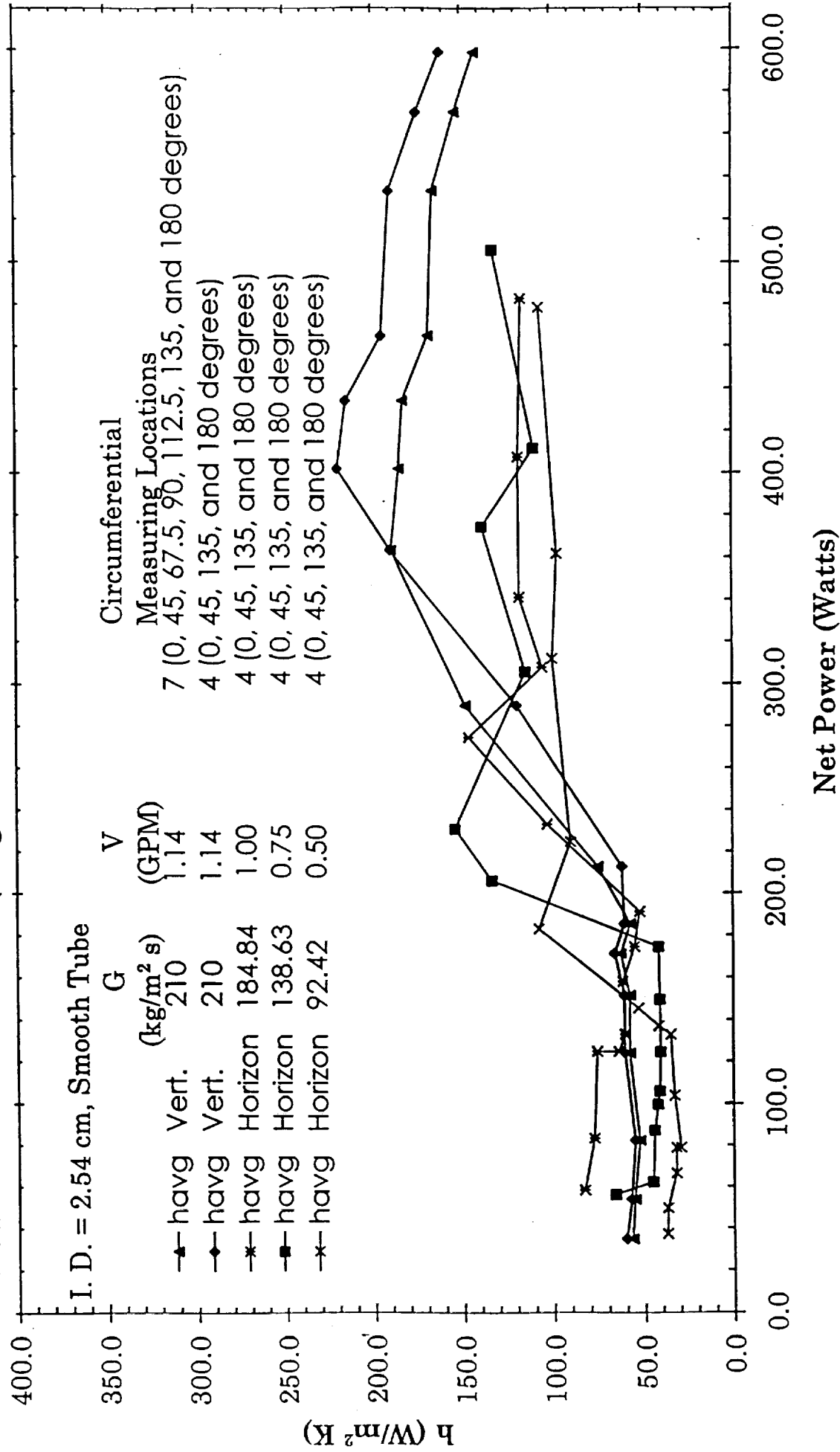
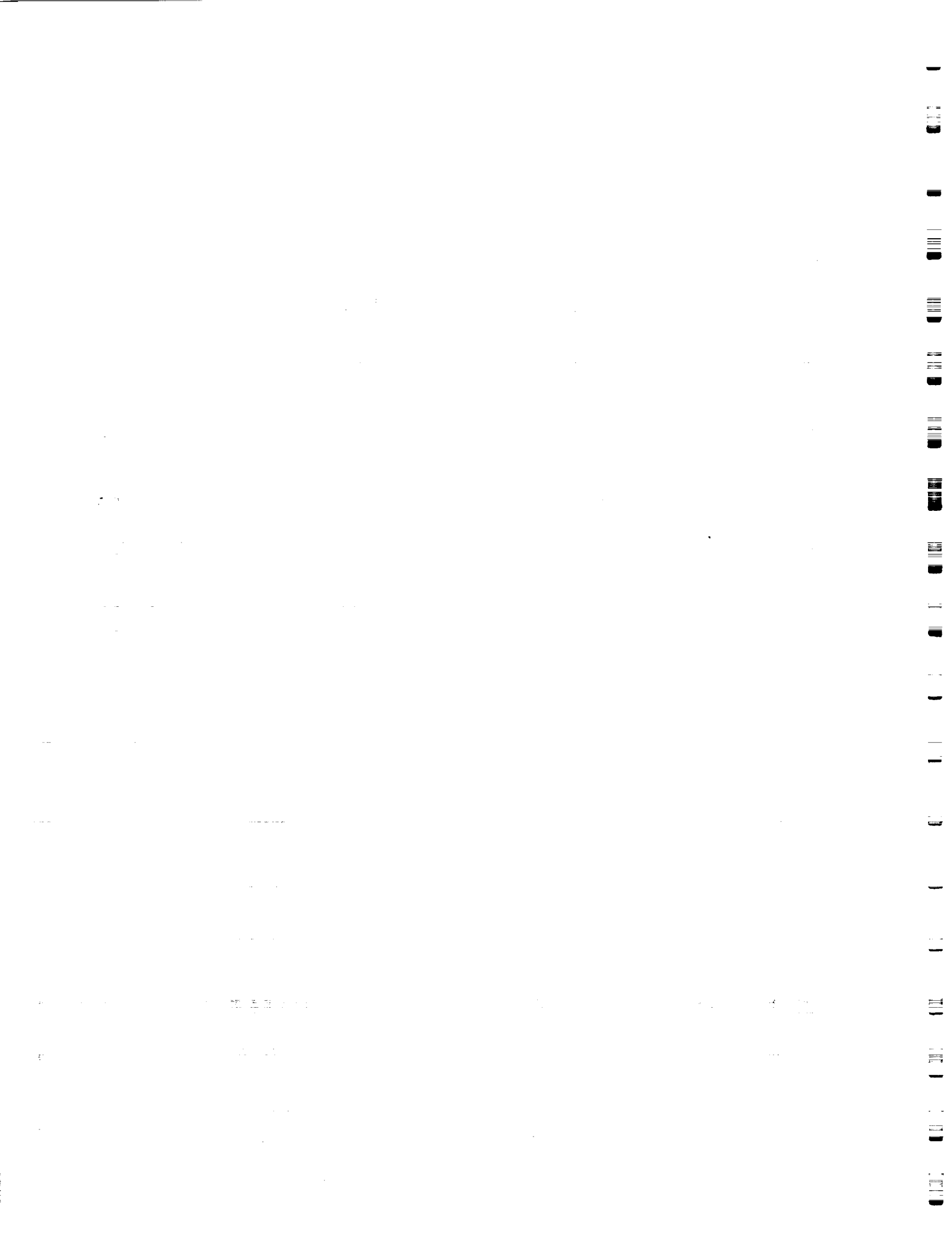


Figure 16-Circumferentially and Axially Averaged Heat Transfer Coefficient as a Function of the Net Power Generation for a Single-Side Heated, Smooth Channel



(1) single-phase flow regime occurs in the region where $\phi > \phi_{\text{ONB}}$, (2) stable nucleate boiling regime occurs in the region $\Delta\phi < \phi < \phi_{\text{ONB}}$, and (3) stable film boiling regime occurs for $\phi < \Delta\phi$. A similar condition was postulated by Boyd et al. [20] and similar observations were recently observed by Marshall et al. [21] who used water as the working fluid. This stable circumferential distribution seems to be preserved by energetic mixing and flow regime interaction. The result of this stable flow is a continual increase in h with power (see Figure 16) until a second and less pronounced CHF occurs. Figures 14a through 14f show that this occurred at a power level of about 500.0 W, which is more than a factor of two above the first CHF.

Figure 16 also compares the overall h obtained for a vertical channel from the present work with similar results for a horizontal channel, which was obtained by Smith [30]. Smith's results for h had to be updated (see Boyd et al., [4]) from the reported circumferentially and axially averaged heat transfer coefficients. Direct comparisons with our mass flow rate of 210.0 kg/m²s cannot be made because of different mass flow rates for horizontal channel. Efforts are on the way to run cases with identical flow rates so quantitative comparisons can be made. However, qualitative comparisons can be made with the horizontal flow case of 184.84 kg/m²s. The heat transfer coefficient, h , increases with power for both cases, but the peak value of h for the horizontal flow (Top-Heating) near the second CHF (ultimate CHF) is almost twenty percent less than that obtained for the vertical. This difference can be attributed to the difference in mass velocity to some extent, but further investigation will indicate the extent of this contribution. The present results for the horizontal case indicate that the mass velocity influence on h is small in the range between 92.0 and 184 kg/m²s, which implies that the difference shown in Figure 16 between the horizontal and vertical flow is due to principally the orientation differences. Finally, the power level at which the second CHF occurred for the horizontal flow is more than forty percent less than that for the vertical flow.

As stated before, the circumferential measurement of wall temperature was made at seven circumferentially locations rather than four as used by Boyd et al. [4], Smith [12], and Turknett [13]. The effect of selected locations for the circumferential temperature measurement on mean heat transfer coefficient is given by Figure 17. Shown are plots of h as a function of power when seven and four circumferential measurement locations were used. It is clear that the more circumferential measurement locations used for the temperature, the more accurate the value of

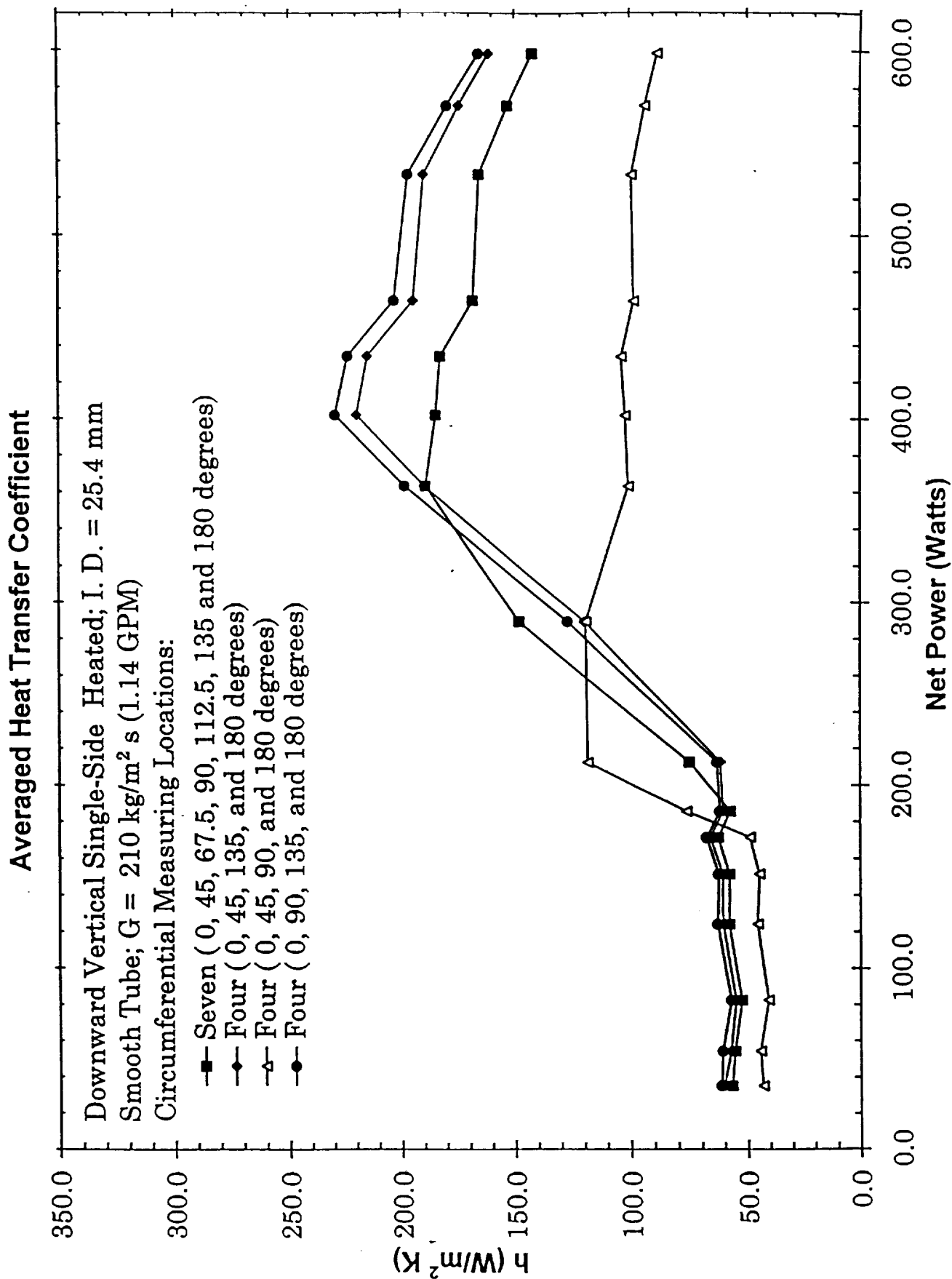
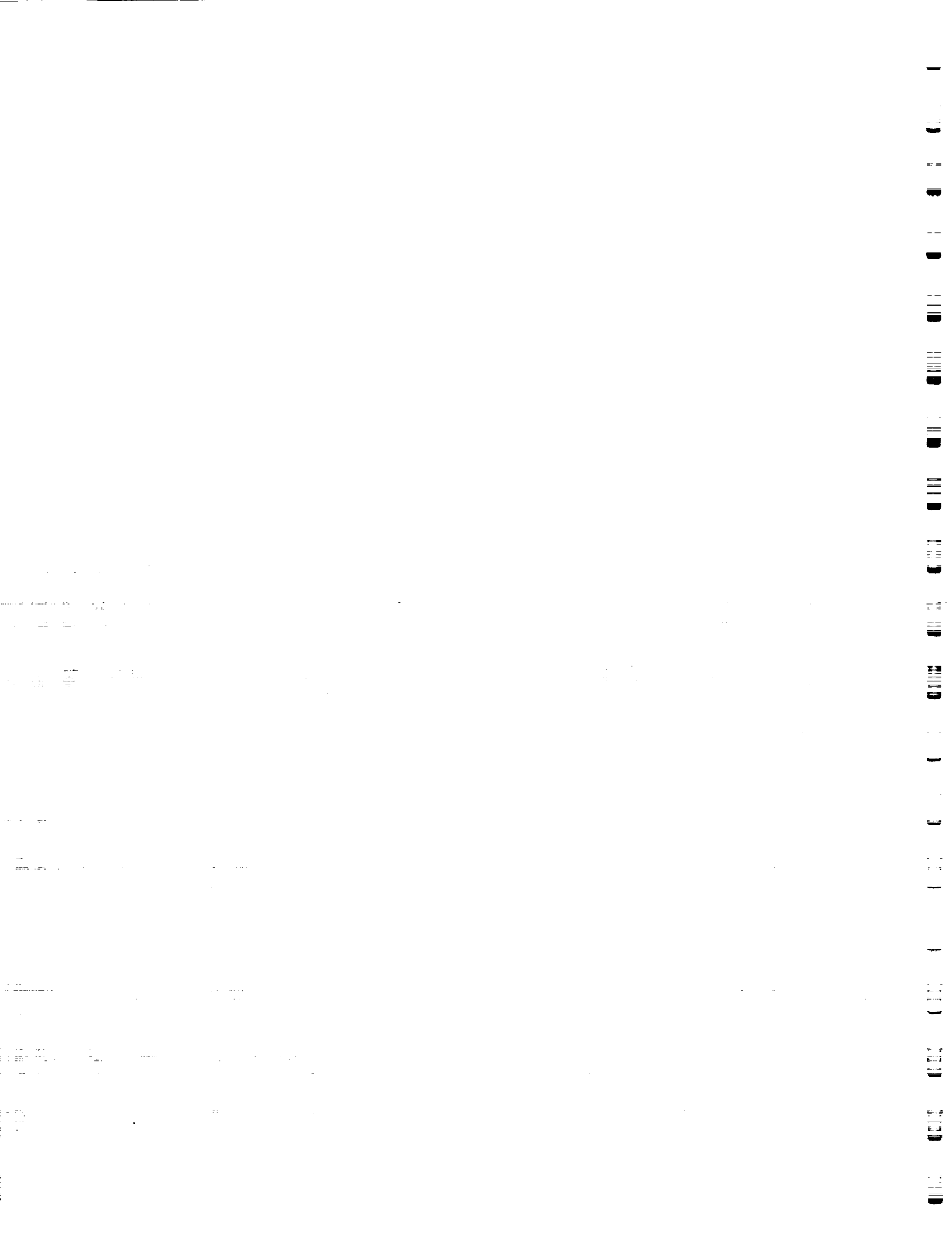


Figure 17: Circumferentially and Axially Averaged Heat Transfer Coefficient for Different Circumferential Temperature Measuring Locations as a Function of the Net Power Generation for a Single-Side Heated, Smooth Channel.



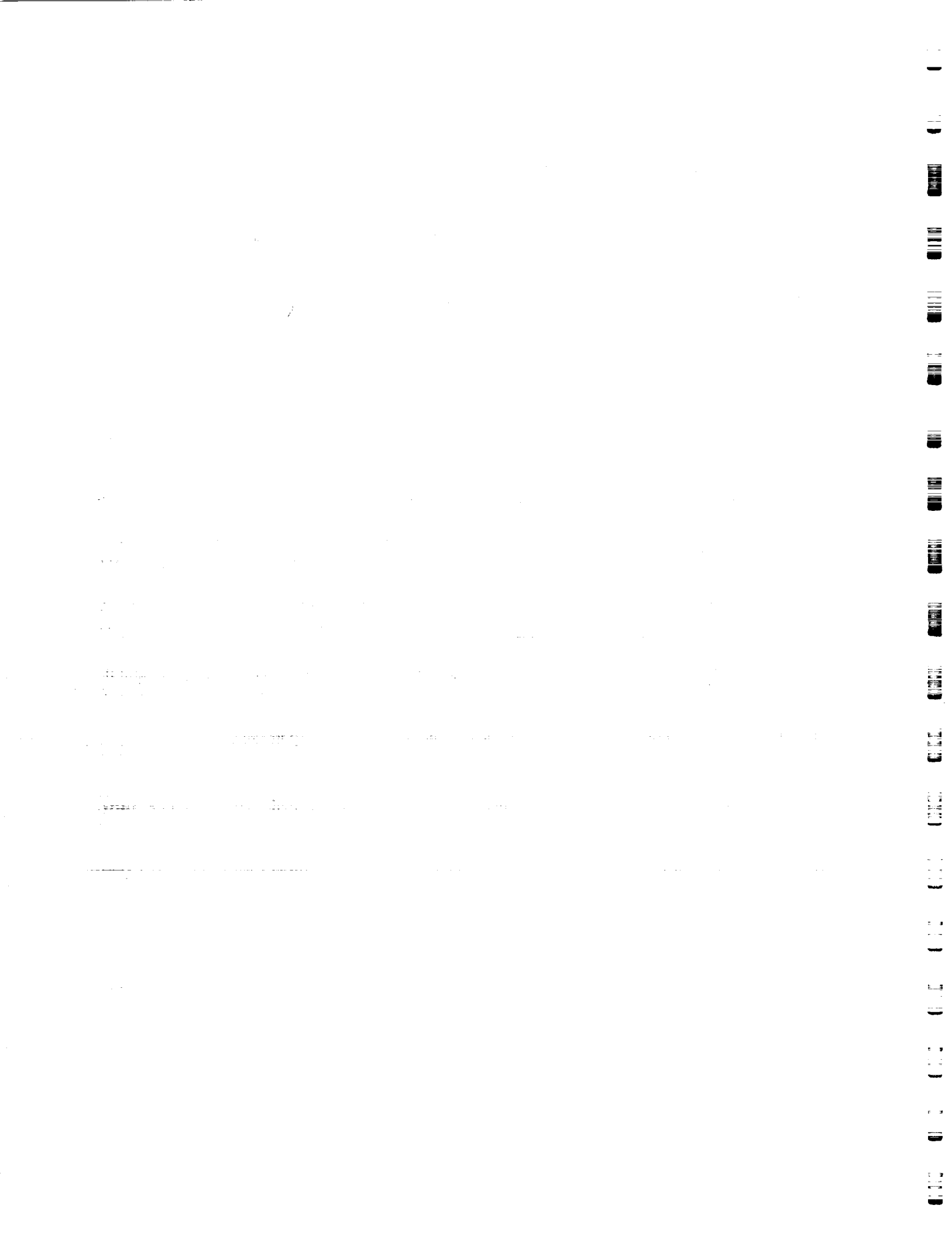
the mean h and better the resolution for later determinations of local variations in the heat transfer coefficient. But if for cost or geometric restrictions of the channel only four circumferential temperature measurements can be made, what are the best locations which will result in a good estimate for h ? The results in Figure 17 show that the circumferential locations used by Boyd et al. [4], Smith [12], and Turknett [13] resulted in the best agreement with the case where seven circumferential locations were chosen (present work). Further efforts are needed to obtain the local (axial and circumferential) heat transfer coefficient using a non-linear inverse conduction approach (Huque and Boyd, [19]).

2.6 SUMMARY

In this work, 2-D (circumferential and axial) wall temperature measurements, and circumferentially-and-axially averaged heat transfer coefficient (h) distributions were presented for the forced convection boiling of Freon-11 in a single-side heated vertical channel with downward flow for a mass flow rate of $210.0 \text{ kg/m}^2\text{s}$. Experimental data was obtained for 2-D wall temperature distributions and axial distributions of mean wall temperature (circumferentially averaged), which was reduced to obtain h .

This work confirms recent observations by Marshall et al. [21] and previous postulations by Boyd et al. [4]. It shows that the effects of single-side heating are to allow multiple levels of critical heat flux to occur before the channel wall is no longer wetted by liquid phase.

Additional work is needed to extend the results to wider ranges of G , inlet temperature, heating configuration, and D so that: (1) further comparisons can be made with horizontal flow, (2) local and mean variations in the heat transfer coefficient can be obtained, and (3) a basis can be established for testing existing and new correlations, as well as forced convection and flow boiling numerical models.



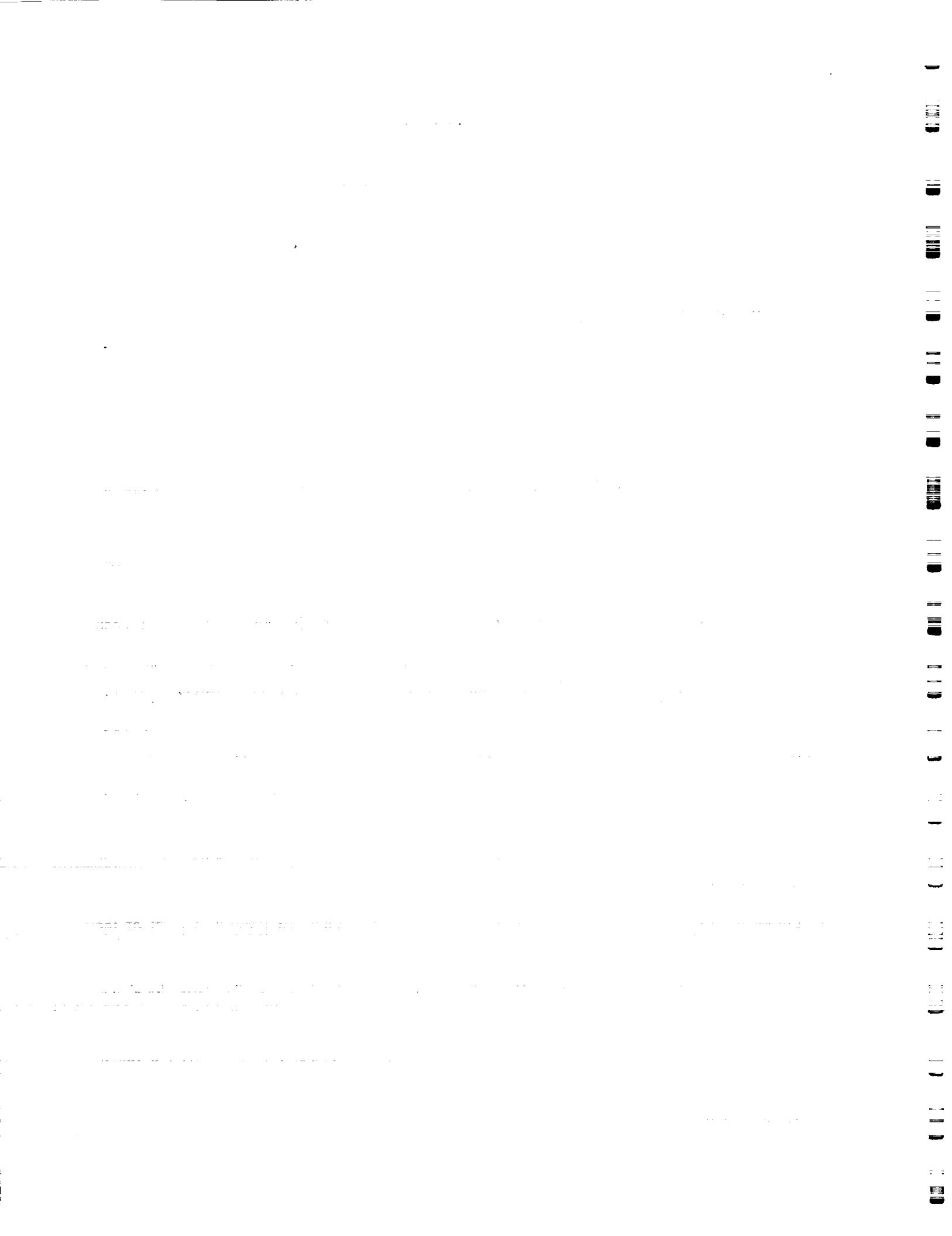
3.0 SUBCOOLED FLOW BOILING IN SINGLE-SIDE HEATED VERTICAL CHANNELS WITH DOWNWARD FLOW; PART I: THE EFFECT OF ORIENTATION BASED ON THE AVERAGED HEAT TRANSFER COEFFICIENT

3.1 INTRODUCTION AND LITERATURE SURVEY

Flow boiling is the most commonly used heat transfer technique in industry. Industries such as aerospace, nuclear, power generation, chemical processing, and electronics use flow boiling heat transfer processes to transport large quantities of power at fairly low wall temperatures.

Due to extensive use of flow boiling heat transfer in industries, basic features of the boiling phenomena have been extensively investigated for more than sixty (60) years, and large data base encompassing a variety of fluids with wide ranges of pressure and flow rates have been developed and correlated.

Most widely quoted flow boiling heat transfer coefficient (h) correlations have been developed from large data banks for vertical upflow with the majority of the data being in the vapor quality range from 0.0 to 0.5. These include correlations by Chen [22], Shah [23], Steiner et al. [24], and Winterton and his coworkers [25 - 27]. Some of these correlations have also been extended to flow boiling inside horizontal tubes. There are several weak points in this approach. First of all, above the stratified flow threshold criterion, it is assumed that there is no tube orientation effect on heat transfer. Below the threshold, there is a reduction in h because the tube circumference is only partially wetted with liquid and dry at the top. This reduction in h is predicted by adding an empirical correction term to the vertical tube correlation. However, these empirical corrections have been developed by statistical regression to improve the fit of the vertical tube correlation to the horizontal tube boiling data bank rather than by a direct comparison of experimental test data for vertical and horizontal flows at the same local test conditions. Consequently, effects other than stratification may be involved. Hence, these potentially important other effects (which could include other stratification influences; e.g. due to reduced gravity) will be manifested as weak influences in existing design correlations for horizontal tubes.



Several researchers have used the threshold criterion in their correlations for both vertical and horizontal flow. The most widely used stratified threshold criterion for applying vertical flow boiling correlations to horizontal flows is the liquid Froude number, defined as

$$Fr_L = G^2 / [g D \rho_L^2]. \quad (3)$$

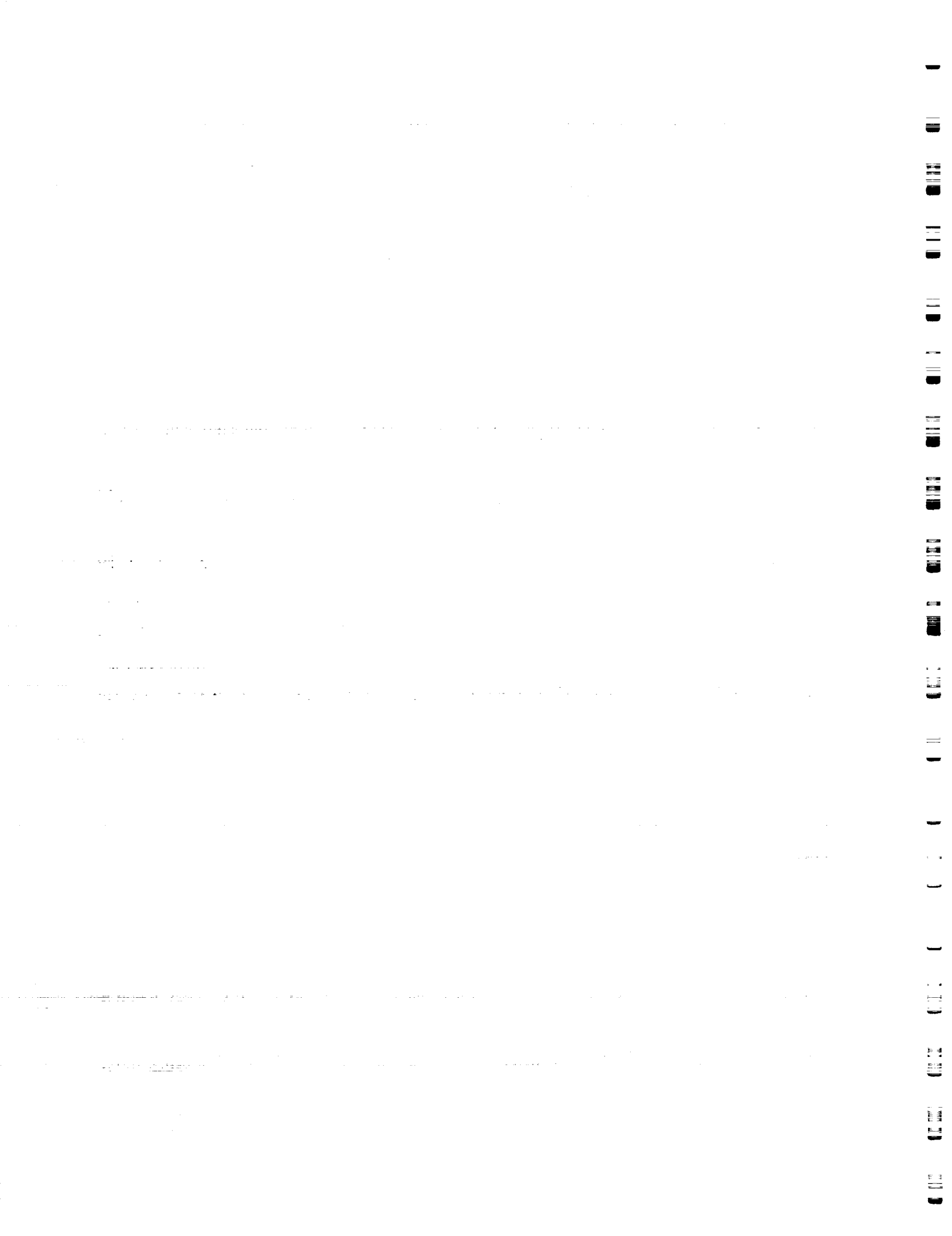
For $Fr_L < 0.04$, Shah [23] recommended that both the convective boiling and nucleate boiling heat transfer coefficient be determined by separate correlations. Gungor and Winterton [26] on other hand defined the threshold for Fr_L to be **0.05**. In addition, they modified both the convection enhancement factor (**F**) by multiplying by a factor E_2 and boiling suppression factor (**S**) by multiplying by a factor E_1 . Both E_2 and E_1 have a reducing effect and are given by

$$E_2 = Fr_L^{[0.1 - 2 Fr_L]} \quad (4)$$

$$E_1 = Fr_L^{0.5}$$

Using a Shah type correlation, Kandlikar [28] developed a new correlation which retained the Shah threshold value of **0.04**. More recently, Kattan et al [29] obtained experimental data on flow regimes and the threshold between stratified and unstratified flow. They found that the liquid Froude number criterion ($Fr_L = 0.04, 0.05$, etc.) used by many flow boiling correlations is incapable of delineating the transition between stratified and unstratified flow data of refrigerants, and called the use of vertical tube correlation to model heat transfer in horizontal tubes “questionable.”

Until recently very few researchers have investigated the effect of orientation based on fundamental flow analysis. Recently, Kattan et. al. [29] studied orientation effects for R-134a flow boiling in horizontal flow, vertical upflow, and vertical downward flow using a 12 mm diameter tube over wide ranges of mass velocities, vapor qualities and heat flux. They found a significant effect of flow direction on local heat transfer coefficient. The experimental data showed that the horizontal tube heat transfer coefficients ranged from 47% to 38% below those for vertical upflow. The vertical downflow data were significantly below the data for **h** for both



horizontal flow and vertical upward conditions. The lower coefficients for downflow compared to upflow and horizontal flow were not expected by Kattan et. al. [29], and they tried to explain this by hypothesizing that buoyancy effects of vapor, which opposes downward flow may reduce its accelerating effects on the liquid and hence diminish the convective contribution to heat transfer. The lower heat transfer coefficients for horizontal tube as compared to vertical upward flow at low flow rates can be explained as a result of flow stratification in the horizontal tube. As they observed, these differences between horizontal and vertical upward flows diminish and even reverse in nature as the heat flux and quality increase.

One other fundamental difference between the boiling in upflow, downflow, and horizontal flow which can have significant effect of heat transfer was also hypothesized by Kattan et. al. as the subcooling effect of the pressure gradient on the process. Very recently, Kirk et. al. [30] looked into the effect of low-velocity subcooled flow boiling at various orientations for R-113 flowing in rectangular channels. They found that at very low velocities where buoyancy is dominant, the effect of orientation is very pronounced. In low-velocity domain, and as the channel is rotated from horizontal position to the vertical upflow position, a significant enhancement of heat transfer takes place at low levels of heat flux with enhancement diminishing as heat flux is increased. They also found that a limiting flow velocity exists beyond which the orientation and gravity can be completely neglected. Both the studies by Kattan et al. and Kirk et al., establishes the fact that the effect of flow velocity on heat transfer is very much dependent on flow orientation and has some surprising influences.

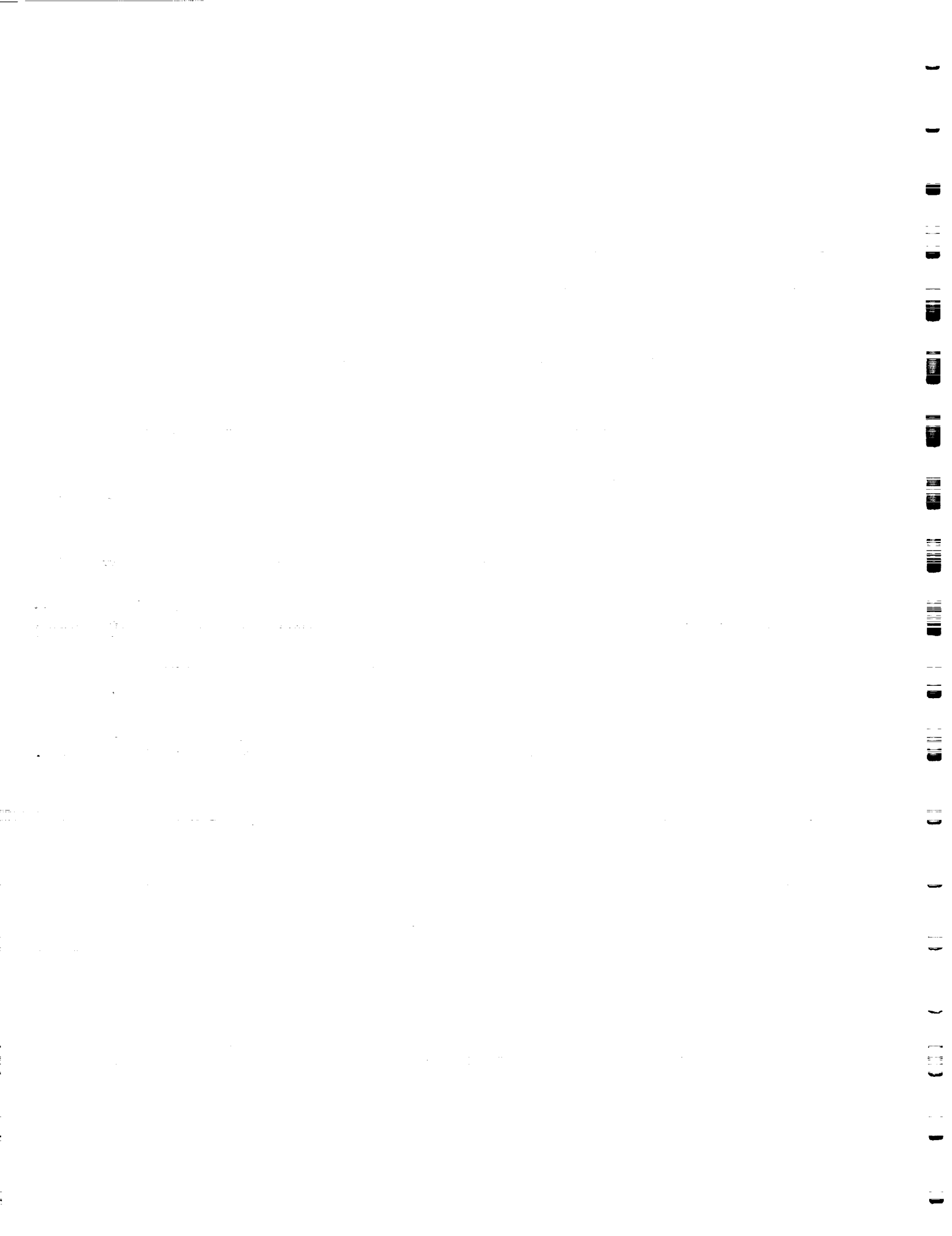
From the discussion above, it is clear that the efforts have just been started in understanding the orientation effects on heat transfer and we have a long way to go. In this work, we extend the previous studies to include single-side heated channels for downward and horizontal flow. Efforts will be made to study the effect of flow orientation using fundamental flow analysis by comparing quasi-boiling curves and heat transfer coefficients for identical flow conditions for a top-side heated horizontal flow and a single-side heated vertical downward flow.

3.2 RESULTS

One of the objectives of this work is to study the effect of flow orientation on flow boiling heat transfer in single-side heated geometries. In order to accomplish this goal, two independent sets of experiments were ran. One setup was to study horizontal flow boiling heat transfer under top-side heating conditions, and the other to study vertical downward flow boiling heat transfer under single-side heating conditions. Although we refer to the channel surface in this paper as being smooth, its surface conditions can be described as: "as received." However, all test sections were thoroughly cleaned with cotton and steel wool. The detailed description of the experimental flow boiling loop, test sections used, and the experimental procedure are explained in detail for both the setups in Section #1, and elsewhere [12]. The readers are also referred to the above references for the procedure of data reduction analysis and thermal modeling which is used to obtain the heat transfer coefficients.

In this work, the results for the three experimental test cases will be presented which were run under identical flow conditions for both horizontal and vertical downflow. The complete 2-D (axial and circumferential) wall temperature distributions, and axially and circumferentially averaged heat transfer coefficient ($h_{a,v}$) distributions will be presented for Freon-11 flowing in a 25.4 mm inside diameter (I. D.) tube, with a mass velocity (G) of 184.0 kg/m²s, an inlet temperature of 22.6 °C, and an exit pressure of 0.1843 MPa (absolute). For the same inlet temperature and exit pressure conditions given above, only axially and circumferentially averaged mean heat transfer coefficients will be presented for Freon-11 flowing in 19.1 mm, and 12.7 mm I. D. (D) tubes with mass flow rates of 246.45 kg/m²s and 520.78 kg/m²s, respectively. Finally, the single-side heating configuration for both orientations consist of: (1) a heated section for the circumferential coordinate (ϕ) between -90.0 degrees to + 90.0 degrees, and (2) an unheated insulated section for 90.0 degrees < ϕ < 270.0 degrees. For the horizontal channel, the heating is top-side heating with the plane of symmetry being vertical. The axial coordinate (Z) is measured from the beginning of the heated section, where the flow is hydrodynamically fully developed at $Z = 0$. The heated length was 1.22 m.

Figures 18a-18d show the distributions as measured outside wall temperature at different circumferential and axial locations for both horizontal and vertical downward flow. The Vertical



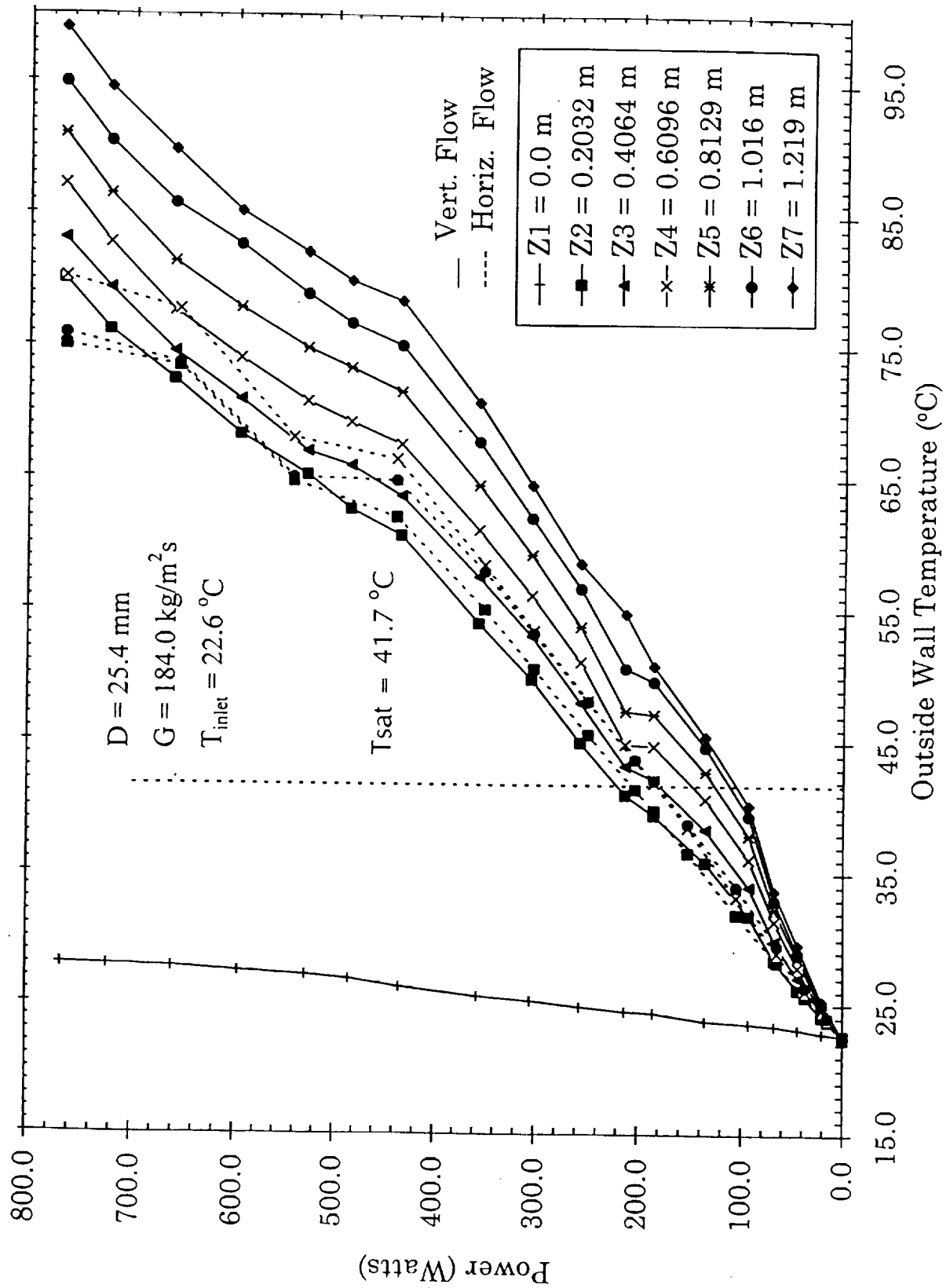


Figure 18a: Measured Outside Wall Temperature (Copper Channel) Axial Variation as a Function of the Net Power Generation for a Single-Side Heated Smooth Channel for Vertical Downward and Horizontal Flow, for $\phi = 0.0$ Degrees.

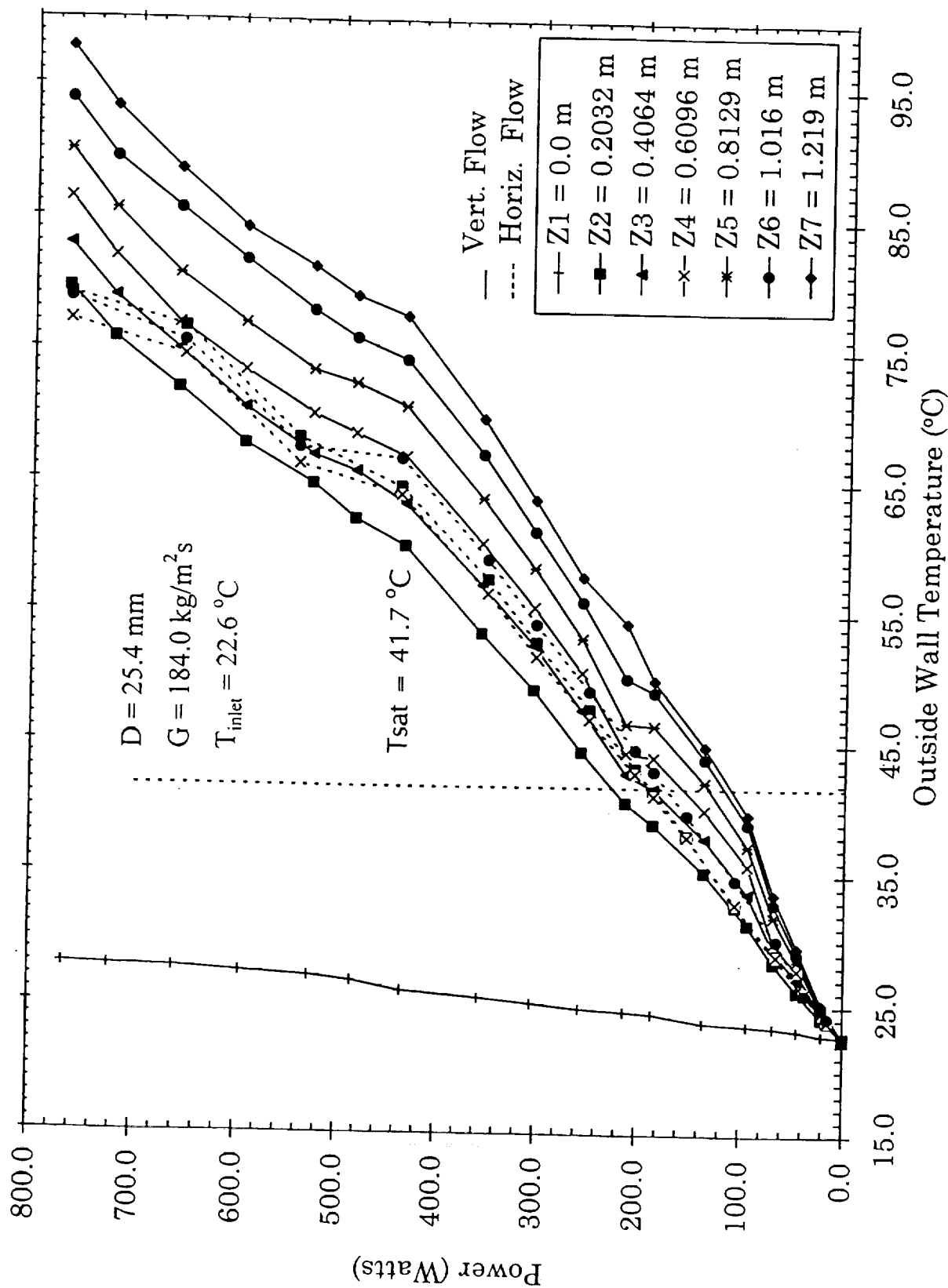
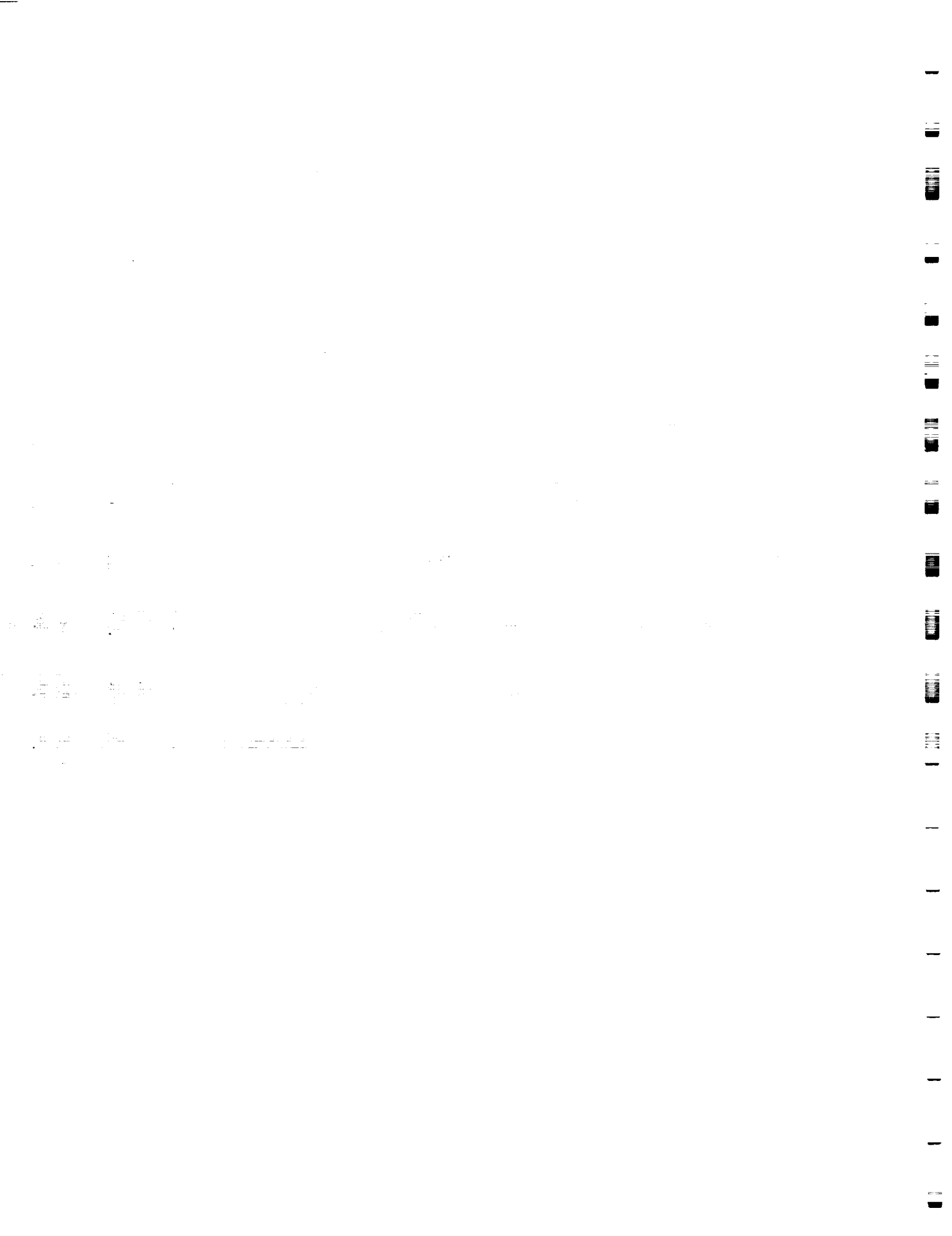


Figure 18b: Measured Outside Wall Temperature (Copper Channel) Axial Variation as a Function of the Net Power Generation for a Single-Side Heated Smooth Channel for Vertical Downward and Horizontal Flow, for $\phi = 45.0$ Degrees.



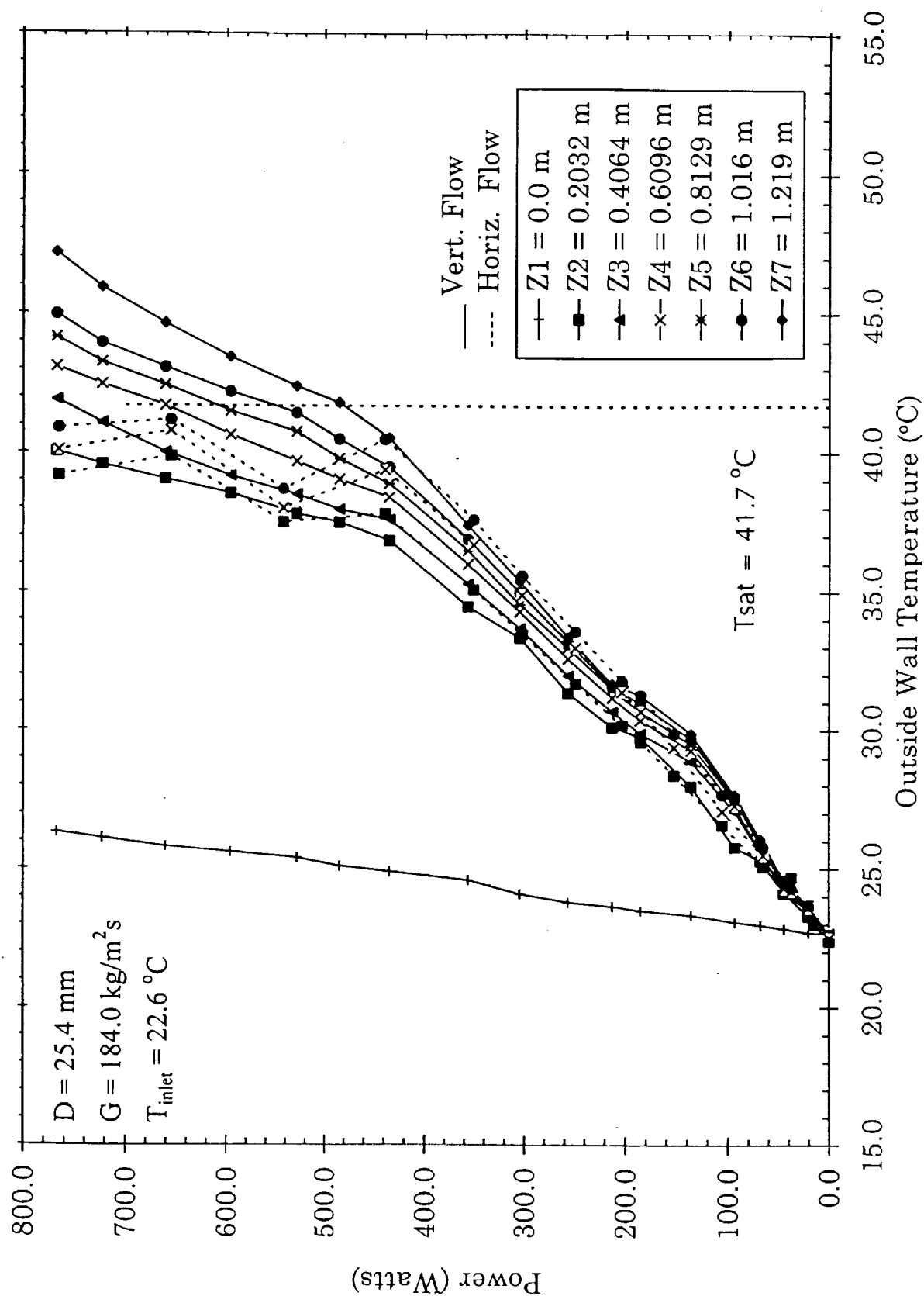
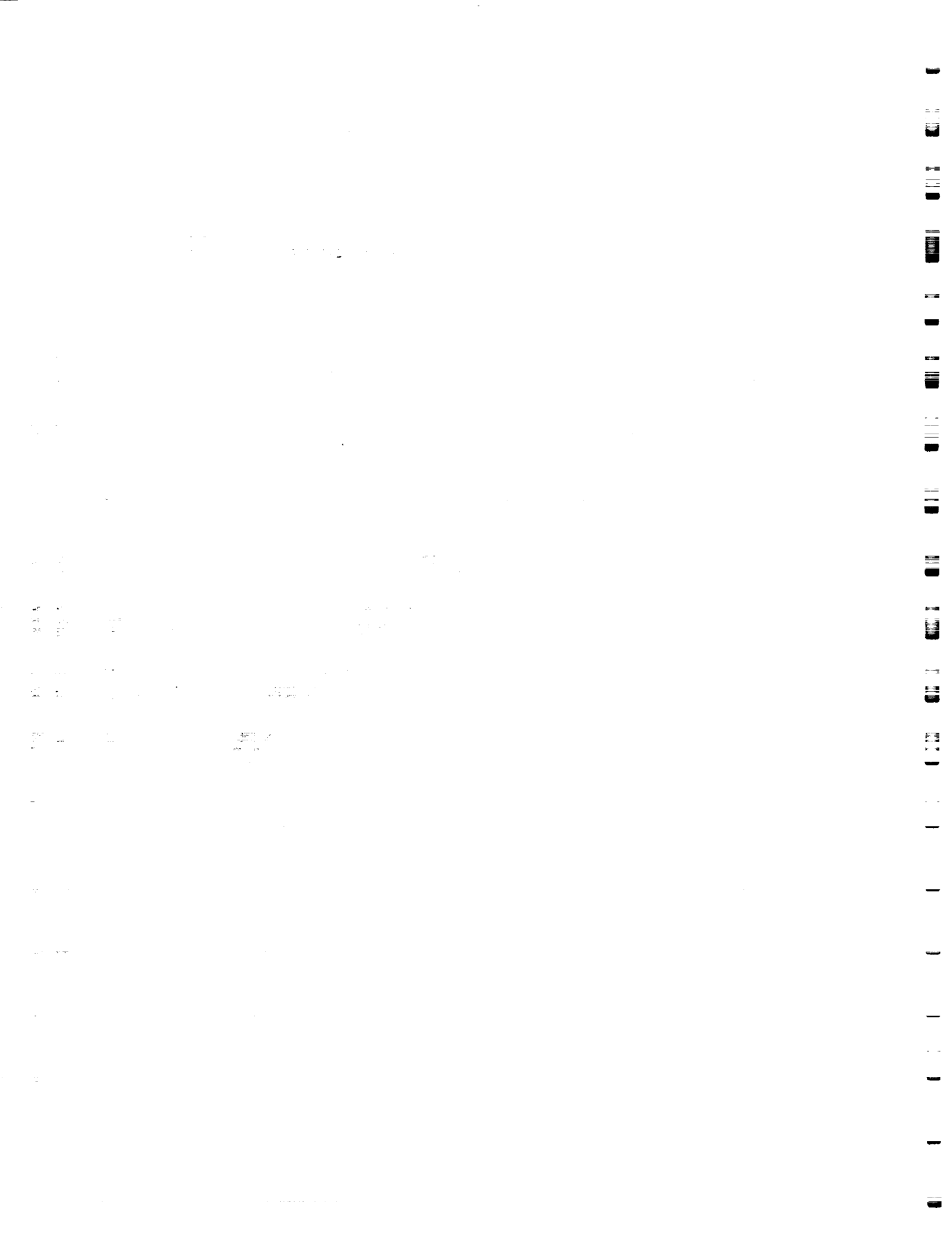


Figure 18c: Measured Outside Wall Temperature (Copper Channel) Axial Variation as a Function of the Net Power Generation for a Single-Side Heated Smooth Channel for Vertical Downward and Horizontal Flow, for $\phi = 135.0 \text{ Degrees}$.



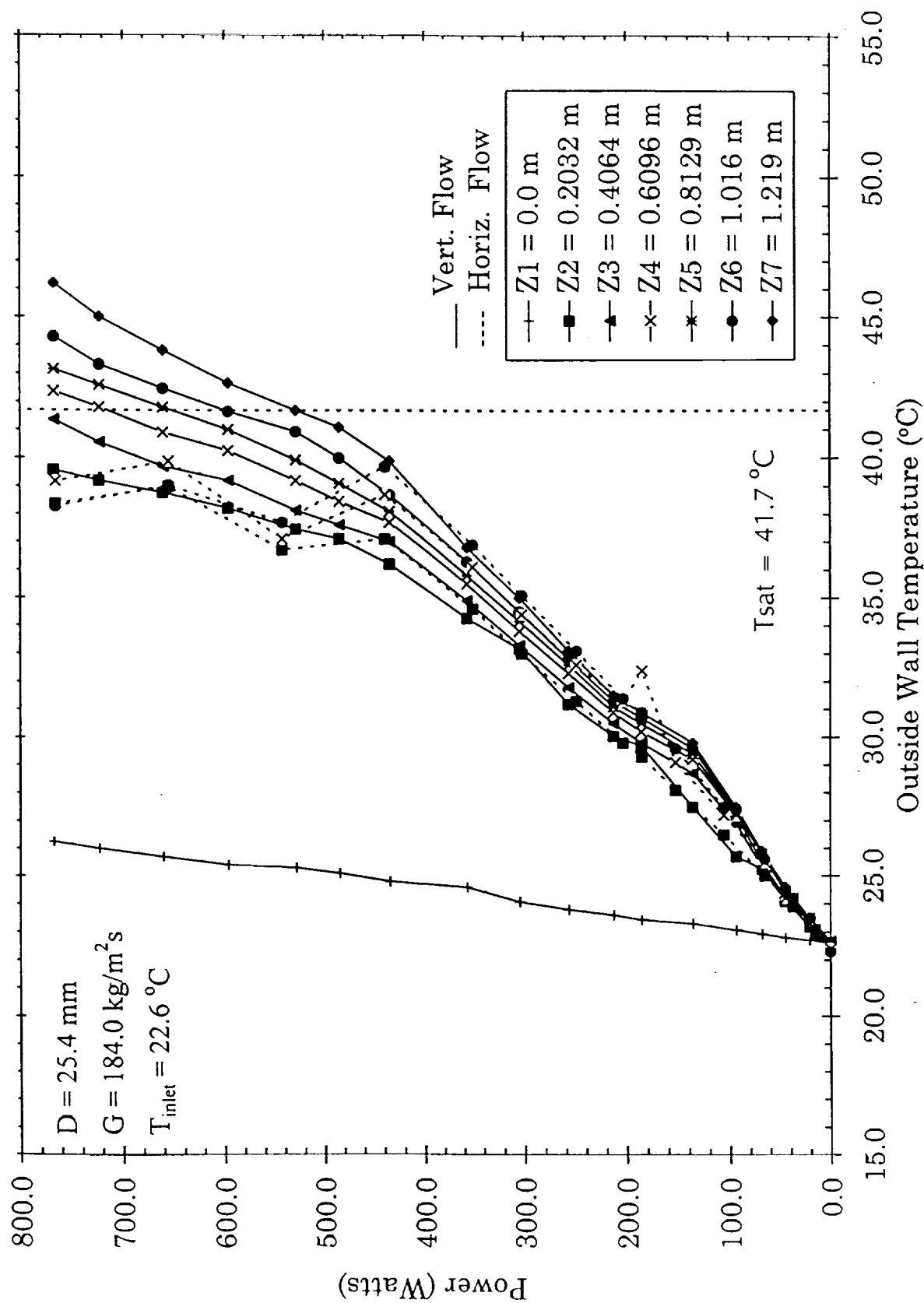
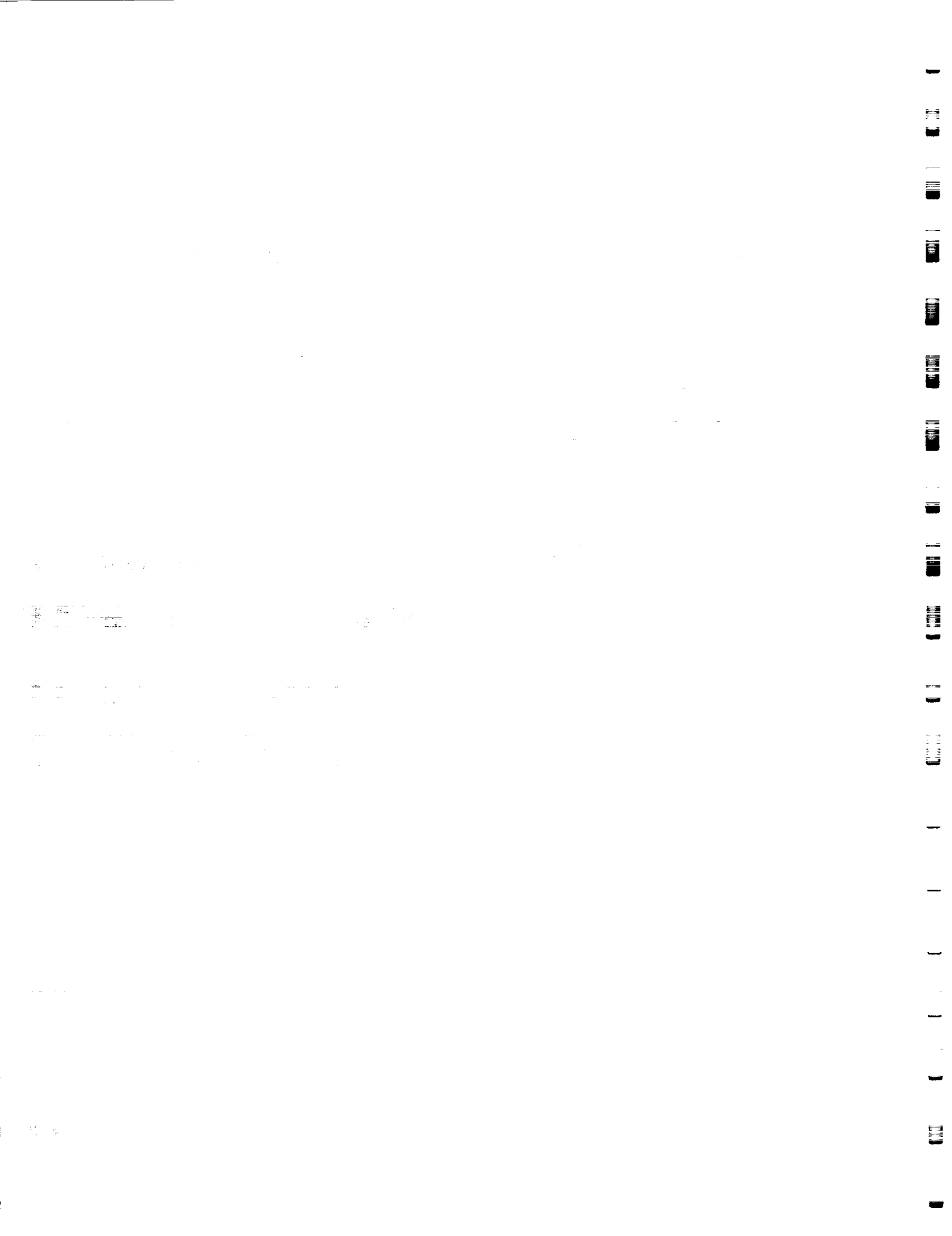


Figure 18d: Measured Outside Wall Temperature (Copper Channel) Axial Variation as a Function of the Net Power Generation for a Single-Side Heated Smooth Channel for Vertical Downward and Horizontal Flow, for $\phi = 180.0$ Degrees.



flow temperature profile is given by solid lines and horizontal by dashed lines. For the vertical downward flow, the wall temperature increased as the fluid flowed from upstream to downstream (axial locations #1 to #7) in the test section. Furthermore as ϕ varied from 0 to π , the temperature decreased circumferentially because of a change from a circumferentially heated region ($\phi = 0$ to $\pi/2$) to a non-heated one ($\phi = \pi/2$ to π). The similar trends can be observed for the horizontal flow case, but here the wall temperature first increased as the fluid flowed from upstream to downstream, axial locations #1 to #4, but later decreased significantly for axial locations #5 to #7. This decrease in the wall temperature for the downstream axial location is not attributed to any physical phenomenon unique to the top-side heating case, but rather it is due to the experimental setup [12], where the chiller which was used to regulate the inlet temperature to the test section was located just after the exit of the test section. This placement of the chiller causes the wall temperature at the axial locations #5, #6 and #7 to be significantly lower than other upstream locations. Accordingly, we have restricted our discussion to axial locations #2 through #4 for the horizontal flow case. From the figures, one observes that the wall temperatures at $\phi = 0$ remain above the saturation temperature ($T_{sat} = 41.65\text{ }^{\circ}\text{C}$) for most power levels and below T_{sat} regardless of the flow orientation for $\phi = 3\pi/4$ and π at all except the highest power levels for $Z < 0.6\text{ m}$.

The onset to nucleate boiling (ONB) was estimated using the Davis-Anderson correlation [17]. For the experimental specifications shown in Figure 18a-18d, the ONB was estimated to occur at an inside wall temperature (ONB) of $43.2\text{ }^{\circ}\text{C}$. Since this temperature cannot be compared directly with the measured outside wall temperatures (T_{wo}) shown in Figure 18a-18d, it can serve as a lower bound for the outside wall temperatures (ONBO) at which ONB occurred at different axial locations. Using ONB as one indicator and the shape changes of the measured net power (P) versus T_{wo} curve, some qualitative descriptions can be made about the evolution of the two-dimensional boiling front with respect to flow orientation for single-side heated channels. From Figure 18a-18d, clear evidence of the orientation effect is manifested by T_{wo} for the horizontal flow boiling being consistently above that for vertical flow for $Z > 0.2\text{m}$ and all values of ϕ . As demonstrated in Figure 19, this has the effect of reducing h_{av} for the horizontal orientation when compared to the vertical flow. At higher power levels above 400.0 W for the

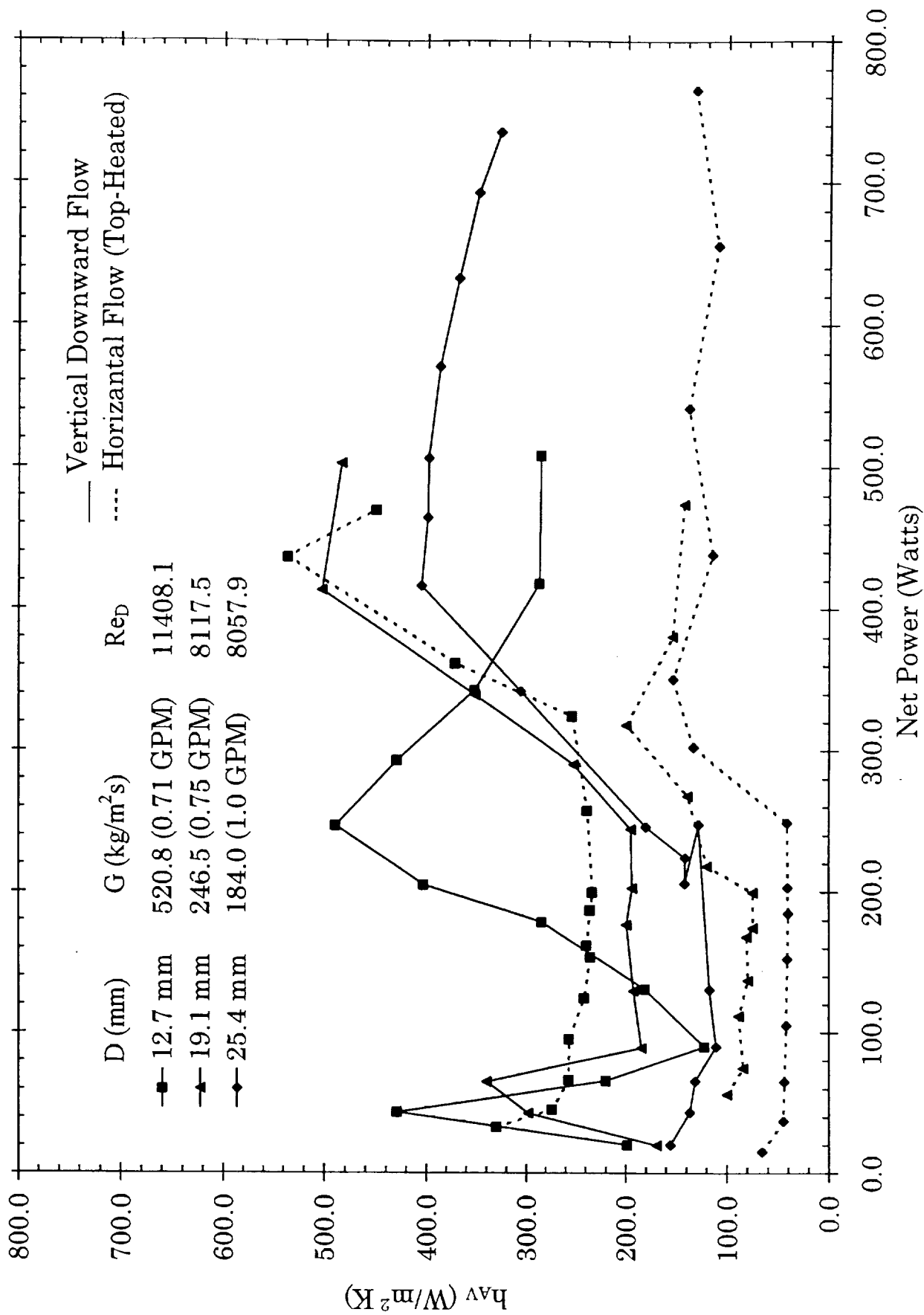


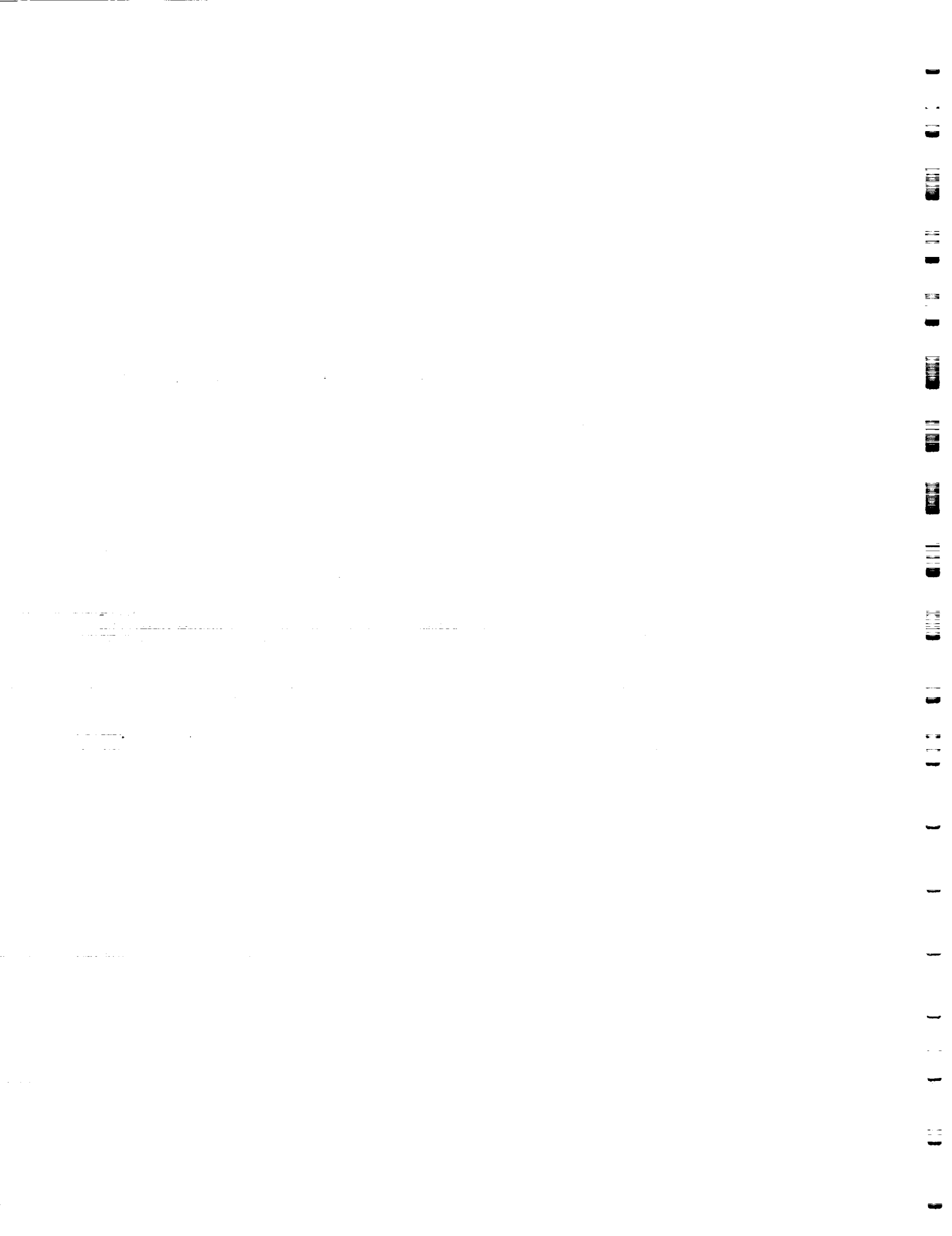
Figure 19: Circumferentially and Axially Averaged Heat Transfer Coefficient as a Function of Net Power Generation for a Single-Side Heated Smooth Channel

horizontal flow, there appears to be rewetting phenomenon which is initiated and then disappears as the power was increased.

In Figure 19, G is increasing and D is decreasing from case to case. However, the Reynolds number for the two largest values of D are almost identical. Although variations of h_{av} with power are different for the two cases, there are some similarities. When one take into account that the L/D are quite different for the two cases, it indicates that a better correlation and comparison could be made by comparing the axial distributions of the circumferentially averaged heat transfer coefficient. For a fifty percent increase in the Reynolds number, h_{av} for the horizontal flow increased by a factor of two in some cases and actually exceeded h_{av} for the vertical downward flow. The present work will be expanded later in a second part to include the effects that both single-side heating and orientation have on the axial distribution of the heat transfer coefficient.

3.3 SUMMARY

In this work, results have been presented for identical test runs for horizontal top-side heated flow, and vertical downward flow to study the effect of orientation on heat transfer data. The results show that horizontal flow heat transfer data is significantly lower than vertical downward flow data, which is the opposite relationship observed for uniformly heated flow channels. However, as both the Reynolds number and heat flux increase, the relationship changes. This study should be extended to investigate these effects further by comparing the axial distributions of the heat transfer coefficient.



4.0 SUBCOOLED FLOW BOILING IN SINGLE-SIDE HEATED VERTICAL CHANNELS WITH DOWNWARD FLOW; PART II: COMPARISONS WITH SELECTED TWO-PHASE CORRELATIONS

4.1 INTRODUCTION

Subcooled flow boiling can accommodate high levels of heat flux in a variety of diverse processes and applications such as advance space thermal management systems, plasma-facing fusion components, electronic and computer components, and manufacturing and material processing.

Subcooled flow boiling heat transfer is a complicated phenomenon involving many factors, among which heat flux distribution on the channel wall is an important one. Beside the heat flux distribution, there are many different variables which influence the flow boiling heat transfer. These variables include pressure, mass flow rate, quality, thermophysical properties, wall material, surface characteristics, and channel geometry. A clear understanding of the influence of different variables on heat transfer during single-phase flow may be obtained through analytical equations and well established empirical correlations, but flow boiling heat transfer is more complex due to interactions between the two phases with the channel in the presence of both convective and boiling modes of heat transfer. However by introducing reasonable physical abstraction, it is sometimes possible to greatly simplify the problem and to obtain acceptable results.

In the past, one of the first simplifying assumptions made to advance the two-phase flow boiling theory was to study heat transfer in uniformly heated tubes. This simple geometry was used usually to: (1) decrease the experimental complexity, (2) directly use previous single-phase data as a basis to isolate the boiling contribution, and (3) to avoid the inclusion of the complexity of circumferential heat flux variations on the channel inner wall. From the literature, it is clear that there has been much work completed for flow boiling heat transfer correlations for a uniform heat flux distribution. Correlations presented by Chen [22], Shah [23], Kandlikar [5], [28], Steiner et.al. [24], Winterton and his co-workers [25, 26] and Boyd and Meng [8] cover different fluids, vast ranges of flow rates, the entire spectrum of quality, and low and high subcooling.

1. *What is the purpose of the study?*
 2. *What are the research objectives?*
 3. *What is the research design?*
 4. *What are the variables?*
 5. *What is the sample size?*
 6. *What are the data sources?*
 7. *What are the data collection methods?*
 8. *What are the data analysis methods?*
 9. *What are the results?*
 10. *What are the conclusions?*
 11. *What are the limitations?*
 12. *What are the recommendations?*
 13. *What are the references?*
 14. *What are the appendices?*
 15. *What are the glossary?*
 16. *What are the abbreviations?*
 17. *What are the acronyms?*
 18. *What are the symbols?*
 19. *What are the units?*
 20. *What are the formulas?*
 21. *What are the equations?*
 22. *What are the diagrams?*
 23. *What are the figures?*
 24. *What are the tables?*
 25. *What are the charts?*
 26. *What are the graphs?*
 27. *What are the plots?*
 28. *What are the maps?*
 29. *What are the photos?*
 30. *What are the videos?*
 31. *What are the audios?*
 32. *What are the interviews?*
 33. *What are the focus groups?*
 34. *What are the surveys?*
 35. *What are the experiments?*
 36. *What are the case studies?*
 37. *What are the case analyses?*
 38. *What are the case reports?*
 39. *What are the case studies?*
 40. *What are the case analyses?*
 41. *What are the case reports?*
 42. *What are the case studies?*
 43. *What are the case analyses?*
 44. *What are the case reports?*
 45. *What are the case studies?*
 46. *What are the case analyses?*
 47. *What are the case reports?*
 48. *What are the case studies?*
 49. *What are the case analyses?*
 50. *What are the case reports?*

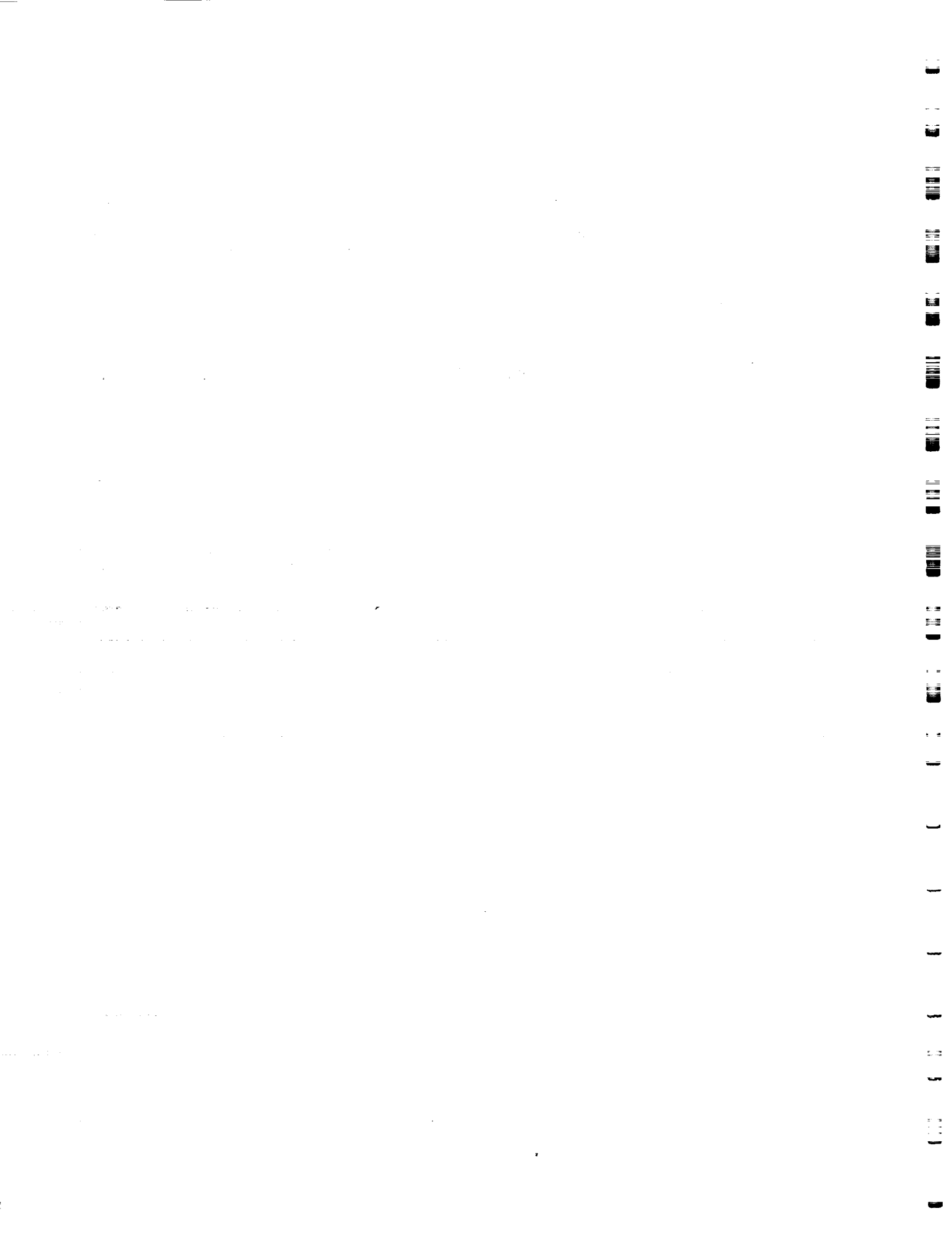
Some of these correlations are recommended for both saturated and subcooled flow boiling. These correlations are valid for only smooth tubes, and one must avoid using them when orientation is important.

As stated above, several researchers have proposed correlations for the prediction of heat transfer coefficients in flow boiling systems. But to simplify the heat transfer modeling and reduce the experimental complexities, most of the research efforts have been limited to heat transfer correlation for uniformly heated channels. In addition, very little effort has been made to study heat transfer in complex and non-uniform heated channels.

In this work, the results of flow boiling heat transfer in non-uniform or single-side heated tubes will be presented, and the experimental heat transfer coefficients will be compared with selected existing single-phase and two-phase flow boiling correlations. In order to establish a basis for the comparisons with data for the single-side heated channel, base-line comparisons for uniformly heated channels will be made with data from: (1) the literature, and (2) from the same flow loop used to produce the single-side heat flux data but with uniformly heated wall conditions. Among the two-phase correlations which will be considered are heat transfer correlations for uniformly heated tubes developed by Shah [23] and Liu and Winterton [25]. Using the results from the above comparisons, we will: (1) assess these correlations and data for the uniform heat flux case, (2) adapt the correlations to the single-side heat flux case, and (3) determine whether more fundamental correlation development work is needed for the single-side heated configurations.

4.2 CORRELATION DESCRIPTION

One objective of the present work is to explore an initial basis for comparisons with heat transfer data in single-side heated channels. As this work is primarily geared toward non-uniform and single-side heat flux boundary conditions, some tests were run under uniform heat flux conditions to provide a baseline check for our single-side heated work. These will be compared first with existing correlations, and then these correlations will be extended to the single-side heated experimental data.



Based on both the criteria of satisfying the range of our experimental parameters and simplicity (or ease of use), two correlations were selected for the comparisons with our single-phase experimental heat transfer data. Accordingly, two different additional correlations were selected for comparisons with the two-phase heat transfer data. Because they are frequently used by many designers and researchers in a variety of engineering fields, the two single-phase correlations selected were: (1) the Dittus-Boelter correlation, and (2) the Petukhov correlation. The two correlations selected for two-phase comparisons were: (1) the Shah correlation, and (2) the Liu-Winterton correlation. A brief description of each of the correlation, along with the procedure of its use, is given below.

Dittus-Boelter Correlation: This correlation is one of the most widely used single-phase heat transfer correlation. The correlation is given below as

$$h_1 = 0.023 \text{ Re}^{0.8} \text{ Pr}^{0.4} (k/D). \quad (5)$$

In this correlation, all the thermophysical properties are evaluated at liquid bulk fluid temperature.

Petukhov's Correlation: This correlation is also one of the most widely used single-phase heat transfer correlation, and is considered to be more accurate than the Dittus-Boelter correlation. Petukhov's correlation is given by

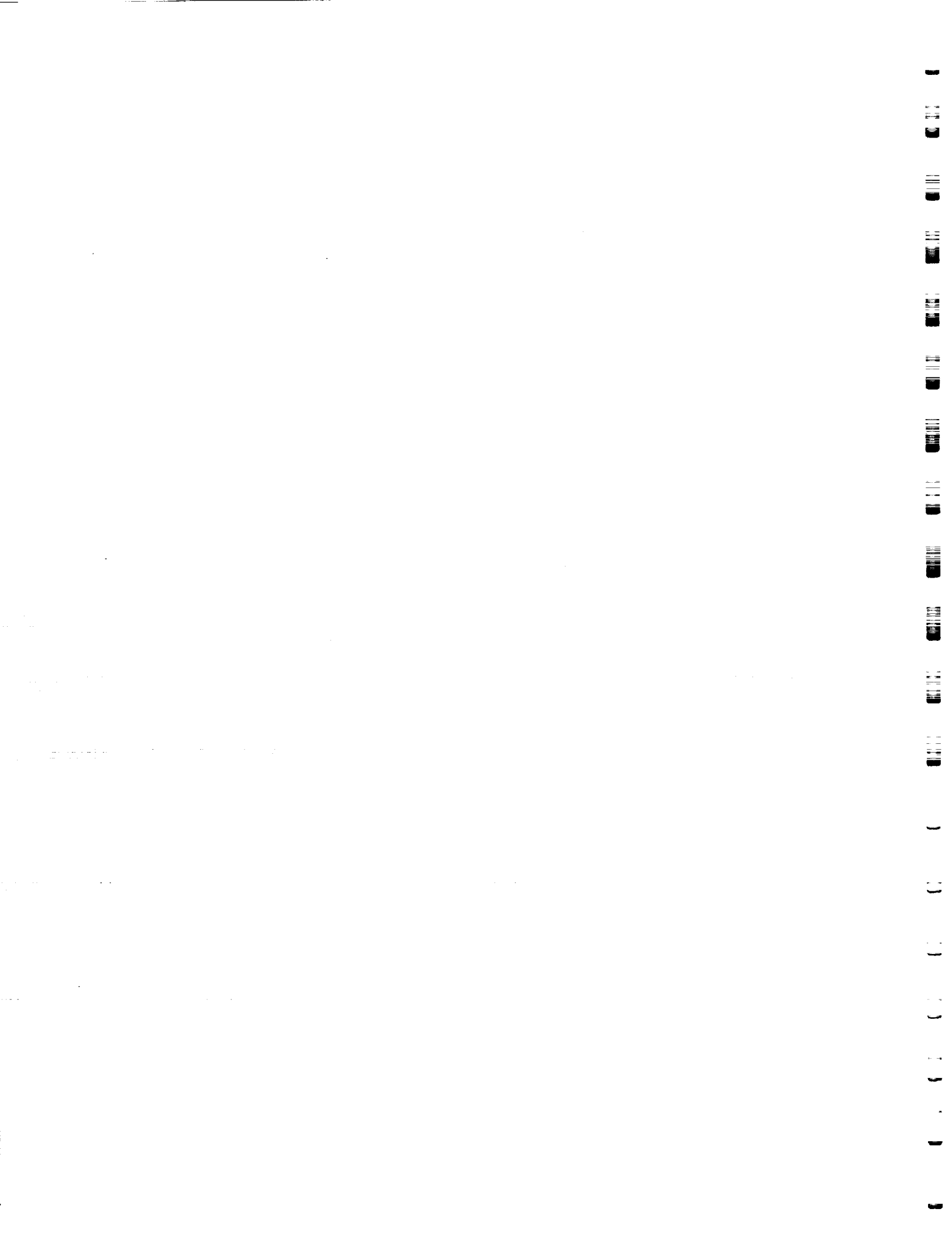
$$h_1 = \frac{(f/8)^{Pe} \left(\frac{\mu}{\mu_w} \right)^n (k/D)}{K_1(f) + K_2(\text{Pr}) \left(\frac{f/8}{\text{Pr}} \right)^{1/2} (\text{Pr}^{2/3} - 1)} \quad (6)$$

$$f = (1.82 \log \text{Re} - 1.64)^{-2}$$

$$K_1(f) = 1 + 3.4 f$$

$$K_2(\text{Pr}) = 11.7 + 1.8 \text{Pr}^{-1/3}$$

$$10^4 < \text{Re} < 5.0 \times 10^6$$



$$0.5 < Pr < 200.0$$

$$n = \begin{cases} 0.11, & \text{for liquid when } T_w > T_b \\ 0.25, & \text{for liquid when } T_w < T_b \\ 0, & \text{for gases and constant heat flux} \\ & \text{boundary conditions.} \end{cases}$$

In the above correlation, all the thermophysical properties are single-phase liquid properties and are evaluated at the film temperature, $(T_w + T_b)/2$.

Shah's Correlation: Shah's correlation is expressed as

$$\frac{h_p}{h_1} = \left[f_1(Bo)^{-1} + x/x^* \right]^{-1} \quad (7)$$

where

$$f_1(Bo) = \begin{cases} 230Bo^{0.5}, & Bo > 3.0 \times 10^{-5} \\ 1 + 46Bo^{0.5}, & Bo \leq 3.0 \times 10^{-5} \end{cases}$$

$$x^* = -\frac{qC_{pc}}{h_1 i_{lg}} = -Bo / St$$

where h_1 is the single-phase heat transfer coefficient. The Dittus-Boelter correlation was suggested for h_1 . In the above correlation, all the thermophysical properties were evaluated at bulk fluid temperature. The standard deviation for this correlation was $\pm 30\%$ over 97% of all the data points.

Liu-Winterton Correlation: The Liu-Winterton correlation was developed for vertical tube flow and is in the form of asymptotic equations, which were correlated using over 3,000 data points. The standard deviation for this correlation was $\pm 25\%$ over the entire range of data.

Their correlation for saturation boiling is given by

$$h_{tp}^2 = (h_l F)^2 + (h_{pool} S)^2 \quad (8)$$

where h_l was evaluated from the Dittus-Boelter correlation. The nucleate boiling heat transfer coefficient, h_{NB} , was evaluated with Cooper's correlation, which is given by

$$h_{pool} = 55 \text{ Pr}^{0.12} q^{\frac{2}{3}} (-\log \text{Pr})^{-0.55} M_w^{-0.5}. \quad (9)$$

The F and S factors are defined as

$$F = \left[1 + x \text{Pr} \left[(\rho_L / \rho_v) - 1 \right] \right]^{0.35}, \quad (10)$$

and

$$S = (1 + 0.055 F^{0.1} \text{Re}^{0.16})^{-1}. \quad (11)$$

For subcooled boiling, eq. (8) was modified by the authors because the driving temperature differences for nucleate boiling and for forced convection are different. Therefore for subcooled flow boiling, Liu and Winterton replaced equation (8) with

$$q^2 = (F h_l \Delta T_b)^2 + (S h_{pool} \Delta T_s)^2 \quad (12)$$

where

$$\Delta T_s = T_w - T_s \text{ and } \Delta T_b = T_w - T_b.$$

For subcooled flow boiling, all the other equations remain the same; but the quality (x) is set to zero and hence $F=1.0$. Eq. (11) is still used to evaluate S . As in our case, the temperature difference ΔT_b is unknown. Therefore, the two-phase heat transfer coefficient was given as

$$h_{tp} = q / \Delta T_b \quad (13)$$

where ΔT_b is obtained from the following equation

$$\Delta T_b = \frac{T_s - T_b}{1 + A_{bp}^2} \left[1 + \sqrt{(1 + (1 + A_{bp}^2)(A_{qp}^2 - 1))} \right], \quad (14)$$

and

$$A_{bp} = (F h_l) / (S h_{pool}),$$

and

$$A_{qp} = q / (S h_{pool} (T_s - T_b)).$$

In this correlation except for the liquid Prandtl and liquid Reynolds numbers which are evaluated at the bulk temperature, all other thermophysical properties were determined at the saturation temperature.

4.3 EXPERIMENTAL SUMMARY

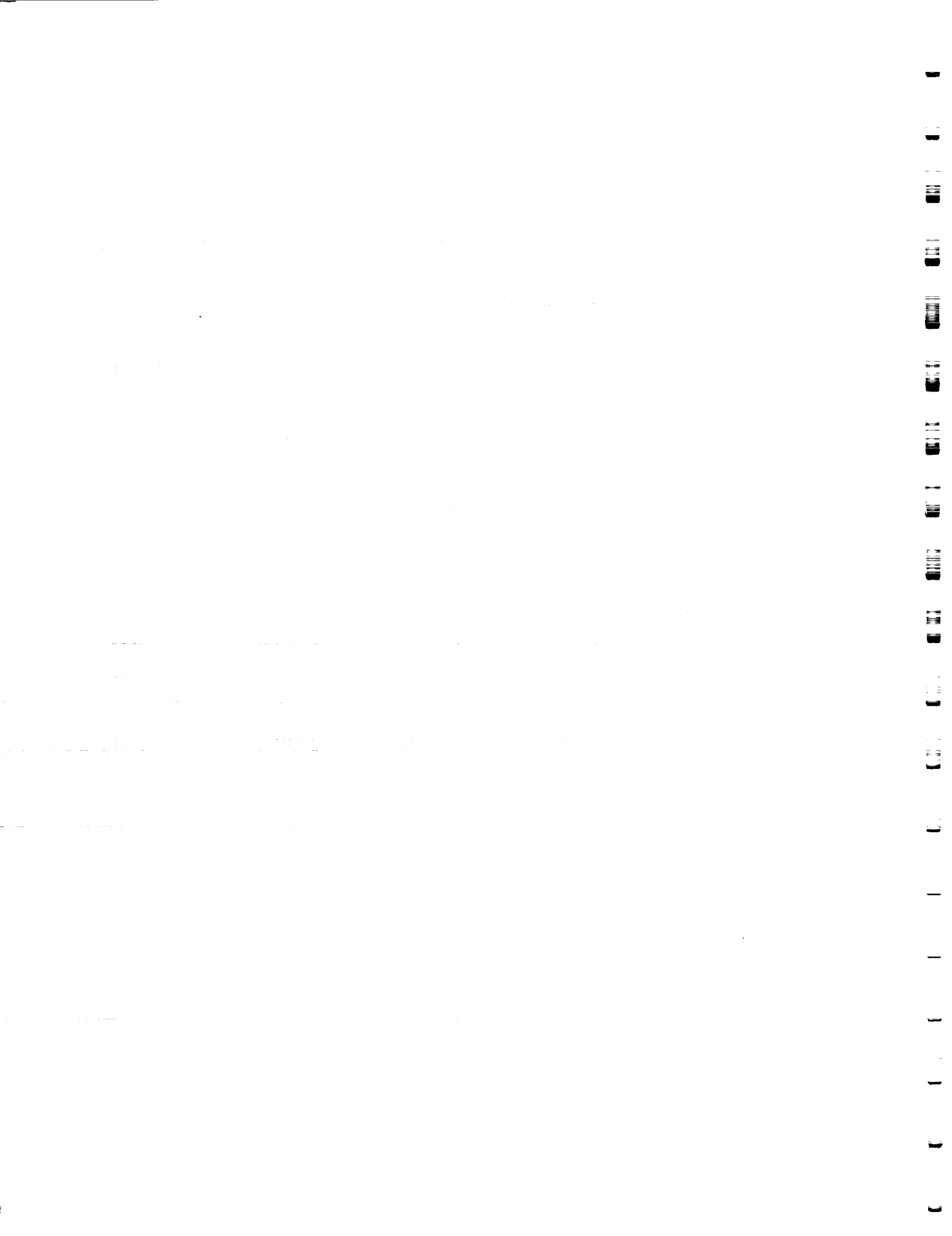
A series of experiments were run to obtain the heat transfer coefficient axial distribution for both the uniform and single-side heating configurations. The detailed description of the error analysis was presented elsewhere (Boyd, [14]).

The results for two experimental test cases will be presented. These cases involve both uniform and single-side heating configurations under identical flow conditions. The results will be presented for Freon-11 flowing in a 25.4 mm inside diameter (I.D.) tube, with mass velocity (G) of $210.0 \text{ kg/m}^2\text{s}$, an inlet temperature of 22.6°C , and an exit pressure of 0.1843 MPa (absolute). The external heated surface area for the single-side heated case was 0.0512 m^2 . The outside diameter of the heated channels was 28.4 mm .

4.4 RESULTS

Before the single-phase correlations were used for comparisons with our experimental data, they were compared with single-phase data produced by Chen and Tuzla [32] and Boyd [33]. These comparisons will also verify the correct usage of the correlations. As shown in Figure 20, both correlations predict T_w within 10.0°C , but the Dittus-Boelter correlation slightly underpredicts T_w . Further, the Dittus-Boelter correlation gave better predictions for h_i than the Petukhov correlation which consistently overpredicted h_i by approximately 20.0%. There may have been some convergence difficulties in using Petukhov's correlation with the present predictions; this will be resolved in the near future. It is important to note that the Chen and Tuzla water data was produced using a very low heat flux of 125.0 kW/m^2 . For comparison at higher heat fluxes, Figure 21 shows that the Petukhov correlation has better success than the Dittus-Boelter correlation. As Boyd and Meng [8] demonstrated, Shah's correlation has good predictability for high heat flux conditions in the fully developed boiling region when it is used along with Petukhov's correlation rather than the Dittus-Boelter correlation.

Figure 22, shows the comparison of our experimental data obtained at an axial location near the middle of the test section with the above noted single-phase and two-phase correlations for



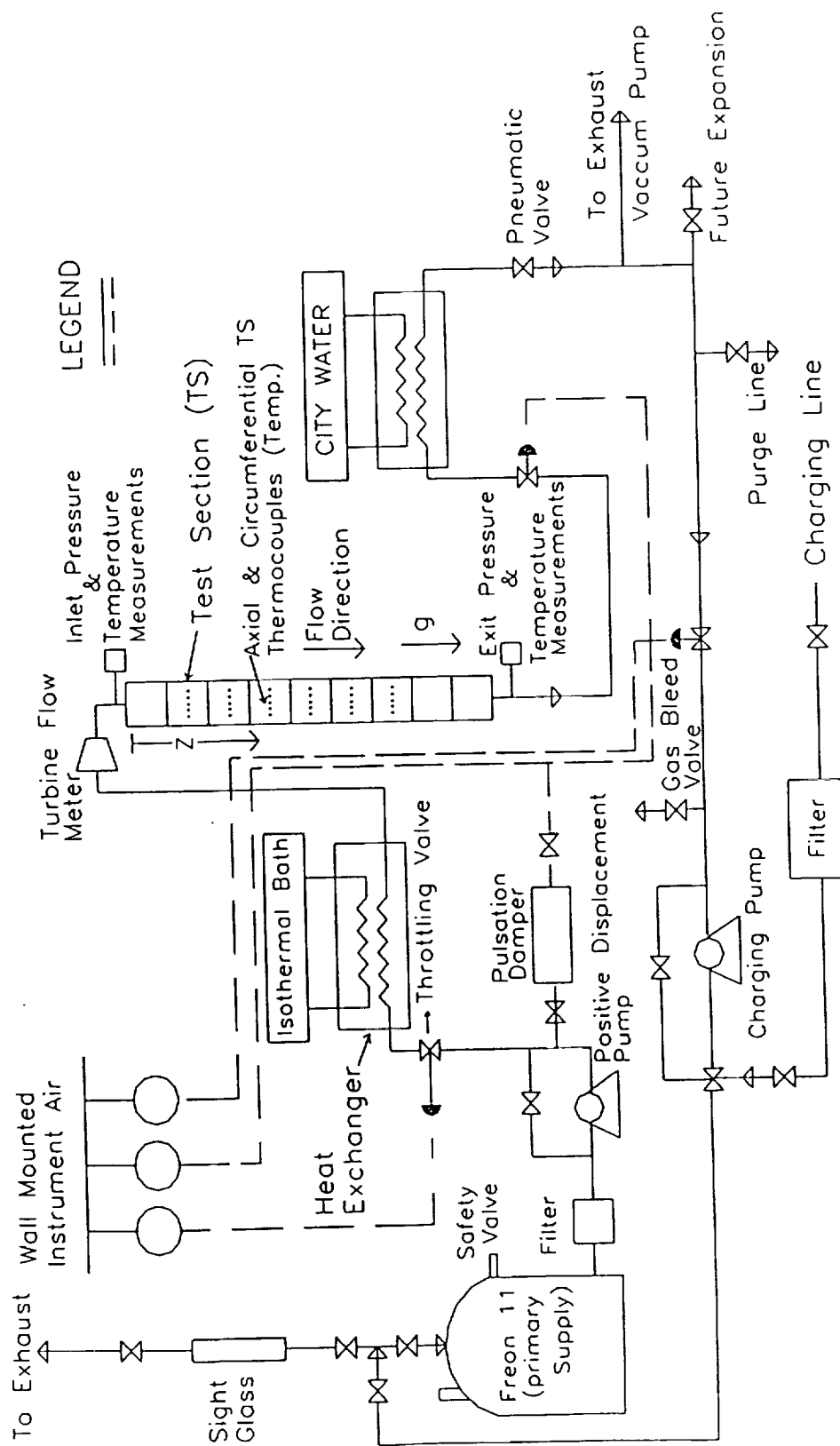


Figure 20: Schematic of the Vertical Downward Flow Boiling Loop



Chen & Tezla Single-Phase Heat Transfer Data Plot (Regenerated)

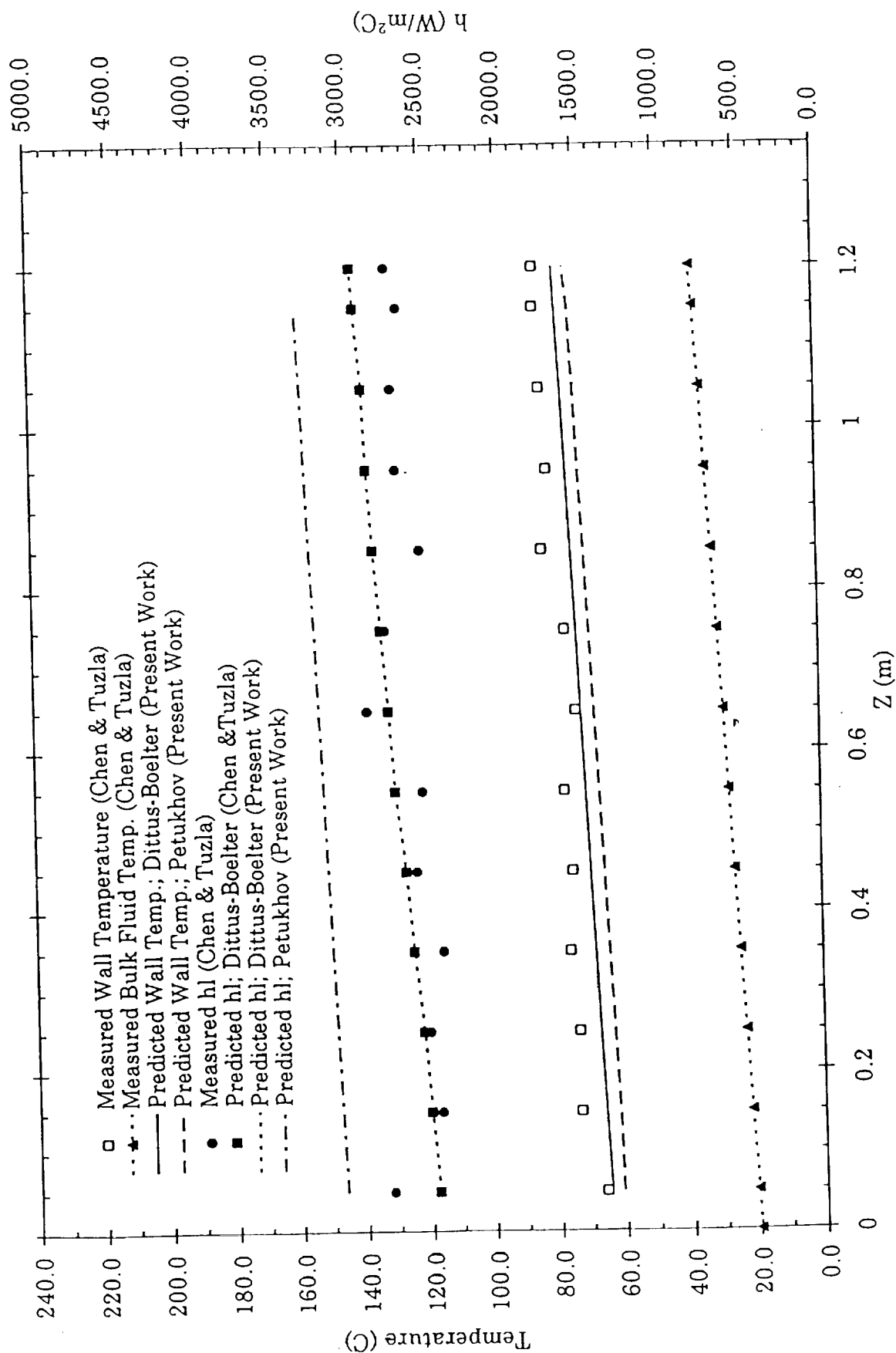
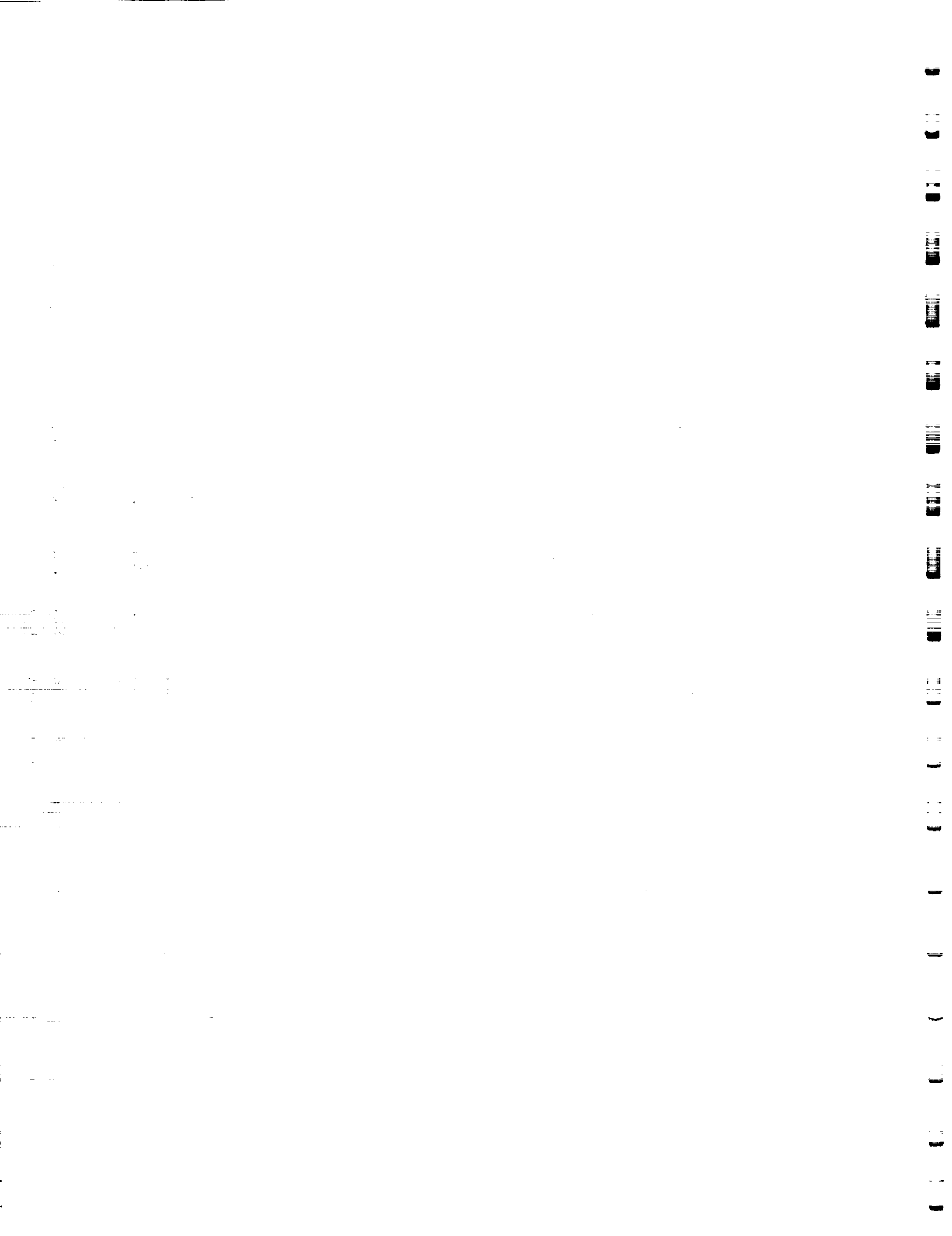


Figure 21: Comparisons of Low Heat Flux, Single-Phase Heat Transfer Data with Predictions. $q = 125.0 \text{ kW/m}^2$; $G = 500.0 \text{ kg/m}^2\text{s}$; $D = 15.7 \text{ mm}$, and $T_{\text{sat}} = 120.0^\circ\text{C}$



Comparisons of Boyd Experimental Data Using Shah's Correlation With both Petukhov's and Dittus-Boelter Correlations for Single-Phase Regime for $P_{exit} = 1.66 \text{ MPa}$, $D = .003 \text{ m}$, $Z = .2866 \text{ m}$, and $G = 31.5 \text{ Mg/m}^2 \text{ s}$

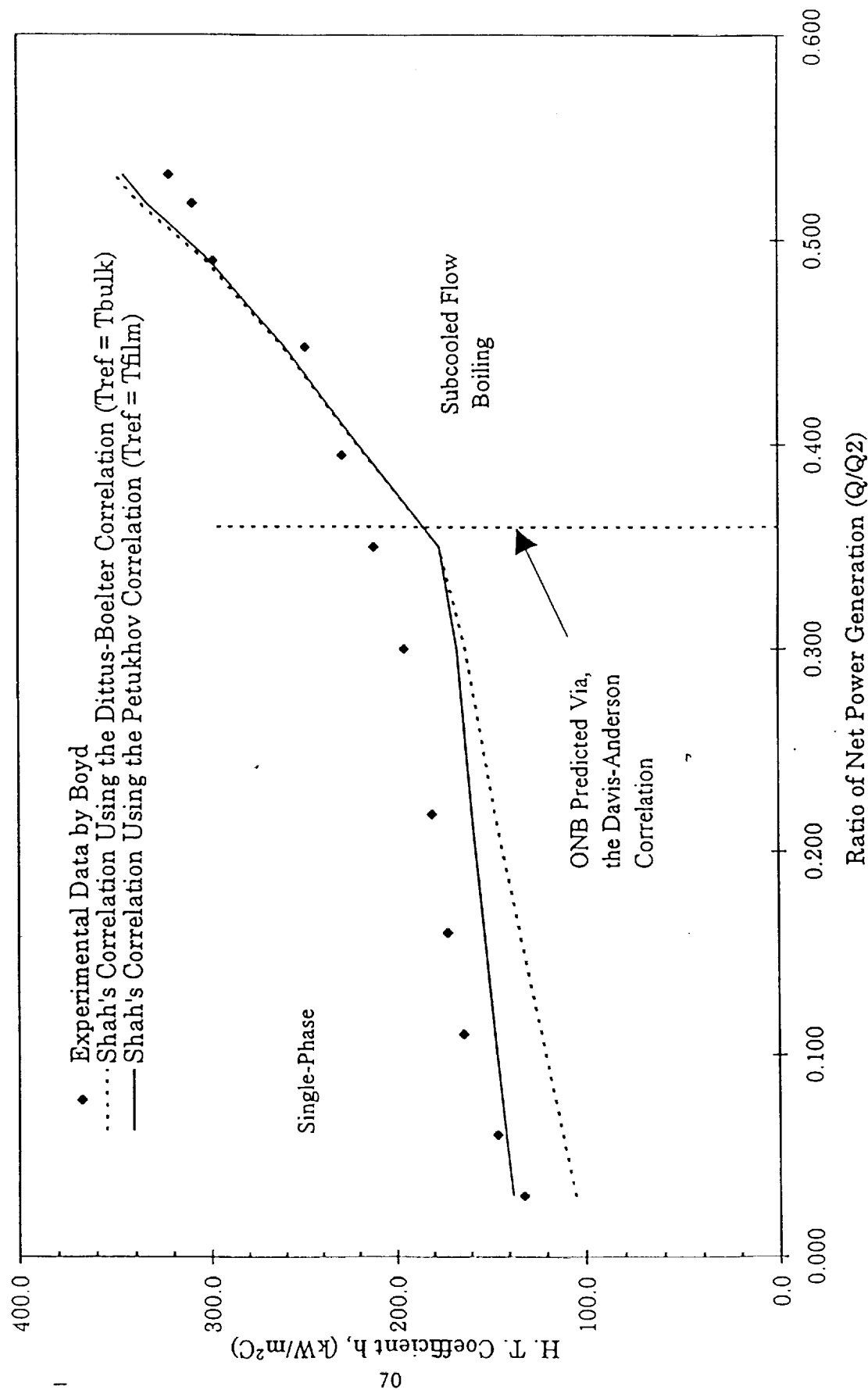
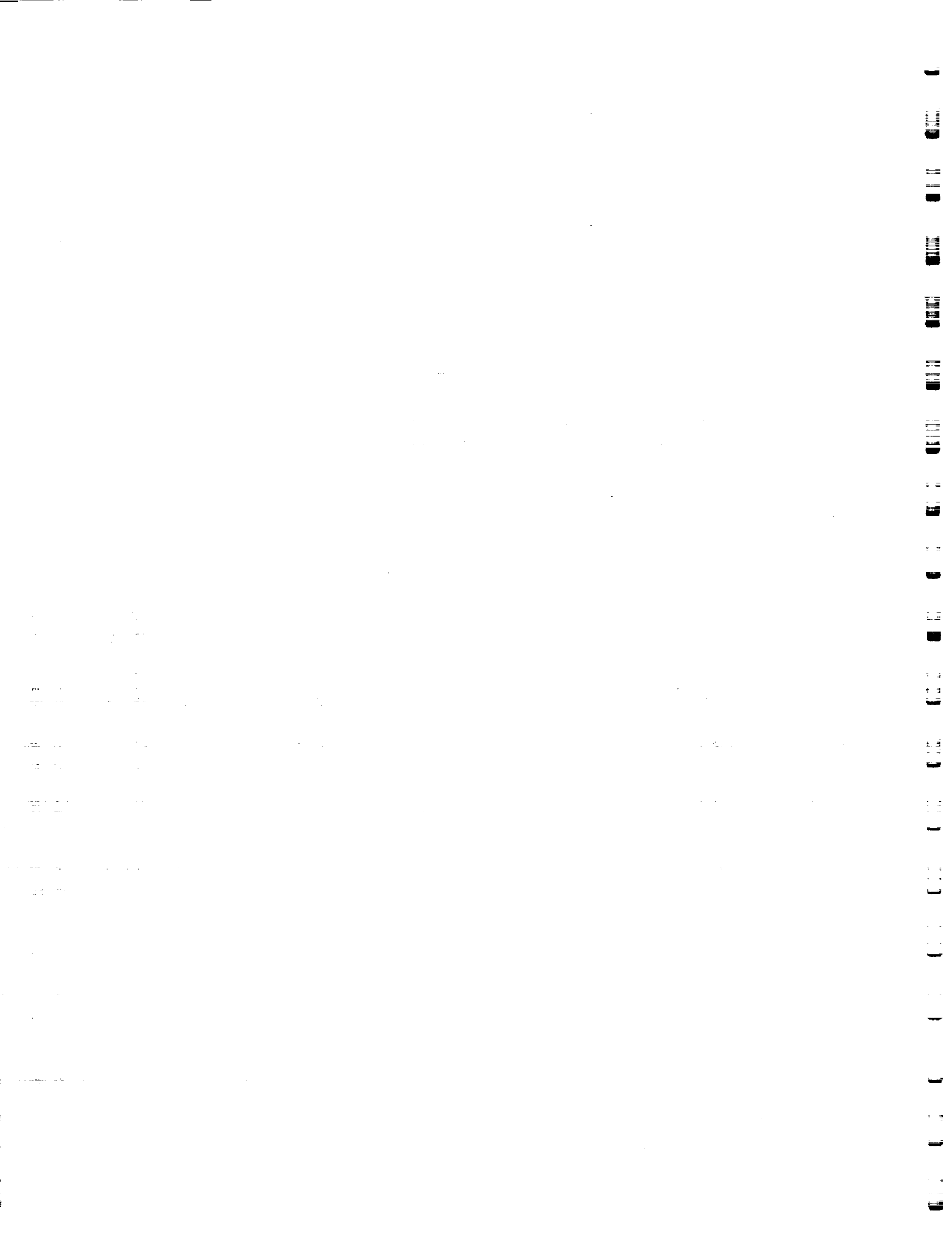


Figure 22: Comparisons of High Heat Flux, Single-Phase and Subcooled Flow Boiling, Water Data with Predictions. $q < 3,500.0 \text{ kW/m}^2$; $G = 31,500 \text{ kg/m}^2 \text{ s}$; $D = 3.0 \text{ mm}$; $Z = 0.287 \text{ m}$; and Exit Pressure MPa (absolute).



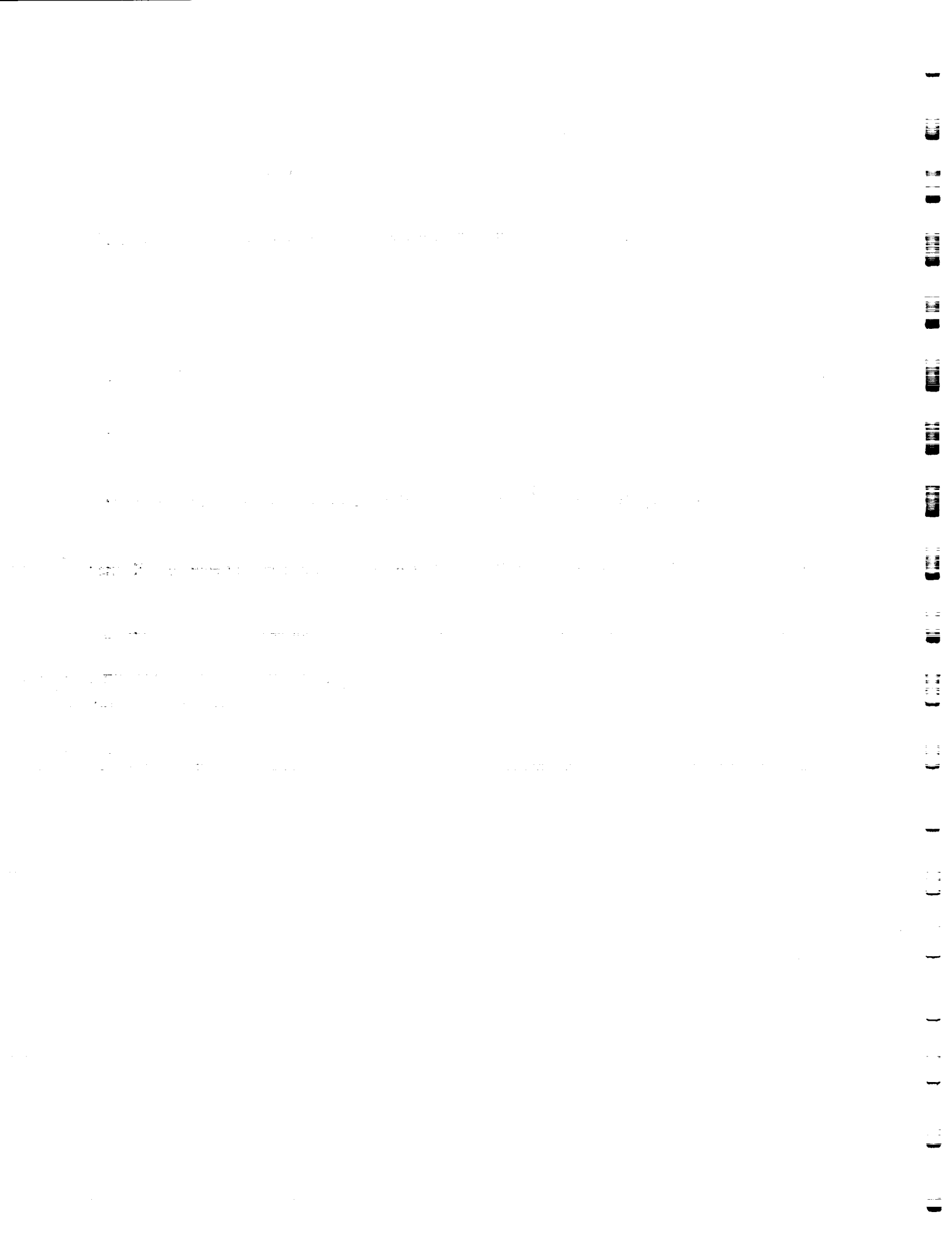
both uniform and single-side heated boundary conditions. Since none of the correlations selected thus far accounts for orientation, we anticipate only qualitative comparisons. Before the comparisons are discussed, it should be noted that the effects of single-side heating was accounted for by using a particular correlation as usual with the exception of using the thermal hydraulic diameter (D_t) as the characteristic length in place of the channel diameter (D). So that, D_t is given by

$$D_t = \frac{4 A_c}{P_H}, \quad (15)$$

where P_H is the heated perimeter and A_c is the flow channel cross-sectional area. With this definition of D_t , one readily observes the effect of the different reference lengths in Figure 23 for both a uniformly heated channel and the single-side heated channel. As shown in the figure, there is qualitative agreement with the data in the single-phase region and good agreement with the Shah correlation in the two-phase region. For the single-side heated case, there is fairly good agreement between all single-phase correlations and the data for Z between 0.203 and 0.416 m. After the ONB, Figure 24 shows that there is better agreement between the data and the Liu-Winterton correlation at upstream locations ($Z < 0.4$ m) and lower power levels. However for increased values of Z between 0.4 m and 0.8 m or at higher levels of power, Figures 22 and 25 show that Shah's correlation gave better predictions. At larger values of Z , all correlations overpredicted the data (see Figure 26).

4.5 SUMMARY

When used directly in the single-phase regime, the Liu-Winterton correlation compared well with the single-side heated Freon-11 data when D_t was chosen as the characteristic length. However, the Shah correlation characterized the data better in the two-phase region. Since all correlations overpredicted the data near the exit of the test section for the two-phase region, additional correlational development will be needed to completely characterize non-uniformly heated circumferential effects. Finally, good agreement was obtained between the correlations for



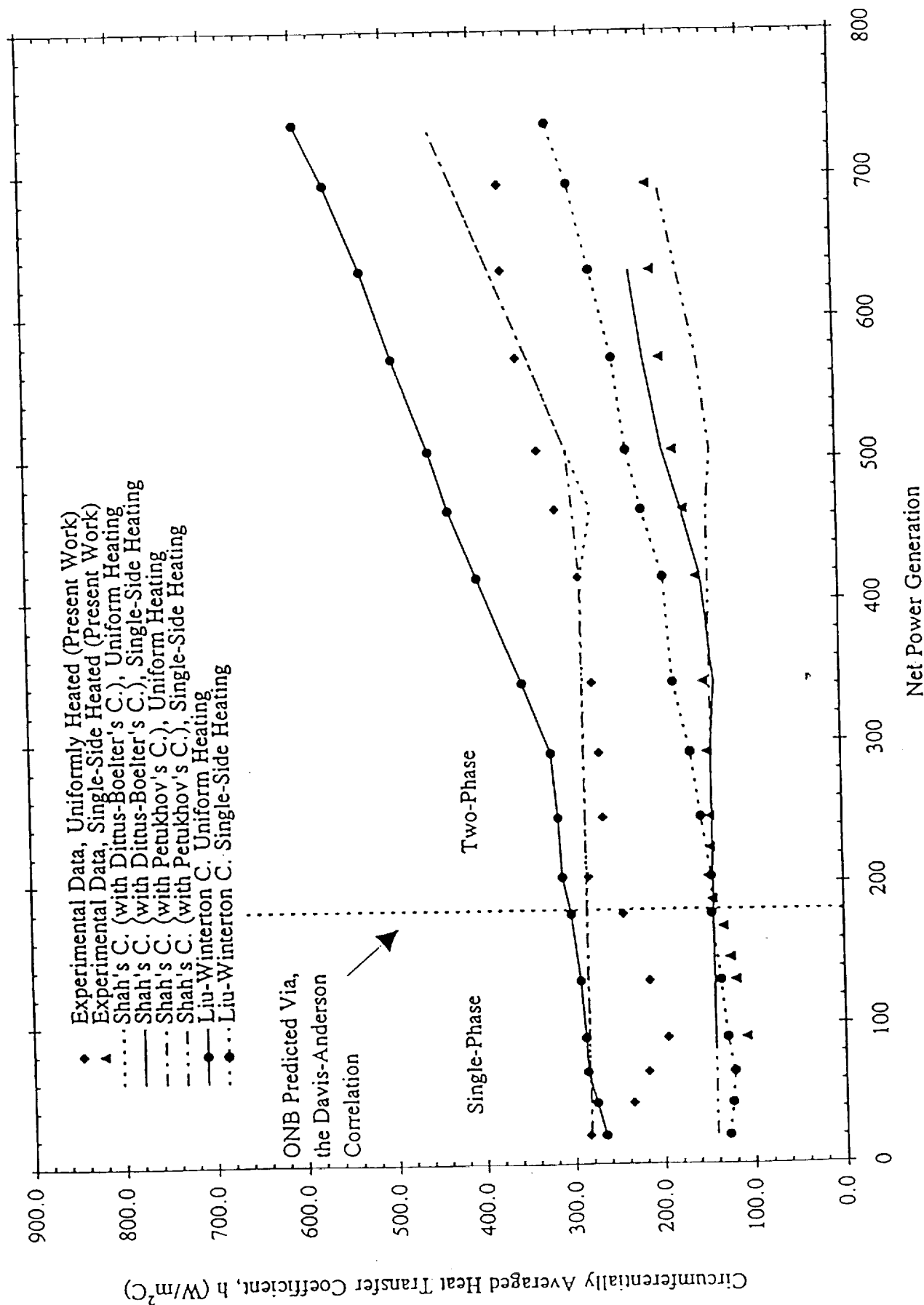
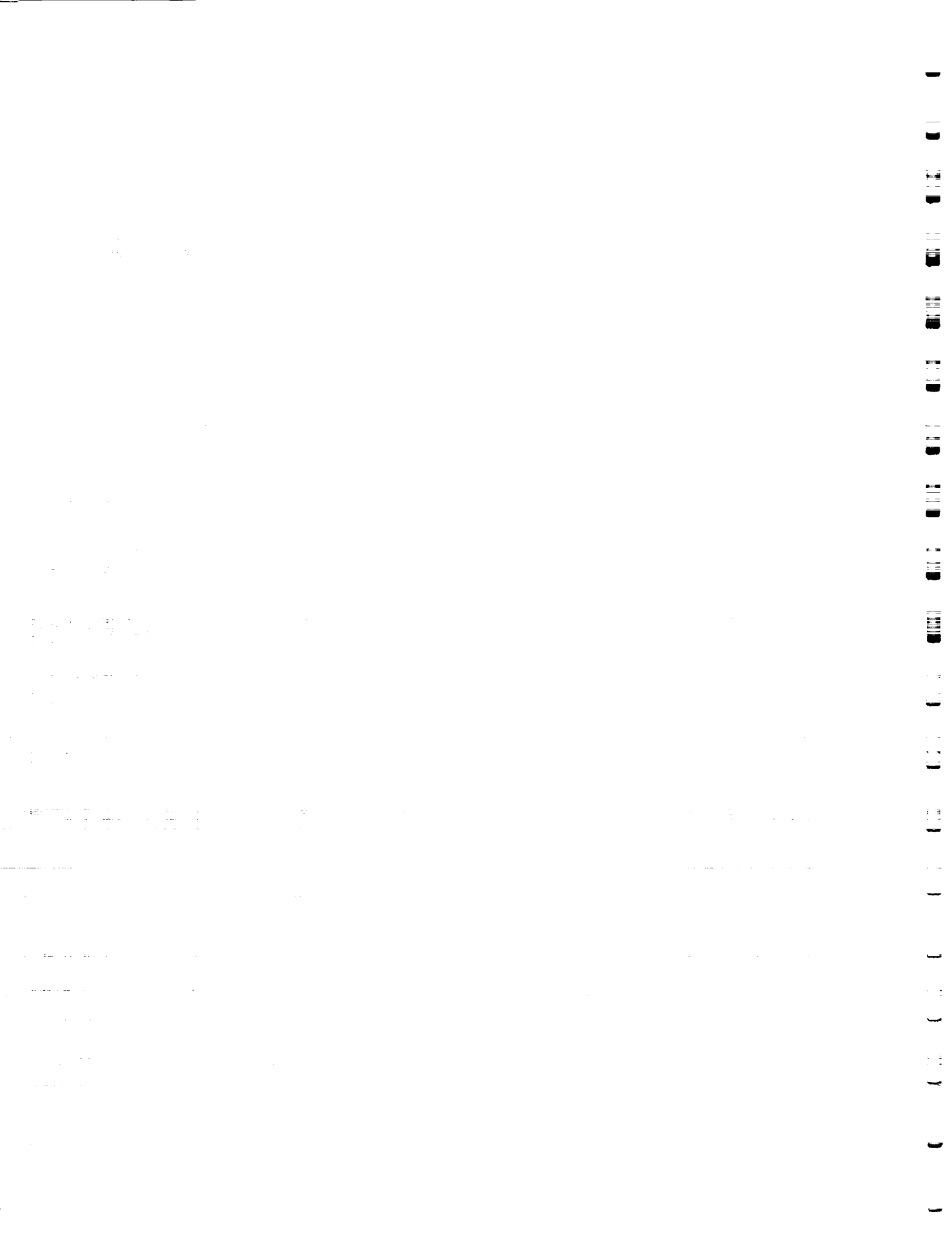


Figure 23: Comparisons of Correlations (C) with Experimental Freon-11 Data for Single-Phase and Two-Phase Heat Transfer Coefficients for Uniform and Single-Side Heated Vertical Smooth Channels with Downward Flow for the Following Flow Conditions: $G = 210.0 \text{ kg/m}^2\text{s}$, $D = 25.4 \text{ mm}$; $Z = Z_4 = 0.6 \text{ m}$, with an Exit Pressure ($@ Z = 2.463 \text{ m}$) of 0.1843 MPa (absolute).



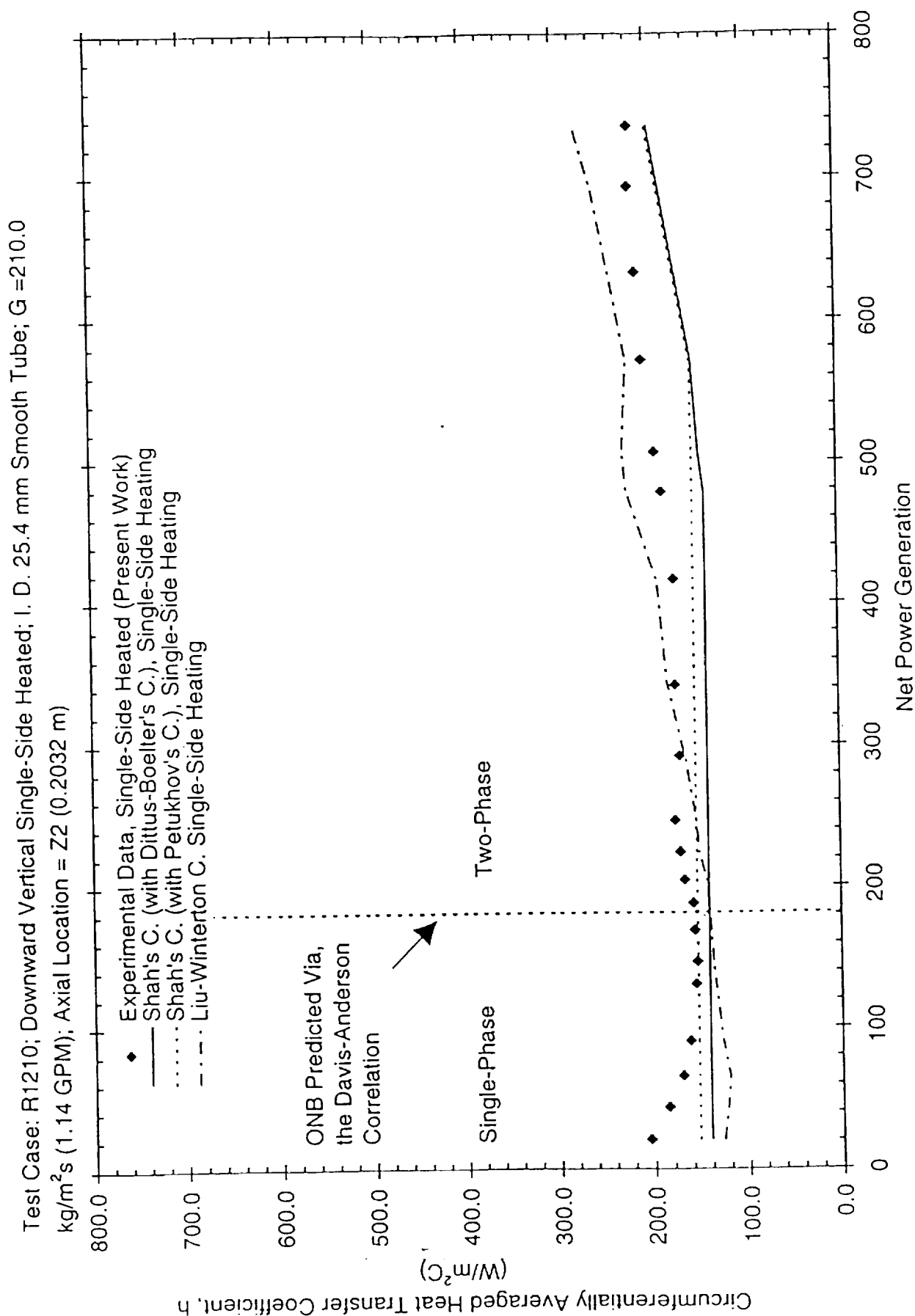


Figure 24: Comparisons of Correlations (C) with Experimental Freon-11 Data for Single-Phase and Two-Phase Heat Transfer Coefficients for Single-Side Heated Vertical Smooth Channels with Downward Flow for the Following Flow Conditions: $G = 210.0$ kg/m²s, $D = 25.4$ mm; $Z = Z_2 = 0.2032$ m, with an Exit Pressure ($@ Z = 2.463$ m) of 0.1843 MPa (absolute).

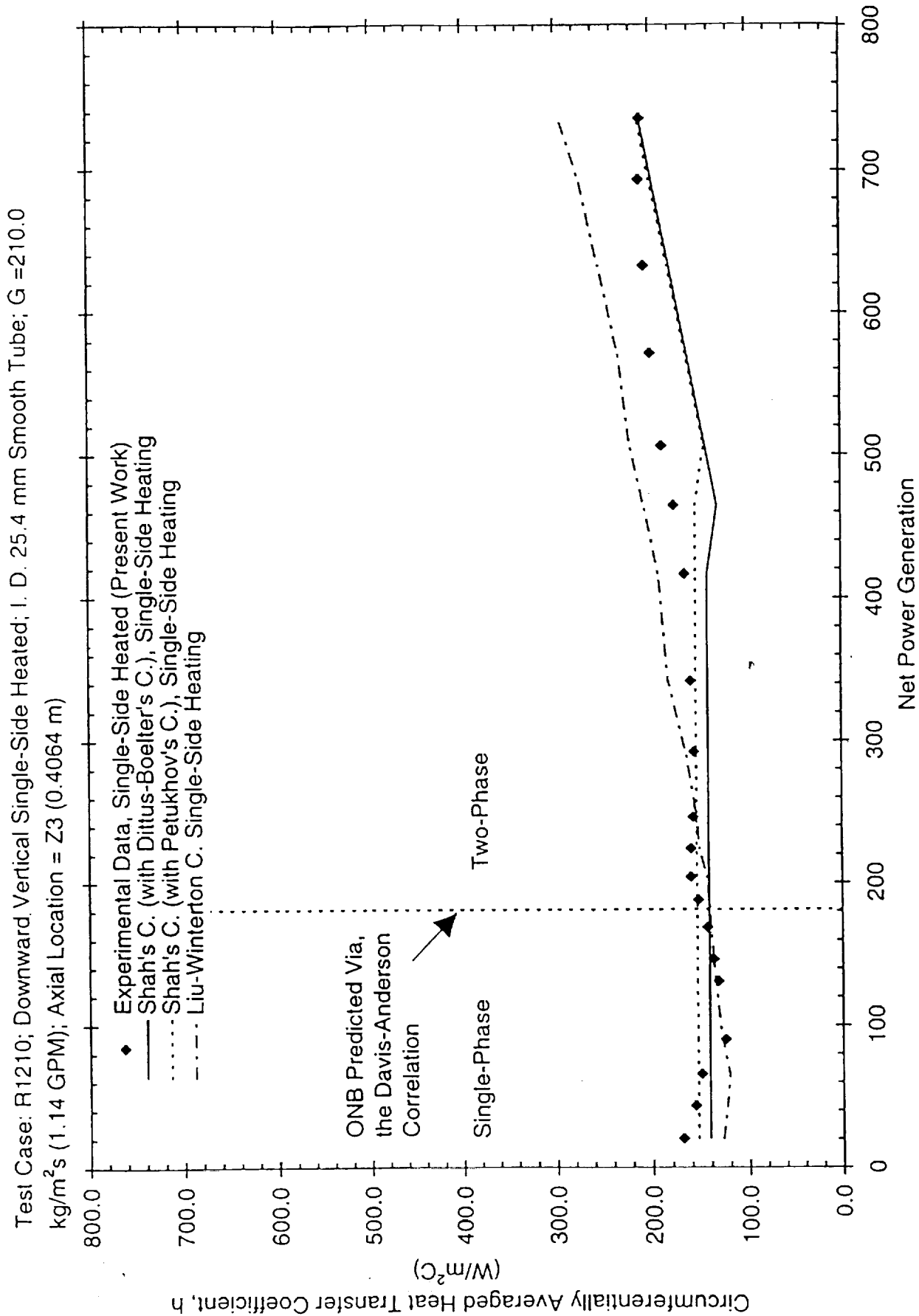


Figure 25: Comparisons of Correlations (C) with Experimental Freon-11 Data for Single-Phase and Two-Phase Heat Transfer Coefficients for Single-Side Heated Vertical Smooth Channels with Downward Flow for the Following Flow Conditions: $G = 210.0$ kg/m²s, $D = 25.4$ mm; $Z = Z_3 = 0.4064$ m, with an Exit Pressure ($@ Z = 2.463$ m) of 0.1843 MPa (absolute).

Test Case: R1210; Downward Vertical Single-Side Heated; I. D. 25.4 mm Smooth Tube; $G = 210.0$

$\text{kg/m}^2\text{s}$ (1.14 GPM); Axial Location = Z6 (1.016 m)

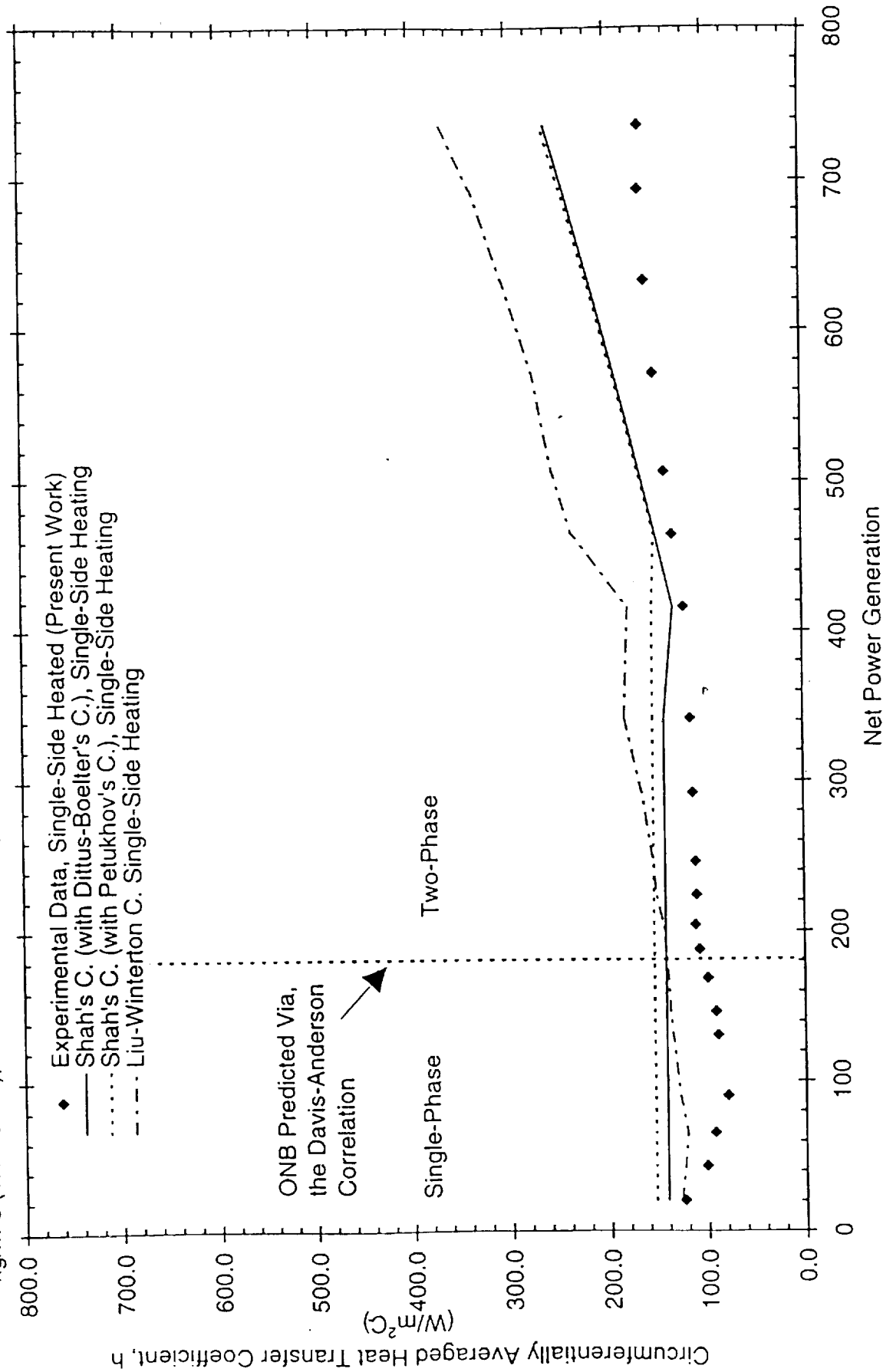


Figure 26: Comparisons of Correlations (C) with Experimental Freon-11 Data for Single-Phase and Two-Phase Heat Transfer Coefficients for Single-Side Heated Vertical Smooth Channels with Downward Flow for the Following Flow Conditions: $G = 210.0 \text{ kg/m}^2\text{s}$, $D = 25.4 \text{ mm}$; $Z = Z_6 = 1.016 \text{ m}$, with an Exit Pressure ($@ Z = 2.463 \text{ m}$) of 0.1843 MPa (absolute).

uniformly heated channels and water data under the following conditions: (1) for low heat fluxes ($q \leq 125 \text{ kW/m}^2$), the Dittus-Boelter is recommended for single-phase convection; (2) for high heat fluxes ($125 \text{ kW/m}^2 < q \leq 30,000 \text{ kW/m}^2$), the Petukhov correlation is recommended for single-phase convection; and (3) for high heat fluxes, the Shah correlation is recommended for fully developed subcooled flow boiling.

5.0 TWO -DIMENSIONAL DATA REDUCTION APPLYING AN INVERSE HEAT CONDUCTION (IHC) TECHNIQUE

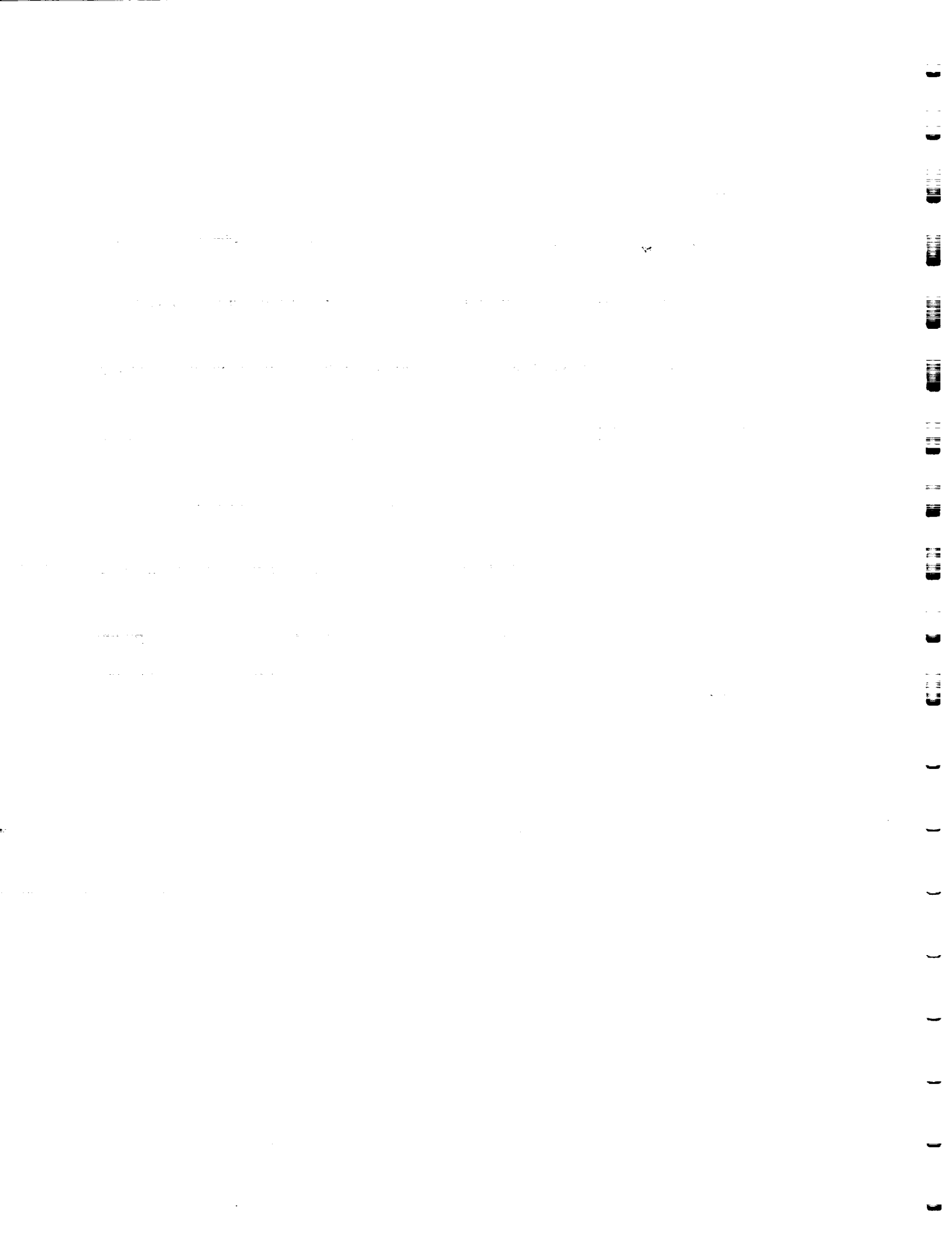
5.1 INTRODUCTION

Flow boiling heat transfer is an efficient method of removing a large quantity of heat per unit area under fairly low temperature difference. A large volume of experimental data are available at the Thermal Science Research Center (TSRC) at Prairie View A&M University on convection and flow boiling. For a various outside heat flux conditions on copper tubes several temperature measurements were performed on the outside of tubes. The working fluid used was Freon-11 with various flow conditions.

A One-Dimensional (1-D) data reduction was performed (Smith [12]) to obtain the circumferential averaged heat transfer coefficient at the inside of the tube from the available temperature and heat flux data. An attempt was also made to obtain the circumferential variation of heat transfer coefficient by using finite difference numerical scheme (Meng [34]). The problem is difficult because it is one of the boundary condition that is unknown and needs to be determined from the known internal temperature data. One of the methods that can be used for 2-D data reduction to obtain the circumferential variation of heat transfer coefficient is by applying steady state Inverse Heat Conduction technique (IHC). This section presents some preliminary results on IHC techniques.

5.2 IHC TECHNIQUE

Inverse Heat Conduction technique are becoming increasingly important tool for mathematical modeling, thermal design and optimization of engineering systems, and experimental data reduction. The development of this method is based on advances in mathematical theory and computer technology. Inverse heat conduction problems are those problems in which references on boundary conditions are made from a set of measured temperature data. The TSRC experiments fall under this category where the heat flux on the outside of the tube are known. Temperature measurements were made at some specific locations on the outside of the tube. It is required to obtain the circumferential variation of the wall temperature and heat transfer coefficient on the inside of the tube.



The present method used was suggested by Naylor and Oosthuizen [35] with simple modification for steady state conditions. The method is also similar to the method used by Dorri and Chandra [36] to measure contact resistance variation with temperature.

In order to obtain the local heat transfer variation on the inner surface, the heat transfer coefficients are assumed to be defined in terms of a series of piece-wise function of N constant values, h_1, h_2, \dots, h_n , where each constant represent the locally averaged heat transfer coefficient over a sub-region of the surface.

If the values of the constants h_1, h_2, \dots, h_n , are guessed, the corresponding variation of temperature (T_c^j) at each of the measurement locations can be calculated. Note that the experimental temperature variation (T_m^j) at each of the measurement points is known. So, the square of the difference between the calculated and measured temperatures, summed over all thermocouples is then calculated as follows:

$$E = \sum_{j=1}^M (T_c^j - T_m^j)^2 \quad (16)$$

where M is the number of measurement points. The superscript j refers to the measurement point and is not an exponent.

The optimum local heat transfer rate distribution is then obtained by minimizing the sum square root E with respect to each unknown coefficients:

$$\frac{\partial E}{\partial h_i} = 2 \sum_{j=1}^M (T_c^j - T_m^j) \frac{\partial T_c^j}{\partial h_i} \quad (17)$$

Let T_{c0}^j be the calculated temperatures for an initial set of coefficients. The term $(T_c^j - T_m^j)$ is then linearized using a Taylor series as follows:

$$(T_c^j - T_m^j) = (T_{c0}^j - T_m^j) + \frac{\partial T_c^j}{\partial h_1} \Delta h_1 + \frac{\partial T_c^j}{\partial h_2} \Delta h_2 + \dots + \frac{\partial T_c^j}{\partial h_N} \Delta h_N \quad (18)$$

Substituting eq. (18) into eq. (17) gives and equation for the corrections to the coefficients Δh_i required to minimize E:

$$\sum_{j=1}^M (T_{c0}^j - T_m^j) \frac{\partial T_c^j}{\partial h_i} + \frac{\partial T_c^j}{\partial h_1} \frac{\partial T_c^j}{\partial h_i} \Delta h_i + \quad (19)$$

$$\frac{\partial T_c^j}{\partial h_2} \frac{\partial T_c^j}{\partial h_i} \Delta h_2 + \dots + \frac{\partial T_c^j}{\partial h_N} \frac{\partial T_c^j}{\partial h_i} \Delta h_N = 0$$

Applying eq. (19) for each of the coefficient $h_i = h_1, h_2, \dots, h_N$ gives a set of N linear equations in $\Delta h_1, \Delta h_2, \dots, \Delta h_N$. The values of $\partial T_c^j / \partial h_i$ in eq. (19) are obtained by calculating the temperatures (T_{c0}^j) from the initial guessed values of h_i and then, one by one, adding a small amount δh_i (e.g. $\delta h_i = 0.01 h_i$) to each of the h_i values T_{cl}^j . The derivative at each segment is approximated by:

$$\frac{\partial T_c^j}{\partial h_i} = \frac{T_c^j - T_{c0}^j}{\delta h_i} \quad (20)$$

The solution steps for the above mentioned IHC technique are as follows:

1. Guess the values of all the h_i coefficients, $i = 1, 2, \dots, N$.
2. Calculate the temperatures at all the measurements points; i.e., T_{c0}^j .
3. Increase h_1 by a small amount, $\delta h_1 = 0.01 h_1$ and recalculate the temperatures, i.e., T_{cl}^j .
4. Repeat step (18) for coefficients h_2, h_3, \dots, h_N .
5. Calculate the derivatives using eq. (20). Using these derivatives, apply eq. (19) for each coefficient to obtain N equations for the N unknown Δh_i values. Solve these equations.
6. Use Δh_i values to get improved values for the coefficients, i.e. $h_1 + \Delta h_1, h_2 + \Delta h_2, \dots, h_N + \Delta h_N$.
7. Repeat steps (2) to (6) until the coefficients cease to change (within a selected tolerance) from one iteration to the next.

5.3 RESULTS AND DISCUSSION

The method is applied to one particular case of horizontal test section experiments. The case chosen is from experiment #R1215 (Smith [12]) with a power level of 144.55 W, which is a top heated case. The axial location chosen for data reduction is at the middle of the test section. The 2-D data reduction was carried out using the commercial finite element code ANSYS along with a set of peripheral programs. The system of peripheral computer codes were developed to

interface with ANSYS for successive iteration calculations. One set of programs reads ANSYS output files, cleans them up, and writes in a desired format. These are then used by another set of programs to carryout the calculations according to IHC technique. The updated values of heat transfer coefficients are obtained and used by ANSYS for the next iteration.

The programs are written with several constraints in order to prevent divergence of the solution. The constraints are the percentage of changes of the values of heat transfer coefficients from one iteration to the next. They also include constraints to prevent the matrix from having a zero determinant. Two data files, one containing the measured temperatures and the other the initial vlaues for heat transfer coefficient on the inner segments are required to initiate the calculation along with the ANSYS program, which is written in batch mode.

For initial runs, the model used had a constant thickness of epoxy layer around the copper tube (see Figure 27: For this case the air and epoxy layer shown is replaced by a continuous epoxy layer). The thermal conductivities used for the copper tube and epoxy were 382.74 W/mK and 1.038 W/mK, respectively. The inner surface was divided into five equal circumferential sections, each of these sections was assumed to have a constant value of the heat transfer coefficient.

After initial iterations, the circumferential variations of the inside heat transfer coefficient showed lower values at the top and higher values at the bottom which is contrary to the expected variations. One of the reasons may be the value of the thermal conductivity of epoxy used. After talking with representative of OMEGA, the manufacturer of the epoxy, a modified value of 0.12 W/mK was taken for new simulation. Initial guessed profiled of heat transfer coefficients was close to a backward "S" shape, which is expected to be the final profile. Figure 28 shows how the sum of the squares of the error changes with the number of iterations. The errors are the differences between the measured and calculated temperatures at each of the four location where measurements were taken during the experiments. According to the figure, the error reaches a value of about 10.0 within 50 iterations and remains steady with successive iterations. Figure 29 shows the circumferential variation of heat transfer coefficients at various stage of iterations. The changes were very small between 150 and 170 iterations, which suggests that the iterations process was close to convergence. The result show an increase of heat transfer coefficient from the top to near 45 degrees and than decreasing drastically towards the bottom.

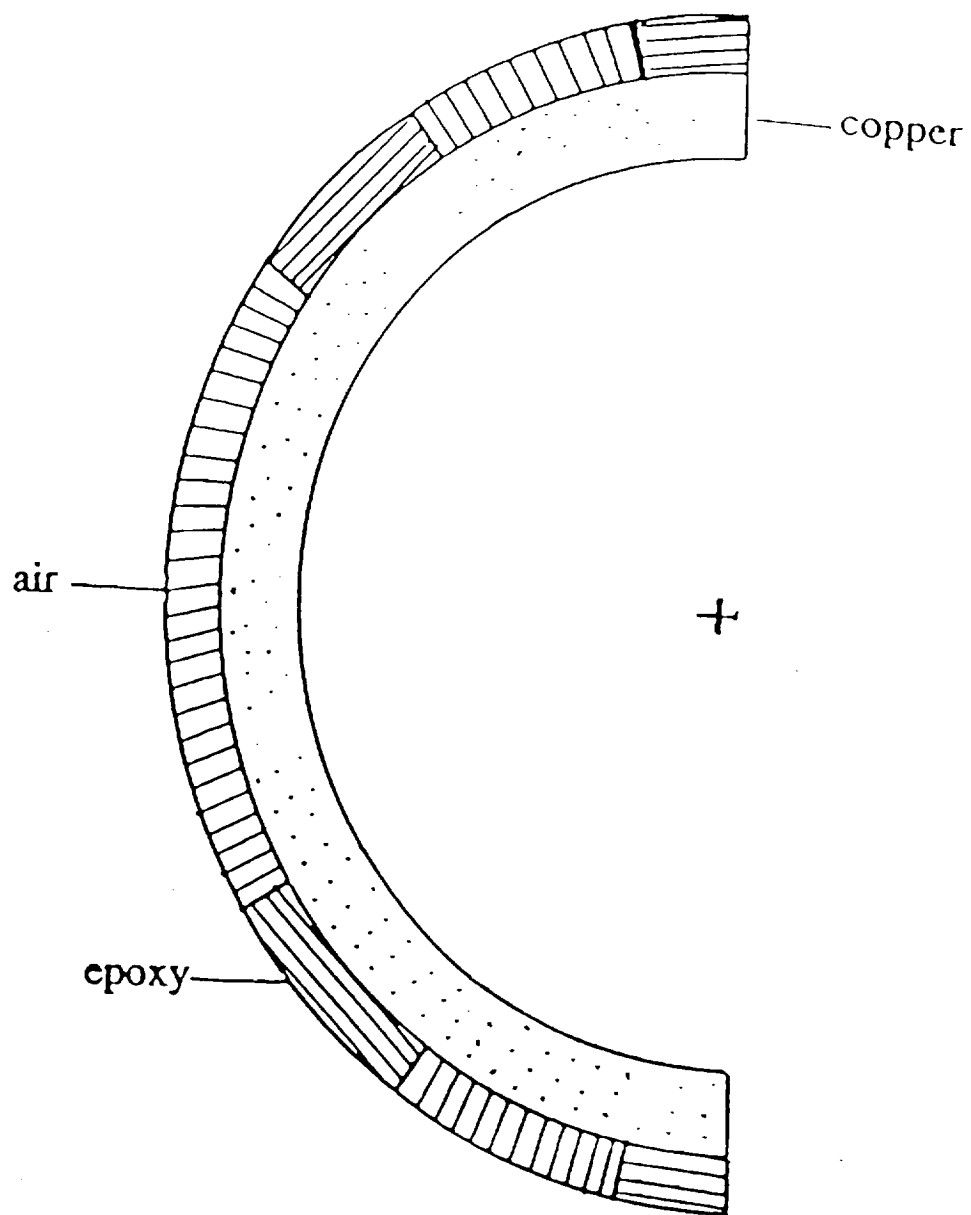


Figure 27: Schematic of the model with air and epoxy on the outer layer.

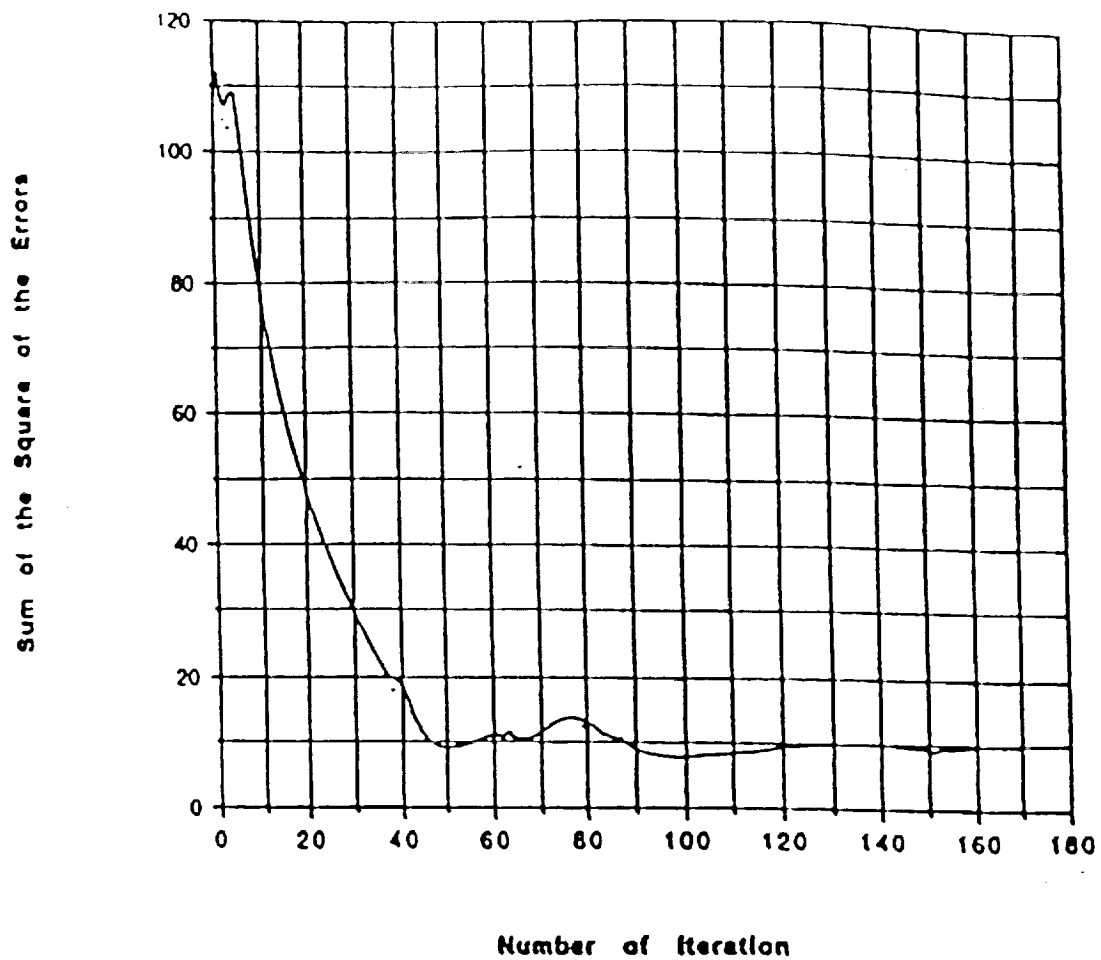


Figure 28: Sum of the squares of the differences between measured and calculated temperatures versus number of iterations.

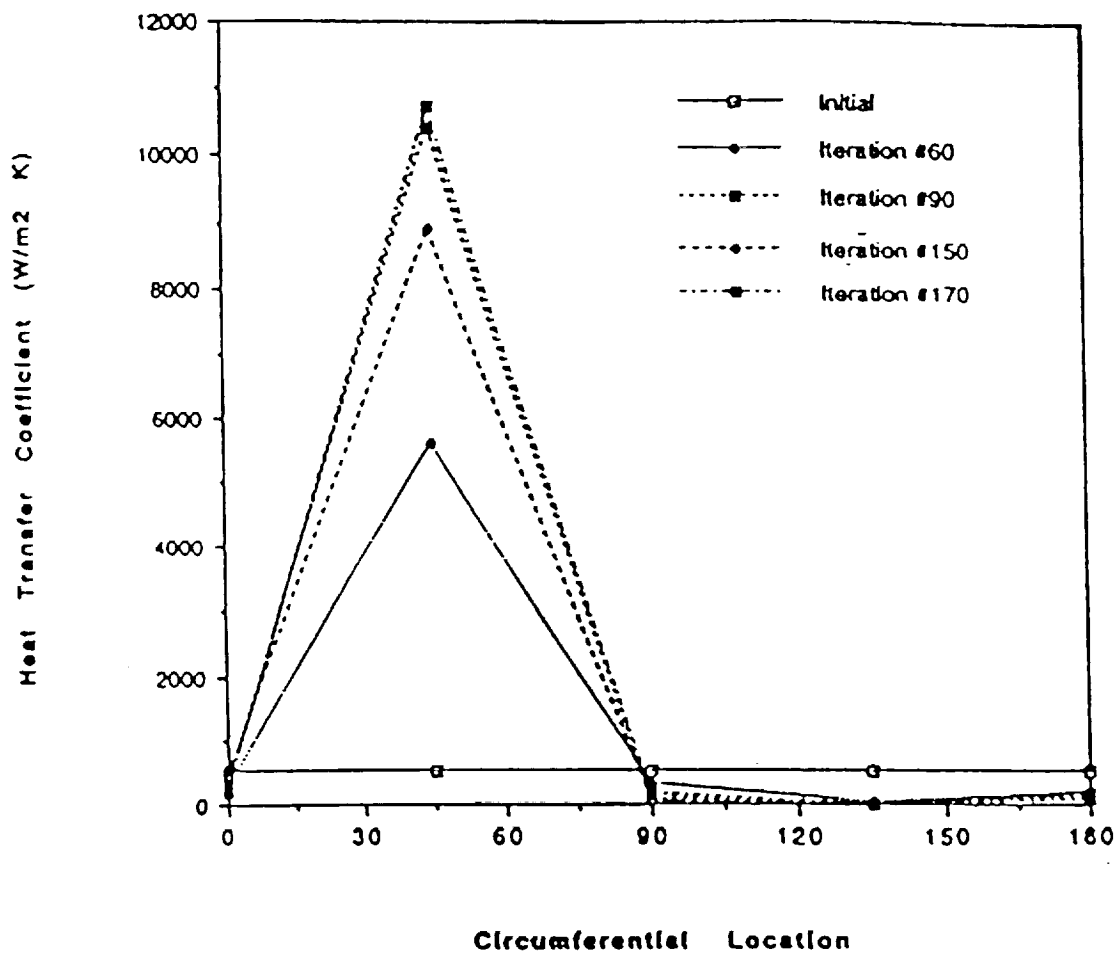


Figure 29: Circumferential variation of heat transfer coefficient at various level of iterations with only epoxy on the outer layer and five inner wall segments.

In order to obtain an improved result, i.e. greeting a heat transfer profile close to a backward “S” shape, a new model was developed where the epoxy layer was not considered to be continuous. The model has epoxy around the four thermocouples and air of equal radial thickness on the rest of the outside surface of copper. The epoxy and air thermal conductivities were taken as 1.038 W/mK and 0.028 W/mK, respectively. For this model Figure 30 shows the highest value of h is still at around 45 degrees. The resulting constant value of E for this case was around 10.0. Assuming that the present profile is due to the limited number of circumferential segments for the convection coefficient (something similar to the number of nodes in finite difference methods) the simulation was discontinued. A new model was developed and programs modified accordingly to include ten circumferential segments for convection coefficients and new iterations were initiated from an assumed backward “S” shaped profile. The result is plotted in Figure 31 and again shows a peak value at around 45 degrees. Although the peak in h remained near 45 degrees using ten inner wall segments as compared to five, the model clearly increased h at zero degree. Similarly some improvement of the results were noticed using five locations for measured temperatures instead of four, i.e., assuming the temperature at 90 degrees from the top to be known. The value was obtained by linear extrapolation of the top two temperatures. The interim results plotted in Figure 32 clearly shows the maximum h to be on the top. The simulation is not yet complete and will continue till convergence has been achieved. Finally, one important constraint which must be imposed on all equations is the zero heat flux condition on the vertical plane of symmetry at each radial location.

5.4 SUMMARY

Initial simulations using a IHC technique were performed. Simulations were performed with both constant thickness epoxy layer and a layer consisting of both epoxy and stationary air. Inside heat transfer profiles were obtained by dividing the inner surface to either five or ten segments. The results showed a peak value of h at around 45 degrees instead of an anticipated backward “S” shaped profile. In future funded work, more simulations must be performed using more than four locations of known measured temperatures and the imposed symmetry conditions.



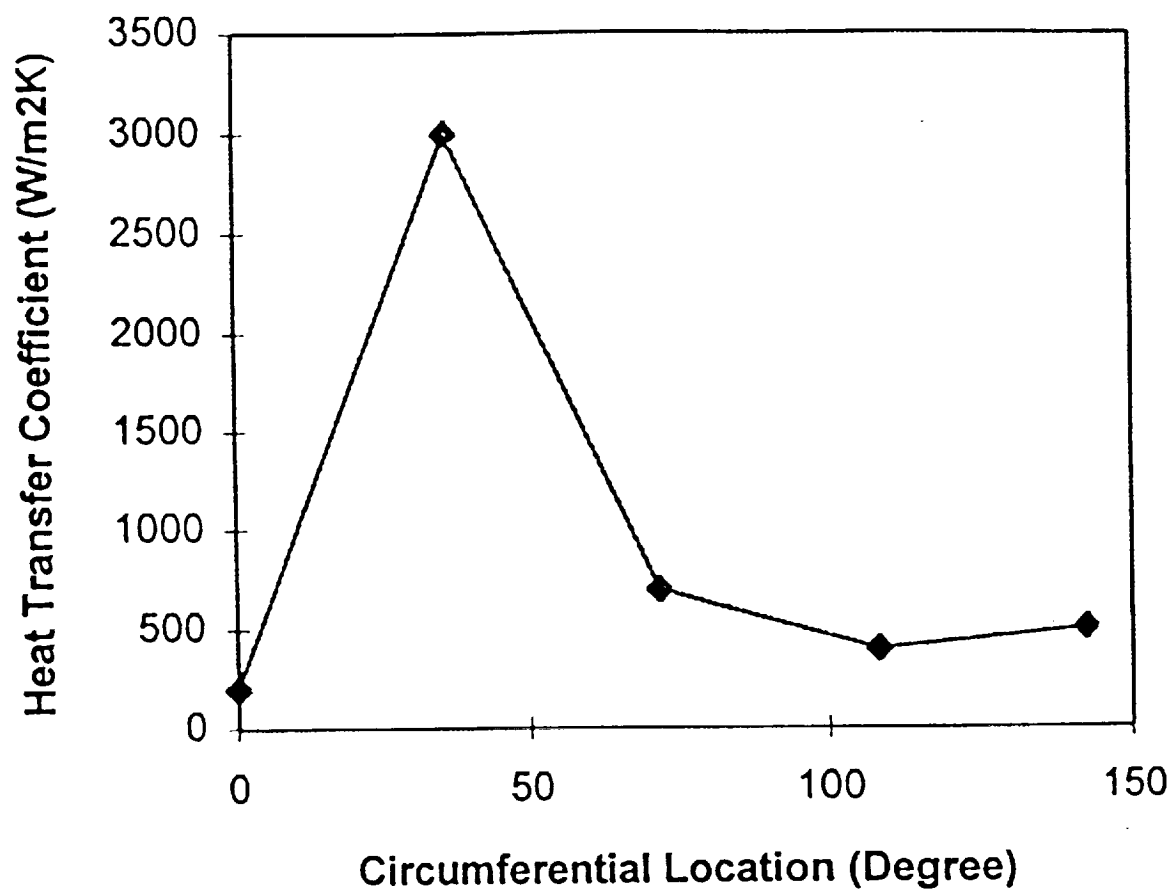


Figure 30: Circumferential variation of heat transfer coefficient with epoxy and air on the outer layer and five inner wall segments.

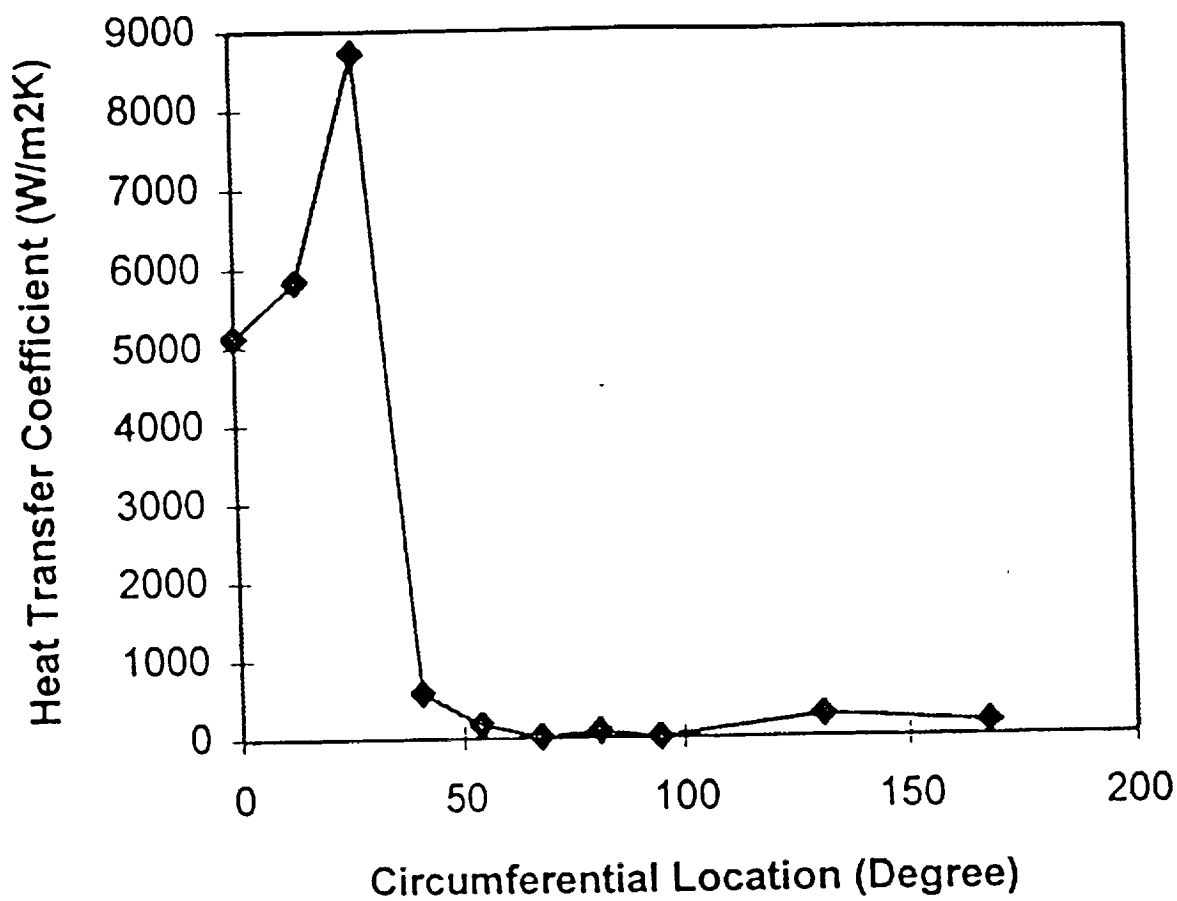


Figure 31: Circumferential variation of heat transfer coefficient with epoxy and air on the outer layer and ten inner wall segments.

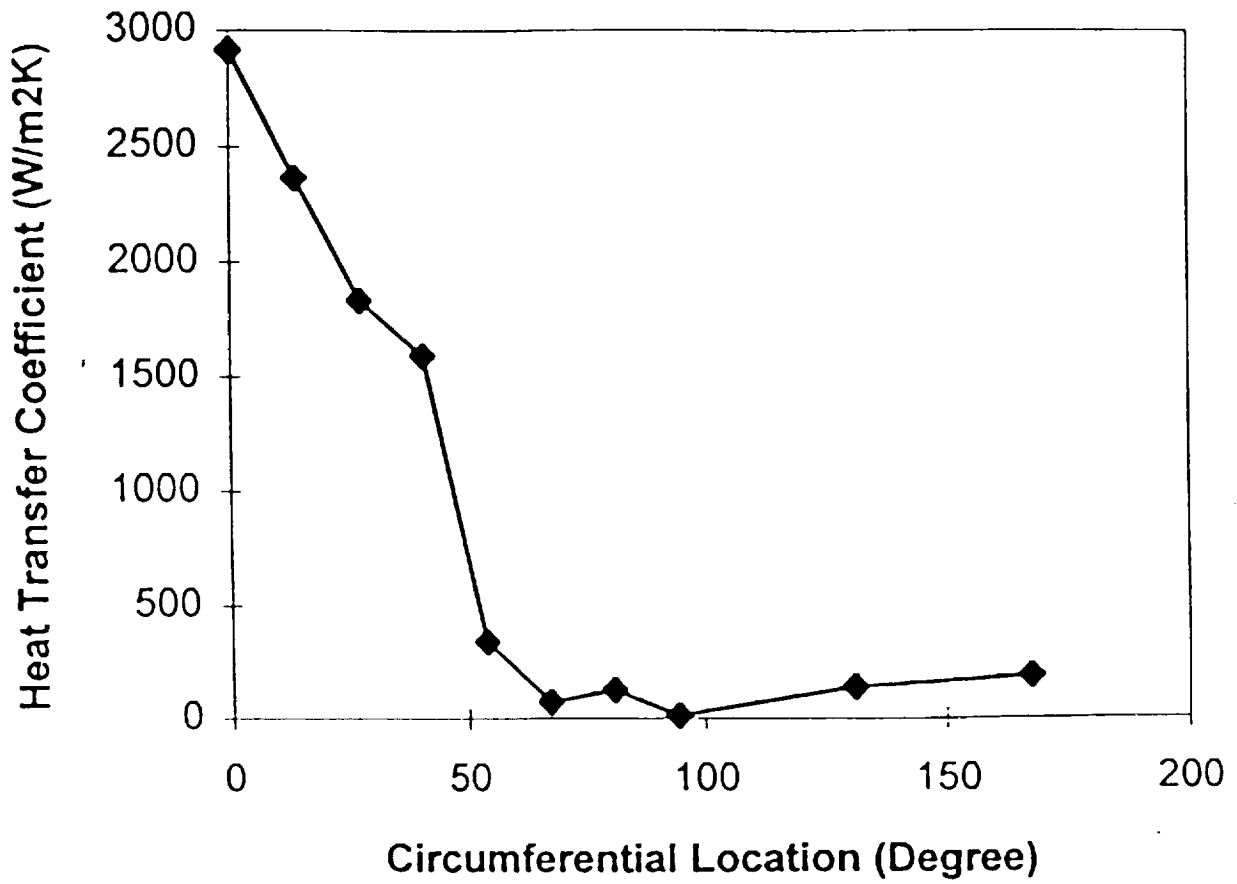


Figure 32: Circumferential variation of heat transfer coefficient with epoxy and air on the outer layer, ten inner wall segments and five measurement locations.



6.0 CONCLUSIONS

A vertical flow loop was designed and assembled to determine the local (circumferential and axial) and mean wall temperature distributions for single-phase and two-phase (subcooled and saturated) downward flow in both uniformly-heated and single-side heated vertical channels. Freon-11 was used as the working fluid in order to directly relate and compare the results with a previous experimental campaign which employed this same working fluid. For a given steady-state experiment, the following parameters were held constant: (1) exit pressure, (2) inlet temperature, and (3) mass velocity. For a given configuration of the 2.2m long cylindrical channel test section, which had a 1.2m long heated section, the applied heat rate was varied from zero through successive quasi-steady states to a level which corresponded to localized film boiling in the test section.

The measurements showed that the boiling curve changes significantly at higher mass velocities with respect to both the circumferential and axial directions. The slope of the boiling curve changes in a non-monotonic fashion with respect to the circumferential directions. The slope of the boiling curve changes in a non-monotonic fashion with respect to the circumferential direction. The measurements point to the existence of a dry-out phenomenon occurring at multiple levels of the applied heat for the single-side heated channel. In comparing the heat transfer for horizontal channel flow with a vertically downward flow, the results show that significantly lower heat transfer occurs in the horizontal flow. However, this trend reverses as both the Reynolds number and the applied heat rate increase.

Both the Liu-Winterton and Shah correlations were compared with the experimental data. The Shah correlation predicted the uniformly heated tube data better. When a thermal hydraulic diameter approach was used for the single-side heated case, the data at upstream locations for $Z/L < 0.5$ was bounded above by the Liu-Winterton correlation and below by the Shah correlation. At $Z/L = 0.5$, the Shah correlation bounded the data; and for $Z/L > 0.5$, both correlations overpredicted the data with the Shah correlation being closest to the data. The present results indicate that additional correlational development is needed.

In addressing some of the advanced space thermal management objectives concerning accommodating high heat fluxes in non-uniformly heated systems, a large battery of experiments

have been completed where local two-dimensional wall temperature variations were measured for both single-phase and two-phase flow in a single-side heated circular tube. As noted above, the results show significant axial and circumferential variations. Accurately accounting for such variations can result in optimized future advanced space, enhanced (high heat flux) thermal management systems.

Although most of the funded NASA work at Prairie View has not resulted in technical papers in national publications, this work has resulted in four (4) papers which appeared in international publications (see the Appendix).

ACKNOWLEDGMENTS

The P. I., and the TSRC students and staff are also appreciative to Vivian Pope for her invaluable assistance in completing this report, and handling matters associated with processing equipment orders, typing, and being part of our team. The P. I. is very grateful to NASA JSC and Headquarters for supporting this work.

REFERENCES

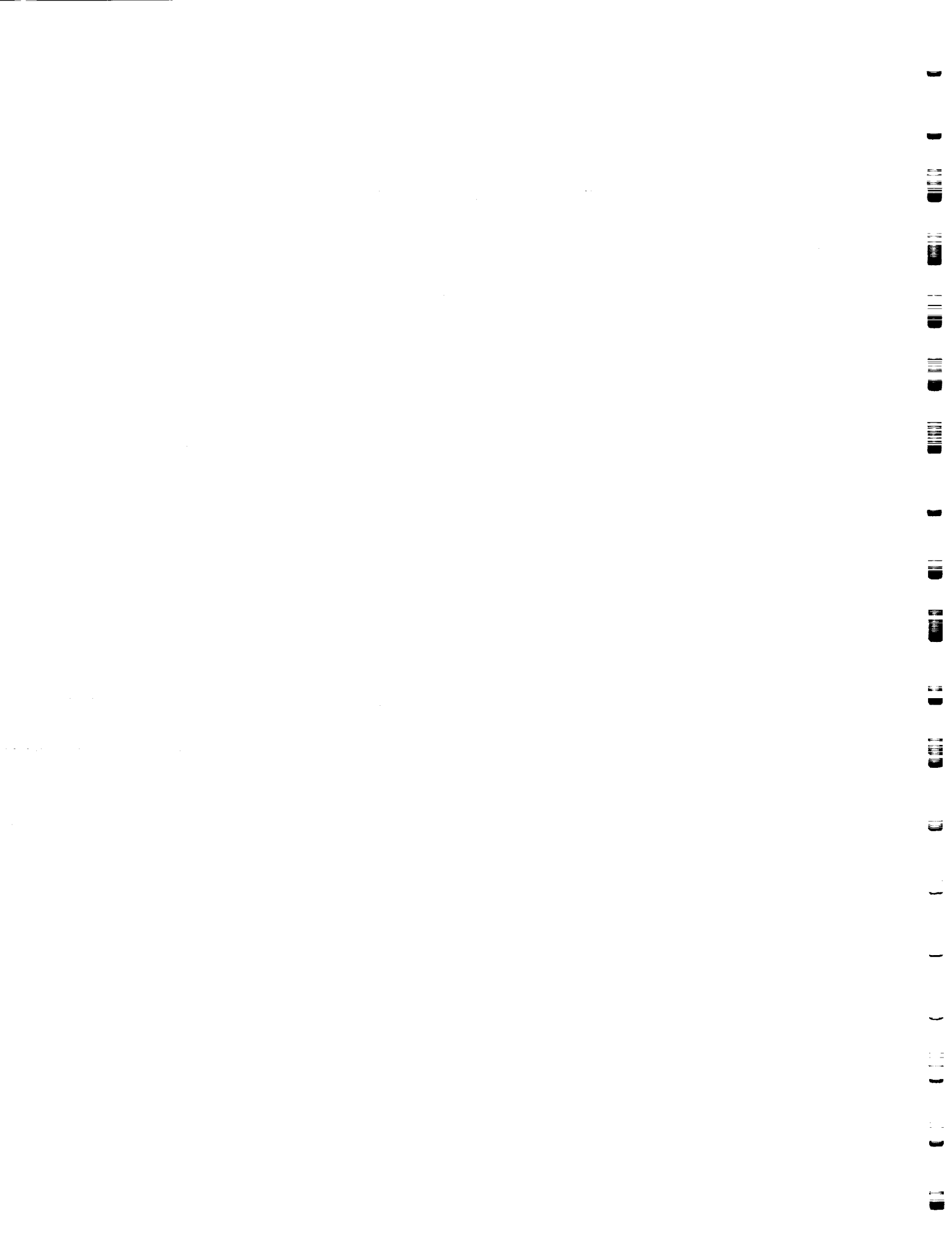
1. Miller, K. M., Ungar, E. K., Dzanitis, J. M., and Wheeler, M., 1993, "Microgravity Two Phase Pressure Drop Data in Smooth Tubing, Lunar,": AMD-Vol. 174/FED-Vol. 175, *Fluid Mechanics Phenomena in Microgravity*, ASME WAM 1993.
2. Ungar, E. K., Miller, K. M., and Chen, I. Y., 1993, "Two Phase Pressure Drop in Lunar and Martian Gravity: Experimental Data and Predictions," ASME FED Vol. 190, pp. 329-342.
3. Reinarts, T. R., Miller, K. M., and Frederick, R. B., 1993, Two Phase Flow Regimes in Smooth Tubing in Microgravity, Lunar Gravity and Martian Gravity, and Earth-Normal Gravity," AMD-Vol. 174/FED-Vol. 175, *Fluid Mechanics Phenomena in Microgravity*, ASME WAM 1993.
4. Boyd, R. D., Smith, A., and Turknett, J., 1995b, "Multi-Dimensional Wall Temperature and Heat Transfer Enhancement for Top-Heated Horizontal Channels with Flow Boiling," *Int. J. of Experimental Heat Transfer, Thermodynamics and Fluid Mechanics*.
5. Kandlikar, S. G., 1991, "Development of Flow Boiling Map for Subcooled and Saturated Flow Boiling of Different Fluids Inside Circular Tubes," *Journal of Heat Transfer*, Vol. 113, February, pp. 190-200.
6. Shah, M. M., 1977, "A General Correlation for Heat Transfer During Subcooled Boiling in Pipes and Annuli," *ASHRAE Transactions*, Vol. 83, pp. 202-215.
7. Gungor, K. E. and Winterton, R. H. S., 1986, "A General Correlation for Flow Boiling in Tubes and Annuli," *International Journal of Heat Transfer*, Vol. 29, No. 3, pp. 351-358.
8. Boyd, R. D. and Meng, X., 1995a, "Boiling Curve Correlation for Subcooled Flow Boiling," *International Journal of Heat Transfer*, Vol. 38, pp. 758-60.
9. Patankar, S. V. and Chai, J. C., 1991, "Laminar Natural Convection in Internally Finned Horizontal Annuli," ASME 91-HT-12.
10. Wen, X. L., Briggs, A., and Rose, J. W., 1991, "Accurate Measurements of Heat Transfer Coefficients for Condensation on Horizontal Integral-Fin Tubes," ASME 91-HT-6.
11. Jaber, M. H., Webb, R. L., and Stryker, P., 1991, "An Experimental Investigation of Enhanced Tubes for Steam Condensers," ASME 91-HT-5.

12. Smith, A., 1992, "Subcooled Freon-11 Flow Boiling Heat Transfer With and Without Enhancement Devices for Top Heated Horizontal Coolant Channel," MS Thesis, Prairie View A&M University.
13. Turknett, J. C., 1989, "Forced Convection and Flow Boiling With and Without Enhancement Devices for Top-Side-Heated Horizontal Channels," MS Thesis, Prairie View A&M University.
14. Boyd, R. D., 1986, "Flow Boiling With and Without Enhancement Devices for Horizontal, Top Heated Coolant Channels for Cold Plate Design Applications, Preliminary Report," Prairie View A&M University, Submitted to NASA (JSC), Contract No. 9-16899.
15. Reid, R. S., Pate, M. B., and Bergles, A. E., 1987, "Evaporation of Refrigerant 113 Flowing Inside Smooth Tubes," ASME 87-HT-51.
16. Huque, Z., Boyd, R. D., and Smith, A., 1993, "Experimental Design for Flow Boiling in Thermal Management Systems," *Proceedings of the Mechanical Engineering Symposium*, Prairie View A&M University, Prairie View, Texas, pp. 117-122.
17. Davis, E. J. and Anderson, G. H., 1966, "The Incipience of Nucleate Boiling in Forced Convection Flow," *AIChE Journal*, Vol. 12, No. 4, pp. 774-780.
18. Perry, R. H. and Green, D., 1984, *Perry's Chemical Engineers' Handbook*, McGraw Hill Publishing Company, Sixth ed., pp. 3-275, 3-276, 3-288.
19. Huque, Z. and Boyd, R. D., 1994, "Two-Dimensional Data Reduction Applying an Inverse Heat Conduction (IHC) Technique," *Proceedings of the Mechanical Engineering Symposium*, Prairie View A&M University, Prairie View, Texas, pp. 66-72.
20. Boyd, R. D., et al., 1984, "Preliminary Design Analysis of ALT-II Limiter for TEXTOR," *Journal of Nuclear Materials*, 121, pp. 309-315.
21. Marshall, T., et al., 1994, "Post Critical Heat Flux and Log of Flow Accident Experiments," US/Japan Helium Cooling Workshop, General Atomics Corporation, San Diego, CA.
22. Chen, J. C., 1966, "A Correlation for Boiling Heat Transfer to Saturated Fluids in Convective Flows," *Industrial and Engineering Chemistry Process Design and Development*, Vol. 5 No. 3, pp. 322-329.
23. Shah, M. M., 1977, "A General Correlation for Heat Transfer During Subcooled Boiling in Pipes and Annuli," *ASHRAE Transactions*, Vol. 83, pp. 202-215.



24. Steiner, D. and Taborek, J., 1992, "Flow Boiling Heat Transfer in Vertical Tubes Correlated by an Asymptotic Model," *Heat Transfer Engineering*, Vol. 13, No. 2, pp. 43-66.
25. Liu, Z. and Winterton, R. H. S., 1991, "A General Correlation for Saturated and Subcooled Flow Boiling in Tubes and Annuli, Based on a Nucleate Pool Boiling Equation," *International Journal Heat Mass Transfer*, Vol. 34, No. 3, pp. 2759-2763.
26. Gungor, K. E. and Winterton, R. H. S., 1986, "A General Correlation for Flow Boiling in Tubes and Annuli," *International Journal Heat Mass Transfer*, Vol. 29, No. 3, pp. 351-358.
27. Gungor, K. E. and Winterton, R. H. S., 1986, "Simplified General Correlation for Saturated Flow Boiling and Comparison of Correlations with Data," *Chem. Eng. Res. Des.*, Vol. 65, pp. 148-156.
28. Kandlikar, S. G., 1990, "A General Correlation of Saturated Two-Phase Flow Boiling Heat Transfer Inside Horizontal and Vertical Tubes," *Journal of Heat Transfer*, Vol. 112, pp. 219-228.
29. Kattan, N., Thome, J. R., and Favrat, D., 1995, "Flow Boiling in Horizontal and Vertical Tubes: The Effect of Tube Orientation on Heat Transfer," *Convective Flow Boiling International Conference Proceedings*, Engineering Foundation, Paper No. IV-1, Banff, Alberta, Canada.
30. Kirk, K. M., Mete, H. Jr., and Keller, R., 1995, "Low-Velocity Subcooled Nucleate Flow Boiling at Various Orientations," *Journal of Heat Transfer*, Vol. 117, pp. 380-385.
31. Peatiwala, Q. and Boyd, R. D., 1995, "Forced Convection and Flow Boiling in a Single-Side Heated Vertical Smooth Channel with Downward Flow," *National Heat Transfer Conference*, Vol. 314, pp. 133-143.
32. Chen, J. C. and Tuzla, K., 1995, "Contribution of Convection and Boiling to Convective Flow Boiling" *Convective Flow Boiling International Conference Proceedings*, Engineering Foundation, Paper No. IV-10, Banff, Alberta, Canada.
33. Boyd, R. D., 1992, "Subcooled Flow Boiling Model Assessment and Development," Interim Report, TSRC-2, NRC-0491364.
34. Meng, X., "Heat Transfer Predictions and Numerical Data Reduction for Freon-11 Boiling in Enhanced and Smooth Wall Channels," MS Thesis, Department of Mechanical Engineering, Prairie View A&M University.

35. Naylor, D. and Oosthuizen, P. H., 1993, "Evaluation of a Inverse Heat Conduction Procedure for Determining Local Convective Heat Transfer Rates," Inverse Problems in Engineering: Theory and Practice, Nicholas Zabarar, et., ed., pp. 125-131.
36. Dorri, B. and Chandra, U., 1991, "Determination of Thermal Contact Resistances Using Inverse Heat Conduction Procedure," Numerical Methods in Thermal Problems: Proceedings of the Seventh International Conference, R. W. Lewis ed., Vol. VII, Part 1, pp. 213-223.



APPENDIX
(REPRINTS of PUBLISHED
TECHNICAL PAPERS)



Two-Dimensional Wall Temperature Measurements and Heat Transfer Enhancement for Top-Heated Horizontal Channels with Flow Boiling

Ronald D. Boyd

Alvin Smith*

Jerry C. Turknett†

*Thermal Science Research Center,
College of Engineering and Architecture,
Prairie View A & M University,
Prairie View, Texas*

■ Two-dimensional (circumferential and axial) wall temperature distributions were measured for top-heated coolant channels with internal geometries that include smooth walls, spiral fins, and both twisted tape and spiral fins. Freon-11 was the working fluid. The flow regimes studied were single-phase, subcooled flow boiling, and stratified flow boiling. The inside diameter of all test sections was near 10.0 mm. Circumferentially averaged heat transfer coefficients at several axial locations were obtained for selected coolant channels for a volumetric flow rate of $4.738 \times 10^{-5} \text{ m}^3/\text{s}$, 0.19 MPa (absolute) exit pressure, and 22.2°C inlet subcooling. Overall (averaged over the entire channel) heat transfer coefficients were compared for the various channel geometries. This comparison showed that the channel with large-pitch spiral fins had higher heat transfer coefficients at all power levels. However, the results appear to indicate that if the twist ratio (ratio of the twisted tape period to the inside diameter) is decreased, the configuration employing both fins and a twisted tape will have had greater enhancements.

Keywords: *two-dimensional, wall temperature, single-side heating, flow boiling, heat transfer coefficient, horizontal channel*

INTRODUCTION

Space commercialization will require efficient heat transfer systems. The future success of many efforts will be based on our understanding of the behavior of two-phase flow boiling in both space (zero g or reduced g) and earth environments. This was emphasized in the Workshop on Two-Phase Fluid Behavior in a Space Environment sponsored by NASA in 1989 [1]. Flow boiling heat transfer offers an enhancement alternative to forced-primed and capillarity heat management systems. The following effects are essential to a better understanding of the factors that affect flow boiling in heated tubes: (1) nonuniform heat flux distribution, (2) local (axial and circumferential) distributions of the heat transfer coefficient, (3) resulting pressure drop and pumping power requirements, (4) single and double enhancement devices, (5) the relative advantages of saturated and subcooled flow boiling regimes, (6) flow channel aspect ratio effects, (7) the relative effects

of heat transfer enhancement techniques, and (8) correlations for mean and local heat transfer and pressure drop.

In the past, significant progress has been made in extending the experimental (e.g., [2–4]) and correlational (e.g., [5–10]) ranges of applicability for two-phase heat transfer in uniformly heated tubes. However, most of the previous work did not include the essential effect of single-side heating. In addition to being applicable to single-side heating and several gravitational levels, future research efforts must also include basic phenomena such as (1) orientation (e.g., vertical flow and bottom-heated flow channels) and Marangoni effects, (2) other working fluids such as ammonia, (3) flow stability, (4) binary fluids, and (5) identification of the threshold inertia (Froude number) beyond which gravity effects would be negligible. For example, threshold inertia determination is necessary to identify when orientation and/or Marangoni effects become important. Although it is not apparent, the devel-

Address correspondence to Professor Ronald D. Boyd, Thermal Science Research Center, College of Engineering and Architecture, Prairie View A & M University, P.O. Box 397, Prairie View, TX 77446.

* Present address: Saturn Corporation, 100 Saturn Parkway, P.O. 1500 MD-K-17, Spring Hill, TN 37174-1500.

† Present address: Westinghouse Savannah River Company, P.O. Box 616, Bldg 705-1c, Aiken, SC 29802.

Experimental Thermal and Fluid Science 1995; 11:372–386

© Elsevier Science Inc., 1995
655 Avenue of the Americas, New York, NY 10010

0894-1777/95/\$9.50
SSDI 0894-1777(95)00060-Y

opment of improved data reduction models is also essential to the accurate representation and interpretation of the heat transfer data.

This work will assist the development of fundamentally based heat transfer correlations that include effects of (1) enhancement device configurations for fluids other than air [11], (2) basic flow parameters that are fluid-independent, and (3) complex heat flux distributions.

This paper examines, experimentally, two-dimensional (2-D) wall temperature variations for turbulent horizontal channel flows that are heated from the top. The Reynolds number (Re) was near 1.5×10^4 , and Freon-11 was the working fluid. The temperature measurements were used to obtain axial variations in the circumferentially averaged heat transfer coefficient (h_m). The overall heat transfer coefficient (h) was determined and compared for four different internal channel enhancement configurations (see Table 1):

1. Smooth wall [$G = 781.2 \text{ kg}/(\text{m}^2 \text{ s})$],
2. Spiral fins with a small pitch (SP, 0.652 fin/mm) and $G = 700.0 \text{ kg}/(\text{m}^2 \text{ s})$,
3. Spiral fins with a larger pitch (LP, 0.4 fin/mm) and $G = 991.0 \text{ kg}/(\text{m}^2 \text{ s})$,
4. Doubly enhanced spiral fins with both large-pitch fins and a twisted tape, $G = 991.0 \text{ kg}/(\text{m}^2 \text{ s})$.

EXPERIMENTAL INVESTIGATION

In this section, brief descriptions are given of the Freon-11 flow loop, test section, and the data reduction procedure.

Flow Loop

The flow loop (see Fig. 1) was a closed system that operates between 0.1 MPa ($T_{\text{sat}} = 24^\circ\text{C}$) and 1.3 MPa ($T_{\text{sat}} = 124^\circ\text{C}$). The total power generation was 2.6 kW, and the maximum mass velocity for these experiments was $1000.0 \text{ kg}/(\text{m}^2 \text{ s})$. Under special circumstances, the loop can be operated at a pressure near 0.04 MPa ($T_{\text{sat}} = 0^\circ\text{C}$). The loop has two reservoirs (0.25 m^3 each). The reservoirs have separate heat exchanger jackets for secondary temperature control. The flow loop tubing was 25.0 mm I.D. stainless steel. The flow loop consists of (1) the freon loop, (2) air lines for pneumatically controlling valves and pulsation damper, and (3) vacuum lines for system evacuation.

The freon loop was designed to study both saturated and subcooled flow boiling regimes. After the loop was evacuated, it was filled with freon until the pressure was slightly above atmospheric. After the charging process, the fluid was circulated through the loop at the desired oper-

ating conditions. Bleed valves were used to purge the loop and transducers of any gases, and the flow conditions were reestablished. During a given test, the heater tape power output was adjusted to a given level. The flow rate of the isothermal bath (50%–50% mixture of ethylene glycol and water) was adjusted until the test section inlet temperature was at the desired level. A steady state was then allowed to occur. After all the desired flow conditions were again verified, the test section's axial and circumferential wall temperature measurements were recorded along with all the flow conditions.

Referring to Fig. 1, the freon flowed from reservoir 1 through a filter to the main pump (positive displacement), which required a net positive suction pressure of at least 0.02 MPa. After leaving the pump, the fluid passed near a pulsation damper, which reduced the pressure and flow oscillations. When the damper was used, a pneumatically controlled metering valve was used to stabilize the flow. After exiting the metering valve, the fluid passed through a turbine flowmeter and then through an unheated flow-developing section (upstream portion of the test section) that had a length greater than 40 times the test section diameter. This flow-developing section had the same diameter as the heated portion of the test section. As the fluid flowed through the test section, the inlet and exit temperatures and pressures were monitored. The downstream portion of the test section was heated (with a heater tape) on its top half. A downstream valve was used to control the test section exit pressure. The fluid then passed through the heat exchanger where the energy generated in the test section was removed. For these tests, the working fluid bypassed both reservoir 2 and the charging pump and then flowed back to reservoir 1.

Test Section

The test section was 2.23 m long and is shown in Figs. 2 and 3. The upstream unheated portion of the test section had smooth walls, and the downstream heated portion (1.219 m long) had either smooth walls or an enhanced wall configuration (spiral fins and/or a twisted tape). In cases where the spiral fins and twisted tape were used simultaneously, the tape twist corresponded to the twist of the spiral fins. The entire test section was insulated and had three main ports (with a fourth extending from the center one), mounted facing downward on either end of the test section. These ports were used to monitor the inlet and exit fluid pressures, temperatures, and test section differential pressure. Each test section had 28 Type K thermocouples mounted on the outside surface of the

Table 1. Test Section Internal Configurations

Tube Type ^a	O.D. (mm)	I.D. (mm)	No. Fins	Fin Height (mm)	Fin Width (mm)	Fins / mm
Spiral fin L.P.	12.7	9.5	16	0.56	3.0	0.4
Spiral fin L.P./tape	12.7	9.5	16	0.56	3.0	0.4
Spiral fin S.P.	12.7	11.3	26	0.56	3.0	0.6
Smooth walls	1.27	1.07	—	—	—	—

^a L.P. and S.P. denote large-pitch and small-pitch fins, respectively.

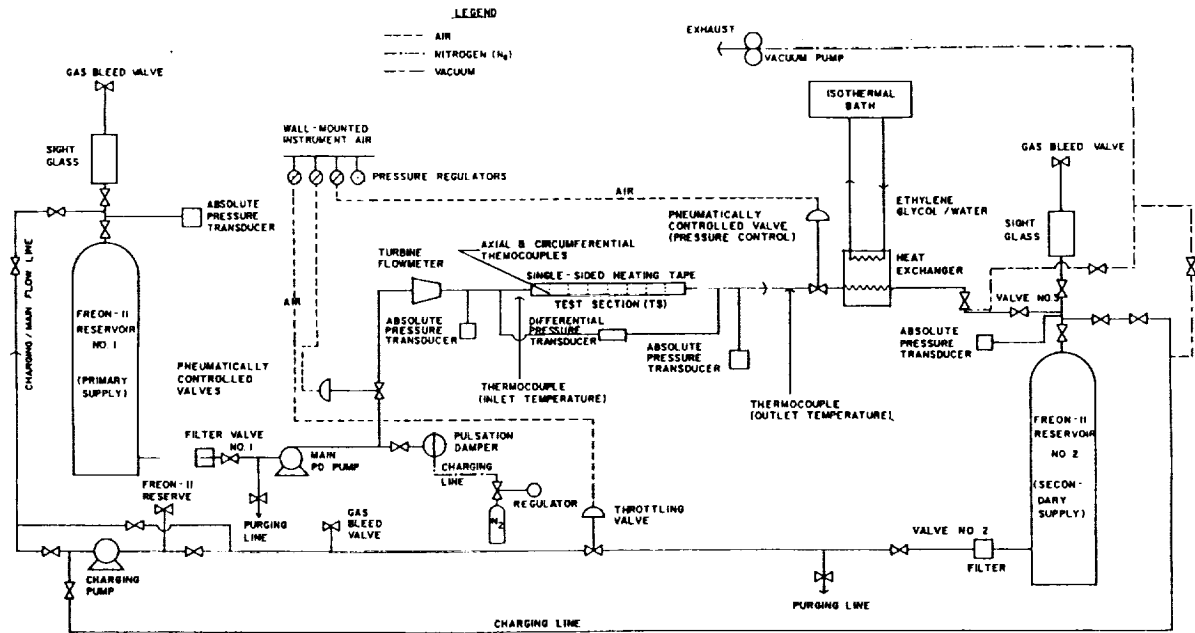


Figure 1. Freon-11 flow loop for both subcooled and saturated flow boiling experiments.

copper flow channel. Seven thermocouples were used to make temperature measurements (T_m) at specific axial locations (see Fig. 3) on the wall of the coolant channel. Figure 3 also shows the four circumferential locations ($\phi = 0, \pi/4, 3\pi/4$, and π radians) at which wall temperature measurements were made for each of the seven axial locations. All measurements were made for flow conditions of 0.19 MPa (absolute) exit pressure, 22.2°C

inlet temperature, and a volumetric flow rate of $4.738 \times 10^{-5} \text{ m}^3/\text{s}$. These wall temperature measurements were used, along with other measured conditions and the data reduction analysis, to determine the unknown steady-state heat transfer coefficients (h and h_m).

Data Reduction

The data reduction approach was based on a heated hydraulic diameter [12] assumption. Figure 4 shows the model used for this approach. This model was used to compute a circumferentially averaged heat transfer coefficient from the circumferentially averaged wall temperature. This latter temperature was computed from the four wall temperature measurements made on the outside of the test section at each of the seven axial locations.

Briefly, this approach involves estimating the inside flow channel's wall temperature by using an equivalent uniformly heated tube whose diameter is equal to the ratio of four times the actual flow channel cross-sectional area to the heated perimeter. This was done using the model in Fig. 4, by accounting for the temperature drop across the flow channel wall and the heat losses (convection and radiation) from the test section to the ambient. An iterative scheme was necessary to compute the inside wall temperature. After accounting for finite heat losses, the circumferentially averaged heat transfer coefficient was given by [12, 13]

$$h_m = A/B, \quad (1)$$

where

$$A = \left(\frac{k_A}{r_A} \right) B_1 \left[\ln \left(\frac{r_D}{r_C} \right) + \frac{k_C}{h_x r_D} \right] - \frac{k_C}{r_A} (T_m - T_x),$$

$$B = B_2 + B_3 + B_4,$$

$$B_1 = P_p r_C / A_s k_B,$$

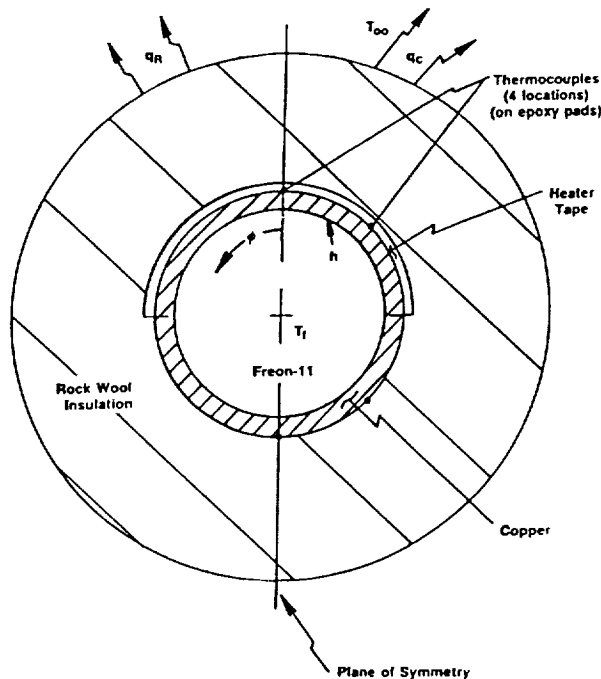


Figure 2. Cross section of the heated portion of the test section.

LOCATION OF MEASUREMENTS (m)

Z1	Z2	Z3	Z4	Z5	Z6	Z7
0.0	0.2032	0.4064	0.6096	0.8128	1.016	1.219

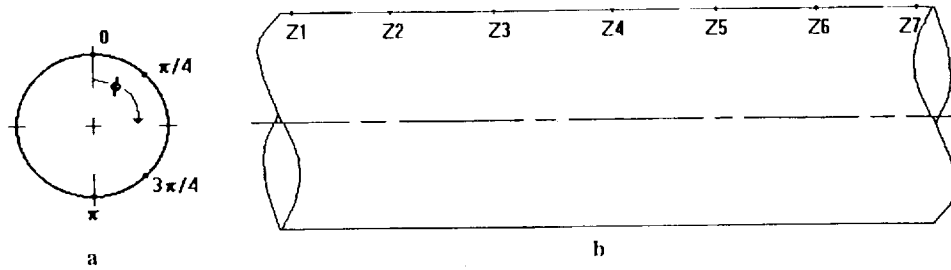


Figure 3. Wall temperature measurement locations. (a) cross section locations; (b) axial locations along heated length.

$$B_2 = (T_m - T_\infty) \left[\ln \left(\frac{r_D}{r_C} \right) + \frac{k_C}{h_z r_D} + \frac{k_C}{k_B} \ln \left(\frac{r_C}{r_B} \right) \right],$$

$$B_3 = (T_m - T_\infty) \left[\frac{k_C}{k_A} \ln \left(\frac{r_B}{r_A} \right) \right]$$

$$- \left[\ln \left(\frac{r_D}{r_C} \right) + \frac{k_C}{h_z r_D} \right] (T_f - T_\infty),$$

and

$$B_4 = B_1 \left[\ln \left(\frac{r_C}{r_B} \right) + \frac{k_B}{k_A} \ln \left(\frac{r_B}{r_A} \right) \right].$$

In Eq. (1) the magnitude of the bulk temperature, T_f , is dependent on T_{av} , which is the circumferentially averaged wall temperature at $r = r_C$ (see Figs. 3 and 4). T_f was determined based on the magnitude of T_{av} relative to the wall temperature, $T_{w,ONB}$, which is the temperature required for the onset of nucleate boiling (ONB). The bulk

fluid temperature is given by

$$T_f = \begin{cases} T_f(z), & T_{av} < T_{w,ONB} \\ T_{sat}, & T_{av} \geq T_{w,ONB} \end{cases} \quad (2)$$

For a given axial location, the measured circumferential values of T_m were related to T_{av} by

$$T_{av} = \frac{T_m(\phi=0) + 3T_m(\phi=\pi/4) + 3T_m(\phi=3\pi/4) + T_m(\phi=\pi)}{8} \quad (3)$$

Finally, the temperature $T_{w,ONB}$ was computed using the correlation of Frost and Dzakowic (see Collier [14]).

$$1.0 = 8.0 St_{ONB} Pe We^{*-1} Ec Ja^* \quad (4)$$

In some cases, the heat transfer coefficient was averaged not only circumferentially but also axially. Although there were seven axial locations at which wall temperature measurements were made, those measurements near either end of the test section heated length were influenced by end losses. Hence, the averaged heat transfer coefficient h was obtained by using the five central axial locations (Z_2, Z_3, Z_4, Z_5 , and Z_6),

$$h = \frac{h_{m_2} + 2h_{m_3} + 2h_{m_4} + 2h_{m_5} + h_{m_6}}{8} \quad (5)$$

so that the values of h_{m_i} (where $i = 2, 3, 4, 5, 6$) correspond to the value of h_m at various locations Z_i .

An uncertainty analysis was developed using the above formulas to estimate the uncertainty, δh_m . Using the approach suggested by Moffat [15, 16], δh_m was found to be $\pm 14.6 \text{ W/(m}^2 \text{ K)}$ (see the Appendix).

RESULTS

For the various internal channel configurations noted above, comparisons were made of the 2-D wall temperature distributions, axial distribution of the mean (circumferentially averaged) heat transfer coefficient h_m , and the totally averaged (circumferentially and axially) or overall heat transfer coefficient h . Additional details and data tabulation can be found in [13, 17].

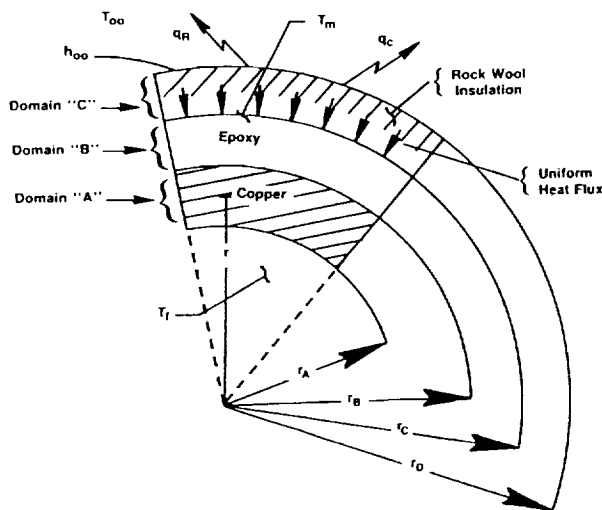


Figure 4. Control volume for the heated hydraulic diameter model.

Overall Heat Transfer

Figure 5 shows a comparison of the overall heat transfer coefficient for the four internal configurations. These comparisons show that the spiral fins with the large pitch resulted in a higher heat transfer coefficient essentially at all power levels. The discontinuities in each curve are due to either nucleate boiling or severe flow structure changes at certain axial or circumferential locations for a given power level. Since the test section was horizontal and the mass velocity level was relatively low (low Froude number), stratification effects were expected and were found to be significant. Stratification conditions reduced the enhancement effectiveness for all internal configurations. Preliminary estimates indicated that these reductions could be as high as a factor of 2 relative to vertical flows.

Although the mass velocity is different for some cases, the Reynolds number (Re) for all cases is nearly the same: (1) 1.61×10^4 for the large-pitch spiral fin tube with and without a twisted tape, (2) 1.43×10^4 for the smooth tube, and (3) 1.35×10^4 for the small-pitch spiral fin tube. Hence, the above-noted differences cannot be attributed to differences in Re .

Two-Dimensional Wall Temperature Distributions

Figures 6 and 7 show the power generation as a function of measured outside wall temperature at various circumferential and axial locations for the cases of large-pitch spiral fins without and with a twisted tape, respectively. The three parts in each of these figures are for three of the four circumferential locations ($\phi = 0, \pi/4$, and π ;

see Fig. 3). As ϕ varied from 0 to $\pi/4$, the peak wall temperatures for the case of large-pitch fins with the twisted tape were consistently higher than those for the channel with only the large-pitch spiral fins. This is displayed more dramatically in Fig. 8, which shows the axial distribution of $T_w (= T_m)$ for the four circumferential locations and constant power. While the wall temperature distributions were essentially identical for $\phi = 3\pi/4$ and π , there were significant differences at $\phi = 0$ and $\pi/4$ (compare Figs. 8a and 8b). It is apparent from the figures that the addition of a tape increased mixing near the top of the channel and hence increased the stratification at downstream locations. For the case without the twisted tape and for $\phi = 0$, the wall temperature in the upstream portion of the test section between Z_2 ($Z = 203.2$ mm) and Z_4 ($Z = 609.8$ mm) was consistently lower than that with the twisted tape. However, this trend reversed downstream of Z_5 ($Z = 812.8$ mm). Since the power level for the large-pitch finned tube in Fig. 8a ($P_p = 493.0$ W) was greater than that for the large-pitch finned tube with a twisted tape (shown in Fig. 8b with $P_p = 480.0$ W), the profiles for the former case will be consistently lower than those for the latter case at the same power level. With the exception of the differences noted at $\phi = 0$ and $\pi/4$, the two profiles were similar. Further, for the case with the twisted tape and the large-pitch fins with $\phi = \pi/4$, the wall temperature varied axially in a periodic manner between maxima of 155°C (upstream) and 90°C (downstream). As there were only seven axial locations in which measurements were made, it was not possible to determine the period of this variation.

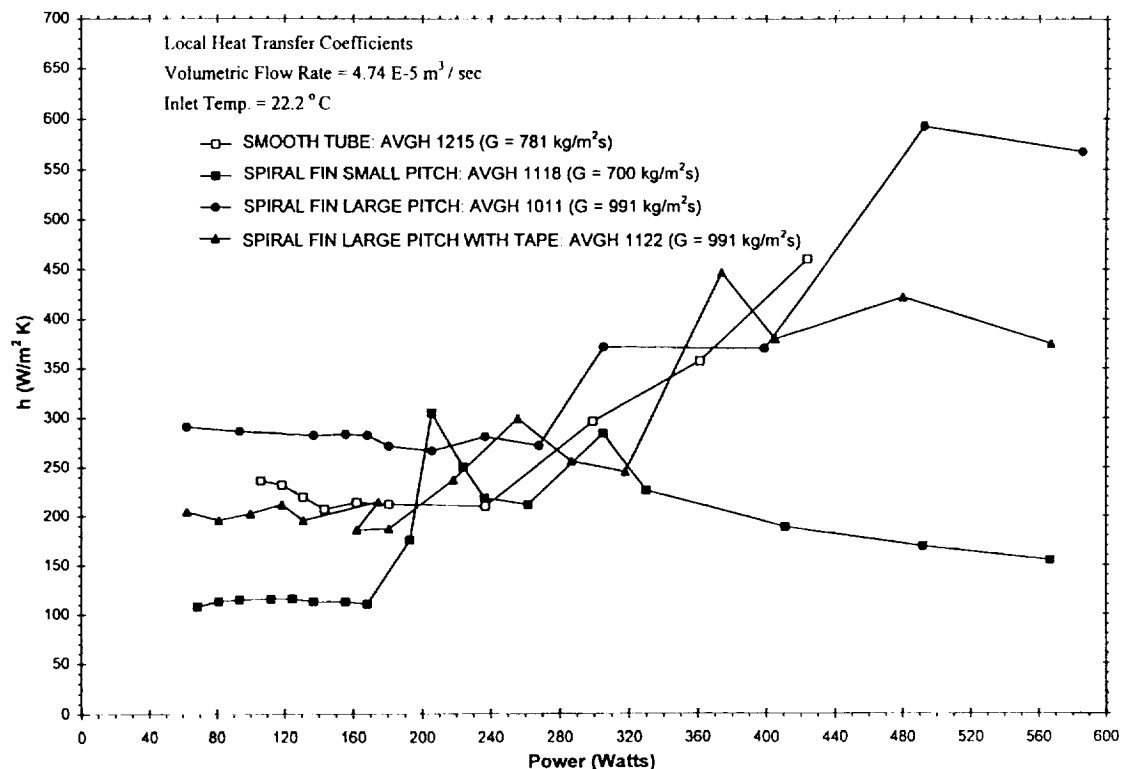
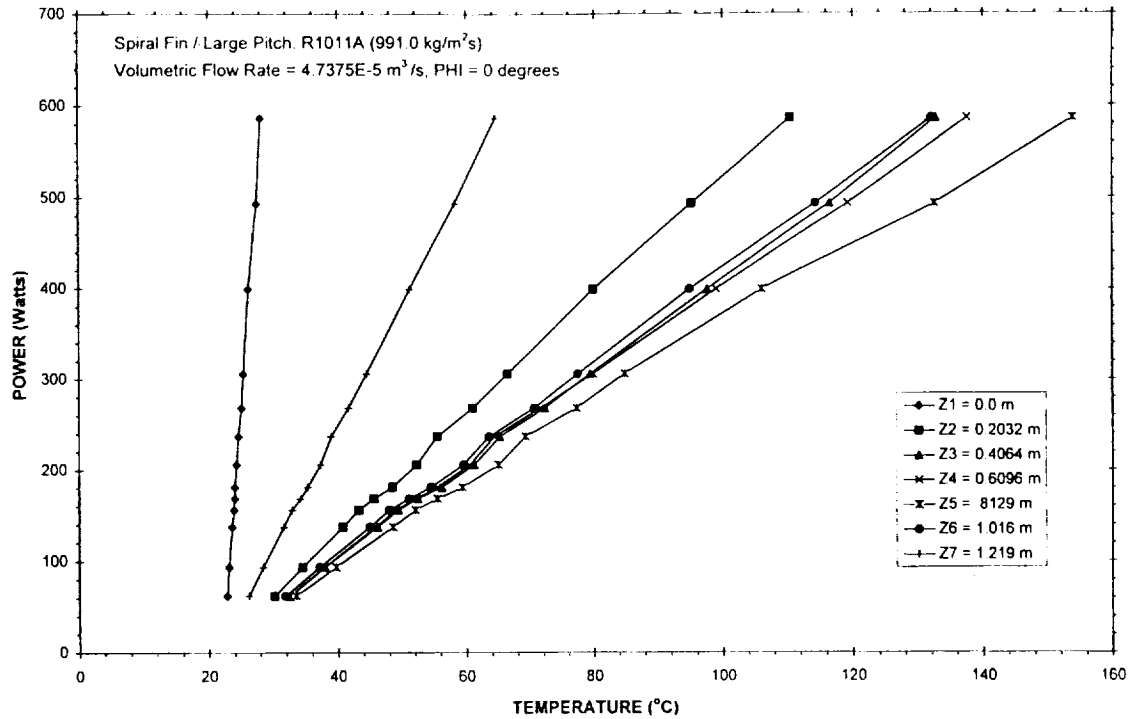
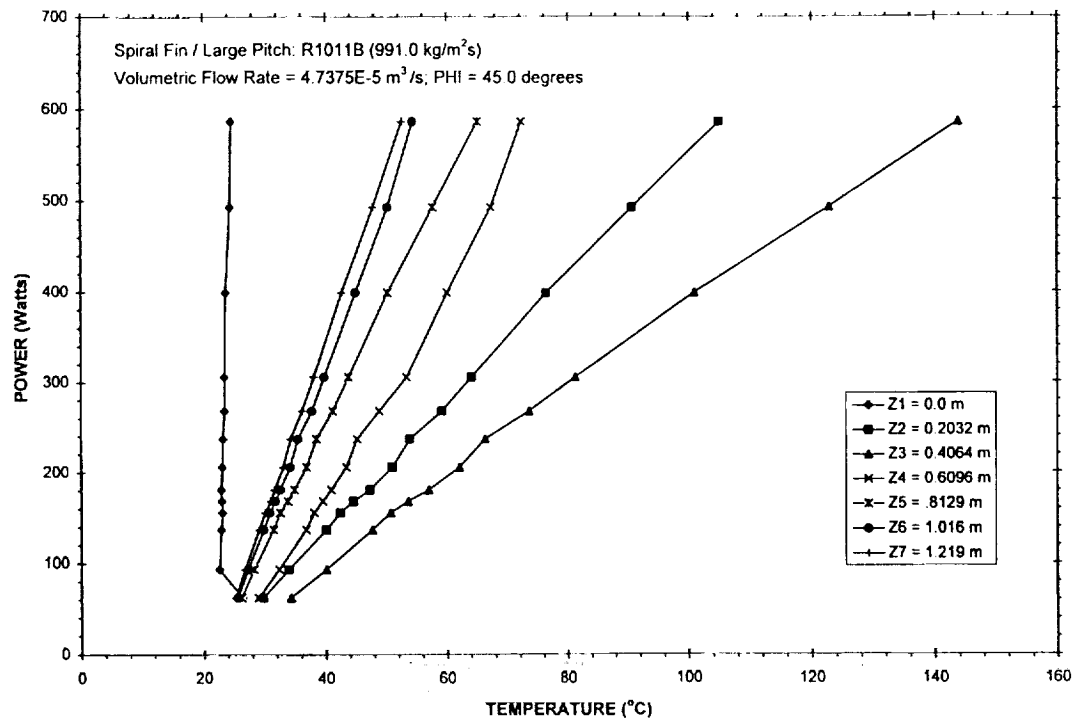


Figure 5. Comparison of the overall heat transfer coefficients for circular coolant channels with different internal configurations.



a



b

Figure 6. Measured outside wall temperature at selected axial locations as a function of the net power generation for the spiral fin, large-pitch internal geometry at (a) $\phi = 0$, (b) $\phi = \pi/4$, (c) $\phi = \pi$.

tion. However, the present measurements indicate that the period was less than 0.4 m. As implied above, the amplitude of the fluctuations decreased as Z increased. These latter trends were influenced possibly by (1) periodic liquid wetting near $\phi = \pi/4$ (off-center from the top

of the channel) due to the swirl flow, (2) liquid entrainment into the vapor flow, and (3) circumferential and axial conduction in the tube.

From Figs. 8a and 8b, stratification effects can be seen to have been significant in that (1) the wall temperatures

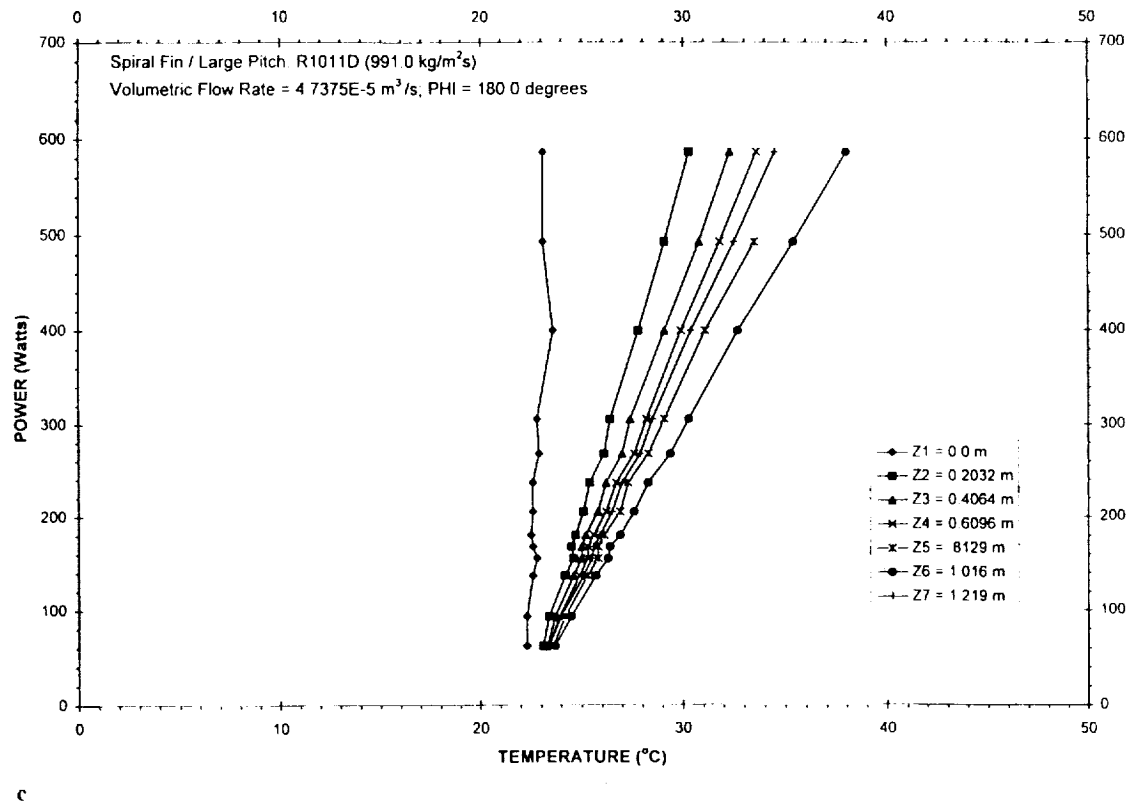


Figure 6. Continued.

at $\phi = 0$ remained significantly above (vapor region) the saturation temperature ($T_{\text{sat}} = 43^\circ\text{C}$) and (2) those wall temperatures at $\phi = 3\pi/4$ and π were consistently below (liquid region) T_{sat} . However, the tubes with the large-pitch fins (with and without the twisted tape) increased stratification at upstream locations more than the small-pitch finned wall tube. This effect could have been caused by reduced radial mixing. However, as Z was increased, the stratification decreased more for the former two configurations than for either the smooth tube or the small-pitch fins (compare Figs. 8a and 8b with 8c and 8d). Although the power levels for the latter two figures are lower than those of the former two, a comparison of the axial distribution of the circumferentially averaged wall temperatures clearly shows larger changes in the gradient of T_w with respect to Z for the large-pitch finned wall. In fact, the large-pitch spiral fin with the twisted tape had the greatest changes.

In all tube configurations, the wall temperature increased (from 22.2°C) with Z near the entrance (Z_1) and later decreased (to near 25.0°C) as Z approached Z_7 , near the exit of the test section.

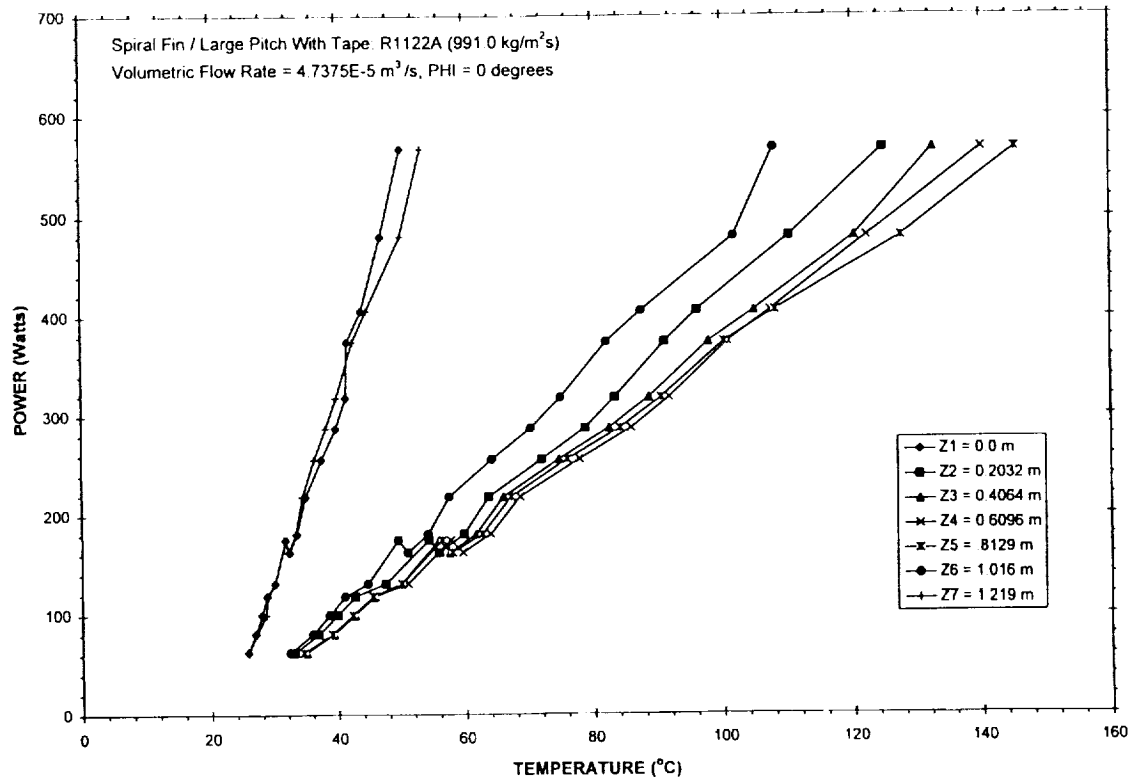
Circumferentially Mean, Axially Distributed Heat Transfer

Figures 8a and 8b emphasize the significance of the circumferential temperature variations in systems with single-side heating. It is apparent that in cases where stratification is important, the addition of a twisted tape will, at some locations, exacerbate (compare Figs. 8a and

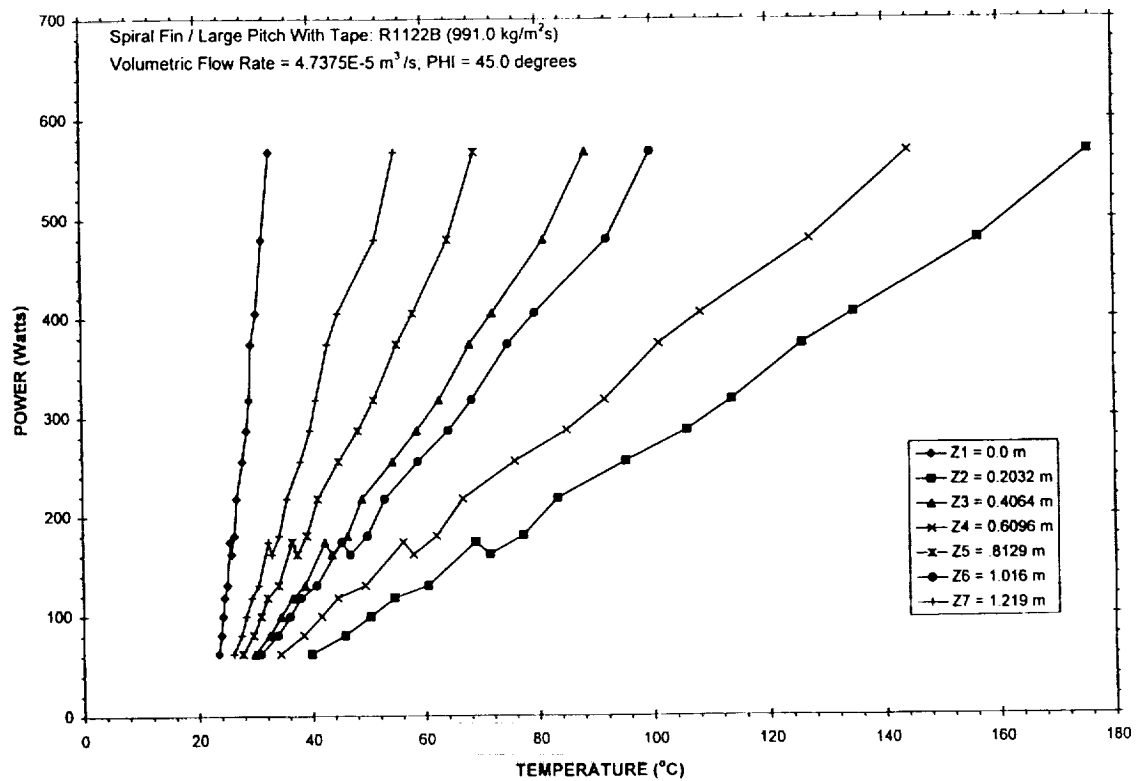
8b for $\phi = \pi/4$) the already high wall temperature and small heat transfer coefficient. However, the data also indicate that the twisted tape will enhance, rather than inhibit, the heat transfer in some cases. Before turning this enhancing effect, the adverse influence of the twisted tape on the heat transfer coefficient will be discussed.

The detrimental influence on h_m due to the addition of the twisted tape was emphasized by considering the circumferentially averaged heat transfer coefficients as a function of the power generation, with Z as a parameter. At each axial location, a sudden rise in h_m was a manifestation of the inside wall temperature (computed from the measured outside wall temperature) exceeding the absolute wall superheat required for the onset of nucleate boiling. Relatively speaking, larger values of $1/[1500\text{--}2000 \text{ W/(m}^2 \text{ K)}]$ were obtained at both the entrance (Z_1) and the exit (Z_7) than at intermediate locations. This is due to (1) entrance effects, (2) the presence of the single-phase liquid at the bottom of the tube, (3) axial conduction losses, and (4) the absence of heating from the heater tape near the exit. Therefore, the data near the test section exit and entrance may not be representative of the actual behavior. Nevertheless, when the values of h_m at the intermediate axial locations are compared, one finds that the levels of h_m before and after ONB were higher for the tube without the twisted tape.

The above trends could possibly be reversed by reconfiguring the twisted tape. The twisted tape twist ratio (τ , ratio of the axial period to the inside diameter) appears to be the underlying factor that could improve the enhance-



a



b

Figure 7. Measured outside wall temperature axial distribution as a function of the net power generation for the spiral fin, large-pitch with a twisted tape internal geometry at (a) $\phi = 0$, (b) $\phi = \pi/4$, and (c) $\phi = \pi$.

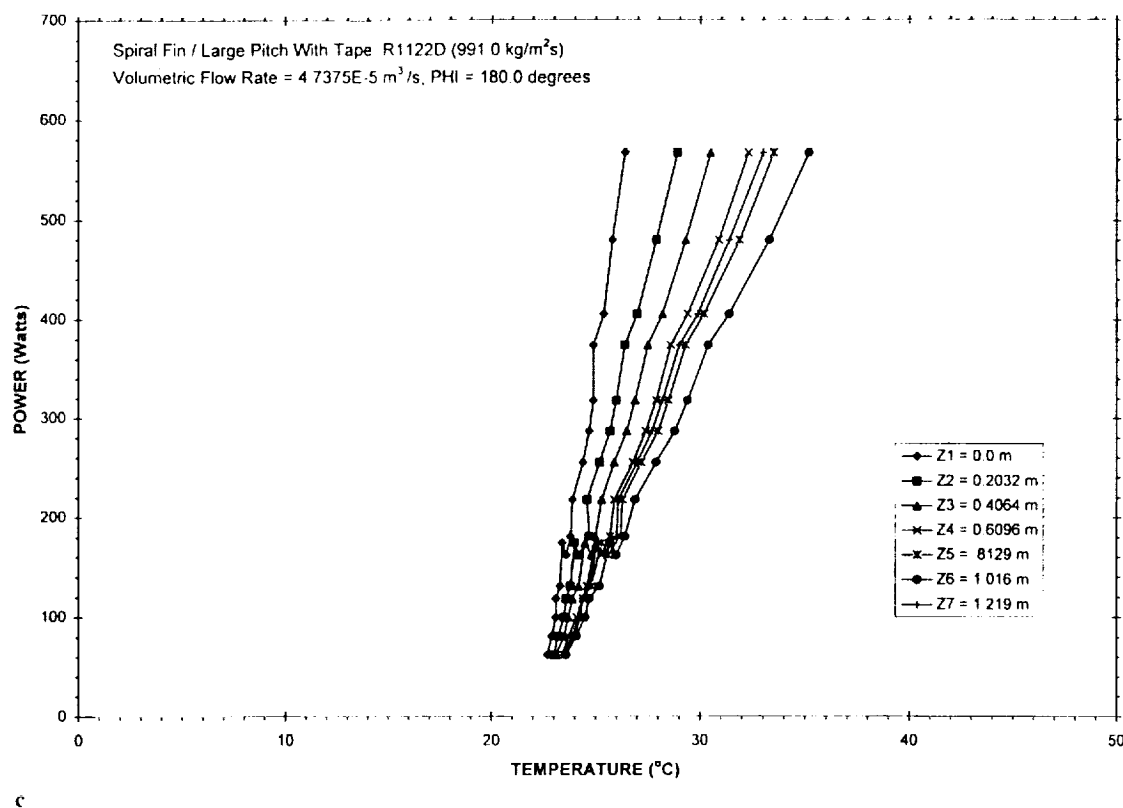


Figure 7. Continued.

ment capabilities of the tube with both fins and a twisted tape. Supporting evidence for this possibility can be observed by comparing either Fig. 6b with Fig. 7b or Fig. 8a with 8b for $\phi = \pi/4$. As noted earlier, the effect of the twisted tape is to raise the local wall temperature at some axial locations and lower it at other locations. In cases where the wall temperature was lowered, these lower values (as well as the peak values) decreased with increasing Z . It would appear that if the period of these temperature fluctuations could be decreased, the lower levels of the wall temperature would prevail over a large portion of the flow channel. Lower temperatures, and hence larger h_m , would result owing to increased mixing between the stratified fluid layers. This overall trend, of enhanced heat transfer accompanying reduced t_T , has been pointed out in the literature (e.g., see Kirishenko [18] and Hong and Bergles [19]) but has never to our knowledge been documented by local measurements on top-heated tubes. However, to verify that this is also true for stratified flows, the present work should be extended to include lower values of t_T .

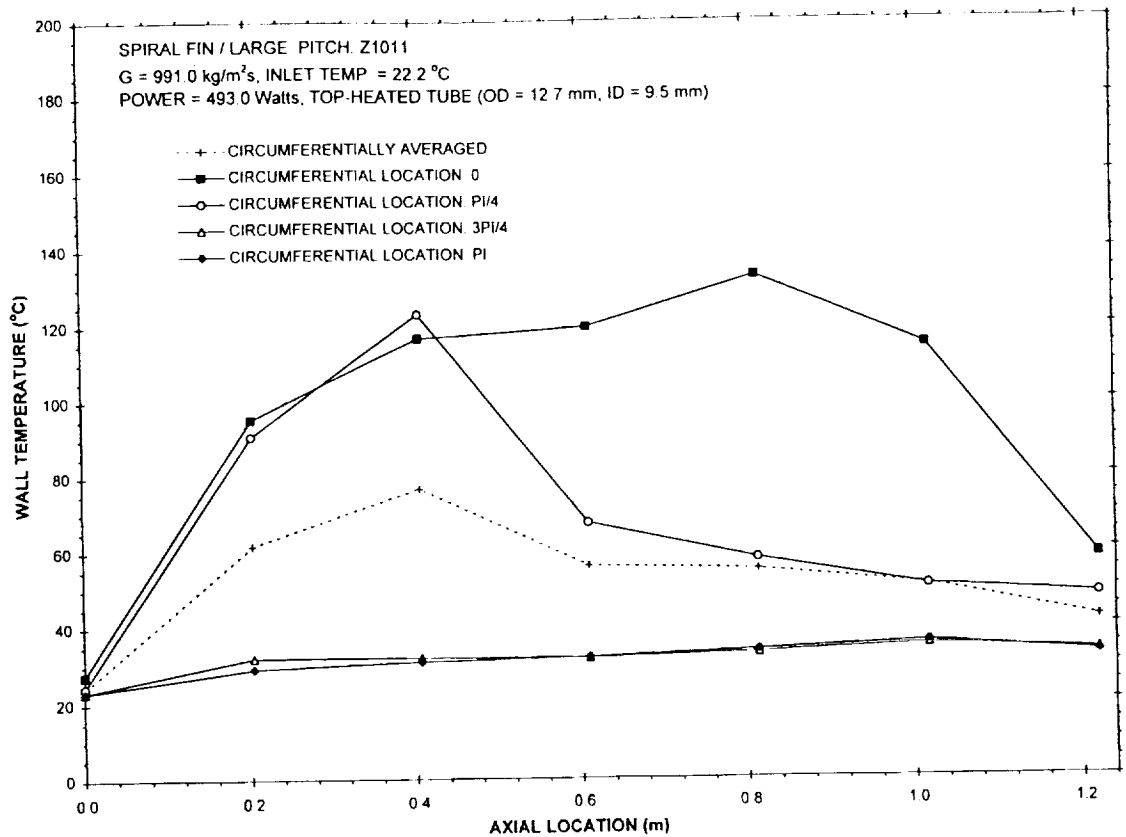
The axial distribution of the circumferential mean heat transfer coefficient (h_m) is shown in Fig. 9 for three of the four internal tube configurations. The axial trends for the smooth wall case in Fig. 9c form a basis for the other cases. The trends in the axial variation of $h_m(Z)$ become increasingly irregular as the internal enhancement progresses from smooth wall tube to small-pitch fins and eventually to large-pitch fins with the twisted tape. There was a reduction and subsequent increase in $h_m(Z)$ as Z increased, which is similar to observations made by Reid

et al. [20] for the case of uniform heating. From Fig. 9c, there was a local (axial) peak in $h_m(Z)$, which moved downstream as the power increased. This may be representative of a slug-type flow and may be a unique consequence of the top-heated boundary condition. The width of the axial distribution and the magnitudes of $h_m(Z)$ increased with the power. For the smooth wall case, all curves appeared to approach an asymptote as Z increased. The addition of enhancement devices disrupted these rather regular trends. The fluctuations of $h_m(Z)$ with increasing Z still existed but became more irregular and greater in amplitude.

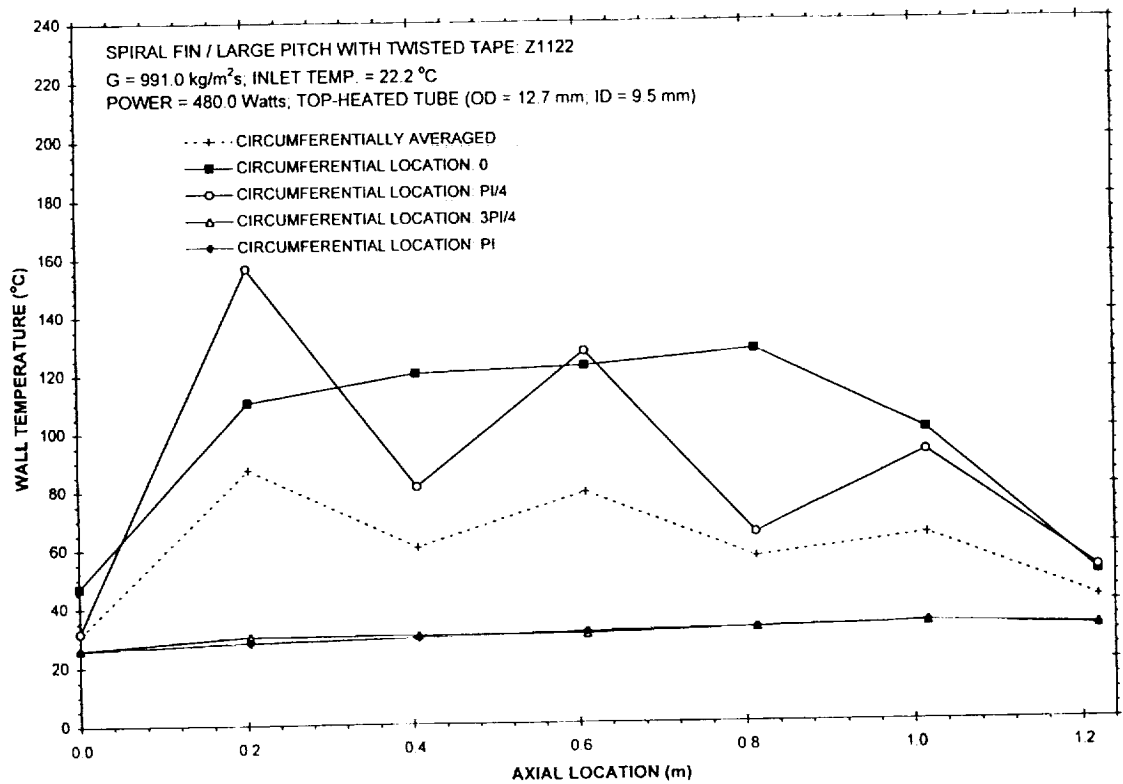
PRACTICAL USEFULNESS/SIGNIFICANCE

This experimental examination of the 2-D local (axial and circumferential) wall temperature variations of a horizontal, top-side-heated coolant channel provides a unique body of single- and two-phase data for (1) the practical configuration of flow channels heated from one side, for which almost no data and/or engineering correlations exist; (2) a basis for the future determination, using inverse conduction techniques, of 2-D local variations in the heat transfer coefficient; and (3) eventually a basis for developing a new generation of engineering correlations that apply to single-side-heated channels with thermally conducting walls for single- and two-phase forced flows.

For practicing engineers, single- and two-phase results are given for (1) the circumferential mean but axially distributed heat transfer coefficient and (2) the circumferential and axial mean heat transfer coefficient. The pres-



a



b

Figure 8. Axial distribution of the wall temperature for the four circumferential locations for (a) large-pitch spiral fins, (b) large-pitch spiral fins with twisted tape, (c) small-pitch spiral fins, and (d) smooth tube.

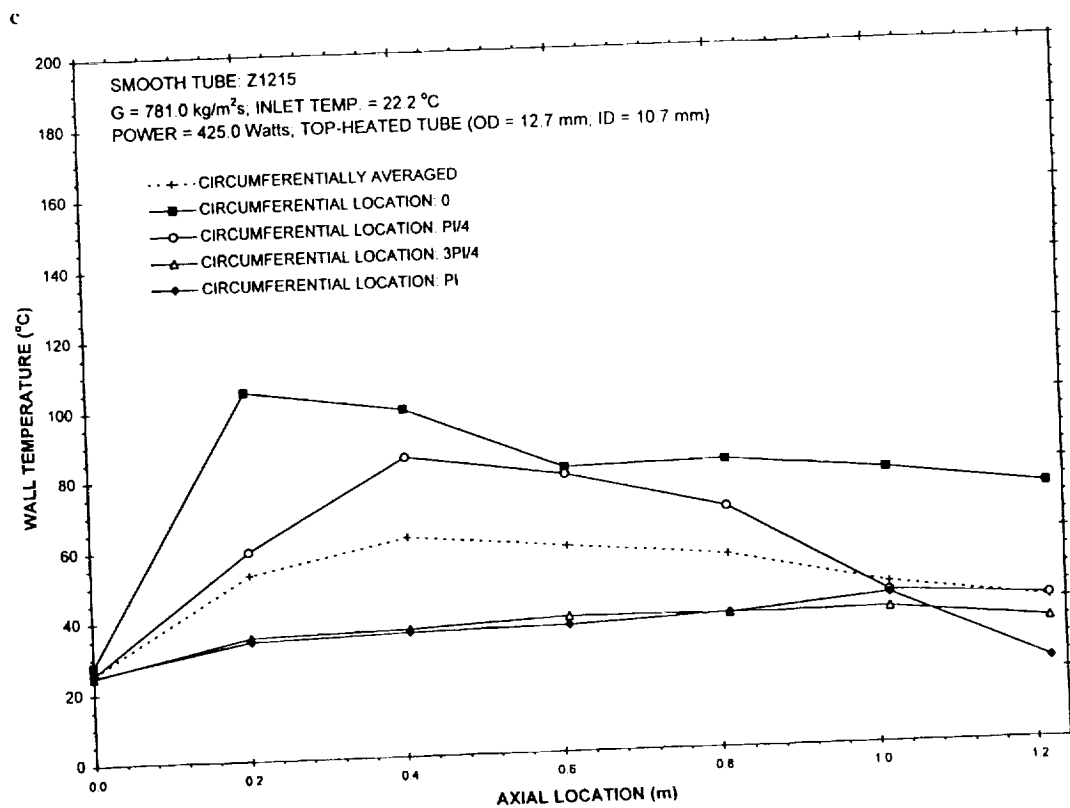
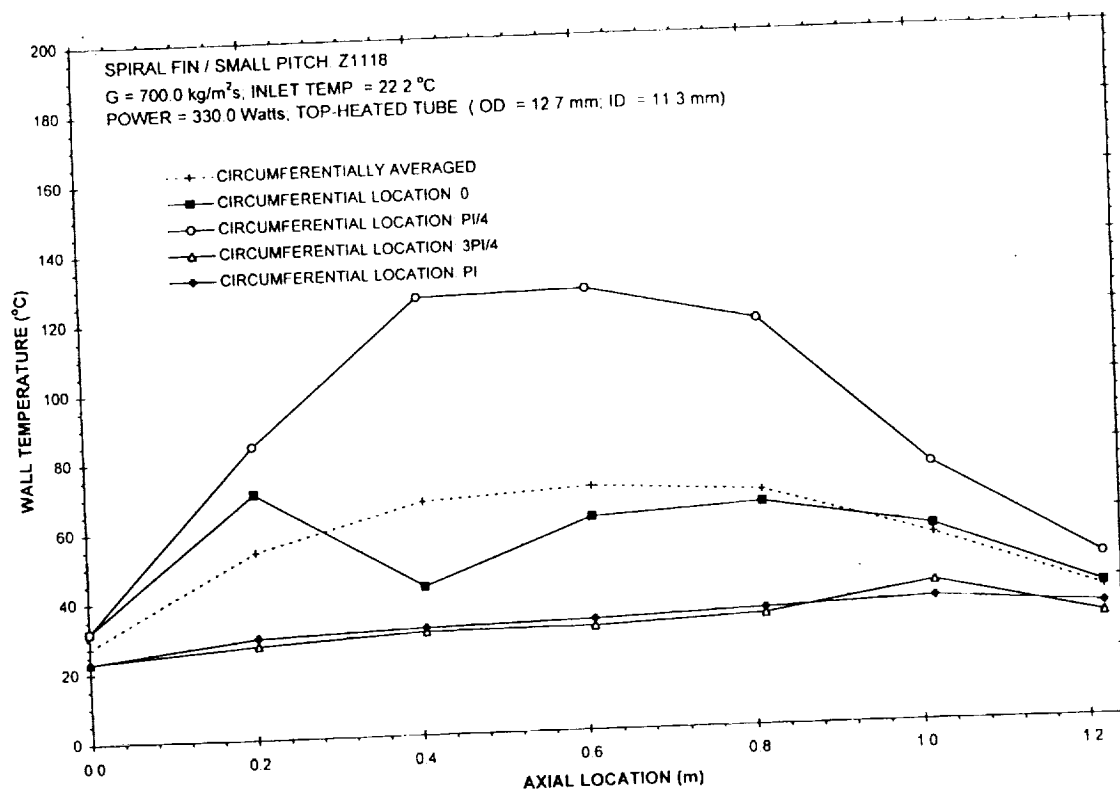
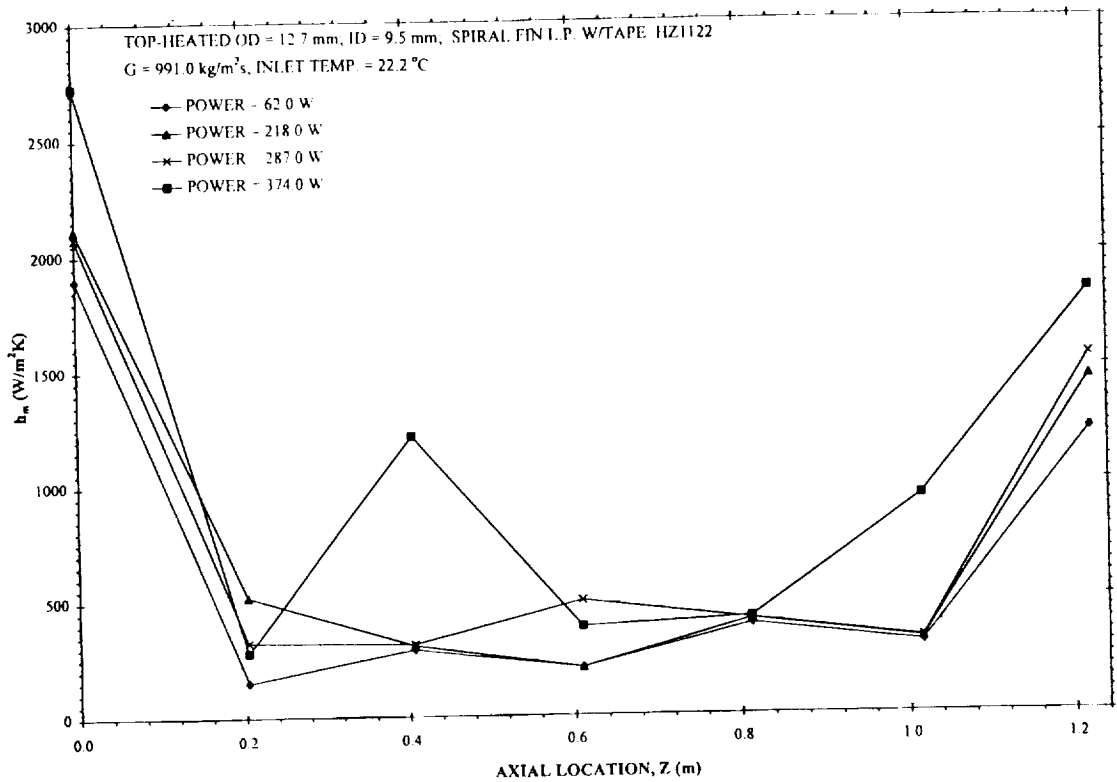
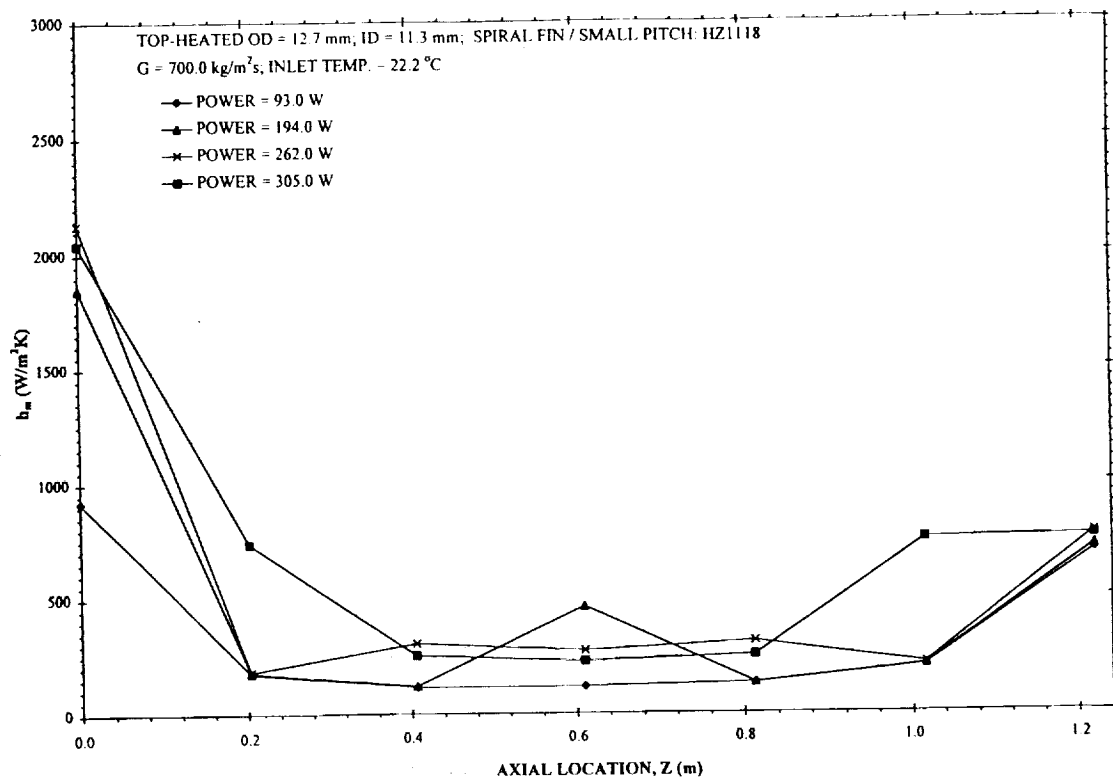


Figure 8. Continued.



a



b

Figure 9. Axial distribution of the circumferentially averaged heat transfer coefficient for (a) large-pitch spiral fins with a twisted tape, (b) small-pitch spiral fins, and (c) smooth wall.

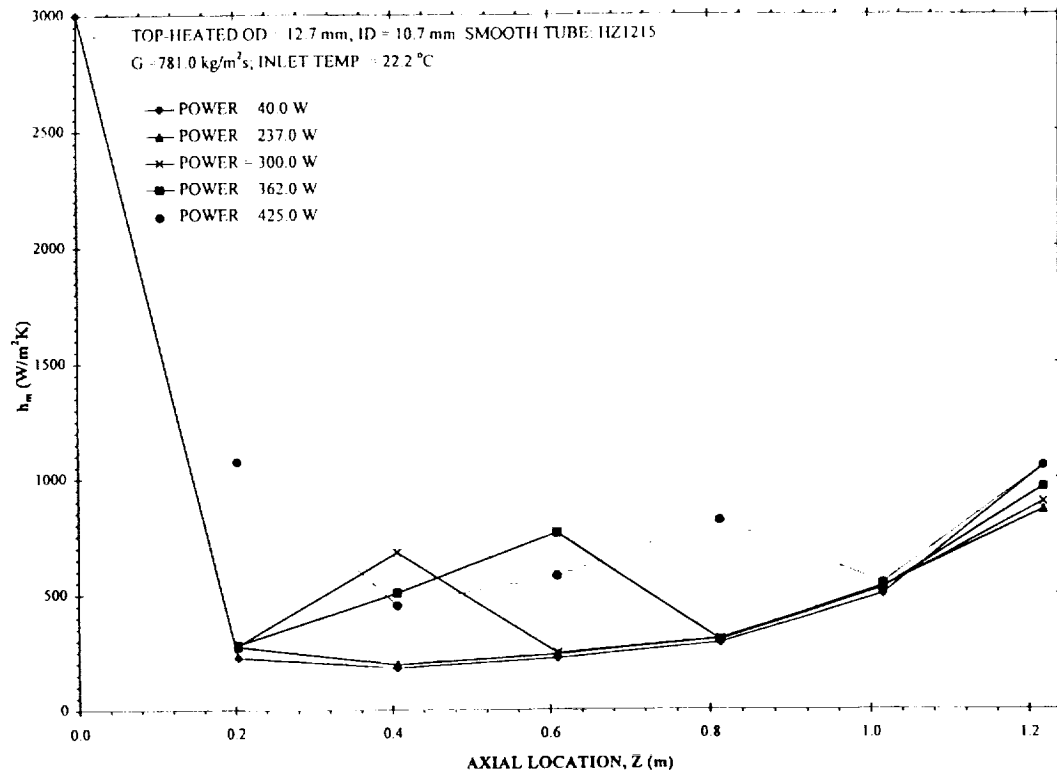


Figure 9. Continued.

ent results can assist the practicing engineer who may be involved with a design using top-side heating to (1) assess the error involved and possible correction factors associated with the use of conventional or classical heat transfer correlations and (2) make preliminary comparisons of the relative merits of various heat transfer enhancement techniques.

CONCLUSIONS

The present work provides experimental data characterizing the localized thermal transport in top-heated horizontal coolant channels with enhancement devices. The present local wall temperature measurements form a basis for future comparisons with three-dimensional numerical predictions. Such comparisons will be useful in explaining the underlying local flow conditions that are favorable to both local and overall heat transfer enhancement in top-heated configurations. This can be demonstrated in a limited way by noting the behavior of the measured wall temperature for $\phi = \pi/4$ in Figs. 8a and 8b. The effect of adding a twisted tape was to move the peak wall temperature upstream. The present cases should be expanded to include additional circumferential and axial resolution of the wall temperature variations and comparisons at additional levels of Re. The two-dimensional wall temperature measurements were used to determine the circumferentially mean but axially dependent heat transfer coefficient. The flow in the thermally conducting coolant channel was hydrodynamically developed but thermally developing with regions of (1) single-phase convection, (2) local subcooled

boiling, and (3) a predominating stratified flow over most of the channel length. In addition, three-dimensional thermal conduction effects were important in the channel wall.

The results show that the coolant channel with the large-pitch spiral fins had a larger overall heat transfer coefficient than smooth tubes or tubes with either small-pitch spiral fins or a combination of large-pitch spiral fin and a twisted tape. However, local measurements indicated that the effectiveness of the latter case will improve for stratified flow as the period of the twisted tape reduced. Although similar observations have been made in the literature for nonstratified flows, the present local measurements not only document this effect but also (1) provide a basis for comparisons with three-dimensional, two-phase, numerical models and (2) form a basis for assessing present and evolving heat transfer correlations.

We thank Dr. Joseph Atkinson, Russ Long, John Thornborrow, and William D. Harwell for their support and assistance. In addition, we wish to express our appreciation to Quaid Peatiwala for replotting the data, drawing Fig. 3, and rechecking the mass velocity specifications. Finally, we are grateful to NASA (JSC and Headquarters) for supporting this work under contracts NAG 9-310 and NAG 9-631.

APPENDIX: UNCERTAINTY ANALYSIS

This study has resulted in the determination of circumferentially mean as well as the axially and circumferentially mean heat transfer coefficients from measurements of (1) the test section outside local wall temperature; (2) the

Freon-11 flow conditions, which include flow rates, exit pressure, and inlet and exit bulk temperatures; and (3) the ambient temperature. The relationships between these quantities were summarized in Eqs. (1)–(5). Following the approach outlined by Moffat [15, 16], the uncertainty in the heat transfer coefficient h_m is

$$\delta h_m = \left[\left(\frac{\partial h_m}{\partial X_i} \delta X_i \right)^2 + \left(\frac{\partial h_m}{\partial C_i} \delta C_i \right)^2 \right]^{1/2}, \quad (\text{A.1})$$

where X_i represents all independent variables and C_i represents corrections used to account for calibration defects, system-sensor interactions, and system disturbance errors. The double indices in Eq. (A.1) imply summation over all independent or correction variables. If effects of C_i are neglected, δh_m is given by

$$\delta h_m \approx \left[\left(\frac{\partial h_m}{\partial A} \delta A \right)^2 + \left(\frac{\partial h_m}{\partial B} \delta B \right)^2 \right]^{1/2}, \quad (\text{A.2})$$

where A and B are given in Eq. (1). Since A and B are not actually independent variables, their relationships with these variables are as follows:

$$\delta A = \text{Function}(T_m, P_p, T_x), \quad (\text{A.3})$$

so that

$$\delta A = \left[\left(\frac{\partial A}{\partial P_p} \delta P_p \right)^2 + \left(\frac{\partial A}{\partial T_m} \delta T_m \right)^2 + \left(\frac{\partial A}{\partial T_x} \delta T_x \right)^2 \right]^{1/2};$$

and

$$\delta B = \text{Function}(T_x, T_m, T_1, P_p), \quad (\text{A.4})$$

so that

$$\delta B = \left[\left(\frac{\partial B}{\partial P_p} \delta P_p \right)^2 + \left(\frac{\partial B}{\partial T_m} \delta T_m \right)^2 + \left(\frac{\partial B}{\partial T_x} \delta T_x \right)^2 + \left(\frac{\partial B}{\partial T_1} \delta T_1 \right)^2 \right]^{1/2}$$

The partial derivatives for A and B were obtained from Eq. (1) [21]. Additional derivations are also needed for both T_1 and P_p . The uncertainties for Z and G were $\delta Z = 0.0016$ m and $\delta G = 8.4$ kg/(m² s), respectively. The uncertainties in measuring all temperatures were assumed equal and will be denoted by δT . If $\delta P_p = 0.1$ W, then $\delta A = 762.3$ W/m², $\delta B = 0.027$ K, $\partial h_m / \partial A = 9.92 \times 10^{-3}$ K⁻¹, $\partial h_m / \partial B = -462.6$ W/(m² K²). This resulted in $\delta h_m \approx \pm 14.6$ W/(m² K).

NOMENCLATURE

A_s	surface area, m ²
c_p	specific heat, kJ/(kg K)
D	thermal hydraulic diameter, m
E_c	Eckert number [= $10^{-3} G^2 / \rho_{\text{liq}}^2 c_p (T_m - T_{\text{sat}})$], dimensionless
G	mass velocity, kg/(m ² s)
h	circumferentially and axially averaged heat transfer coefficient W/(m ² K)

h_m	axially distributed but circumferentially averaged heat transfer coefficient, W/(m ² K)
h_c	heat transfer coefficient due to natural convection (see Fig. 4), W/(m ² K)
i_{lg}	specific latent heat of vaporization, kJ/kg
$i_{\text{sub,liq}}$	enthalpy subcooling of the fluid, kJ/kg
Ja^*	Jakob number (= $\Delta i_{\text{sub,liq}} / i_{\text{lg}}$), dimensionless
k	thermal conductivity, W/(m K)
Pe	Peclet number (= Re Pr), dimensionless
P_p	net power generation, W
q_c	heat flux due to natural convection from outside of test section (see Fig. 4), W/m ²
q_R	heat flux due to radiation from the outside of the test section, W/m ²
r	radial coordinate for the data reduction model (see Fig. 4), m
St_{ONB}	Stanton number at onset of nucleate boiling, dimensionless
T_1	bulk temperature of the flowing fluid (see Fig. 2), °C
$T_m(\phi, Z)$	local measured outside wall temperature of the test section (see Figs. 3 and 4), °C
$T_w(\phi, Z)$	outside wall temperature of the test section [= $T_m(\phi, Z)$], °C
T_{sat}	saturation temperatures (316 K at 0.19 MPa for Freon-11), °C
T_x	ambient temperature, °C
We^*	modified Weber number (= $\rho_g G^2 D / \rho_{\text{liq}}^2 \sigma$), dimensionless
Z	axial coordinate for the heated portion of the test section (see Fig. 3), m

Greek Symbols

ϕ	circumferential coordinate; see Figs. 2, 3, and 6. In some figures ϕ is written out as phi. dimensionless
π	half of a full rotation or 180°; in some figures, π is written out as pi
ρ_g	density of gaseous phase of fluid, kg/m ³
ρ_{liq}	density of liquid phase of fluid, kg/m ³

Subscripts

A, B, C	denote domains A, B, C (see Fig. 4)
i	axial location (= 1, 2, ..., 7) (see Fig. 3)
w	wall

REFERENCES

- Swanson, T. D., Juhasz, A., Long, W. R., and Ottenstein, L., *Workshop on Two-Phase Fluid Behavior in a Space Environment*, 1989, NASA Conf. Publ. 3043.
- Zyslin, L. V., and Dorfman, E. A., Heat Transfer in Channels on Transition from Convection to Developed Boiling, *Heat Transfer—Sov. Res.*, **20**(6), 720–727, 1988.
- Gotovskiy, M. A., Zaletnev, A. F., Shemyakin, S. Yu., Fyodorov, A. V., and Isakov, S. B., Subcooled Boiling Heat Transfer to a Liquid in Tubes, *Heat Transfer—Sov. Res.*, **20**(6), 728–737, 1988.
- Jung, D. S., McLinden, M., Radermacher, R., and Didion, D., Horizontal Flow Boiling Heat Transfer Experiments with a Mixture of R22/R114, *Int. J. Heat Mass Transfer*, **32**(1), 131–145, 1989.

5. Gungor, K. E., and Winterton, R. H. S., A General Correlation for Flow Boiling in Tubes and Annuli, *Int. J. Heat Mass Transfer*, **29**(3), 351–358, 1986.
6. Shah, M. M., A General Correlation for Heat Transfer During Subcooled Boiling in Pipes and Annuli, *ASHRAE Trans.* **83**(2443), 202–217, 1977.
7. Liu, Z., and Winterton, R. H. S., A General Correlation for Saturated and Subcooled Flow Boiling in Tubes and Annuli, Based on a Nucleate Pool Boiling Equation, *Int. J. Heat Mass Transfer*, **34**(11), 2759–2766, 1991.
8. Klimenko, V. V., A Generalized Correlation for Two-Phase Forced Flow Heat Transfer, *Int. J. Heat Mass Transfer*, **31**(3), 541–552, 1988.
9. Steiner, D., and Taborek, J., Flow Boiling Heat Transfer in Vertical Tubes Correlated by an Asymptotic Model, *Heat Transfer Eng.*, **13**(2), 43–69, 1992.
10. Kandlikar, S. G., Development of a Flow Boiling Map for Subcooled and Saturated Flow Boiling of Different Fluids Inside Circular Tubes, *J. Heat Transfer*, **113**, 190–200, 1991.
11. Carnovos, T. C., Cooling Air in Turbulent Flow with Internally Finned Tubes, in *Process Heat Transfer*, AIChE HT & EC Division, National Heat Transfer Conf., pp. 32–37, 1977.
12. Boyd, R. D., and Turknett, J. C., Forced Convection and Flow Boiling With and Without Enhancement Devices for Top-Side-Heated Horizontal Channels, NASA Space Sci. Eng. Res. Forum, Alabama A & M University, Huntsville, AL, Mar. 22–23, 1989, pp. 363–370.
13. Smith, A., Subcooled Freon-11 Flow Boiling Heat Transfer With and Without Enhancement Devices for Top-Heated Horizontal Coolant Channels, M.S. Thesis, Mech. Eng. Dept., Prairie View A & M Univ., Prairie View, TX, 1992.
14. Collier, J. G., 1981, *Convective Boiling and Condensation*, 2nd ed., McGraw-Hill, New York.
15. Moffat, R. J., Estimating the Credibility of Experimental Work, Dept. Mech. Eng., Stanford Univ., Stanford, CA, 1990.
16. Moffat, R. J., Describing the Uncertainties in Experimental Results, *Exp. Thermal Fluid Sci.*, **1**, 3–17, 1988.
17. Turknett, J. C., Forced Convection and Flow Boiling With and Without Enhancement Devices for Top-Side-Heated Horizontal Channels, M.S. Thesis, Mech. Eng. Dept., Prairie View A & M Univ., Prairie View, TX, 1989.
18. Kirishenko, Yu. A., Investigation of Effect of Subcooling on Centrifugal Acceleration on Nucleate Boiling Heat Transfer to Cryogenic Fluids, *Heat Transfer—Sov. Res.*, **12**(2), 57, 1980.
19. Hong, S. W., and Bergles, A. E., Augmentation of Laminar Flow Heat Transfer in Tubes by Means of Twisted-Tape Inserts, *J. Heat Transfer*, May, 251–256, 1976.
20. Reid, R. S., Pate, M. B., and Bergles, A. E., Evaporation of Freon-113 Flowing Inside Smooth Tubes, Natl. Heat Transfer Conf., Pittsburgh, PA, ASME 87-HT-51, August 1987.
21. Boyd, R. D., Flow Boiling with Enhancement Devices for Cold Plate Coolant Channel Design, Thermal Sci. Res. Center Rep. NAG 9-310 (NASA), December 1991.

Received August 9, 1992; revised March 20, 1995

MEASUREMENTS OF LOCAL HEAT TRANSFER FOR FORCED CONVECTION AND FLOW BOILING IN HORIZONTAL, UNIFORMLY HEATED SMOOTH TUBES

Ronald D. Boyd, Alvin Smith, Xiaowei Meng, and Jerry Turknett
Thermal Science Research Center (TSRC),
College of Engineering and Architecture, Prairie View A & M University,
Prairie View, Texas, USA

This work deals with improved ways to characterize the local heat transfer inside smooth circular channels. The objectives are to: (1) measure local (axial) channel wall temperatures, and (2) make comparative predictions of local subcooled flow-boiling heat transfer for the case of the a uniformly heated channel. Flow boiling experiments were conducted with Freon-11 in horizontal, copper, uniformly heated coolant channels with smooth walls. Temperature measurements were made on the outside surface of the copper channel at four circumferential and seven axial locations. Comparisons were made for inside computed wall temperature and the axial mean circumferential heat transfer coefficient with a subcooled flow-boiling model based on the assumption of large Froude number. The predictions served as a comparative baseline and a qualitative check for the data.

Flow-boiling heat transfer plays an important part in engineering and in today's high-technology fields, such as space-station energy systems, microelectronic devices, and nuclear reactors. Based on theoretical and numerical analysis as well as the large amount of available data, investigators have been able to create advanced software for both predictions of local heat transfer and experimental data reduction for single-phase and some two-phase flows in vertical channel geometries with uniform-heat-flux boundary conditions. Although it has been known for decades that flow boiling increases and enhances heat transfer, little attention beyond the work of Bergles and Rohsenow [1] and Shah [2] has been given to advanced heat transfer model development for subcooled flow boiling inside channels or ducts with uniform circumferential heating.

In the past, there have been (1) a large number of experimental investigations made for flow boiling heat transfer for different fluids, (2) large pressure and flow rate ranges, and (3) a large number of the empirical models for single-phase convection, subcooled flow boiling, saturated flow boiling, and critical heat flux. The present work involves the measurement and prediction of local wall temperature for Freon-11 in an uniformly heated, smooth horizontal channel.

The present address of Jerry Turknett is Westinghouse Savannah River Company, P.O. Box 616, Bldg. 705-1c, Aiken, SC 29802.

Address correspondence to Professor Ronald D. Boyd, Department of Mechanical Engineering, Prairie View A & M University, P.O. Box 397, Prairie View, TX 77446.

Experimental Heat Transfer, 7:19-29, 1994

Copyright © 1994 Taylor & Francis

0891-6152/94 \$10.00 + .00

19

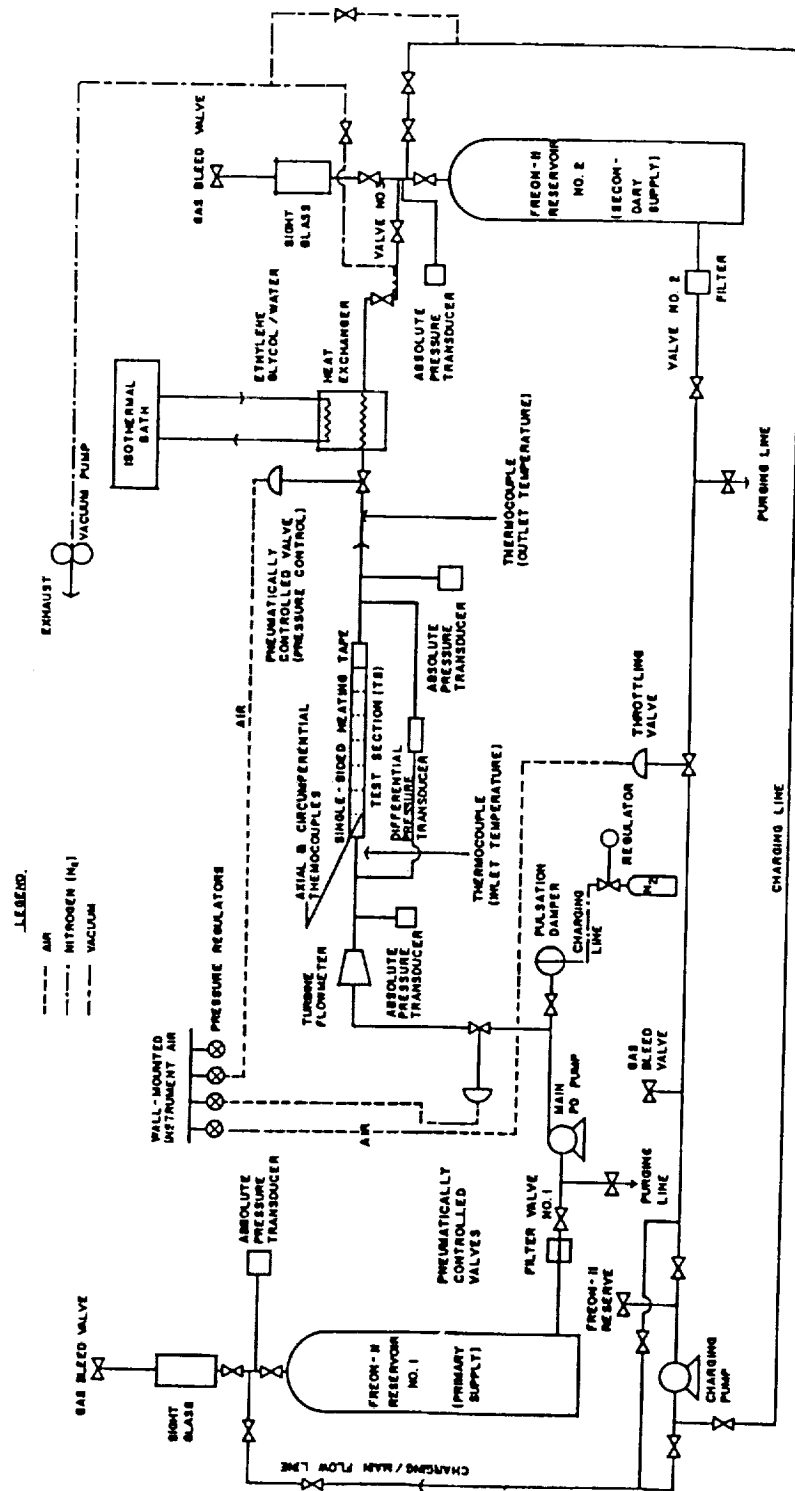


Figure 1. Freon-11 flow loop for both subcooled and saturated-flow boiling experiments.

sponding to volumetric flow rates of the turbine flowmeter, and (3) heater tape voltage and current measurements. The test section pressures (inlet and exit) were also measured using membrane transducers.

DATA REDUCTION

The data reduction approach was based on a heated hydraulic diameter [3] assumption. Figure 2 shows the model used for this approach. This model was used to compute a circumferentially averaged heat transfer coefficient from the circumferentially averaged wall temperature. This latter temperature was computed from the four wall temperature measurements made on the outside of the test section at each of the seven axial locations. The model in Figure 2 accounts for the temperature drop across the flow channel wall, and the heat losses (convection and radiation) from the test section to the ambient. An iteration scheme was necessary to compute the inside wall temperature. After accounting for finite heat losses, the circumferentially averaged heat transfer coefficient was given by

$$h_m = \frac{A}{B} \quad (1)$$

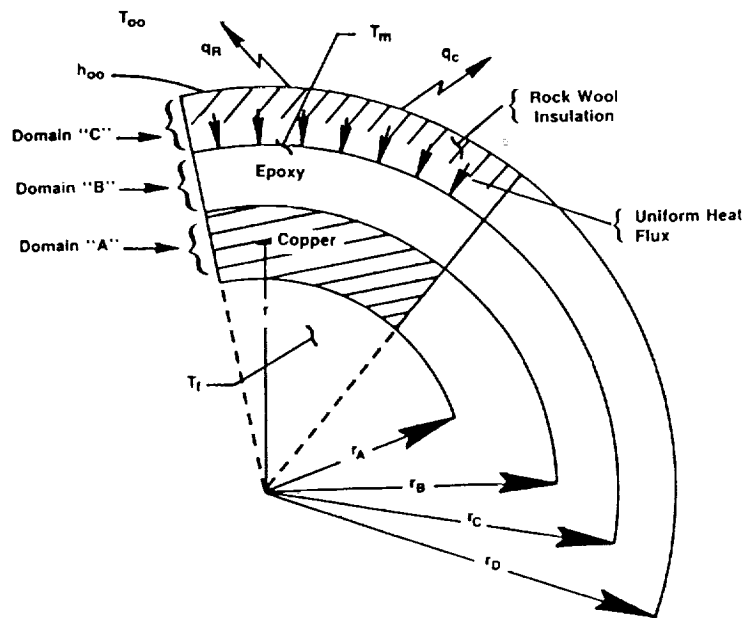


Figure 2. Control volume for the heated hydraulic diameter model. $r_A = 0.475$ cm, $r_B = 0.635$ cm, $r_C = 0.6985$ cm, and $r_D = 3.2385$ cm.

where

$$A = \left(\frac{k_A}{r_A} \right) B_1 \left[\ln \left(\frac{r_D}{r_C} \right) + \frac{k_C}{h_\infty r_D} \right] - \left(\frac{k_C}{r_A} \right) (T_m - T_\infty)$$

$$B = B_2 + B_3 + B_4$$

$$B_1 = \frac{P_p r_C}{A_s k_B}$$

$$B_2 = (T_m - T_\infty) \left[\ln \left(\frac{r_D}{r_C} \right) + \frac{k_C}{h_\infty r_D} + \left(\frac{k_C}{k_B} \right) \ln \left(\frac{r_C}{r_B} \right) \right]$$

$$B_3 = (T_m - T_\infty) \left[\frac{k_C}{k_A} \ln \left(\frac{r_B}{r_A} \right) \right] - \left[\ln \left(\frac{r_D}{r_C} \right) + \frac{k_C}{h_\infty r_D} \right] (T_b - T_\infty)$$

and

$$B_4 = B_1 \left[\ln \left(\frac{r_C}{r_B} \right) + \left(\frac{k_B}{k_A} \right) \ln \left(\frac{r_B}{r_A} \right) \right].$$

In the above expression for the circumferentially averaged heat transfer coefficient (h_m), the magnitude of the bulk temperature, T_b , is dependent on T_{av} , which is the circumferentially averaged wall temperature at $r = r_C$. T_b was determined based on the magnitude of T_{av} relative to the wall temperature, $T_{w_{ONB}}$, which is the temperature required for the onset of nucleate boiling. The bulk fluid temperature was given by

$$T_b = \begin{cases} T_b(z) & \text{for } T_{av} < T_{w_{ONB}} \\ T_{sat} & T_{av} \geq T_{w_{ONB}} \end{cases} \quad (2)$$

where $T_{w_{ONB}}$ was computed using the Frost and Dzakowic correlation [7]. Although the flow is subcooled, the onset of ONB did not occur simultaneously around the circumference of the horizontal test section. As a result, a portion of the inside surface could be experiencing fully developed boiling while another circumferential portion of the same cross section could be experiencing single-phase flow, and still another portion could be experiencing subcooled film boiling. As a first attempt to reconcile these different processes occurring in the same cross section, the above approximation was made. For a given axial location, the measured circumferential values of T_m were used to obtain a circumferentially averaged temperature, T_{av} . Using the approach suggested by Moffat [8, 9], the complete uncertainty analysis for h_m was developed; it can be found in [6]. The uncertainty in the heat transfer data was found to be $\pm 14.6 \text{ W/m}^2 \text{ K}$.

FLOW BOILING MODEL

The local (axial) heat transfer coefficient is defined as the ratio of local applied heat flux to the difference between the local inside wall temperature and the local fluid bulk temperature.

The local film temperature was used to evaluate all the thermophysical properties in all correlations.

The local mean bulk temperature was calculated from the first law of thermodynamics for given values of the applied heat flux q'' , location Z , mass flux G , and inlet fluid temperature T_{inlet} . From the first law,

$$i_b(Z) = i_{inlet} + \frac{q'' A_s(Z)}{GA_c} \quad (3)$$

The local bulk temperature, $T_b(Z)$, was obtained from $i_b(Z)$ via the saturation table.

The developed flow boiling model [5, 6] was used to predict local heat transfer coefficients and local wall temperatures for uniformly heated vertical channels for flow in the following regimes: (1) single phase, (2) partial nucleate boiling, and (3) fully developed boiling.

In order to use the film temperature as the reference temperature for temperature-dependent thermophysical properties, the wall temperature must be known for each of the above three regimes. A straightforward trial-and-error method was used to find T_w [6]. Once the local wall temperature was determined, the local (axial) heat transfer coefficient was computed. Fluid property data sources are from DuPont [10], Kreith [11], and Vargaftik [12].

RESULTS

Comparisons were made between the data and an existing flow boiling model [5, 6]. The data sets involved a horizontal test section and included two flow rate levels, five axial locations, and four circumferential locations. All data involved uniformly heated tubes. Since the models apply only within the nucleate subcooled boiling region, data in the saturation boiling region ($x \geq 0$) was not reduced, and all predictions stopped beyond this region.

Comparison of the THM data with predictions of the local (axial) heat transfer coefficients for Freon-11 are presented in Figures 3 through 8. It is essential to note that since the predictive models neglect gravitational effects, only qualitative comparisons can be made with 155 data points, which apply to a horizontal uniformly heated flow channel. As noted with the comparisons with the water data in [6], the predictive models strictly apply to thermally fully developed flows.

With the above in mind, comparisons of flow boiling model show that the best agreement is obtained with the data when most of the above conditions are not violated. This occurs at the larger values of the axial coordinate ($Z = Z5 = 81.28$ cm, and $Z = Z6 = 101.60$ cm), and higher mass velocities. Poorer agreement was obtained at upstream locations ($Z < 81.28$ cm) and at the lower mass velocity,

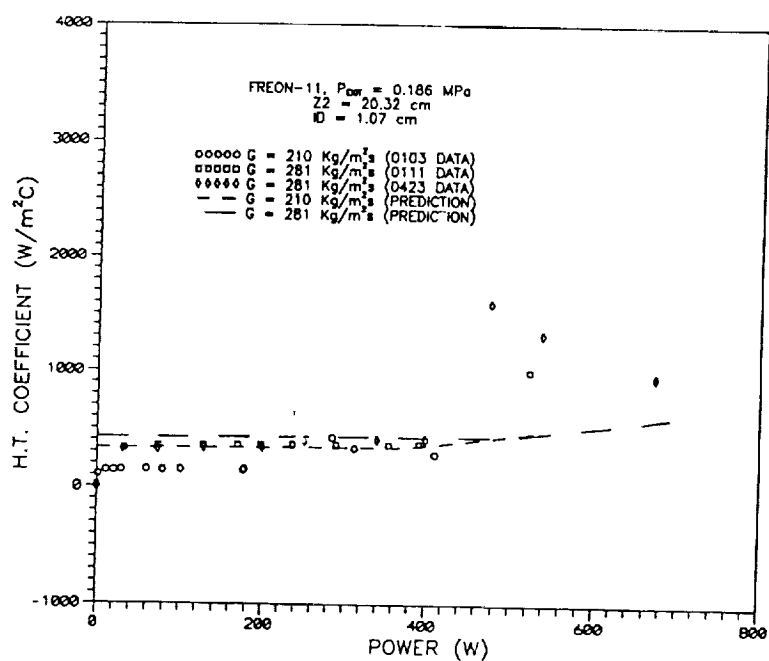


Figure 3. Heat transfer coefficient comparison for $Z = 20.32 \text{ cm}$ (near entrance) and $ID = 1.07 \text{ cm}$.

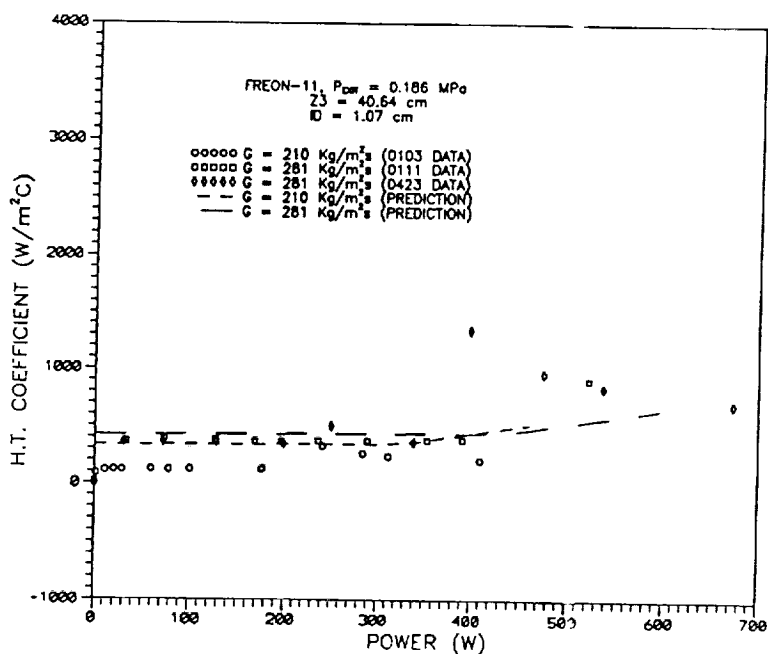


Figure 4. Heat transfer coefficient comparison for $Z = 40.64 \text{ cm}$ and $ID = 1.07 \text{ cm}$.

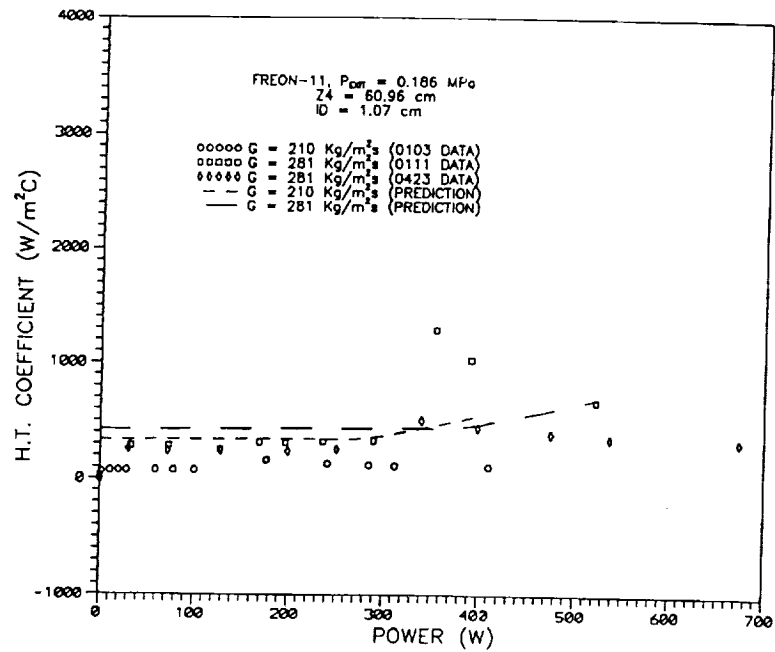


Figure 5. Heat transfer coefficient comparison for $Z = 60.96 \text{ cm}$ and $I.D. = 1.07 \text{ cm}$.

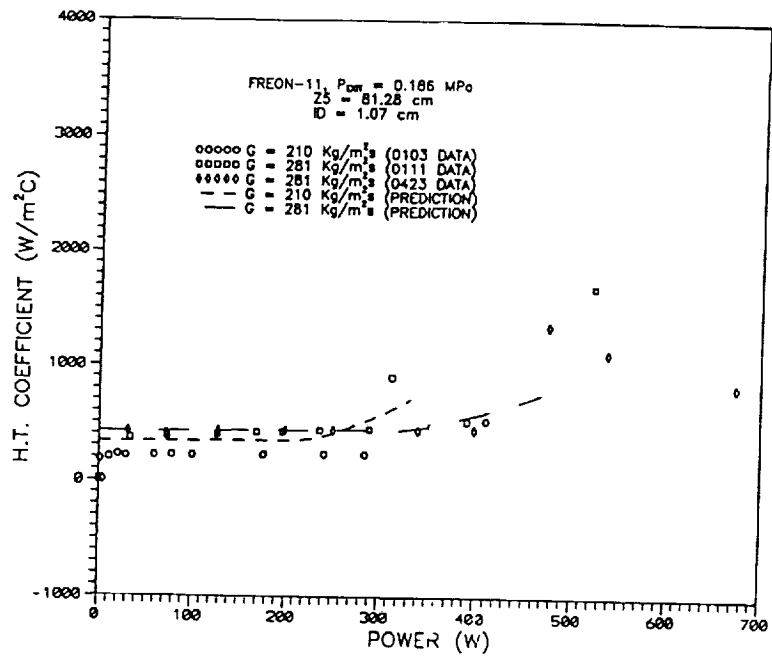


Figure 6. Heat transfer coefficient comparison for $Z = 81.28 \text{ cm}$ and $I.D. = 1.07 \text{ cm}$.

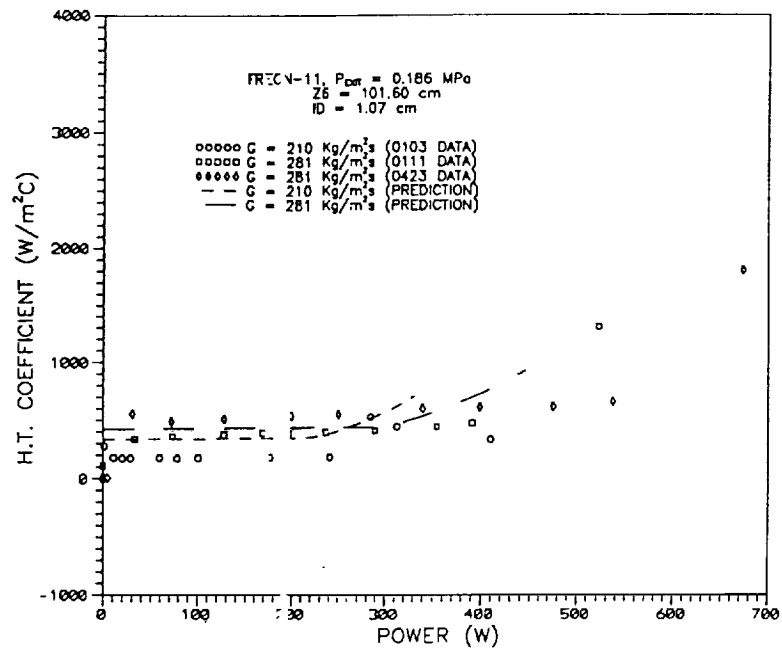


Figure 7. Heat transfer coefficient comparison for $Z = 101.60 \text{ cm}$ (22.0 upstream of exit) and I.D. = 1.07 cm.

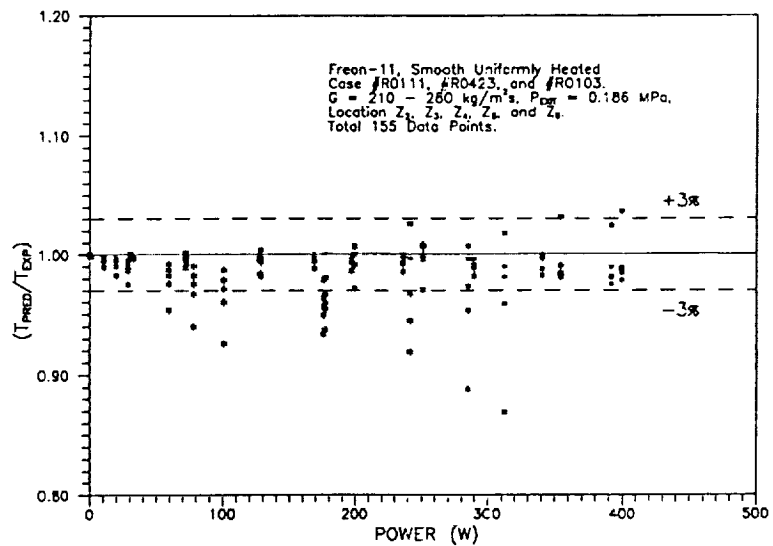


Figure 8. Inside wall temperature comparisons for thermal hydraulic model data reduction and flow boiling model predictions.

where flow developing and orientation effects appear important. This is due mainly to the fact that the experimental flow configuration is horizontal and the Froude number is relatively small.

Inspection of Figures 3 through 7 show a different functional relationship between h_m and power (P_p) as P_p increases. Initially, h_m increases gradually with P_p , and later h_m decreases with increasing P_p . These changes in trend are a result of a localized boiling front (1) increasing in intensity, (2) propagating circumferentially, and (3) eventually, in part, forming a localized film boiling region over a portion of the circumference. The first two noted events cause h_m to increase with P_p . However, the occurrence of a partial (growing) film boiling circumferential patch or region reversed this trend, so that at sufficiently high values of P_p , h_m decreased as P_p increased. In the latter case, for large values of P_p and at a given axial location, the wall-fluid interface had stable circumferential patches, which were (1) single phase, (2) subcooled partial and fully developed boiling, and finally (3) subcooled with film boiling. Additional work is proceeding to expand this study to include wider ranges of mass velocity and subcooling and additional quantitative measurements of the heat transfer coefficient with respect to the circumferential coordinate.

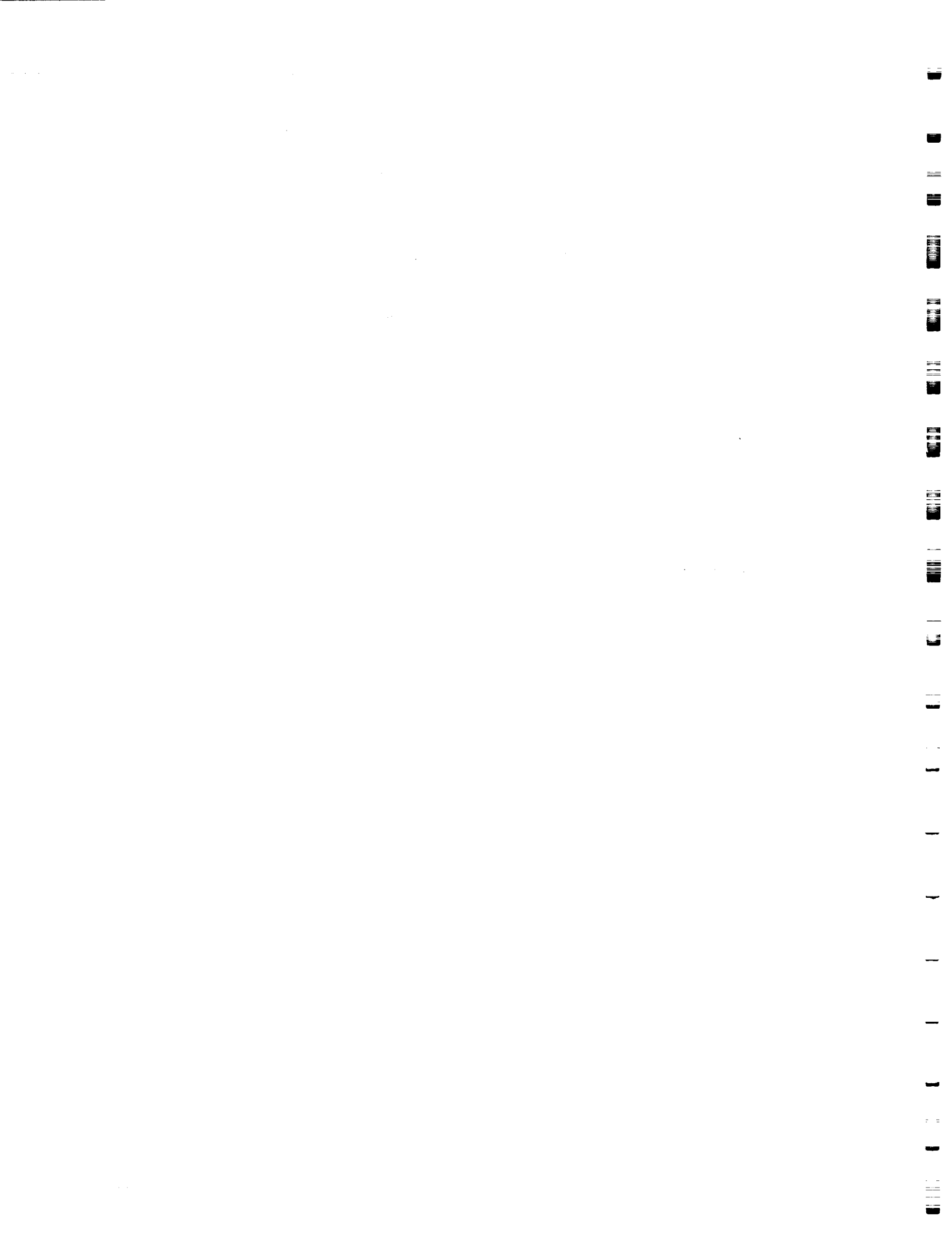
CONCLUSIONS

New subcooled flow-boiling wall temperature data for a uniformly heated, horizontal flow channel have been obtained. The predictions served as an initial baseline or limit for the data. However, additional work is needed to expand the present data reduction model to one that includes circumferential and orientation effects.

REFERENCES

1. A. E. Bergles and W. M. Rohsenow, The Determination of Forced Convection Surface Boiling Heat Transfer, *J. Heat Transfer*, p. 365, Aug. 1964.
2. M. M. Shah, A General Correlation for Heat Transfer During Subcooled Boiling in Pipes and Annuli, *ASHREA Trans.*, vol. 83, pp. 202-215, 1970.
3. A. Smith, Subcooled Freon-11 Flow Boiling Heat Transfer with and Without Enhancement Devices for Top-Heated Horizontal Coolant Channels, M.S. thesis, Prairie View A & M University, Prairie View, TX, May 1992.
4. J. C. Turknett, Jr., and R. D. Boyd, Forced Convection and Flow Boiling with and without Enhancement Devices for Top-Side-Heated Horizontal Channels, M.S. thesis, Mechanical Engineering Department, Prairie View A & M University, Prairie View, TX, Feb. 1989.
5. R. D. Boyd and X. Meng, Local Heat Transfer for Subcooled Flow Boiling with Water, *Fusion Technol.*, vol. 22, pp. 501-510, Dec. 1992.
6. X. Meng and R. D. Boyd, Heat Transfer Predictions and Numerical Data Reduction for Freon-11 Flow Boiling in Enhanced and Smooth Wall Channels, M.S. thesis, Mechanical Engineering Department, Prairie View A & M University, Prairie View, TX, Dec. 1992.
7. J. C. Collier, *Convective Boiling and Condensation*, pp. 152-153, McGraw-Hill, New York, 1972.

8. R. J. Moffat, Estimating the Credibility of Experimental Work, Department of Mechanical Engineering, Stanford University, Stanford, CA, 1990.
9. R. J. Moffat, Describing the Credibility of Experimental Work, Department of Mechanical Engineering, Stanford University, Stanford, CA, 1990.
10. *Thermodynamic Properties of Freon-11*, E. I. DuPont De Nemours and Company, Wilmington, DE, 1965.
11. F. Kreith, *Fluid Flow Data Book*, Genium Publishing Corporation, Schenectady, NY, sec. 411, 1988.
12. N. B. Vargaftik, *Tables of the Thermophysical Properties of Liquids and Gases*, John Wiley, New York, 1975.





AIAA-95-3511

**Multi-Dimensional Wall Temperature and
Boiling Curves For a Single-Side Heated
Vertical Channel with Downward Flow**

Q. Peatiwala, R. Boyd, and Z. Huque

**Prairie View A&M University
Prairie View, TX**

**1995 ASME/AIAA National Heat Transfer
Conference
August 6-9, 1995/Portland, OR**

Multi-Dimensional Wall Temperature and Boiling Curves For a Single-Side Heated Vertical Channel With Downward Flow

Quaid Peatiwala,[†] Ronald D. Boyd,[‡] and Ziaul Huque^{††}

Thermal Science Research Center (TSRC)

Department of Mechanical Engineering

Prairie View A&M University

Prairie View, Texas 77446

Abstract

A vertical flow loop was designed to determine local (circumferential and axial) and mean wall temperature distributions for saturated and subcooled flow boiling in a single-side heated vertical channel with downward flow. Experimental results are given for flow with Freon-11 mass velocities of 280, 210.0, and 140.0 kg/m²s. The measurements indicate a significant circumferential variation in the temperature. The data also indicate that a different mode of heat transfer is present at each circumferential location. The two-dimensional local measurements of the channel wall temperature show that corresponding local heat transfer coefficient variations will be significant.

Nomenclature

G Mass Velocity (kg/m²s)
 T_{av} Circumferentially averaged wall temperature (°C)
 Z_j Axial coordinate or measurement location (m)

Greek

ϕ Circumferential coordinate or measurement location (degrees)

Subscripts

j Axial location index

Introduction and Objectives

Future space programs and commercialization will require an active thermal control system (Miller et al.¹) to provide moderate temperature heat rejection for different system modules. It is essential that the thermal rejection system selected be able to operate under a variety of complex and non-uniform heat flux distributions. Other requirements for the selected system include minimum overall system mass, and pumping power (Ungar et al.² and Reinarts et al.³). The high heat flux potential and low mass requirement of the two-phase thermal control system makes them an attractive option for advanced space applications. Although work is proceeding in studying the two-phase pressure drop^{3,3}, little efforts are being devoted to

studying heat transfer related topics in single-side heated systems. In particular, optimization of the heat transfer, with accompanying reduced mass and pumping power requirements, will require a knowledge of the two-dimensional wall temperature distributions in advanced and commercial space systems (Boyd et al.⁴). Implementation of two-phase thermal control system will also require additional emphasis on flow boiling phenomenon as it pertains to non-uniform heat flux distributions, resulting wall temperature distributions, heat transfer coefficients, flow channel aspect ratio, and orientation.

From the literature review, there has been much work completed for the two-phase heat transfer correlations for a uniform heat flux distribution. Correlations presented by Kandlikar,⁵ Shah,⁶ Gungor and Winterton,⁷ and Boyd and Meng⁸ cover different fluids, vast ranges of flow rates, the entire spectrum of quality, and low and high subcoolings. The former three correlations were only recommended for saturated flow boiling and the latter for subcooled flow boiling. These correlations are valid for only smooth tubes, and one must avoid using them when orientation is important. The former three correlations were derived from the data collected from horizontal flow boiling, where as the latter for high Froude number (> 50.0). Recently, several researchers have considered the effect of heat transfer enhancement devices (fins, and twisted tapes) and have presented correlations, but most of these are again for horizontal flow boiling or condensation on horizontal tubes. Patankar et al.,⁹ Wen et al.,¹⁰ and Jaber et al.,¹¹ have studied the effect of fins on the heat transfer coefficient for condensation. While Wen et al.¹⁰ presented experimental data to facilitate theoretical model development of heat transfer coefficient for condensation on horizontal integral-finned tubes, Jaber et al.¹¹ found that the condensation heat transfer coefficient can be increased by up to 280% for copper if commercially available enhanced tubes are used in condensers over smooth copper tubes. He also looked at copper alloy tubes and found that heat transfer is enhanced by an average of over 30% with finned tubes relative to smooth tubes. Boyd et al.,⁴ Smith,¹² and Turknitt,¹³ have studied the flow boiling in horizontal channels

[†] Graduate Student, Mechanical Engineering, Member ASME

[‡] Honeywell Professor and Director of the TSRC, Mechanical Engineering, Member ASME

^{††} Assistant Professor, Mechanical Engineering, Member ASME

with uniform and top-side heating with and without enhancements. They made measurements of the two-dimensional axial and circumferential wall temperature distributions, and presented results for the axial distribution of the heat transfer coefficient for four internal tube configurations.

As stated before almost all of the work done in two phase flow is for uniform heat flux and for this heat loading condition, there is no circumferential variation in wall temperature. Hence, at any power level only single mode of heat transfer is used to calculate heat transfer coefficient at a given axial location. It is understandable that by using a uniform heat flux distribution, the modeling for heat transfer coefficient is greatly simplified; but in engineering applications with non-uniform circumferential heat flux distributions, this work will show that the wall temperature variations are significant. Some applications where this may be important include thermal management for the advanced space systems, high heat flux fusion components, high heat flux electronic components, in-tube boiling systems, boilers, condensers, and heat exchangers. It should be made clear here that great care must be taken when approximating a non-uniform heat flux condition with a uniform one because by using this approximation, severe restricts or even anomalies may result. This is another reason why applications requiring single-side heating of channels with flow boiling will be better characterized by measurements of the local 2-D wall temperature and heat transfer variations.

For advanced space thermal management systems to become a reality, extensive efforts are needed to collect and correlate 2-D two-phase experimental data for heat transfer correlations for complex heat flux distributions. The long-range scope of this study includes making 2-D wall temperature measurements as a function of mass velocity, inlet subcooling, tube diameter, tube internal geometry, tube orientation, gravity level, and heating configuration. The anticipated Freon-11 mass velocity and tube diameter range between 95.0 and 1,300.0 kg/m²s, and between 9.5 and 25.4 mm, respectively. The tube inside wall configuration will include smooth wall, finned wall, and combined twisted tape and finned walls. In the present paper, we present an example of 2-D outside wall temperature measurements made with subcooled Freon-11 flowing downward in a smooth vertical channel with single-sided heating and study the effects of different mass velocities on wall temperature distribution.

Experimental Setup

The system used to perform forced convection boiling experiments in vertical tubes (downward flow) was based on the system initially developed by Boyd et al.⁴ and later used by Smith,¹² Boyd,¹⁴ and Turknett¹³. Figure 1a shows the Freon-11 vertical flow boiling loop. This closed loop is constructed of stainless steel and copper, and operates between 3.4 kPa and 0.17 MPa. The maximum power generation capability is 2.7 kW and the maximum volume flow rate is approximately 2.97E-4 m³/sec. The Freon-11 is stored in a reservoir which is filled

using a chemical resistance centrifugal pump. After filling the reservoir, the Freon-11 is circulated through the closed loop at the desired operating pressure and flow rate. By circulating the Freon-11 before any data is recorded, any leaks in the system can be detected by using a halogen leak detector. Then the desired inlet temperature is obtained by properly adjusting the chiller/isothermal bath. The energy is transferred between the chiller and Freon-11 by way of a commonly connected heat exchanger. During testing, the outlet temperature of the chiller is adjusted to maintain a constant inlet Freon-11 temperature for a given experimental run. The working fluid for the chiller is a 60/40 ethylene glycol - distilled water mixture.

A description of the closed flow loop and the function of its components is instructive. The Freon-11 flows from the reservoir to the filter, where all the contaminants are removed before the fluid enters the positive displacement pump. The positive displacement pump requires a net positive suction of at least 0.02 MPa. This pump was selected for durability. After leaving the pump, the fluid passes through the pulsation damper. The damper reduces the pressure and flow oscillations. The pressure fluctuations are also minimized by using the pneumatically controlled metering valve. Exiting the control valve, the fluid flows to the heat exchanger, where its temperature is set at a desired value by adjusting the chiller parameters. After exiting the heat exchanger, the fluid passes through the turbine flow meter and enters the unheated "flow developing" section or upstream part of the test section which has a length greater than forty (40) times the test section diameter. The fluid then enters the heated section of the test section. A downstream pneumatically controlled valve is used to control the test section exit pressure. The heated fluid then passes through another heat exchanger where the energy generated is removed partially by using tap water. Finally, the fluid flows back to the reservoir and the flow cycle is complete.

The test sections used in this experiment are the same as used by Boyd et al.⁴ The test sections are 2.235 m long copper tubes (see Figure 1b), and consists of two parts: (1) Upstream unheated section to facilitate flow development, and (2) A downstream single-side heated section. For the present case, the inside diameter (D) was 25.4 mm and the outside diameter was 28.5 mm.

The heated section has a smooth inside surface. The test section was heated with heater tapes which varied in width based on tube diameter and are 1.22 m long. Each tape has power generation capacity of 2.66 kW. The test section was designed with flexibility and ease of replacement in mind. Although, the pressure losses due to union connector at both top and bottom ends of the test section are assumed to be small, computations and additional measurements, will be performed later to estimate these losses. The entire test section was insulated to minimize the heat losses. In addition to the primary two parts of the main test section, each part had pressure-temperature measurement ports upstream and downstream of the test section.

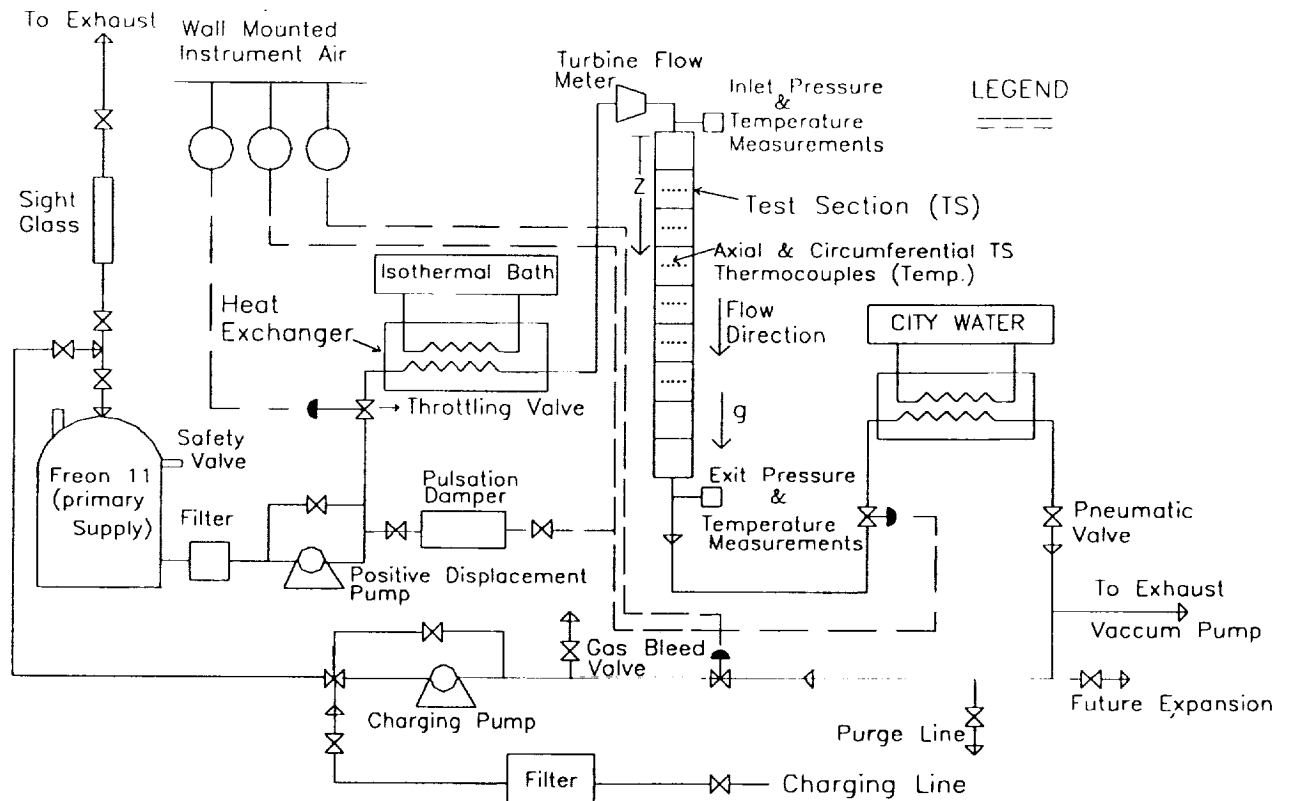


Figure 1a: Schematic of the Vertical Downward Flow Boiling Loop

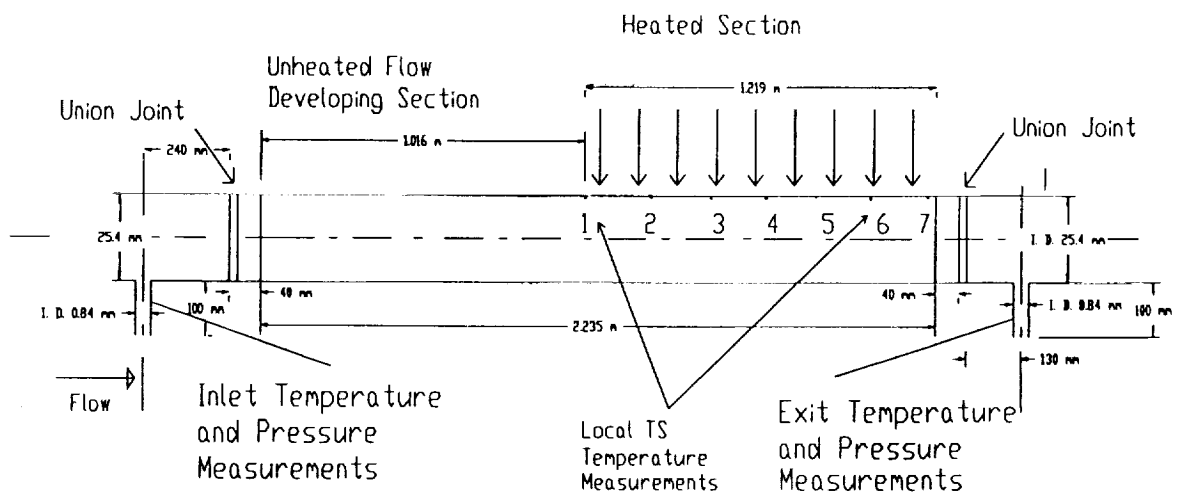


Figure 1b: Test Section (TS) Configuration for Temperature and Pressure Measurements Test Section Description

The heated part of the test section was divided into seven .203 m axial intervals. At each of the axial locations there are seven thermocouples installed circumferentially at 0 , $\pi/4$, $3\pi/8$, $\pi/2$, $5\pi/8$, $3\pi/4$, and π degrees (see Figure 2), with 0 being at the top heated portion of vertical symmetry plane in Figure 2. This test section thermocouple arrangement will allow better circumferential resolution of the wall temperature variation than

previous test sections (Boyd,¹⁴ Smith,¹² and Turknett,¹³) because seven circumferential locations were used rather than four.

The thermocouples were installed by using high thermal conductivity epoxy. Special care was taken when thermocouples were adhered to the tube. The thermocouple beads were placed in good contact with the tube so that as little epoxy as possible was used. Based on forty repeated measurements of the epoxy

thickness between the thermocouple and the copper tube, the mean thickness was 0.194 mm, and the standard deviation was 0.007 mm.

Data Reduction Analysis

Forty-nine (49) local temperature measurements were made on the outside surface of the heated portion of the test section for each experiment. These outside temperatures must be related to the inside wall temperature so that the inside heat transfer coefficient can be computed. Two techniques will be used to reduce the wall temperature data: (1) the heated thermal hydraulic approach (Boyd et al.⁴) (see Figure 3), and (2) a multi-dimensional inverse conduction analysis using a numerical finite element computation code called ANSYS.

The initial data reduction is based on the heated hydraulic approach used by Boyd et al.⁴ In this analysis, we compute circumferentially averaged heat transfer coefficient from circumferentially averaged wall temperature. The circumferentially averaged temperature was computed from the seven wall temperature measurements made on copper tube outside surface at each axial location by using the piece-wise linear approach similar to that used by Reid et al.¹⁵ Using their approach, the circumferentially averaged outside wall temperature can be related to the seven circumferential measured temperatures (T_{m1} at 0 degrees, T_{m2} at $\pi/4$, T_{m3} at $3\pi/8$ etc.) by the equation given below:

$$T_{av} = \frac{2T_{m1} + 3T_{m2} + 2T_{m3} + 2T_{m4} + 2T_{m5} + 3T_{m6} + 2T_{m7}}{16} \quad (1)$$

The temperature T_{av} was used with the model presented by Boyd et al.⁴ to account for temperature drop across channel walls, and convective and radiative heat losses to the surroundings. Using this model, the mean heat transfer coefficient (h_{mv}) at a given axial location can be obtained.

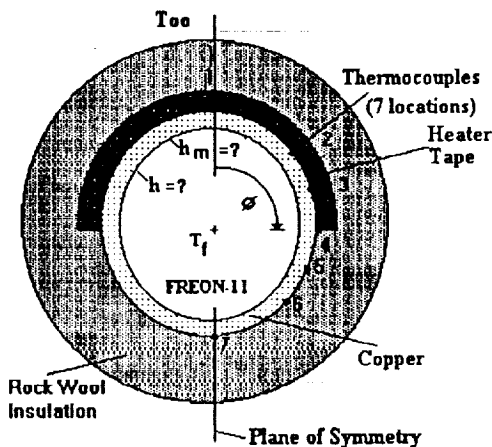


Figure 2: Cross-section of Heated Portion of the Vertical Test Section

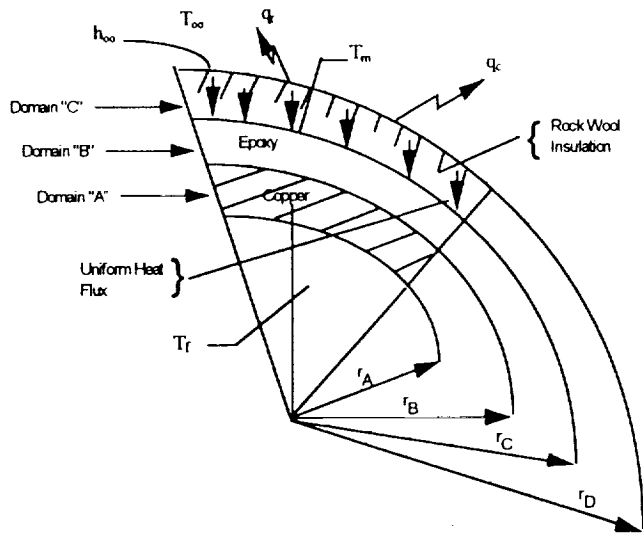


Figure 3: Thermal Hydraulic Model

The uncertainties for each measurement in this experiment are as follows: (1) for geometric measurements, ± 0.001 mm; (2) for voltage, ± 0.05 mV; (3) for current, ± 0.005 mA; (4) for pressure, ± 0.7 Pa; (5) for flow rate, $\pm 6.3E-7$ m³/s; and the resulting uncertainty in wall temperature was estimated to be ± 0.2 °C.

Results

For a 25.4 mm inside diameter single-side heated test section, 2-D (axial and circumferential) wall temperature distribution results are presented for mass velocities (G) of 280.0, 210, and 140 kg/m²s, for an inlet temperature of 22.6 °C, and an exit pressure of 0.1843 MPa (absolute).

2-D Wall Temperature Distribution

Figures 4 through 10 show the distributions as measured outside wall temperature at different circumferential and axial locations for mass velocities of 280.0, 210, and 140 kg/m²s. The wall temperature increased as the fluid flowed from upstream to downstream (axial locations #1 to #7) in the test section. Furthermore as ϕ varied from 0 to π , the temperature decreased circumferentially because of a change from a circumferentially heated region ($\phi = 0$ to $\pi/2$) to a non-heated one ($\phi = 5\pi/8$ to π) for all the flow rates. This change in temperature can be observed clearly in Figures 4 through 10.

It is desired to present the local 2-D wall temperature profile with respect to the net power generation for all forty-nine axial and circumferential locations for three different levels of mass velocity. In order to facilitate this, Figures 4 through 10 contain the profiles for $\phi = 0$ to 180.0 degrees, where Figures a and b (e.g., 4a and 4b) in this figure series contain profiles for different axial locations. Figures 4a, 5a, 6a, etc. each contain profiles for axial location Z_1 , Z_2 , Z_3 , and Z_4 . Finally, Figures 4b, 5b, 6b, etc. each contain profiles for axial locations Z_5 , Z_6 , and Z_7 .

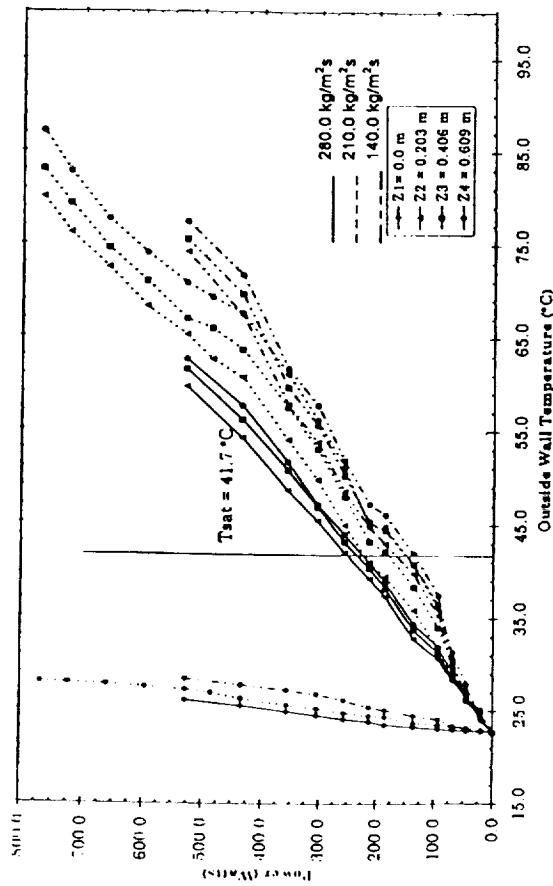


Figure 4a ($\phi = 0.0$ Degrees)

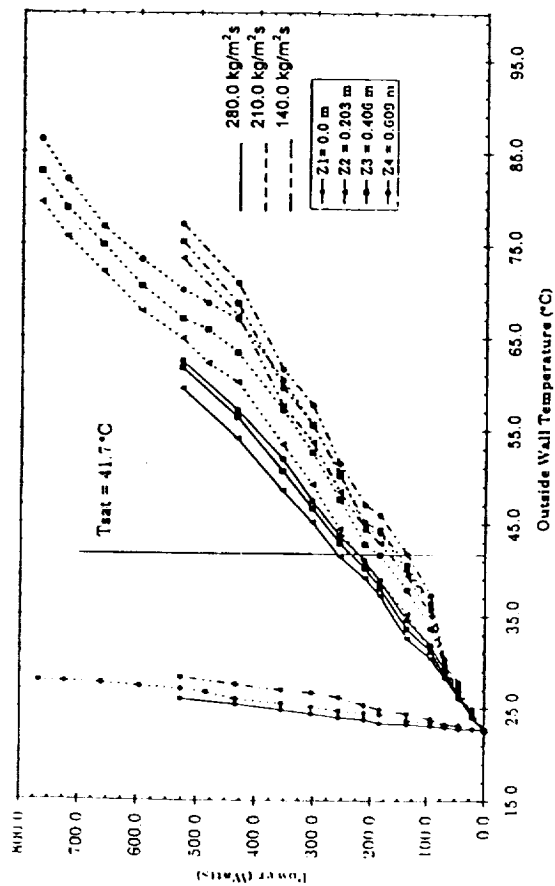


Figure 5a ($\phi = 45.0$ Degrees)

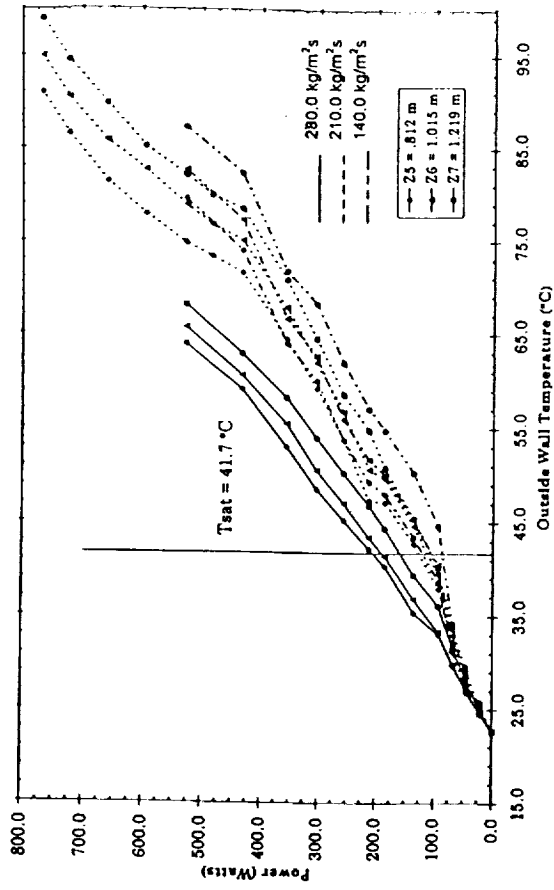


Figure 4b ($\phi = 0.0$ Degrees)

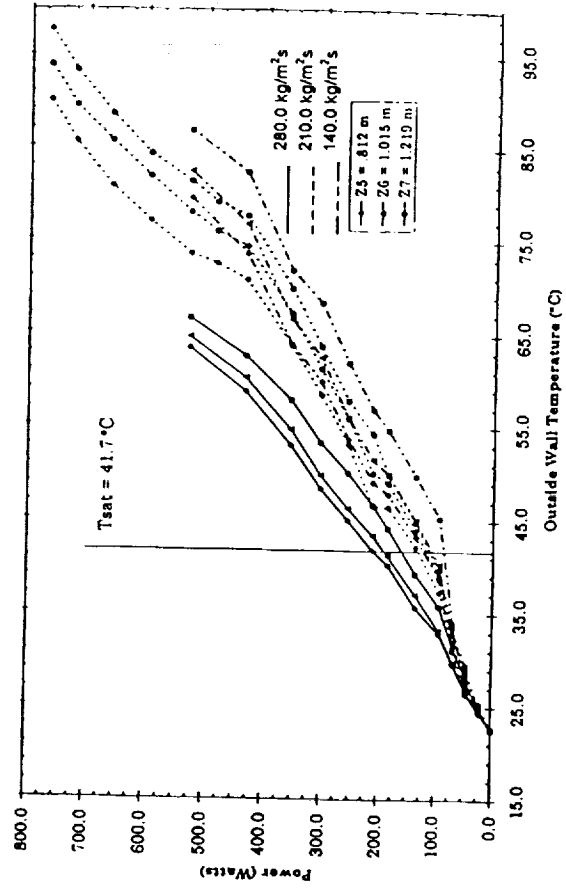


Figure 5b ($\phi = 45.0$ Degrees)

Figures 4a-5b: Measured Outside Wall Temperature (Copper Channel) Axial Distribution as a Function of Net Power Generation for Single-Side Heated Smooth Channel for Different Mass Velocities; Tube ID = 25.4 mm, Inlet Temp = 22.6 °C, and Exit Pressure = .1843 MPa (absolute).

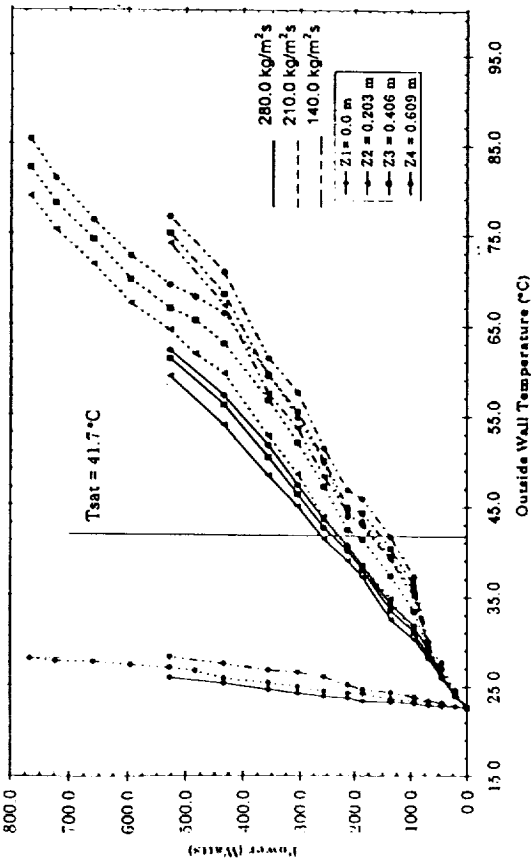


Figure 6a ($\phi = 67.5$ Degrees)

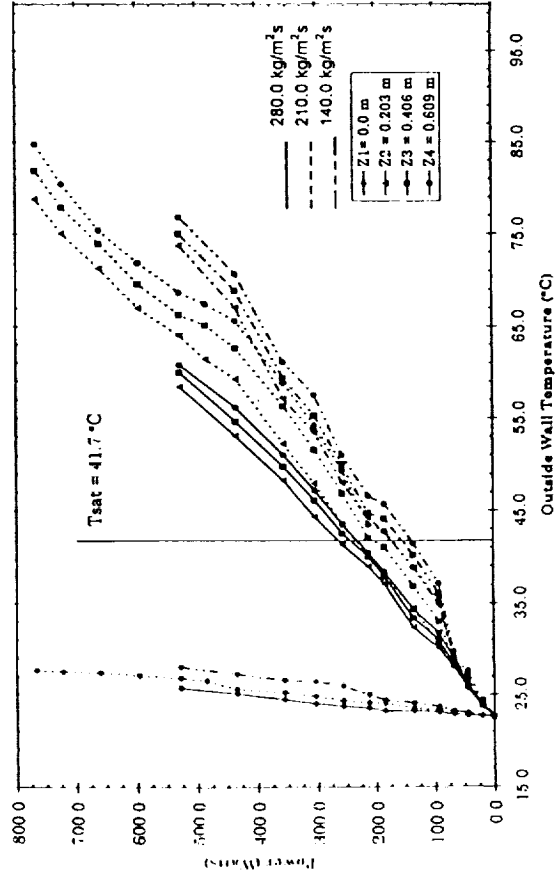


Figure 7a ($\phi = 90.0$ Degrees)

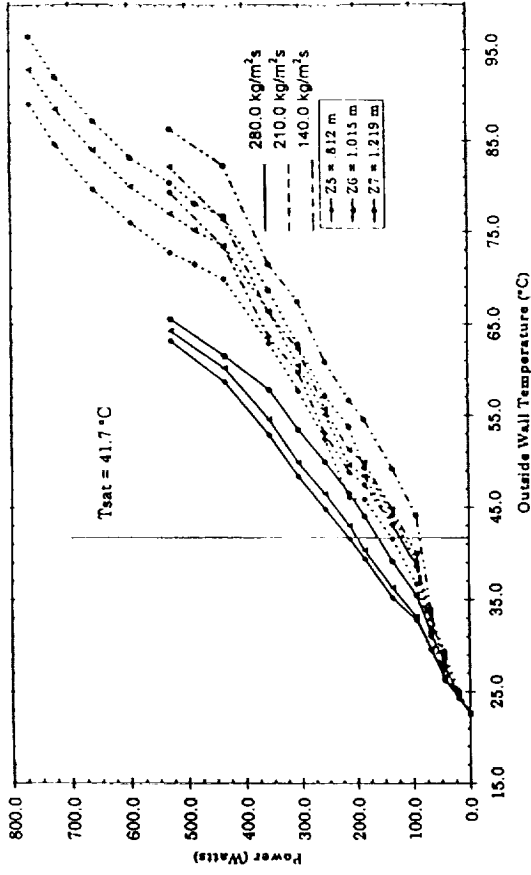


Figure 6b ($\phi = 67.5$ Degrees)

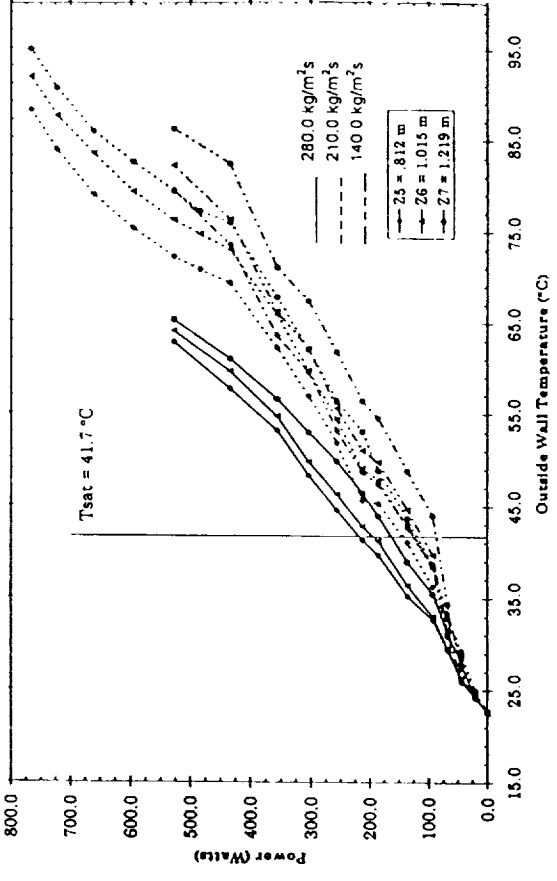


Figure 7b ($\phi = 90.0$ Degrees)

Figures 6a-7b: Measured Outside Wall Temperature (Copper Channel) Axial Distribution as a Function of Net Power Generation for Single-Side Heated Smooth Channel for Different Mass Velocities; Tube ID = 25.4 mm, Inlet Temp = 22.6 °C, and Exit Pressure = .1843 MPa (absolute).

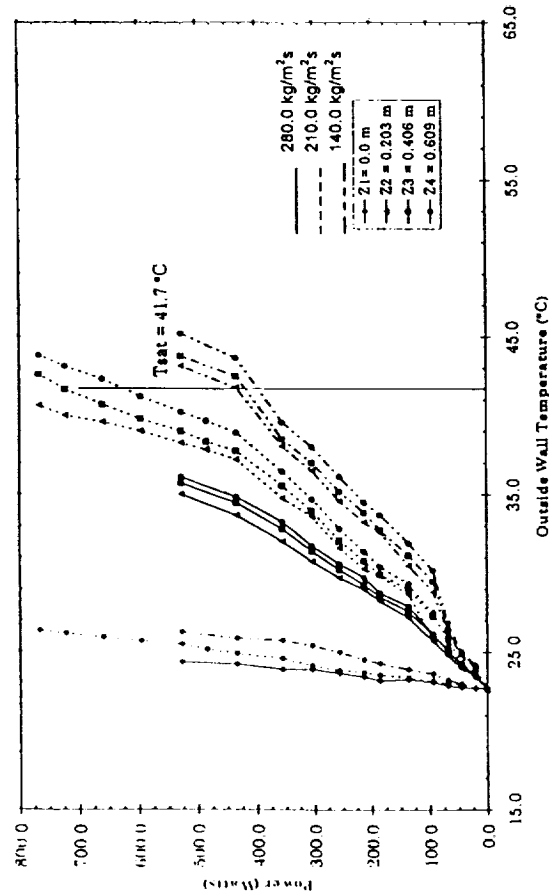


Figure 8a ($\phi = 112.5$ Degrees)

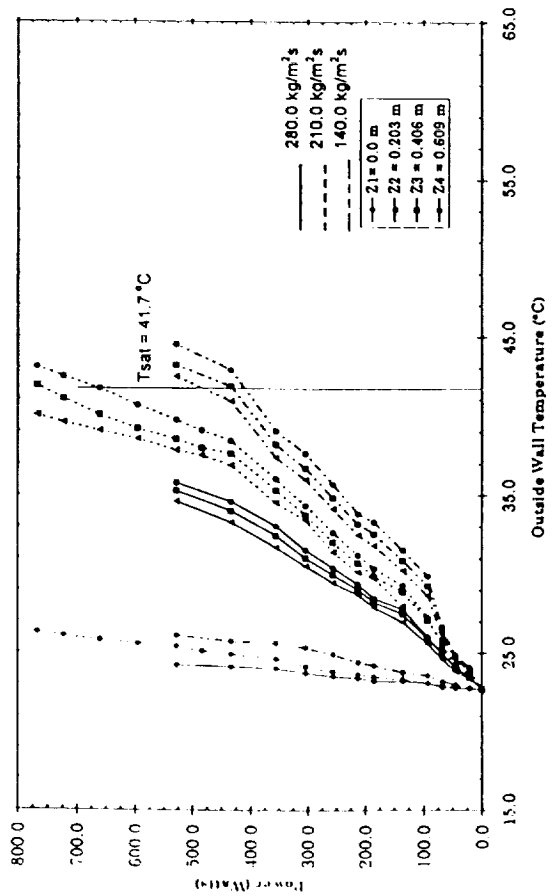


Figure 9a ($\phi = 135.0$ Degrees)

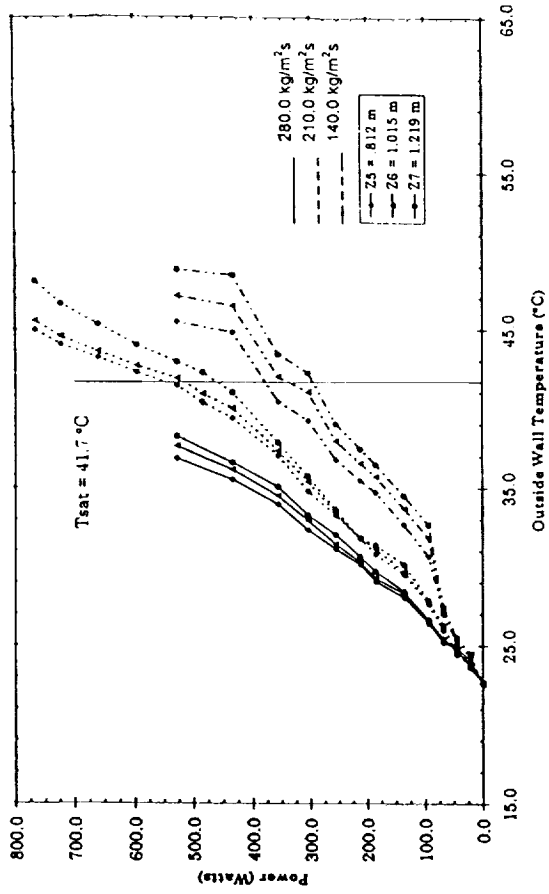


Figure 8b ($\phi = 112.5$ Degrees)

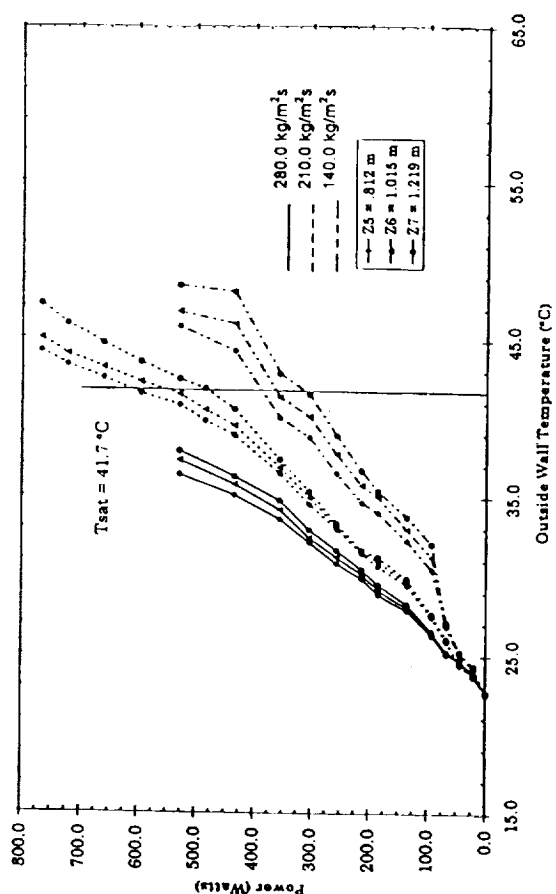


Figure 9b ($\phi = 135.0$ Degrees)

Figures 8a-9b: Measured Outside Wall Temperature (Copper Channel) Axial Distribution as a Function of Net Power Generation for Single-Side Heated Smooth Channel for Different Mass Velocities; Tube ID = 25.4 mm, Inlet Temp = 22.6 °C, and Exit Pressure = .1843 MPa (absolute).

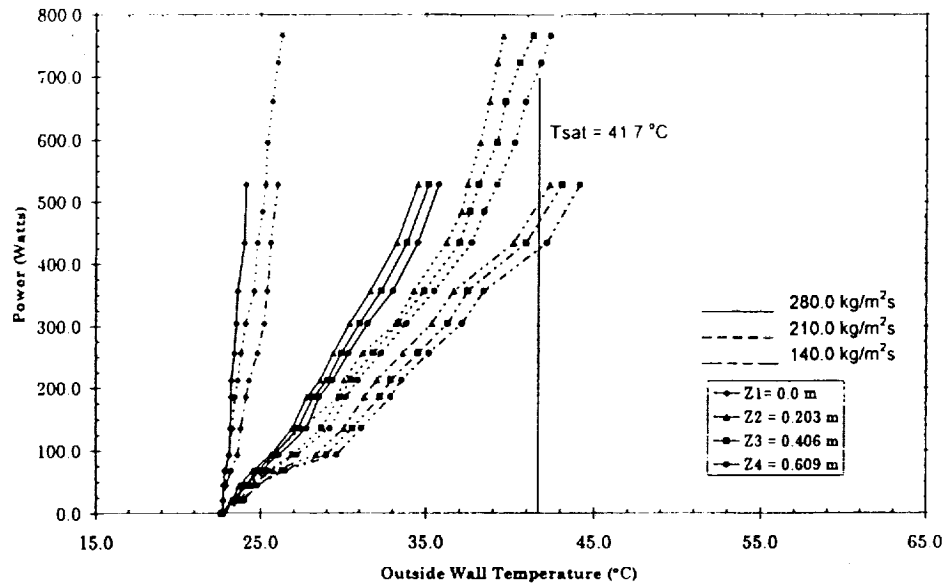


Figure 10a ($\phi = 180.0$ Degrees)

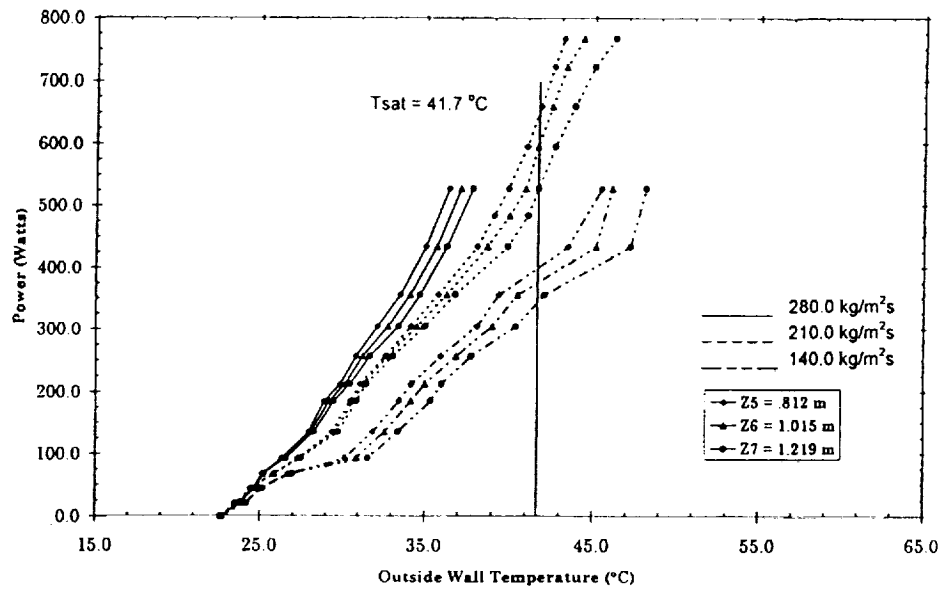


Figure 10b ($\phi = 180.0$ Degrees)

Figure 10: Measured Outside Wall Temperature (Copper Channel) Axial Distribution as a Function of Net Power Generation for Single-Side Heated Smooth Channel for Different Mass Velocities; Tube ID = 25.4 mm, Inlet Temp = 22.6 °C, and Exit Pressure = .1843 MPa (absolute).

From these figures, it can be seen that the wall temperature distributions are closely spaced for $\phi = 0$ to $\pi/2$ and $\phi = 5\pi/8$ to π . This is to be expected because of single-side heating. From the plots, one can also observe that the wall temperature at $\phi = 0$ remains above the saturation temperature ($T_{sat} = 41.65^\circ\text{C}$) and the wall temperatures at $\phi = 5\pi/8$, $3\pi/4$, and π were consistently below T_{sat} for all the mass velocities except at the highest power levels.

Although the data analysis is continuing, preliminary computations using the Davis-Anderson correlation (Davis and Anderson,¹⁷) indicate that the onset to nucleate boiling occurs at a wall temperature of 45.7°C , 44.1°C , and 42.45°C for mass velocities of 280, 210, and 140 $\text{kg/m}^2\text{s}$, respectively. For the computations, all Freon-11 properties were evaluated at the saturation temperature using Perry's handbook.¹⁸ Using these computations as a basis and the basic characteristics of the boiling curve, both axial and circumferential influences on the quasi-boiling curve are displayed in Figure 4 through 10. Figure 4 ($\phi = 0.0$ degrees) through Figure 7 ($\phi = 90.0$ degrees) show that the onset of nucleate boiling (ONB) at $G = 210.0 \text{ kg/m}^2\text{s}$ does occur slightly above 41.7°C simultaneously over the heated section. For the conditions shown, this occurred at a power below 181.2 W simultaneously at all axial locations between locations #2 and #6. For $G = 280.0 \text{ kg/m}^2\text{s}$, ONB in a similar fashion occurred below 312.0 W. The onset to fully developed boiling (OFDB) for $G = 210.0 \text{ kg/m}^2\text{s}$ occurred simultaneously at all these locations at a power level of 181.2 W. Although further data reduction is needed to determine actual inside wall temperatures, it is clear from the figures that the boiling curve will shift to the right with higher values of Z . The data also show a slight increase in $[T_w]_{out}$ (outside wall temperature) in the circumferential direction from $\phi = 90.0$ degrees to 0.0 degrees. These data provide a quantitative record which shows the regions or patches where various simultaneous boiling phenomena occurred. Even though the test section was made of highly conducting copper, the measured outside wall temperatures cannot be used directly to correlate ONB or CHF. However, these measurements are closely linked to the local variations of the inside wall temperature and hence are related to the local two-dimensional boiling heat transfer at the inside wall.

From the above discussion of wall temperature distributions, some additional characteristics of the curves become apparent. The critical heat flux occurred between $\phi = 0.0$ and 90.0 degrees at power levels above 212.7 W for 210.0, and near 212.7 W for 140.0 $\text{kg/m}^2\text{s}$. The data for 280.0 $\text{kg/m}^2\text{s}$ must be extended so that similar observations can be made.

Effect of Mass Velocity Variations

In this paper we have presented the complete wall temperature profile for three different mass velocities namely, 280.0, 210.0 and 140.0 $\text{kg/m}^2\text{s}$ for the same tube of inside diameter of 24.5 mm. Figures 4 through 10 show the complete profile of the wall temperature for all the three mass velocities. From these plots, it is clear that there is significant effect of

mass velocity on the wall temperature for this single-side heating configuration. From Figures 4 through 10, the effect of mass velocity at lower power levels on wall temperature and mode of heat transfer are not significant. However for higher power levels, increases in the mass velocity shift the quasi-boiling curve to the left with a corresponding increase in slope in both the heated and unheated regions.

Figures 4 through 10 show also a clear change in the shape of the boiling curve with respect to both mass velocity and circumferential orientation. For ϕ less than or equal to 90.0 degrees, increasing the mass velocity by identical increments from 140.0 $\text{kg/m}^2\text{s}$ to 210.0 $\text{kg/m}^2\text{s}$ and from 210.0 $\text{kg/m}^2\text{s}$ to 280.0 $\text{kg/m}^2\text{s}$ results in greater heat transfer enhancement for the latter range. Further, these figures show that for moderate power levels the flow structure results in the boiling curves for the former range almost overlaying one another. However, the boiling curves for latter or higher mass velocity range are completely separated one from another. At the higher mass velocities and for $\phi < 90.0$ degrees, the slope of the boiling curves increases and later decreases as ϕ increases. This emphasizes the three dimensional nature of the flow, and in particular the circumferential dependence due to single-side heating. Finally, the circumferential propagation of the boiling front can be seen by comparing Figures 4 through 7 with Figures 8 through 10 for $G = 140.0 \text{ kg/m}^2\text{s}$. At lower values of ϕ , ONB occurs below 181.0 W; however for larger ϕ , ONB occurs near 420.0 W. So as ϕ increases from 90.0 degrees, the stratified nature of the flow is obvious at all axial locations and all mass velocities for this downward vertical flow in a single-side heated channel.

Work is ongoing to obtain the axial distribution of the circumferentially averaged heat transfer coefficient using the thermal hydraulic approach (Boyd et al.⁴) for different diameters and different mass flow rates. Further efforts are in process to obtain the local (axial and circumferential) heat transfer coefficient using a non-linear inverse conduction approach (Huque and Boyd¹⁹).

Conclusions

Two-dimensional wall temperature measurements were presented for the forced convection boiling of Freon-11 in a single-side heated vertical channel with downward flow for a mass flow rate of 280.0, 210.0, and 140.0 $\text{kg/m}^2\text{s}$. Experimental data was obtained for circumferential and axial wall temperature distributions. The measurements show that the boiling curve changes significantly at higher mass velocities and with respect to both circumferential and axial coordinates. Due to circumferential transport, the slope of the boiling curve changes in a non-monotonic fashion as ϕ increases.

References

1. Miller, K. M., Ungar, E. K., Dzanitis, J. M., and Wheeler M., 1993, "Microgravity Two Phase Pressure Drop Data in

- Smooth Tubing, Lunar," AMD-Vol. 174/FED-Vol. 175, *Fluid Mechanics Phenomena in Microgravity*, ASME WAM 1993.
2. Ungar, E. K., Miller, K. M., and Chen, I. Y., 1993, "Two Phase Pressure Drop in Lunar and Martian Gravity: Experimental Data and Predictions," ASME FED Vol. 190, pp. 329-342.
3. Reinarts, T. R., Miller, K. M., and Frederick, R. B., 1993, "Two Phase Flow Regimes in Smooth Tubing in Microgravity, Lunar Gravity and Martian Gravity, and Earth-Normal Gravity," AMD-Vol. 174/FED-Vol. 175, *Fluid Mechanics Phenomena in Microgravity*, ASME WAM 1993.
4. Boyd, R. D., Smith, A., and Turknett, 1995b. "Multi-Dimensional Wall Temperature and Heat Transfer Enhancement for Top-Heated Horizontal Channels with Flow Boiling," *Int. J. of Experimental Heat Transfer, Thermodynamics and Fluid Mechanics* (to be published).
5. Kandlikar, S. G., 1991, "Development of Flow Boiling Map for Subcool and Saturated Flow Boiling of Different Fluids Inside Circular Tubes," *Journal of Heat Transfer*, Vol. 113, February, pp. 190-200.
6. Shah, M. M., 1977, "A General Correlation for Heat Transfer During Subcooled Boiling in Pipes and Annuli," *ASHRAE Transactions*, Vol. 83, pp. 202-215.
7. Gungor, K. E. and Winterton, R. H. S., 1986, "A General Correlation for Flow Boiling in Tubes and Annuli," *International J. Heat Mass Transfer*, Vol. 29, No 3, pp. 351-358.
8. Boyd, R. D. and Meng, X., 1995a, "Boiling Curve Correlation for Subcooled Flow Boiling," *International J. Heat and Mass Transfer*, Vol. 38, pp. 758-60.
9. Patankar, S. V., and Chai, J. C., 1991, "Laminar Natural Convection in Internally Finned Horizontal Annuli," ASME 91-HT-12.
10. Wen, X. L., Briggs, A., and Rose, J. W., 1991, "Accurate Measurements of Heat Transfer Coefficients for Condensation on Horizontal Integral-Fin Tubes," ASME 91-HT-6.
11. Jaber, M. H., Webb R. L., and Stryker, P., 1991, "An Experimental Investigation of Enhanced Tubes for Steam Condensers," ASME 91-HT-5.
12. Smith, A., 1992, "Subcooled Freon-11 Flow Boiling Heat Transfer with and Without Enhancement Devices for Top Heated Horizontal Coolant Channel," MS Thesis, Prairie View A&M University.
13. Turknett, J. C., 1989, "Forced Convection and Flow Boiling With and Without Enhancement Devices for Top-Side-Heated Horizontal Channels," MS Thesis, Prairie View A&M University.
14. Boyd, R. D., 1986, "Flow Boiling With and Without Enhancement Devices for Horizontal, Top Heated Coolant Channels for Cold Plate Design Applications, Preliminary Report," Prairie View A&M University., Submitted to NASA (JSC), Contract No. 9-16899.
15. Reid, R. S., Pate, M. B., and Bergles, A. E., 1987, "Evaporation of Refrigerant 113 Flowing Inside Smooth Tubes," ASME 87-HT-51.
16. Huque, Z., Boyd, R. D., and Smith, A., 1993, "Experimental Design for Flow Boiling in Thermal Management Systems," *Proceedings of Engineering and Architecture Symposium*, Prairie View A&M University, Prairie View, Texas, pp. 117-122.
17. Davis, E. J. and Anderson, G. H., 1966, "The Incipience of Nucleate Boiling in Forced Convection Flow," *AIChE Journal*, Vol. 12, No. 4, pp. 774-780.
18. Perry, R. H. and Green, D., 1984, *Perry's Chemical Engineers' Handbook*, McGraw Hill Publishing Company, Sixth ed. pp. 3-275- 3 -276, 3-288.
19. Huque, Z. and Boyd, R. D., 1994, "Two-Dimensional Data Reduction Applying an Inverse Heat Conduction (IHC) Technique," *Proceedings of the Mechanical Engineering Symposium*, Prairie View A&M University, Prairie View, Texas, pp. 66-72.



FORCED CONVECTION AND FLOW BOILING IN A SINGLE-SIDE HEATED VERTICAL SMOOTH CHANNEL WITH DOWNWARD FLOW

Quaid Peatiwala and Ronald D. Boyd
Thermal Science Research Center (TSRC)
P. O. Box 397
Department of Mechanical Engineering
Prairie View A&M University
Prairie View, Texas 77446

Abstract

The results for the vertical downward flow in a single-side heated channel with a Freon-11 mass flow rate of $210.0 \text{ kg/m}^2\text{s}$ are given. The two-dimensional local (axial and circumferential) measurements of the channel outside wall temperature were obtained experimentally and the corresponding axially and circumferentially mean heat transfer coefficients (h) were calculated. This flow configuration was shown to have twenty percent higher values of h and forty percent higher ultimate critical heat flux than the case of a top-heated channel with horizontal flow. The data points to the existence of multiple levels of critical heat flux, which is unique to the single-side heated geometry. Finally, these averaged heat transfer coefficients ranged from 30.0 to $230.0 \text{ W/m}^2\text{K}$ for the net heat flux range of 180.0 to $11,000.0 \text{ W/m}^2$.

Nomenclature

G	Mass Velocity ($\text{kg/m}^2\text{s}$)
h	Circumferentially and axially mean heat transfer coefficient ($\text{W/m}^2\text{K}$)
h_{mj}	Circumferentially-averaged but axially distributed heat transfer coefficient ($j = 1, 2, \dots, 7$) ($\text{W/m}^2\text{K}$)
T_{av}	Circumferentially averaged wall temperature ($^{\circ}\text{C}$)
Z	Axial coordinate or measurement location (m)

Greek

ϕ	Circumferential coordinate or measurement location (degrees)
--------	--

Subscripts

i	Circumferential location index
j	Axial location index

Introduction and Objectives

Near and long term missions of the National Aeronautics and Space Administration (NASA), including Space Station Freedom and contemplated missions to the Moon and to Mars, will require the use of advanced thermal control concepts to efficiently transport large amount waste heat over long distances (Miller et al., 1993). These missions will require an active thermal control system to provide moderate temperature heat rejection for different system modules. It is essential that the thermal rejection system selected be able to operate under a variety of complex and non-uniform heat flux distributions. Other requirements for the selected system include minimum overall system mass, and pumping power (Ungar et al., 1993). The high heat flux potential and low mass requirement of the two-phase thermal control system makes them an attractive option for advanced space applications.

Before a two-phase thermal control system can be implemented in the space project, there are several phenomena that must be clearly understood. Among the many important aspects of two-phase thermal control and transfer systems needing further study are the two-phase pressure drops and the two-dimensional (2-D) heat transfer coefficient distributions in smooth and enhanced tubes for various gravity levels including normal earth gravity, zero gravity, lunar gravity, and Martian gravity (Reinarts et al., and Ungar et al., 1993). For the case of normal earth gravity, this study investigates 2-D wall temperature variations, and mean heat transfer coefficient variations as a function of applied power. Other gravity conditions will be considered in future studies.

Recently, increased emphasis has been placed on understanding the pressure drop in two-phase flows in earth, low

gravity lunar, and Martian environments. Ungar et al. (1993) and Reinarts et al. (1993) studied the pressure drop and flow profiles for lunar-g and Martian-g two-phase flow. They have developed an extensive data base for these two reduced gravities and have recommended correlations for two-phase flow pressure drop under these conditions. Miller et al. (1993) reviewed many two-phase frictional pressure drop prediction methods for smooth tubes under normal and microgravity conditions. For qualities greater than 0.50, they recommended Troniewski and Ulbrich's correlation. However for qualities less than 0.50, the Lockhart-Martinelli/Chisholm correlation was recommended.

Another important aspect of two-phase thermal control system is the development and understanding of fundamental characteristics of flow boiling heat transfer at different gravity levels. In particular, optimization of the heat transfer, with accompanying reduced mass and pumping power requirements, will require a knowledge of the two-dimensional heat transfer coefficient distributions in advanced and commercial space systems (Boyd et al., 1995b). Implementation of two-phase thermal control system will also require additional emphasis on flow boiling phenomenon as it pertains to non-uniform heat flux distribution, resulting heat transfer coefficients, flow channel aspect ratio, and orientation.

From the literature review, it is clear that progress is being made on the prediction of pressure drop for two-phase thermal control systems for various gravity levels and flow conditions. However, the same cannot be said for the local heat transfer coefficients for two-phase flow boiling. There has been much work completed for the two-phase heat transfer correlations for a uniform heat flux distribution. Correlations presented by Kandlikar (1991), Shah (1977), Gungor and Winterton (1986), and Boyd and Meng (1995a) cover different fluids, vast ranges of flow rates, the entire spectrum of quality, and low and high subcooling. The former three correlations were only recommended for saturated flow boiling and the latter for subcooled flow boiling. These correlations are valid for only smooth tubes, and one must avoid using them when orientation is important. The former three correlations were derived from the data collected from horizontal flow boiling, where as the latter for high Froude number (> 50.0). Recently, several researchers have considered the effect of heat transfer enhancement devices (fins, and twisted tapes) and have presented correlations, but most of these are again for horizontal flow boiling or condensation on horizontal tubes. Patankar et al. (1991), Wen et al. (1991), and Jaber et al. (1991), have studied the effect of fins on the heat transfer coefficient for condensation. While Wen et al (1991) presented experimental data to facilitate theoretical model development of heat transfer coefficient for condensation on horizontal integral-finned tubes, Jaber et al. (1991) found that the condensation heat transfer coefficient can be increased by up to 280% for copper if commercially available enhanced tubes are used in condensers

over smooth copper tubes. He also looked at copper alloy tubes and found that heat transfer is enhanced by an average of over 30% with finned tubes relative to smooth tubes. Boyd et al. (1995b), Smith (1992), and Turknett (1989) have studied the flow boiling in horizontal channels with uniform and top-side heating with and without enhancements. They made measurements of the two-dimensional axial and circumferential wall temperature distributions, and presented results for the axial distribution of the heat transfer coefficient for four internal tube configurations.

The literature search suggests that: (1) there is a lack of local experimental data and local heat transfer correlations for an external single-side heat flux distribution, and (2) very few studies have been completed on investigating the flow aspect ratio, and orientation effects for uniform and non-uniform heat flux distributions.

In addition to the advanced space system, single-side heat flux boundary conditions appears in many other applications. Such advanced applications include high heat fusion components, high heat flux electronic components, in-tube boiling systems, boilers, condensers, and heat exchangers. Therefore, advanced applications requiring flow boiling will necessitate better characterizations of the local 2-D heat transfer variations for single-side heated conditions.

For optimized 2-D two-phase thermal management systems to become a reality, extensive efforts are needed to collect and correlate experimental data for heat transfer correlations for complex heat flux distributions. This is the **long-term objective** of this ongoing study. The long-range scope of this study includes making 2-D wall temperature measurements as function of mass velocity, inlet subcooling, tube diameter, tube internal geometry, tube orientation, gravity level, and heating configuration. The anticipated Freon-11 mass velocity and tube diameter range between 95.0 and 1,300.0 kg/m²s, and between 9.5 and 25.4 mm, respectively. The tube inside wall configuration will include smooth wall, finned wall, and combined twisted tape and finned walls. In the present paper, we present an example of 2-D outside wall temperature measurements made with subcooled Freon-11 flowing downward in a smooth vertical channel with single-sided heating. These wall temperature data were then used to obtain circumferentially and axially averaged heat transfer coefficients. Finally, comparisons were made with a similar flow in a horizontal channel (Boyd et al., 1995b).

Experimental Setup

The system used to perform forced convection boiling experiments in vertical tubes (downward flow), was based on the system initially developed by Boyd et al. (1995b) and later used by Smith (1992), Boyd (1986), and Turknett (1989). Figure 1a shows the Freon-11 (R-11) vertical flow boiling loop. This closed loop is constructed of stainless steel and copper, and

operates between 3.4 kPa and 17 MPa. The maximum power generation capability is 2.7 kW and the maximum volume flow rate is approximately $2.97 \times 10^{-4} \text{ m}^3/\text{sec}$. The Freon-11 is stored in a reservoir which is filled using a chemical resistance centrifugal pump. After filling the reservoir, the R-11 is circulated through the closed loop at the desired operating pressure and flow rate. By circulating the R-11 before any data is recorded, any leaks in the system can be detected by using a halogen leak detector. Then the desired inlet temperature is obtained by properly adjusting the chiller/isothermal bath. The energy is transferred between the chiller and R-11 by way of a commonly connected heat exchanger. During testing, the outlet temperature of the chiller is adjusted to maintain a constant inlet R-11 temperature for a given experimental run. The working fluid for the chiller is a 60/40 ethylene glycol - distilled water mixture.

A description of the closed flow loop and the function of its components is instructive. The R-11 flows from the reservoir to the filter, where all the contaminants are removed before the fluid enters the positive displacement pump. The positive

displacement pump requires a net positive suction of at least 0.02 MPa. This pump was selected for durability. After leaving the pump, the fluid passes through the pulsation damper. The damper reduces the pressure and flow oscillations. The pressure fluctuations are also minimized by using the pneumatically controlled metering valve. Exiting the control valve, the fluid flows to the heat exchanger, where its temperature is set at a desired value by adjusting the chiller parameters. After exiting the heat exchanger, the fluid passes through the turbine flow meter and enters the unheated "flow developing" section or upstream part of the test section which has a length greater than forty (40) times the test section diameter. The fluid then enters the heated section of the test section. A downstream pneumatically controlled valve is used to control the test section exit pressure. The heated fluid then passes through another heat exchanger where the energy generated is removed partially by using tap water. Finally, the fluid flows back to the reservoir and the flow cycle is complete.

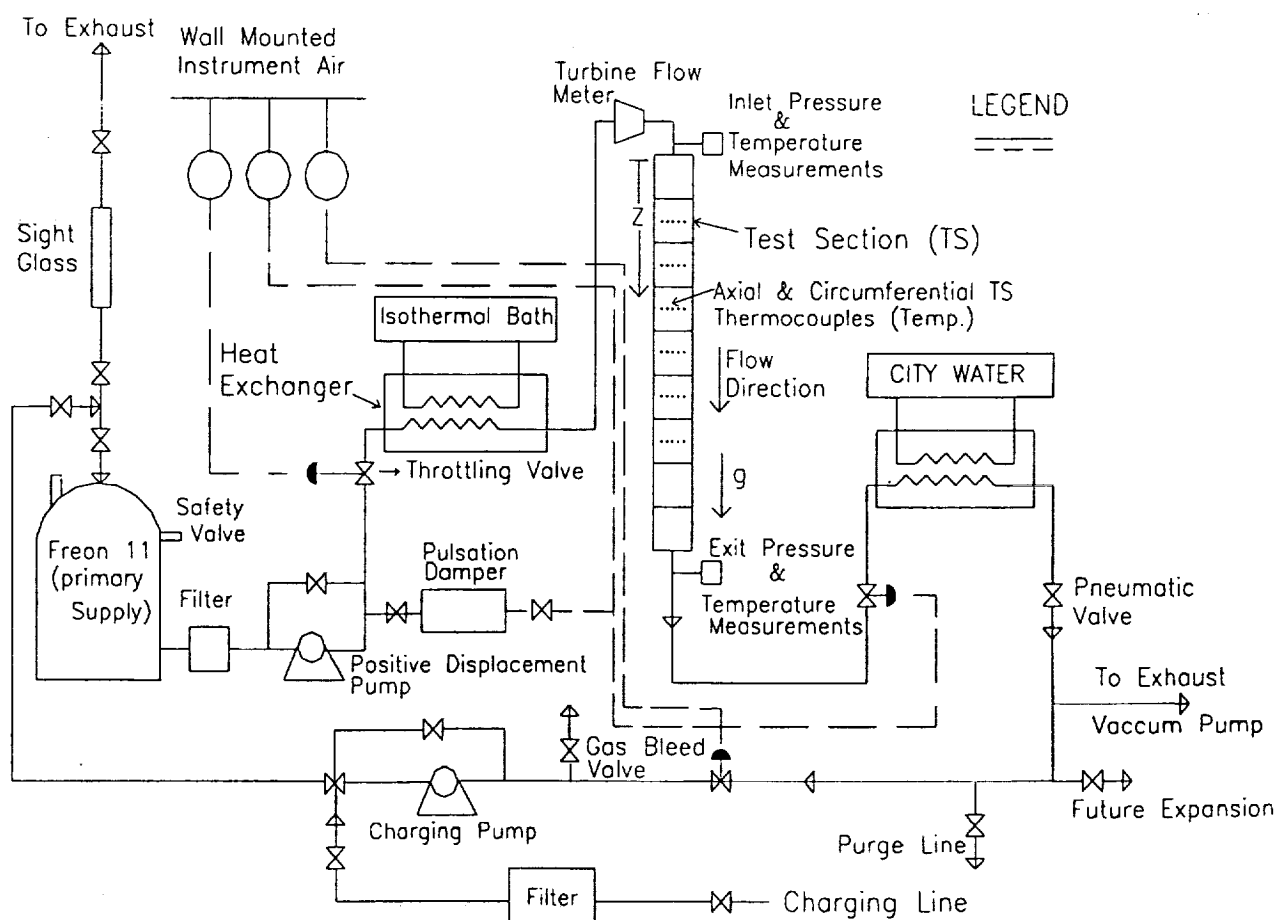


Figure 1a: Schematic of the Vertical Downward Flow Boiling Loop

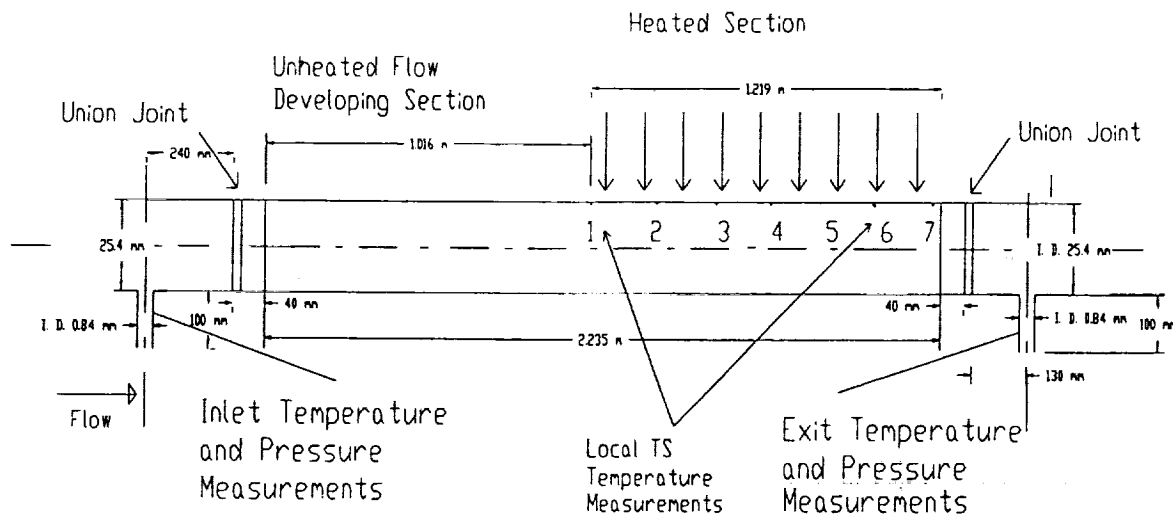


Figure 1b: Test Section (TS) Configuration for Temperature and Pressure Measurements

Test Section Description

The test sections used in this experiment are the same as used by Boyd et al. (1995b). The test sections are 2.235 m long copper tubes (see Figure 1b), and consists of two parts: (1) Upstream unheated section to facilitate flow development, and (2) A downstream single-side heated section. For the present case, the inside diameter (D) was 25.4 mm and the outside diameter was 28.5 mm.

The heated section has a smooth inside surface. The test section is heated with heater tapes which vary in width based on tube diameter and are 1.22 m long. Each tape has power generation capacity of 2.66 kW. The test section was designed with flexibility and ease of replacement in mind. Although, the pressure losses due to union connector at both top and bottom ends of the test section are assumed to be small, computations and additional measurements, will be performed later to estimate these losses. The entire test section was insulated to minimize the heat losses. In addition to the primary two parts of the main test section, each part had pressure-temperature measurement ports upstream and downstream of the test section.

The heated part of the test section was divided into seven 203 mm axial intervals. At each of the axial locations there are seven thermocouples installed circumferentially at 0 , $\pi/4$, $3\pi/8$, $\pi/2$, $5\pi/8$, $3\pi/4$, and π , and degrees (see Figure 2), with 0 being at the top heated portion of vertical symmetry plane in Figure 2. This test section thermocouple arrangement will allow better circumferential resolution of the wall temperature variation than previous test sections (Boyd, 1986, Smith, 1992, and Turknett, 1989) because seven circumferential locations are used rather than four.

The thermocouples were installed by using high thermal conductivity epoxy. Special care was taken when thermocouples

were adhered to the tube. The thermocouple beads were placed in good contact with the tube so that as little epoxy as possible was used. Based on repeated measurements (forty) of the epoxy thickness between the thermocouple and the copper tube, the mean thickness was 0.194 mm, and the standard deviation was 0.007 mm.

Data Reduction Analysis

Forty-nine (49) local temperature measurements were made on the outside surface of the heated portion of the test section for each experiment. These outside temperatures must be related to the inside wall temperature in order for us to calculate the inside heat transfer coefficient. Two techniques will be used to reduce the wall temperature data: (1) the heated thermal hydraulic approach (Boyd et al., 1995b) (see Figure 3), and (2) a multi-dimensional inverse conduction analysis using numerical finite element computation code called ANSYS.

The initial data reduction is based on the heated hydraulic approach used by Boyd et al. (1995b). In this analysis, we compute circumferentially averaged heat transfer coefficient from circumferentially averaged wall temperature. The circumferentially averaged temperature is computed from the seven wall temperature measurements made on copper tube outside surface at each axial location by using the piece-wise linear approach used by Reid et al. (1987). Using their approach, the circumferentially averaged outside wall temperature can be related to the seven circumferential measured temperatures (T_{m1} at 0 degrees, T_{m2} at $\pi/4$, T_{m3} at $3\pi/8$ etc.) by the equation given below:

$$T_{av} = \frac{2T_{m1} + 3T_{m2} + 2T_{m3} + 2T_{m4} + 2T_{m5} + 3T_{m6} + 2T_{m7}}{16} \quad (1)$$

coefficient was estimated by Boyd et al. (1995b), and Huque et al. (1993) to be less than 10 percent.

Results

For a 25.4 mm inside diameter single-side heated test section, results are presented for a mass velocity (G) of 210.0 kg/m²s, an inlet temperature of 22.6 °C, and an exit pressure of 0.1843 MPa (absolute). The results include:

1. 2-D (axial and circumferential) wall temperature distributions;
2. Axial distributions of mean wall temperature (circumferentially averaged); and,
3. Axially and circumferentially averaged mean heat transfer coefficient distributions.

2-D Wall Temperature Distribution

Figures 4a-4g, and Figure 5, show the distributions as measured outside wall temperature at different circumferential and axial locations. The wall temperature increased as the fluid flowed from upstream to downstream (axial locations #1 to #7) in the test section. Furthermore as ϕ varied from 0 to π , the temperature decreased circumferentially because of a change from a circumferentially heated region ($\phi = 0$ to $\pi/2$) to a non-heated one ($\phi = 5\pi/8$ to π).

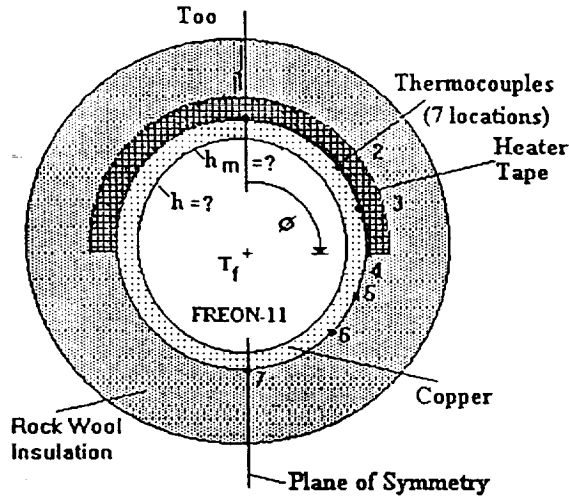


Figure 2: Cross-section of Heated Portion of the Vertical Test section

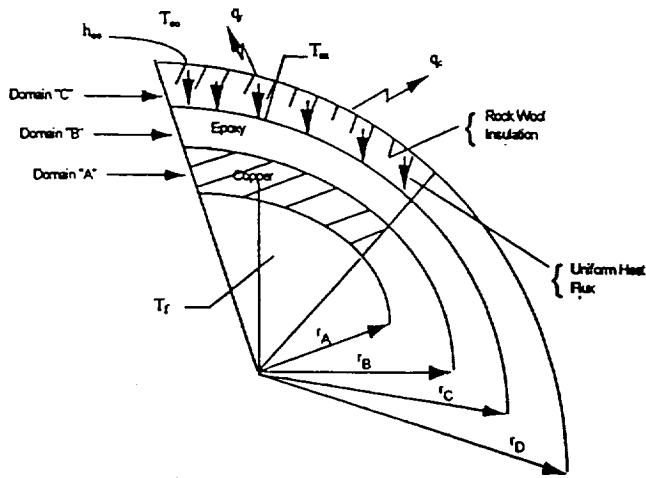


Figure 3: Thermal Hydraulic Model

The temperature T_{av} was used with the model presented by Boyd et al. (1995b) to account for temperature drop across channel walls, and convective and radiative heat losses to the surroundings. Using this model, the mean heat transfer coefficient ($h_{m,j}$) at a given axial location was obtained.

The uncertainties for each measurement in this experiment are as follows: (1) for geometric measurements, ± 0.001 mm; (2) for voltage, ± 0.05 mV; (3) for current, ± 0.005 mA; (4) for pressure, ± 0.7 Pa; (5) for flow rate, $\pm 6.3E-7$ m³/s; and (6) for temperature, ± 0.17 °C. The resulting uncertainty in heat transfer

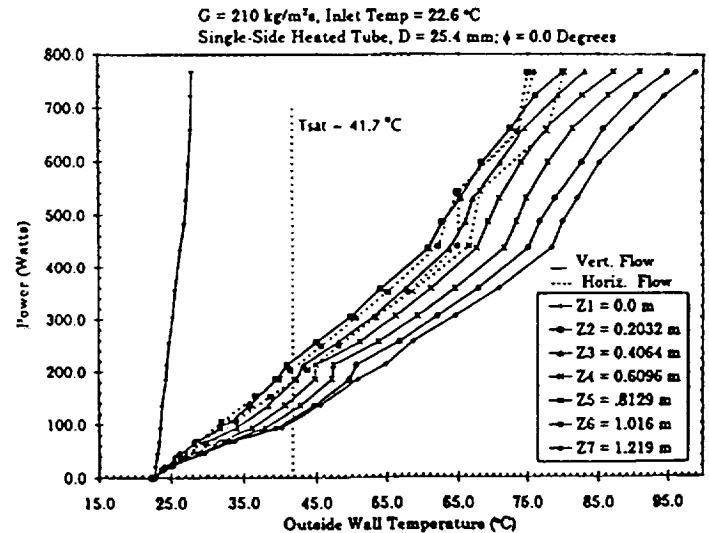
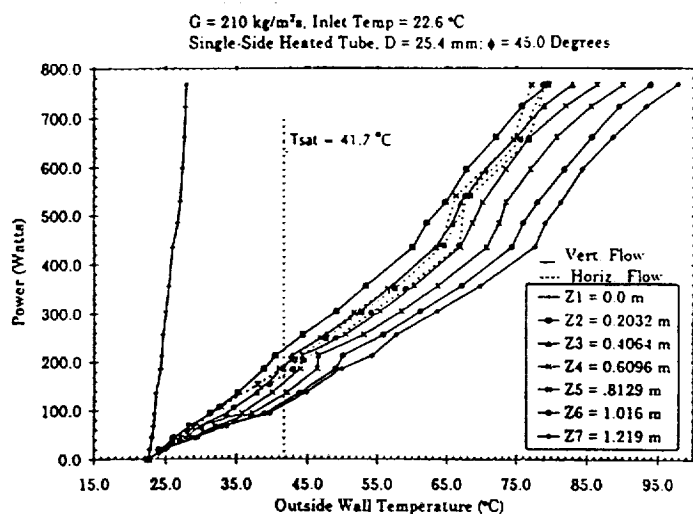
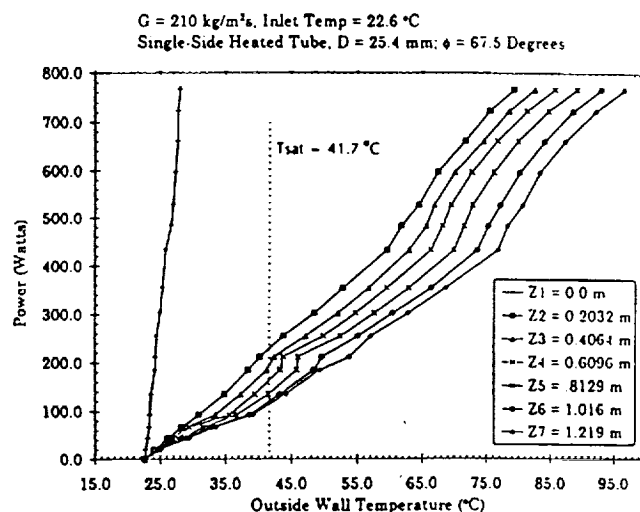


Figure 4a: Measured Outside Wall Temperature (Copper Channel) Axial Variation as a Function of the Net Power Generation for a Single-Side Heated Smooth Channel; $\phi = 0.0$ Degrees

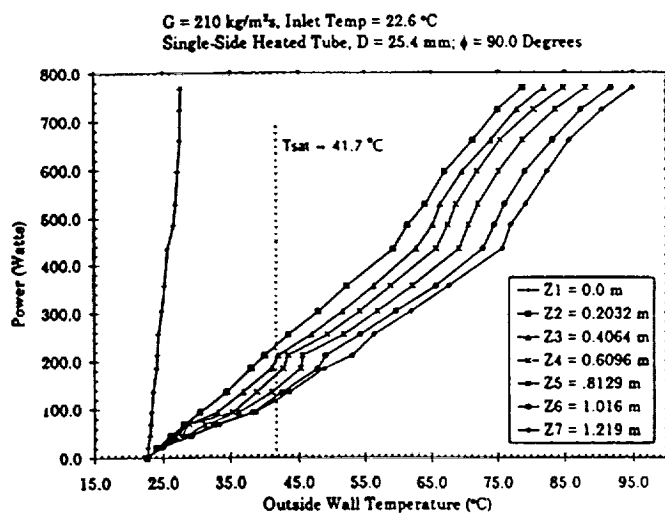
This change in temperature can be observed clearly in Figures 5. This figure shows the axial distributions for the wall temperature for seven circumferential locations, as well as the



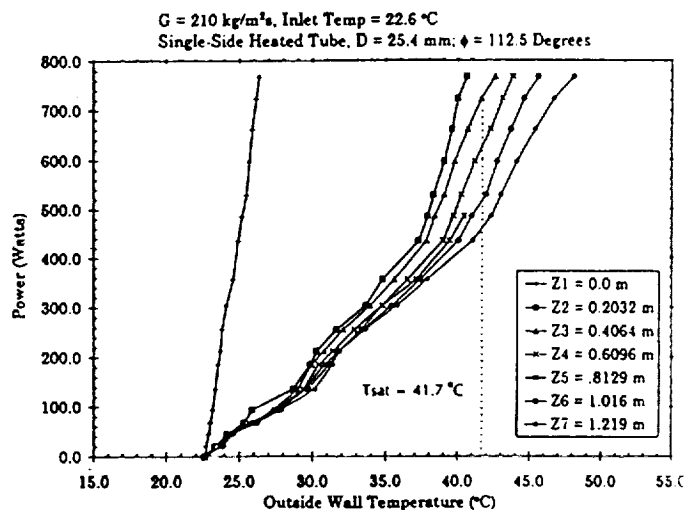
(b) $\phi = 45.0^\circ$ Degrees



(c) $\phi = 67.5^\circ$ Degrees

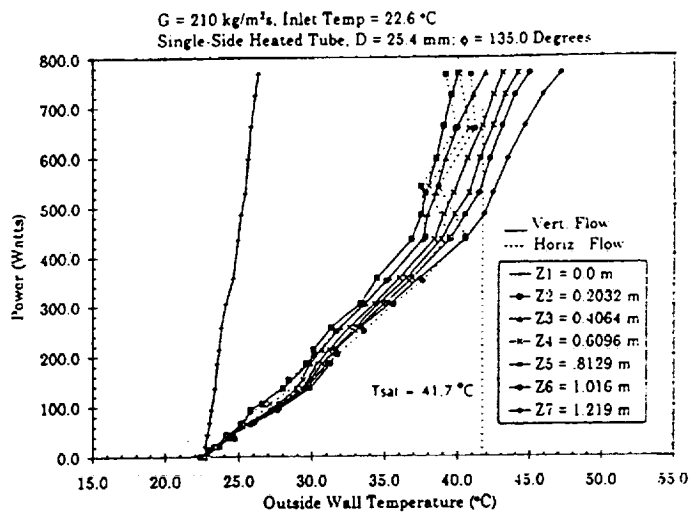


(d) $\phi = 90.0^\circ$ Degrees

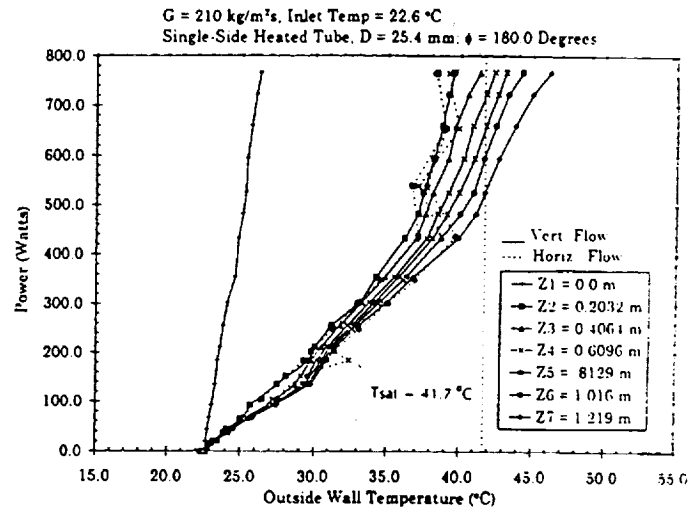


(e) $\phi = 112.5^\circ$ Degrees

Figure 4: Measured Outside Wall Temperature (Copper Channel) Axial Variation as a Function of the Net Power Generation for a Single-Side Heated Smooth Channel.



(f) $\phi = 135.0^\circ$



(g) $\phi = 180.0^\circ$

Figure 4: Measured Outside Wall Temperature (Copper Channel) Axial Variation as a Function of the Net Power Generation for a Single-Side Heated Smooth Channel.

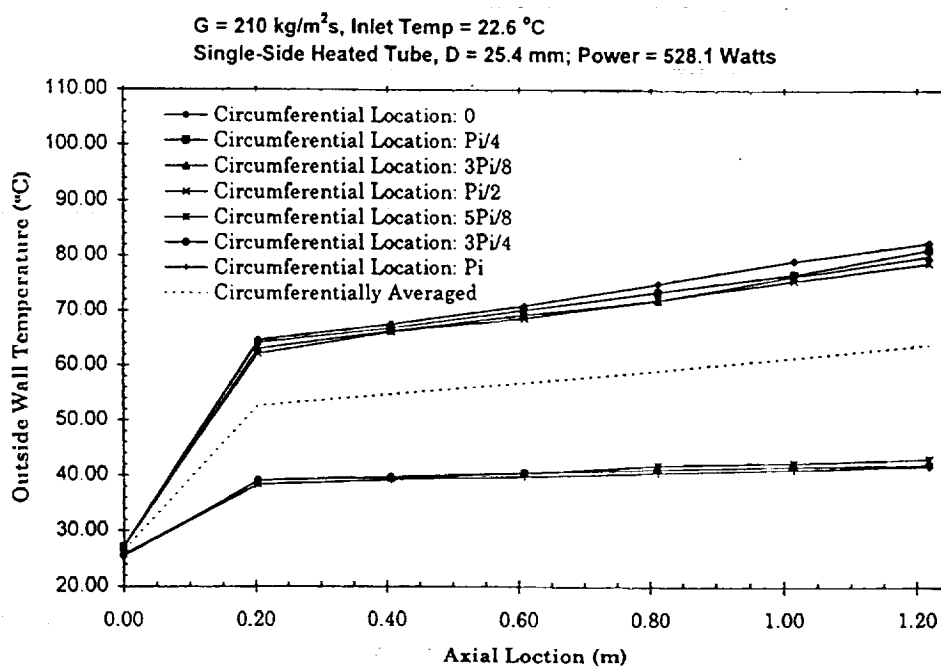


Figure 5: Axial Distribution of the Wall Temperature for Seven Circumferential Locations for the Smooth Tube for the Net Power Generation of 528.1 Watts.

circumferentially averaged wall temperature (dotted line). From these figures, it can be seen that the wall temperature distributions are closely spaced for $\phi = 0$ to $\pi/2$ and $\phi = 5\pi/8$ to π . This is to be expected because of single-side heating. From the plots, one can also observe that the wall temperature at $\phi = 0$ remains above the saturation temperature ($T_{sat} = 41.65^\circ\text{C}$) and the wall temperature at $\phi = 5\pi/8$, $3\pi/4$, and π were consistently below T_{sat} .

Although the data analysis is continuing, preliminary computations using the Davis-Anderson correlation (Davis and Anderson, 1966) indicate that the onset to nucleate boiling occurs at a wall temperature of 44.1°C . For the computations, all Freon-11 properties were evaluated at the saturation temperature using Perry's handbook (1984). Using this computation as a basis and the basic characteristics of the boiling curve, both axial and orientation influences on the quasi-boiling curve are displayed in Figure 4a through 4g. Figure 4a ($\phi = 0.0$ degrees) through Figure 4d ($\phi = 90.0$ degrees) show that the onset of nucleate boiling (ONB) does occur slightly above 41.7°C simultaneously over the heated section from $\phi = 0.0$ to 90.0 degrees. For the conditions shown, this occurred at a power below 181.2 W simultaneously at all axial locations between locations #2 and #6 but at different outside wall temperatures. Similarly, the onset to fully developed boiling (OFDB) occurred simultaneously at all these locations at a power level of 181.2 W. Although further data reduction is needed to determine actual inside wall temperatures, it is clear from the figures that the boiling curve will shift to the right with higher values of Z . The data also show a slight increase in $[T_w]_{out}$ (outside wall temperature) in the circumferential direction from $\phi = 90.0$ degrees to 0.0 degrees. These data provide a quantitative record which shows the regions or patches where various simultaneous boiling phenomena occurred. Even though the test section was made of highly conducting copper, the measured outside wall temperatures cannot be used directly to correlate ONB or CHF. However, these measurements are closely linked to the local variations of the inside wall temperature and hence are related to the local two-dimensional boiling heat transfer at the inside wall.

Heat Transfer Coefficient

Once the local wall temperature distribution was obtained, the mean (circumferentially averaged) wall temperature was computed and this temperature was used in the heated thermal hydraulic approach (Boyd et al., 1995b) to obtain the circumferentially averaged heat transfer coefficient for each axial location and for different power levels. Then, this circumferentially averaged heat transfer coefficient ($h_{m\phi}$) was used to obtain overall (circumferentially and axially mean) heat transfer coefficient using the equation (2), which is based on a linear piece-wise approximation between each axial location. The 1st and the 7th axial locations are not included due to end

losses. Hence, the axially and circumferentially mean heat transfer coefficient was defined as

$$h = \frac{h_{m2} + 2h_{m3} + 2h_{m4} + 2h_{m5} + h_{m6}}{8.0} \quad (2)$$

The mean heat transfer coefficient distribution for the mass flow rate of $210.0 \text{ kg/m}^2\text{s}$ is given on Figure 6. From the above discussion of wall temperature distribution, the OFDB occurred at power level of 181.2 W, and the critical heat flux occurred between $\phi = 0.0$ and 90.0 degrees at a power level of 212.7 W. This can be confirmed again from the mean h distribution given in Figure 6. It is clear from Figure 6 that, at the OFDB, there is an increase in the mean h which occurs at a power of 181.2 W. This agrees with the above noted predictions using the Davis-Anderson correlation.

Since the flow channel is heated from one side, the CHF occurred locally in a small circumferential angular interval $\Delta\phi$ directly below the heater and extending from $\phi = 0$ to $\phi = \Delta\phi$. As the power level is increased, $\Delta\phi$ increases and the ONB occurs at successively larger values of ϕ . If the largest value of ϕ at which the ONB occurs is denoted by ϕ_{ONB} , then the: (1) single-phase flow regime occurs in the region where $\phi > \phi_{ONB}$, (2) stable nucleate boiling regime occurs in the region $\Delta\phi < \phi < \phi_{ONB}$, and (3) stable film boiling regime occurs for $\phi < \Delta\phi$. A similar condition was postulated by Boyd et al. (1984) and similar observations were recently observed by Marshall et al. (1994) who used water as the working fluid. This stable circumferential distribution seems to be preserved by energetic mixing and flow regime interaction. The result of this stable flow is a continual increase in h with power (see Figure 6) until a second and less pronounced CHF occurs. Figures 4a through 4f show that this occurred at a power level of about 500.0 W, which is more than a factor of two above the first CHF.

Figure 6 also compares the overall h obtained for a vertical channel from the present work with similar results for a horizontal channel, which was obtained by Smith (1992). Smith's results for h had to be updated (see Boyd et al, 1995b) from the reported circumferentially and axially averaged heat transfer coefficients. Direct comparisons with our mass flow rate of $210.0 \text{ kg/m}^2\text{s}$ cannot be made because of different mass flow rates for horizontal channel. Efforts are on way to run cases with identical flow rates so quantitative comparisons can be made. However, qualitative comparisons can be made with the horizontal flow case of $184.84 \text{ kg/m}^2\text{s}$. The heat transfer coefficient, h , increases with power for both cases, but the peak value of h for the horizontal flow (Top-Heating) near the second CHF (ultimate CHF) is almost twenty percent less than that obtained for the vertical. This difference can be attributed to the difference in mass velocity to some extent, but further investigation will indicate the extent of this contribution. The present results for the horizontal case indicate that the mass

Heat Transfer Coefficient Comparison for Horizontal (Top Heated) And Downward Vertical Flow (Single-Side heated).

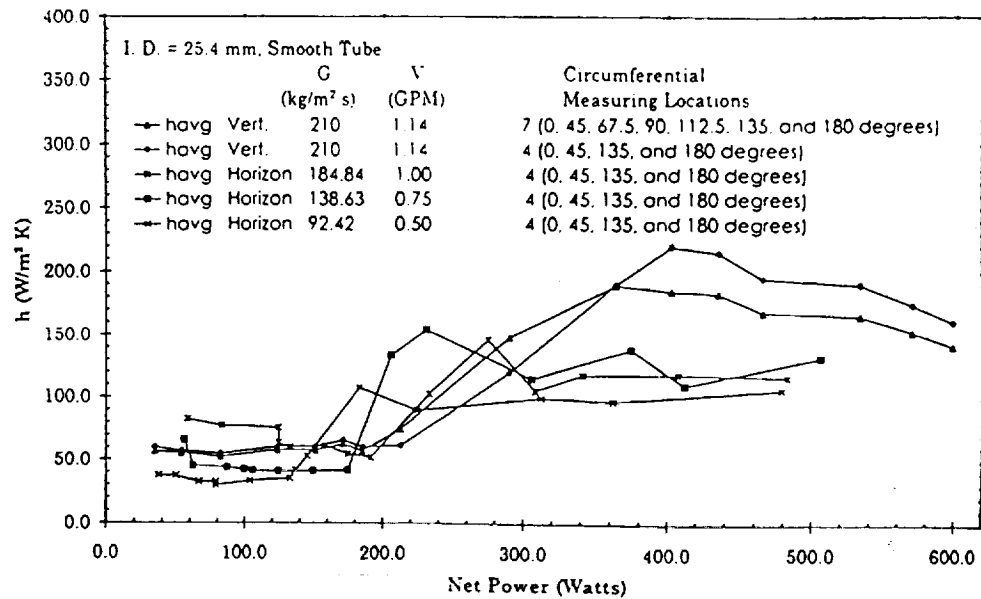


Figure 6: Circumferentially and Axially Averaged Heat Transfer Coefficient as a Function of the Net Power Generation for a Single-Side Heated, Smooth Channel.

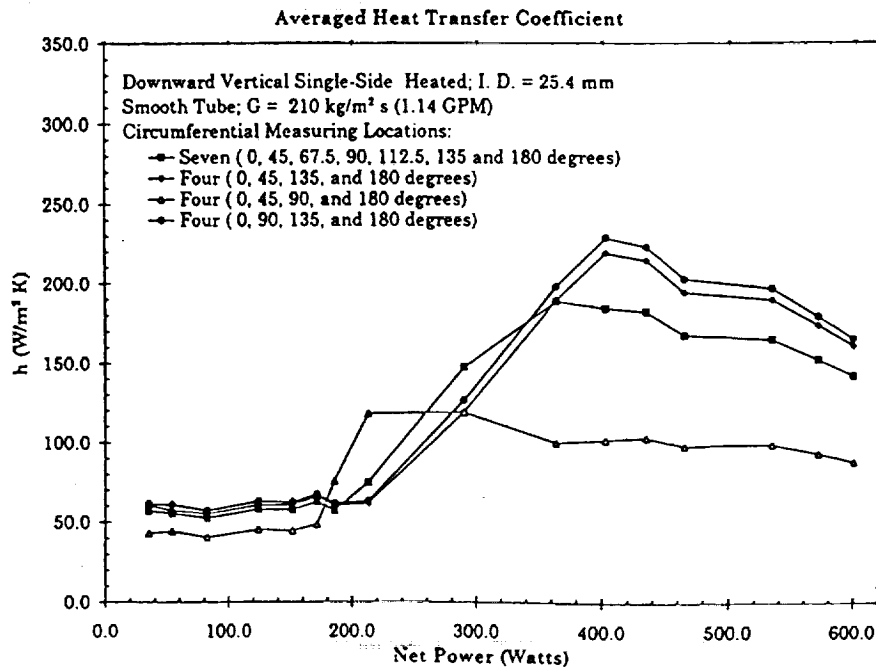


Figure 7: Circumferentially and Axially Averaged Heat Transfer Coefficient For Different Temperature Measuring Locations as a Function of the Net Power Generation for a Single-Side Heated, Smooth Channel.

velocity influence on h is small in the range between 92.0 and 184 kg/m²s, which implies that the difference shown in Figure 6 between the horizontal and vertical flow is due to principally the orientation differences. Finally, the power level at which the second CHF occurred for the horizontal flow is more than forty percent less than that for the vertical flow.

As stated before, the circumferential measurement of wall temperature was made at seven circumferentially locations rather than four as used by Boyd et al. (1995b), Smith (1992), and Turknett (1989). The effect of selected locations for the circumferential temperature measurement on mean heat transfer coefficient is given by Figure 7. Shown are plots of h as a function of power when seven and four circumferential measurement locations were used. It is clear that the more circumferential measurement locations used for the temperature, the more accurate the value of the mean h and better the resolution for later determinations of local variations in the heat transfer coefficient. But if for cost or geometric restrictions of the channel only four circumferential temperature measurements can be made, what are the best locations which will result in a good estimate for h ? The results in Figure 7 show that the circumferential locations used by Boyd et al. (1995b), Smith (1992), and Turknett (1989) resulted in the best agreement with the case where seven circumferential locations were chosen (present work). Work is ongoing to obtain the axial distribution of the circumferentially averaged heat transfer coefficient using the thermal hydraulic approach (Boyd et al. 1995b) for different diameters and different mass flow rates. Further efforts are in process to obtain the local (axial and circumferential) heat transfer coefficient using a non-linear inverse conduction approach (Huque and Boyd, 1994).

Conclusions

In this paper, 2-D (circumferential and axial) wall temperature measurements, and circumferentially-and-axially averaged heat transfer coefficient (h) distributions were presented for the forced convection boiling of Freon-11 in a single-side heated vertical channel with downward flow for a mass flow rate of 210.0 kg/m²s. Experimental data was obtained for 2-D wall temperature distributions and axial distributions of mean wall temperature (circumferentially averaged), which was reduced to obtain h .

This work confirms recent observations by Marshall et al. (1994) and previous postulations by Boyd et al. (1984). It shows that the effects of single-side heating are to allow multiple levels of critical heat flux to occur before the channel wall is no longer wetted by liquid phase.

Additional work is needed to extend the results to wider ranges of G , inlet temperature, heating configuration, and D so that: (1) further comparisons can be made with horizontal flow, (2) local and mean variations in the heat transfer coefficient can be obtained, and (3) a basis can be established for testing

existing and new correlations, as well as forced convection and flow boiling numerical models.

References

- Boyd, R. D. and Meng, X., 1995a, "Boiling Curve Correlation for Subcooled Flow Boiling," *International J. Heat and Mass Transfer*, Vol. 38, pp. 758-60.
- Boyd, R. D., Smith, A., and Turknett, 1995b, "Multi-Dimensional Wall Temperature and Heat Transfer Enhancement for Top-Heated Horizontal Channels with Flow Boiling," *Int. J. of Experimental Heat Transfer, Thermodynamics and Fluid Mechanics* (to be published).
- Boyd, R. D., 1986, "Flow Boiling With and Without Enhancement Devices for Horizontal, Top Heated Coolant Channels for Cold Plate Design Applications, Preliminary Report," Prairie View A&M University, Submitted to NASA (JSC), Contract No. 9-16899.
- Boyd, R. D. et al., 1984, "Preliminary Design Analysis of ALT-II Limiter for TEXTOR," *Journal of Nuclear Materials*, 121, pp. 309-315.
- Cheremisinoff, N. P., 1986, *Hand Book of Heat and Mass Transfer. Volume 1: Heat Transfer Operations*, Gulf Publishing Company, pp. 303-327.
- Davis, E. J. and Anderson, G. H., 1966, "The Incipience of Nucleate Boiling in Forced Convection Flow," *AIChE Journal*, Vol. 12, No. 4, pp. 774-780.
- Gungor, K. E. and Winterton, R. H. S., 1986, "A General Correlation for Flow Boiling in Tubes and Annuli," *International J. Heat Mass Transfer*, Vol. 29, No. 3, pp. 351-358.
- Huque, Z. and Boyd, R. D., 1994, "Two-Dimensional Data Reduction Applying an Inverse Heat Conduction (IHC) Technique," *Proceedings of the Mechanical Engineering Symposium*, Prairie View A&M University, Prairie View, Texas, pp. 66-72.
- Huque, Z., Boyd, R. D., and Smith, A., 1993, "Experimental Design for Flow Boiling in Thermal Management Systems," *Proceedings of Engineering and Architecture Symposium*, Prairie View A&M University, Prairie View, Texas, pp. 117-122.
- Jaber, M. H., Webb, R. L., and Stryker, P., 1991, "An Experimental Investigation of Enhanced Tubes for Steam Condensers," ASME 91-HT-5.
- Kandlikar, S. G., 1991, "Development of Flow Boiling Map for Subcool and Saturated Flow Boiling of Different Fluids Inside Circular Tubes," *Journal of Heat Transfer*, Vol. 113, February, pp. 190-200.
- Marshall, T., et al. 1994, "Post Critical Heat Flux and Log of Flow Accident Experiments," US/Japan Helium Cooling Workshop, General Atomics Corporation, San Diego, CA.

Miller, K. M., Ungar, E. K., Dzanitis, J. M., and Wheeler M., 1993, "Microgravity Two Phase Pressure Drop Data in Smooth Tubing, Lunar," AMD-Vol. 174/FED-Vol. 175, *Fluid Mechanics Phenomena in Microgravity*, ASME WAM 1993.

Patankar, S. V., and Chai, J. C., 1991, "Laminar Natural Convection in Internally Finned Horizontal Annuli," ASME 91-HT-12

Perry, R. H. and Green, D., 1984, *Perry's Chemical Engineers' Handbook*, McGraw Hill Publishing Company, Sixth ed. pp. 3-275-3-276, 3-288.

Reid, R. S., Pate, M. B., and Bergles, A. E., 1987, "Evaporation of Refrigerant 113 Flowing Inside Smooth Tubes," ASME 87-HT-51

Reinarts, T. R., Miller, K. M., and Frederick, R. B., 1993, "Two Phase Flow Regimes in Smooth Tubing in Microgravity, Lunar Gravity and Martian Gravity, and Earth-Normal Gravity," AMD-Vol. 174/FED-Vol. 175, *Fluid Mechanics Phenomena in Microgravity*, ASME WAM 1993.

Shah M. M., 1977, "A General Correlation for Heat Transfer During Subcooled Boiling in Pipes and Annuli," *ASHRAE Transactions*, Vol. 83, pp. 202-215.

Smith, A., 1992, "Subcooled Freon-11 Flow Boiling Heat Transfer with and Without Enhancement Devices for Top Heated Horizontal Coolant Channel," MS Thesis, Prairie View A&M University.

Turknett, J. C., 1989, "Forced Convection and Flow Boiling With and Without Enhancement Devices for Top-Side-Heated Horizontal Channels," MS Thesis, Prairie View A&M University.

Ungar, E. K., Miller, K. M., and Chen, I. Y., 1993, "Two Phase Pressure Drop in Lunar and Martian Gravity: Experimental Data and Predictions," ASME FED Vol. 190, pp. 329-342.

Wen, X. L., Briggs, A., and Rose, J. W., 1991, "Accurate Measurements of Heat Transfer Coefficients for Condensation on Horizontal Integral-Fin Tubes," ASME 91-HT-6.

DISTRIBUTIONS:

1. NASA Lyndon B. Johnson Space Center (original)
ATTN: BE13/Keith D. Hutto
2101 NASA Road 1
Houston, TX 77058-3696
2. Mr. William Harwell/EC2
NASA Johnson Space Center
Mail Code: EC2
Houston, TX 77058
3. NASA Center for Aerospace Information (CASI)
ATTN: Accessioning Department
800 Elkridge Landing Road
Linthicum Heights, Maryland 21090-2934
4. Mrs. Estella Hernandez Gillette
Director of Equal Opportunity Programs
National Aeronautics and Space Administration
Lyndon B. Johnson Space Center
2101 NASA Road 1
Mail Code: AJ
Houston, TX 77058-3695
5. Mrs. Lupita M. Armendariz
Equal Opportunity Specialist
NASA Johnson Space Center
2101 NASA Rd. 1,m/c:AJ
Houston, TX 77058
6. Dr. Joseph Atkinson, Jr.
Director of Minority University
Research & Education Program (AP-2)
NASA Johnson Space Center
Houston, TX 77058
7. Mrs. Oceola Hall
Deputy Associate Administrator for the Office of Equal Opportunity Programs
NASA Headquarters
Two Independent Square
Lab 300 E. St., SW
Washington, DC 20546

8. Ms. Bettie White
Director of Minority University Research and Education Division
NASA Headquarters
Two Independent Square
Lab 300 E. St., SW
Washington, DC 20546
9. Mr. George Reese
Associate Administrator for the Office of Equal Opportunity Programs
NASA Headquarters
Two Independent Square
Lab 300 E. St., SW
Washington, DC 20546
10. Captain James Wetherbee, USN
Deputy Director
NASA Johnson Space
2101 NASA Road 1
Houston, TX 77058
11. Mr. Alfred H. Ottley
604-A Persimmon Lane
Shepherdstown, WV 25443
12. Dr. Milton Bryant, Dean
College of Engineering
Prairie View A&M University
P. O. Box 397
Prairie View, TX 77446-0397
13. Dr. Charles Hines, President
P. O. Box 188
Prairie View A&M University
Prairie View, TX 77446
14. Mrs. Marilyn Donald
National Aeronautics and Space Administration
Lyndon B. Johnson Space Center
Mail Code: AJ
Houston, TX, 77058

15. Mrs. Ann Craddock
Research Foundation
Prairie View A&M University
Prairie View, TX 77446
16. Dr. Ronald Boyd, (6)
Director of the TSRC and Honeywell Professor of Engineering
Department of Mechanical Engineering
College of Engineering and Architecture
P. O. Box 397
Prairie View A&M University
Prairie View, TX 77446-0397
17. Mr. Will Ellis, Chief
Crew and Thermal Systems Division
NASA-JSC
Mail Code-EC 2101 NASA Road 1
Houston, TX 77058
18. Mr. George W. L. Abbey, Director
NASA Johnson Space Center
Mail Code-AA 2101 NASA Road 1
Houston, TX 77058
19. Mr. Henry L. Davis Director
Technology Transfer and Commercialization
NASA Johnson Space Center
Mail Code-HA 2101 NASA Road 1
Houston, TX 77058
20. Mr. Randolph H. Brinkley, Manager
Space Station Program
NASA Johnson Space Center
Mail Code-OA 2101 NASA Road 1
Houston, TX 77058
21. Mr. Frank L. Culbertson, Jr., Manager
Phase 1 Program
NASA Johnson Space Center
Mail Code-CB 2101 NASA Road 1
Houston, TX 77058

22. Mr. Tommy W. Holloway, Manager
Space Shuttle Program
NASA Johnson Space Center
Mail Code-MA 2101 NASA Road 1
Houston, TX 77058
23. Mr. John W. O'Neil, Manager
Space Operations
NASA Johnson Space Center
Mail Code-TA 2101 NASA Road 1
Houston, TX 77058
24. Mr. Donald R. McMonagle, Manager
EVA Project
NASA Johnson Space Center
Mail Code-XA 2101 NASA Road 1
Houston, TX 77058
25. Mr. Leonard Nicholson
Engineering Directorate
NASA Johnson Space Center
Mail Code-EA 2101 NASA Road 1
Houston, TX 77058
26. Dr. E. Joahanne Thomas-Smith
Provost & Vice President for Academic Affairs
P. O. Box 2777
Prairie View A&M University
Prairie View, TX 77446
27. TSRC Files (6)

